



**UNIVERSITÀ
DI TORINO**

University of Torino

Department of Molecular Biotechnology and Health Sciences

Ph.D. Program in
“Biomedical Sciences and Oncology”
35th Cycle

**Development and Characterization of PI3K γ /PKA Peptide
Disruptors as New Therapeutic Tools for the Treatment of
Obstructive Airway Diseases**

Tutor:

Prof. Alessandra Ghigo

Coordinator:

Prof. Emilio Hirsch

Candidate:

Angela Della Sala

Academic Years: 2019-2023
Bio13

Abstract

Progressive obstructive airway diseases, including asthma, chronic obstructive pulmonary disease, and the genetic disorder cystic fibrosis (CF), represent a major health burden worldwide. Cyclic AMP (cAMP) elevating agents, like β 2-adrenergic receptor agonists and phosphodiesterase inhibitors, are a mainstay in the treatment of these conditions, but their clinical use is limited by unwanted side effects due to global cAMP elevation. Compartment-restricted cAMP modulation can be achieved by manipulating the function of A-kinase anchoring proteins (AKAPs) which anchor protein kinase A (PKA) to its substrates and regulators, including enzymes involved in cAMP generation and destruction, in specific cellular locations. For instance, blocking the AKAP activity of phosphoinositide 3-kinase γ (PI3K γ) has been identified as a strategy to improve lung function by inducing cAMP-mediated bronchorelaxation, ion transport and anti-inflammatory responses. This study focuses on the development and the characterization of PI3K γ /PKA peptide disruptors as valuable tools for manipulating β 2-AR/cAMP signaling in the lungs for the treatment of chronic obstructive airway diseases. We characterized the aerodynamic properties of a PI3K γ mimetic peptide (MP) that we previously demonstrated being effective in the airway tract of mice upon intratracheal administration, where it safely boosts airway cAMP without altering cAMP homeostasis in organs in which its elevation would not be desirable, such as in the heart. Here we found that this compound has favourable proteolytic stability, mucus permeability and aerodynamic behaviour that confirm the possibility of using this preclinical advanced compound for inhaled therapy of all pulmonary conditions where local cAMP elevation is desirable, including but not limited to COPD and CF. In parallel, we report the generation of a novel non-natural peptide, DRI-Pep #20, optimized to disrupt the AKAP function of PI3K γ . DRI-Pep #20 mimics the native interaction between the N-terminal domain of PI3K γ and PKA, demonstrating nanomolar affinity for PKA, high resistance to protease degradation and high permeability to the pulmonary mucus barrier. DRI-Pep #20 triggers cAMP elevation both *in vivo* in the airway tract of mice upon intratracheal administration, and *in vitro* in bronchial epithelial cells of CF patients. In CF cells, DRI-Pep #20 rescues the defective function of the cAMP-operated channel cystic fibrosis conductance regulator (CFTR), by boosting the efficacy of approved CFTR modulators. These results position DRI-Pep #20 as a potent PI3K γ /PKA disruptor for achieving therapeutic cAMP elevation in respiratory disorders. Overall, these data point to the use of PI3K γ /PKA peptide disruptors as effective tools to manipulate the cAMP/PKA signaling in a compartmentalized manner, paving the way for targeted therapies with fewer side effects and improved efficacy in the realm of respiratory obstructive disease.

Index

List of Abbreviations.....	3
1. Introduction	4
1.1. Obstructive airways diseases.....	4
1.2. A-kinase Anchoring Proteins (AKAPs)	5
1.3. The AKAP function of PI3K γ	7
1.4. PI3K γ /PKA peptide disruptors in obstructive airways diseases	8
2. Material and Methods	11
2.1. Peptides and reagents	11
2.2. Cell lines	12
2.3. Animals	12
2.4. Isolation of murine peritoneal macrophages	12
2.5. cAMP measurements	13
2.6. Cell viability assay	13
2.7. CFTR activity measurements	13
2.8. CF sputum samples	14
2.9. PAMPA assay	15
2.10. PKA-RII α bioconjugation and fluorescence spectroscopy	15
2.11. Circular dichroism	17
2.12. Transmission Electron Microscopy and Dynamic Light Scattering	17
2.13. Next Generation Impactor (NGI) studies	17
2.14. Peptide mutagenesis	19
2.15. Protein structure prediction	19
2.16. Peptide Structure Prediction	20
2.17. Docking studies	20
2.18. Statistical analysis	21
3. Results	22
3.1. PI3K γ mimetic peptide (PI3K γ MP) binds selectively PKA-RII α	22
3.2. PI3K γ MP overcomes the biobarriers in obstructive airways diseases	23
3.3. PI3K γ MP is delivered to the lower respiratory airways	24
3.4. DRI-Pep #20 as a novel PI3K γ /PKA disruptor with high affinity for PKA..	24
3.5. DRI-Pep #20 mimics the native interaction between PI3K γ and PKA-RII α ..	25
3.6. DRI-Pep #20 has favorable mucus permeability and protease resistance....	27
3.7. DRI-Pep #20 promotes cAMP-dependent activation of wild-type and F508del-CFTR in human bronchial epithelial cells.....	28
4. Discussions	29
5. Figures and Tables	34
6. References	55
7. Patent and Publications	62

List of Abbreviations

AKAPs, A-kinase Anchoring Proteins;
ANOVA, Analysis of Variance;
ATP, Adenosine Triphosphate;
COPD, Chronic Obstructive Pulmonary Disease;
cAMP, 3'-5'-cyclic Adenosine Monophosphate;
CF, Cystic Fibrosis; CFTR,
Cystic Fibrosis Transmembrane Conductance Regulator;
DLS, Dynamic Light Scattering;
ED, Emitted Dose;
ETI, Elexacaftor/ Tezacaftor/ Ivacaftor;
FPF, Fine Particle Fraction;
GPCR, G Protein-Coupled Receptor;
GSD, Geometric Standard Deviation;
HADDOCK, High Ambiguity Driven Biomolecular DOCKing;
HEMT, Highly Effective Modulator Therapies;
HEN, Human Neutrophil Elastase;
HFIP, Hexafluoroisopropanol;
HS-YFP, Halide-Sensitive Yellow Fluorescent Protein;
I-TASSER, Iterative Threading ASSEMBLY Refinement;
IC₅₀, Half-maximal inhibitory Concentration;
Ivacaftor, VX-770,
K_D, Dissociation Constant;
K_{on}, Association rate Constant;
K_{off}, Dissociation rate Constant;
Lumacaftor, VX-809;
LD₅₀, Lethal Dose 50%;
MMAD_{exp}, Mass Median Aerodynamic Diameter;
NGI, Next Generation Impactor;
Penetratin 1, P1;
PI3K γ , Phosphoinositide 3-Kinase gamma;
PKA, Protein Kinase A;
RMSD, Root-Mean Square Deviation;
SEM, Standard Error of the Mean;
Tezacaftor, VX-661;
TEM, Transmission Electron Microscopy.

1. Introduction

1.1. Obstructive airways diseases

Obstructive airways diseases, including asthma, chronic obstructive pulmonary disease (COPD), and the genetic disorder cystic fibrosis (CF), are a diversified group of pathological conditions manifesting with shortness of breath, wheezing, coughing, chest tightness and frequent respiratory infections. Together, these pathologies with approximately 4 million deaths every year, represent the third cause of mortality and the leading cause of morbidity worldwide ¹. The World Health Organization estimates that currently hundreds of millions of people suffer from these diseases and a growing trend is expected for the upcoming years ² and so is the number of CF patients requiring long-term care, as survival is progressively improving as a result of intensive follow-up and better treatments.

Despite the diversity in terms of etiology, pathogenetic mechanisms and clinical manifestations, these conditions share common features such as airway hyper-reactivity, persistent respiratory tract inflammation, and mucus hypersecretion with consequent airway mucus plugging and airflow obstruction ^{3,4}.

The mainstay treatment for obstructive respiratory diseases includes β_2 -adrenergic receptors (β_2 -ARs) agonists and PDE inhibitors, cyclic AMP (cAMP) elevating agents known to regulate airway inflammation and reverse airway constriction ⁵. β_2 -ARs agonists acts as a bronchodilator via cAMP-mediated protein kinase A (PKA) activation that, by phosphorylating several targets within the cell, leads to the activation of myosin light chain phosphatase and inhibition of myosin light chain kinase, and thus mediate airway smooth muscle relaxation ⁶. β_2 -ARs agonists, similar to PDEs inhibitors, also have strong anti-inflammatory effects on infiltrating leukocytes ⁷ as, by boosting cAMP levels in inflammatory cells, promote the production of pro-resolving mediators and anti-inflammatory cytokines ⁸. In addition, PKA activation can reduce the expression of pro-inflammatory genes via inhibiting the transcriptional activity of NF- κ B ⁹.

Furthermore, these drugs can also be exploited to promote the activation of cystic fibrosis transmembrane conductance regulator (CFTR), contributing to proper airway hydration and mucus clearance ¹⁰. Mutations in the gene encoding for the CFTR are responsible for causing CF ⁴ and CFTR dysfunction of non-genetic origin has been demonstrated in asthma ¹¹ and COPD ¹². A high percentage of severe asthmatic patients affected by airway

mucus hypersecretion have been found to express polymorphisms in the CFTR gene¹³. Additionally, cigarette smoke, the leading cause of COPD, has been found to impair both CFTR expression and function in airway epithelia, spanning from reduced transcription to protein degradation, and resulting in “acquired” CFTR dysfunction¹⁴. Overall, disfunction of the CFTR channel leads to defects in ion-fluid transport, in particular in water secretion across the airway epithelium, with the consequent production of a dehydrated, hyper-concentrated mucus that accumulates in the airways causing airflow obstruction and inflammation¹². cAMP elevating agents are potent inducers of the CFTR, since both channel opening and stability at the plasma membrane rely on the cAMP signaling pathway¹⁵. In agreement, cAMP elevating agents can be administered to CF patients since they strongly improve the efficacy of the newly approved CFTR modulators to target the most prevalent channel mutant in CF (F508del)¹⁵.

Unfortunately, the clinical use of current cAMP modulating agents is hindered by unwanted side effects, including but not limited to tachyphylaxis, arrhythmias, diarrhea, and weight loss, arising from global cAMP elevation in both the airways and distant organs^{16,17,18}. Therefore, there is an urgent need for novel and safer approaches to manipulate locally the β_2 -AR/cAMP signaling axis for the treatment of obstructive airways diseases. For instance, compartment-restricted cAMP modulation can be achieved by manipulating the function of A-kinase anchoring proteins (AKAPs) which anchor PKA to its substrates and regulators, including enzymes involved in cAMP generation and destruction, in specific cellular locations^{19,20}. Pharmacological strategies aimed at modulating selective cAMP signalosomes rely on the design of compounds that can selectively affect the interactions between AKAPs and PKA.

1.2. A-kinase Anchoring proteins (AKAPs)

A-kinase anchoring proteins (AKAPs) are key players of the cAMP/PKA system, representing a diverse family of scaffolding proteins known for directly binding PKA. By tethering PKA to specific subcellular compartments, AKAPs create local signaling hubs, termed “signaling islands”, that prevents undesired cAMP responses and are crucial for normal cellular functions²¹. Perturbations in the fine control of cAMP compartmentalization are implicated in various pathologies, including cardiovascular diseases, pulmonary disorders, cancer, neurological conditions, and inflammation²⁰.

Although extensive work has characterized the myriad of protein-protein interactions involving AKAPs and PKA, the complete picture of their impact on cellular signaling in physiology and in disease remains to be fully elucidated.

AKAPs were first identified as a family of fifty structurally diverse but functionally related scaffold proteins that share the capacity to directly interact with the regulatory subunits (R) of the PKA holoenzyme²². The PKA holoenzyme consists of two regulatory subunits, each binding, and thus maintaining in an inactive state, one catalytic subunit²³. External signals activating G protein-coupled receptors (GPCRs) lead to cAMP synthesis, which, in turn, binds to the R subunits of PKA, causing the release and thus activation of the catalytic subunits²³. AKAPs tether PKA to specific cellular components, restricting the activation of the enzyme in space and in time and granting access to a limited number of substrates.

The interaction between AKAPs and PKA is multifaceted, involving A kinase-binding (AKB) domains and distinct targeting sequences²⁴. Importantly, AKAPs do not only direct PKA action but also engage with various signaling molecules, including other kinases, phosphatases, and PDEs in a sophisticated regulatory framework²⁵. AKAPs coordinate and contribute to signaling specificity by their ability to interact with either type I (RI) or type II (RII) PKA regulatory subunits. The complexity is further heightened by the existence of four distinct regulatory subunit isoforms (RI α , RI β , RII α , and RII β), each with unique tissue distribution, cAMP sensitivity, and AKAP-mediated localization²³. The vast majority of AKAPs selectively bind the RII isoform; however, a limited number can interact with RI, while a third class, termed dual-specific AKAPs, can bind both the RI and RII isoforms²⁶. Canonical AKAPs interact via their structurally conserved AKB domains with the dimerised N-terminal dimerization and docking (D/D) domains of the R subunits of PKA. AKB domains are 14–25 amino acids in length and form amphipathic helices that dock with their hydrophobic face into a hydrophobic pocket formed by the D/D domain²⁷. However, some AKAPs, known as “non-canonical”, can interact with the R subunits through regions different from the usual AKB. For example, pericentrin binds PKA via a 100-amino acid long motif, while other proteins such as RSK1 and α/β tubulin do not have the classical AKB domain²⁸.

Extensive work from our group has characterized phosphoinositide 3-kinase γ (PI3K γ) as a “non-canonical” AKAPs, binding to the regulatory subunit RII α of PKA through the

126-150 residues of its N-terminal domain ^{29,30}. This specific amino acid motif plays a crucial role in guiding the interaction with PKA in the context of the regulation of the β_2 -ARs and cAMP signaling in both the heart and the lungs ^{29,30}, as detailed in the following paragraphs.

1.3. The AKAP function of PI3K γ

PI3K γ is constitutively found in certain cell types, including leukocytes and cells of the airway respiratory tract ^{31,32}, while its expression is increased by various stresses in cardiomyocytes, vascular smooth muscle cells, and microglia ^{29,33}.

As a kinase, PI3K γ phosphorylates phosphatidylinositol 4,5-bisphosphate (PIP₂) into phosphatidylinositol 3,4,5-trisphosphate (PIP₃), a key step in the activation of various signaling pathways, primarily Akt-mediated pro-survival responses ³⁴. The activation of PI3K γ is typically initiated by G-protein coupled receptors (GPCRs), which in turn lead to the dissociation of the G $\beta\gamma$ dimer from the G-protein, its interaction with PI3K γ regulatory subunits, and the subsequent recruitment and activation of p110 γ subunit, the catalytic subunit of PI3K γ that is responsible of the kinase function of the enzyme. Interestingly, in cardiomyocytes, the catalytic subunit, p110 γ serves as the anchor for PKA, that tethers the cAMP-dependent kinase to PDE3 and PDE4, favouring their PKA-mediated phosphorylation and activation, eventually leading to cAMP downregulation. This tethering mechanism allows localized PDE stimulation for the precise modulation of cAMP signaling downstream of β_2 -ARs, influencing vital processes such as heart rhythm control ³⁵. While p110 γ appears to behave like an AKAP in that it directly binds the RII α subunit, its PKA-anchoring site appears to be atypical. In contrast to classical AKAPs that bind to PKA-RII α through a conserved amphipathic helix ²⁷, the p110 γ subunit is not predicted to form a helical domain. The interaction with PKA-RII α appears to rely on positively charged residues through the 126-150 residues of its N-terminal domain ³⁵. However, the molecular mechanisms operating this interplay remain unclear. Disruption of the scaffold but not the kinase activity of PI3K γ results in β_2 -AR/cAMP amplification in cardiomyocytes, and the ensuing development of lethal ventricular arrhythmias ³⁵.

PI3K γ is also expressed in pulmonary cells³² where the AKAP function of PI3K γ ³² is key to the negative regulation of the cAMP/PKA signaling cascade downstream of the β_2 -AR/cAMP axis. In this tissue, PI3K γ serves as an AKAP that tethers PKA to PDE3 and 4, thereby favoring their PKA-mediated phosphorylation and activation. Accordingly, basal cAMP levels in tracheas of mice lacking PI3K γ (PI3K $\gamma^{-/-}$) are 2-fold higher compared to wild-type animals and to mice expressing a kinase-inactive PI3K γ (PI3K $\gamma^{KD/KD}$), indicating that the same kinase-independent regulation of cAMP by PI3K γ found in cardiomyocytes is also preserved in airway cells³⁰. Moreover, a significant reduction of the catalytic activity of PDE4B and PDE4D is detected in tracheas of PI3K $\gamma^{-/-}$ mice, while their function is maintained in PI3K $\gamma^{KD/KD}$ tissues, corroborating the notion that PI3K γ restrains airway cAMP levels downstream of β_2 -ARs through a kinase-independent activation of PDE4³⁰. Because molecules that disrupt the interaction between AKAPs and components of the cAMP signaling pathway show promise in modulating specific cAMP signals and influencing cellular responses³⁶, we speculated that pharmacological targeting of PI3K γ scaffold activity could be exploited to achieve therapeutic cAMP elevation in the airways. In particular, we conceived a cell-permeable PI3K γ -derived mimetic peptide (PI3K γ MP) (Patent n° PCT/IB2015/059880-WO/2016/103176 by Kither Biotech S.r.l.) that disrupt the AKAP function of PI3K γ within the lungs and enhances β_2 -AR/cAMP signaling in human bronchial smooth muscle, immune and epithelial cells³⁰.

1.4. PI3K γ /PKA peptide disruptors in obstructive airways diseases

The pharmacological actions of the PI3K γ MP arise from its ability to displace PKA from the PI3K γ complex, thereby preventing PKA-mediated stimulation of a pool of PDE4 and enhancing β_2 -AR/cAMP responses, lead to smooth muscle relaxation, immune cell inhibition, and epithelial fluid secretion in the airways³⁰ (Fig. A). This latter event is linked to the activation of the cystic fibrosis transmembrane conductance regulator (CFTR), which promotes mucus hydration and clearance in CF as well as other obstructive airway diseases like asthma COPD^{37,30}. Although in the last decade numerous inhibitors of the kinase activity of PI3K γ have been developed, many of which are currently in clinical development for treating neoplastic diseases^{38,39}, PI3K γ MP

represents the first compound ever developed to selectively interfere with the anchoring function of PI3K γ ³⁰.

We have demonstrated that intratracheal instillation of the PI3K γ MP in mice induces a significant and dose-dependent increase in cAMP in both tracheas and lungs, which persists in the airways up to 24 hours without altering cAMP homeostasis in other organs, underlying the advantage of using this compound instead of β_2 -adrenergic agonists or PDE inhibitors, that holds several systemic side effects^{16,17,18}. Consistent with the prorelaxing action of cAMP and anti-inflammatory properties of PDE4⁴⁰, PI3K γ MP has been found to avert both bronchoconstriction in airway smooth muscle and neutrophil lung infiltration in a murine model of asthma³⁰. Another effect of targeting PDE4 is the cAMP/PKA-dependent gating of the CFTR channel, increasing airway surface liquid and facilitating mucus clearance. Of note, in human airway epithelial cells the PI3K γ MP not only increases CFTR gating but also restores the function of the most prevalent CFTR mutant in CF (F508del) by potentiating the effects of approved CFTR modulators³⁰.

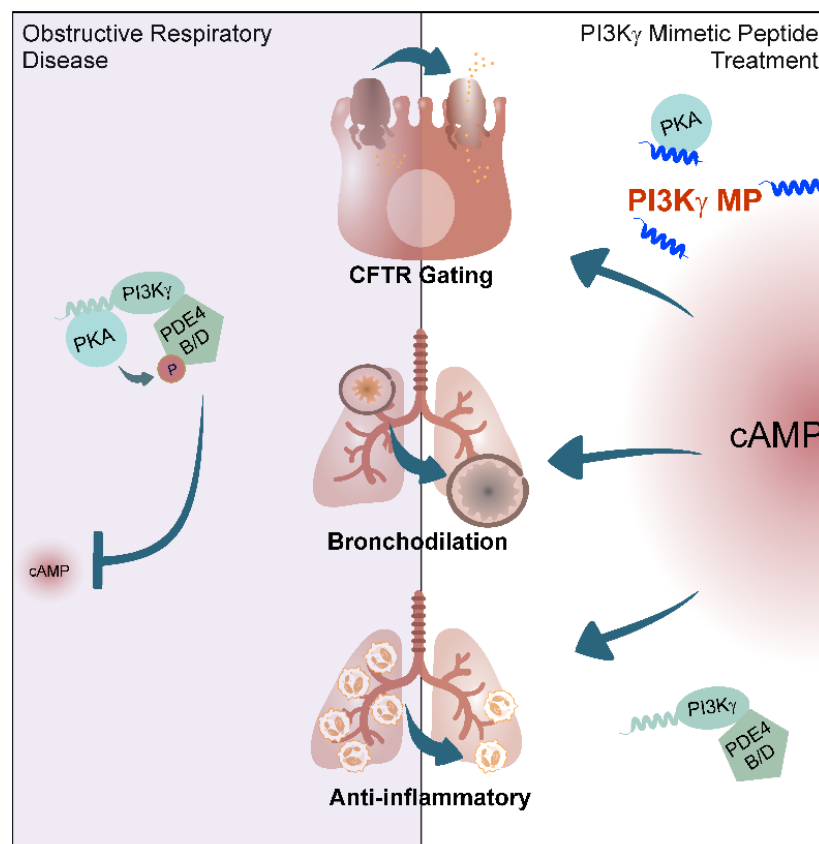
Overall, by disrupting the PI3K γ /PKA interaction locally in the airways, PI3K γ MP may represent a promising inhaled therapy for enhancing β_2 -AR/cAMP signaling in obstructive airways diseases. Inhalation of peptides offers a major advantage over that of classical small molecules, including high target selectivity and efficacy, as well as limited systemic toxicity⁴¹. Nonetheless, clinical outcomes of inhaled therapies strongly depend on the ability of the drug to deposit along the airways and to overcome barriers imposed by the diseased lungs, especially mucus⁴². The accumulation of an abnormally thick mucus layer and high concentrations of proteolytic enzymes significantly hamper peptide delivery in the airways of patients with obstructive airways diseases⁴².

In this context, our study was to confirm and extend our previous data indicating that the PI3K γ MP can overcome, at least partially, these obstacles. This was demonstrated via aerodynamic properties and thorough physico-chemical analysis of PI3K γ MP taking into consideration critical factors such as molecular dimensions, membrane permeability, and proteolytic stability were conducted.

We found that this peptide has favourable proteolytic stability, mucus permeability and aerodynamic behaviour that confirm the possibility of using this preclinical advanced compound for inhaled therapy of all pulmonary conditions where local cAMP elevation is desirable, including but not limited to COPD and CF.

In parallel, we report the generation of a novel non-natural peptide, DRI- Pep #20 (Patent pending n° BIT28754-CF/PS), optimized to disrupt the AKAP function of PI3K γ . DRI- Pep #20 acted as a potent disruptor of the PI3K γ /PKA complex by mimicking the core of the native interaction of PI3K γ with PKA, and that was characterized by nanomolar affinity for PKA, high resistance to protease degradation and high permeability to the pulmonary mucus barrier.

Overall, our study supports the use of natural and non-natural PI3K γ /PKA peptide disruptors as effective tools to manipulate the cAMP/PKA signaling complex in the lungs for therapeutic purposes.



Ghigo, Murabito et al., *Sci. Transl. Med.*, 2022

Figure A. Targeting the AKAP function of PI3K γ with a cell-permeable PI3K γ -derived mimetic peptide (PI3K γ MP) (Patent n° PCT/IB2015/059880-WO/2016/103176 by Kither Biotech S.r.l.)

2. Material and Methods

2.1. Peptides and reagents

Peptides were synthesized by GenScript (Piscataway, NJ) at >95% purity. The sequences of all peptides are as follows;

P1 RQIKIWFQNRRMKWKK	Pep #21 KGNHR
DRI-Pep #20 RHQGK	Pep #22 KNLHR
Pep #01 KATHRSPGQIHLVQRHPPSEESQAF	Pep #23 KSLHR
Pep #02 KATHRSPGQIHLVQRHPP	Pep #24 KCNHR
Pep #03 KATHRSPGQIHLVQRHP	Pep #25 KNCHR
Pep #04 KATHRSPGQIHLVQRH	Pep #26 KGSHR
Pep #05 KATHRSPGQIHLVQR	Pep #27 KATHR
Pep #06 KATHRSPGQIHLVQ	Pep #28 KNSHR
Pep #07 KATHRSPGQIHLV	Pep #29 KSCHR
Pep #08 KATHRSPGQIHL	Pep #30 KLGHR
Pep #09 KATHRSPGQIH	Pep #31 KQCHR
Pep #10 KATHRSPGQI	Pep #32 KLSHR
Pep #11 KATHRSPGQ	Pep #33 KCCHR
Pep #12 KATHRSPG	Pep #34 KSNHR
Pep #13 KATHRSP	Pep #35 KCGHR
Pep #14 KATHRS	Pep #36 KSGHR
Pep #15 KATHR	Pep #37 KGCHR
Pep #16 KATH	Pep #38 KGLHR
Pep #17 KAT	Pep #39 KLLHR
Pep #18 KA	Pep #40 KCSHR
Pep #19 K	Pep #41 KLCHR
Pep #20 KGQHR	Pep #42 KCLHR
	Pep #43 KGGHR

Recombinant human PKA regulatory subunit RII α (PKA-RII α) and PI3K γ catalytic subunit (p110 γ) were purchased by Biaffin GmbH & Co KG (Kassel, DE) and Origene Technologies (TP307790, Rockville, US), respectively.

Human neutrophil elastase was purchased from Sigma-Aldrich (CAS 9004-06-2, Sigma-Aldrich, Saint Louis, MO) and reconstituted in 50 mM sodium acetate, pH 5.5, with 200 mM NaCl. VX-809 (Lumacaftor), VX-770 (Ivacaftor), VX-661 (Tezacaftor) and VX-445 (Elexacaftor) were purchased from MedChemExpress LLC (Princeton, USA). Propranolol, Hexafluoroisopropanol, Forskolin and CFTRinh-172 were purchased from Sigma-Aldrich (CAS 318-98-9, 920-66-1, 66575-29-9, 307510-92-5 Sigma-Aldrich, Saint Louis, MO).

2.2. Cell lines

Immortalized normal human bronchial epithelial cells (16HBE14o-) were kindly provided by Dr. Gruenert (University of California San Francisco, San Francisco, CA). Cystic fibrosis bronchial epithelial (CFBE41o-) cells stably expressing F508del-CFTR (F508del-CFTR-CFBE41o-) were kindly provided by L. Fu from the UAB Research Foundation (Birmingham, AL). Cells were grown in Minimum Essential Medium (MEM) supplemented with 10% FBS, 5 mM L-Glutamine, 100 U/ml penicillin and 100 µg/ml streptomycin (Thermo Fisher Scientific, Waltham, MA) on culture dishes pre-coated with human fibronectin (1 mg/ml; Sigma-Aldrich, Saint Louis, MO), bovine collagen I (3 mg/ml; Sigma- Aldrich, Saint Louis, MO) and bovine serum albumin (0.1%; Sigma-Aldrich, Saint Louis, MO) diluted in LHC-8 basal medium (Invitrogen, Waltham, MA). Cells up to passage 15 were used for experiments. All cells were cultured at 37°C and under a 5% CO₂ atmosphere.

2.3. Animals

PI3K γ -deficient mice (PI3K γ ^{-/-}) were described previously³⁰. Mutant mice were back-crossed with C57Bl/6j mice for 15 generations to inbreed the genetic background and C57Bl/6j were used as controls (WT). Mice used in all experiments were 8 to 12 weeks of age. Mice were group-housed, provided free-access to standard chow and water in a controlled facility providing a 12-hour light/dark cycle and were used according to institutional animal welfare guidelines and legislation, approved by the local Animal Ethics Committee. All animal experiments were approved by the animal ethical committee of the University of Torino and by the Italian Ministry of Health (Authorization n°757/2016-PR).

2.4. Isolation of murine peritoneal macrophages

Peritoneal macrophages were prepared from 8- to 12-week- old wild-type (WT) and PI3K γ ^{-/-} mice, as described previously³⁰. Briefly, cells were collected from euthanized animals by peritoneal lavage with 5 mL of PBS, supplemented with 5 mM EDTA. Cells were centrifuged for 3 min at 300 g and the pellet was resuspended in culture media including Roswell Park Memorial Institute (RPMI) media, 100 U/ml penicillin and 100 µg/ml streptomycin, and 10% heat-inactivated FBS (Thermo Fisher Scientific, Waltham,

MA). Macrophages were seeded in 96-well plates (1×10^6 cells/well) and maintained at 37°C with 5% CO₂ for at least 16/18 h before treatment with the peptide and cAMP quantification.

2.5. cAMP measurements

From cells: cAMP content was measured in 16HBE14o- cells at the indicated time points after treatment with the indicated doses of peptides using the Promega cAMP-Glo™ Assay kit (Promega, Milano, IT), according to the manufacturer's protocol.

From tissues: lungs, tracheas and hearts were collected from euthanized mice 24 h after intratracheal instillation of different doses of the peptide (0 to 750 mg/kg in a final volume of 50 µl of PBS). Snap-frozen tissues were powdered in liquid nitrogen and extracted with cold 6% trichloroacetic acid. Samples were sonicated for 10 sec, incubated at 4°C under gentle agitation for 10 min and then centrifuged at 13000 rpm at 4°C for 10 min. Supernatants were washed four times with five volumes of water saturated with diethyl ether and lyophilized. cAMP content was detected with Cyclic AMP ELISA Kit (Cayman Chemical, Michigan, USA), according to the manufacturer's protocol.

2.6. Cell viability assay

Human bronchial epithelial cells (16HBE14o-) were seeded in 96-well plates (2×10^4 cells/well) and incubated for at least 16/18 hours at 37°C with 5% CO₂ before experiments. Non-adherent cells were eliminated by washing with PBS and cells were then stimulated with 8 different doses of the indicated peptide (0 µM – 1 mM range) for 24h. ATP levels were evaluated as an indicator of viable cells using the Cell Titer-Glo® Luminescent Cell Viability Assay (Promega, Milano, IT), according to the manufacturer's protocol. The lethal dose (LD₅₀) was calculated with respect to untreated control cells, whose viability was set to 100%.

2.7. CFTR activity measurements

CFTR-mediated anion transport was measured by using the Premo™ Halide Sensor (Thermo Fisher Scientific, Waltham, MA) which allows assessment of CFTR activity by measuring the rate of YFP fluorescence quenching caused by iodide/chloride exchange across the plasma membrane. Briefly, the halide-sensitive yellow fluorescent protein

(HS-YFP) was expressed in 16HBE14o- and F508del-CFTR-CFBE41o- cells through the BacMam technology, according to the manufacturer's protocol. Cells expressing the HS-YFP were cultured on 96-well plates and treated with the indicated peptides/compounds for the indicated time. Fluorescence was evaluated in a plate reader immediately after addition of 150 μ l of Halide stimulus buffer (an NaI-containing solution) leading to a final NaI concentration in the wells of 75 mM. Fluorescence was continuously read (1 point per second) starting at 1 s before Halide stimulus buffer addition and up to 120 s. CFTR activity was expressed as $\Delta F/F_0$ where ΔF was obtained by subtracting the background fluorescence (fluorescence of cells not expressing HS-YFP) to the fluorescence measured at the specific time point after addition of NaI. ΔF was then normalized to the initial fluorescence F_0 (fluorescence of HS-YFP-expressing cells immediately after addition of NaI) to obtain a measure of relative fluorescence $\Delta F/F_0$.

2.8. CF sputum samples

Spontaneous expectorated sputum samples from CF patients in stable clinical conditions were collected at the Bronchiectasis and Cystic Fibrosis Programs of the Respiratory Department of Fondazione IRCCS Ca' Granda Ospedale Maggiore Policlinico in Milan (Italy) and processed as previously described⁴³. The study protocol was approved by local institutional review boards (594_2016bis) and all participants provided written informed consent to the collection and use of their biological samples. Briefly, samples were first processed by eliminating saliva, then sputum plugs were selected and weighted. Samples were diluted 8X in PBS, vortexed until sputum dissolution and centrifuged for 15 min at 3000 g. Supernatants were recovered and stored at -80 °C, thawed overnight at 4 °C, and all subsequent experiments were undertaken within 24h from thawing. Neutrophil elastase was quantified as described previously⁴³ and sputum samples containing 20 μ g/mL of active neutrophil elastase were used to assess the activity of peptides in 16HBE14o- cells in the presence of CF sputum. Briefly, cells were seeded in 96-well plates (2×10^4 cells/well) and incubated for at least 16/18 h at 37 °C with 5% CO_2 before experiments. Subsequently, peptides were diluted in PBS at a final concentration of 25 μ M and a PBS:sputum mixture (1:1) was added on the top of adherent cells (100 μ l/well). cAMP levels were quantified at the indicated time points using the Promega cAMP-Glo™ Assay kit (Promega, Milano, IT), according to the manufacturer's protocol.

2.9. PAMPA assay

To assess the permeability of peptides through a CF sputum layer, a parallel artificial membrane permeability system (PAMPA) (Corning Gentest Pre-coated PAMPA, 353015, USA plates) that allows to measure the ability of drugs to diffuse from a donor compartment, through an artificial membrane, into an acceptor compartment, was used as described previously⁴⁴. The bottom wells of the PAMPA system (“acceptor” wells) were filled with 300 μ L of PBS (10mM, 150 mM NaCl, pH 7.4), while “donor” wells were filled with 200 μ L of the peptide solution (2 mg/mL in 10mM PBS, 150 mM NaCl, pH 7.4), in the absence or presence of CF sputum. In the latter case, 40 μ L of CF sputum was first deposited over the PAMPA membrane, and the peptide solution was subsequently added over the CF sputum layer. Afterwards, the two wells were coupled and incubated for 5h at RT. At the end of the incubation, the plates were split, and the amount of peptide diffused into the acceptor well was quantified by fluorescence spectroscopy using a Horiba Jobin Yvon Fluorolog 3 TCSPC fluorimeter (Horiba, Kyoto, Japan) equipped with a 450-W xenon lamp and a R928 photomultiplier (Hamamatsu Photonics, Hamamatsu, Japan). Excitation was performed at 280nm while emission was recorded in the spectral region of 290-500 nm (maximum of emission at 362 nm). Excitation and emission slits were set at 4 and 5 nm, respectively. The concentration of the peptide was calculated using a 6-points calibration curve. The apparent permeability coefficient (P_{app}) was expressed according to this relationship:

$$P_{app} = \frac{dQ/dt}{C_0 \times A}$$

derived from Fick’s law for steady-state conditions⁴⁵, where dQ is the quantity of drug expressed as moles permeated into the acceptor compartment at time t (18000 sec), C_0 is the initial concentration of the peptide in the donor well, and A is the area of the well membrane (0.3 cm²).

2.10. PKA-RII α bioconjugation and fluorescence spectroscopy

Recombinant PKA-RII α was bio-conjugated to fluorescein 5-maleimide (F5M), as described previously⁴⁶, using 75 μ g of PKA-RII α and a 50-fold excess of F5M. After bioconjugation, the derivative was immediately purified using a Sephadex® G-25 desalting column and phosphate-buffered saline solution (PBS) (20 mM, 150 mM NaCl, pH 7.2) as eluent. To evaluate F5M labelling efficiency, the dye/protein ratio (D/P) of the

conjugates was determined by the absorption spectra of the labelled proteins in PBS (20 mM, 150 mM NaCl, pH 7.2), according to the following equation:

$$\frac{D}{P} = \frac{A_{max} e_{prot}}{(A_{280} - cA_{max}) e_{dye}}$$

where A_{280} is the absorption of the conjugate at 280 nm; A_{max} is the absorption of the conjugate at the absorption maximum of the corresponding F5M; c is a correction factor ($c = 0.29$); e_{prot} ($25,169 \text{ M}^{-1}\text{cm}^{-1}$) and e_{dye} ($63,096 \text{ M}^{-1} \text{ cm}^{-1}$) are the molar extinction coefficients of PKA and F5M, respectively. PKA-RII α presents six cysteine residues, and the final D/P value was 0.2.

UV-visible absorption spectra were measured with a UH5300 spectrophotometer (Hitachi, Tokyo, Japan) at RT, using 1 cm pathway length quartz cuvette. Fluorescence emission spectra in steady-state mode were acquired at RT using a Jobin Yvon Fluorolog 3 TCSPC fluorimeter (Horiba, Kyoto, Japan) equipped with a 450-W Xenon lamp and a R928 photomultiplier (Hamamatsu Photonics, Hamamatsu, Japan). Steady-state fluorescence spectra were recorded in the 500-600 nm range. The excitation wavelength was set on 490 nm and the excitation and emission slits were set on 2 and 4, respectively. Equilibrium binding constants (K_D and K_A) were obtained from steady-state data.

Fluorescence kinetics were measured using an Applied Photophysics SX20 stopped-flow spectrophotometer (Applied Photophysics, North Carolina, US) fitted with a 495 nm cut-off filter between the cell and the fluorescence detector, and equipped with a thermostat bath set at $25 \pm 0.2^\circ\text{C}$. Association and dissociation rate constants (k_{on} and k_{off}) were calculated from stopped-flow kinetics data. Data acquisition, visualization and analysis were performed with Pro-Data software from Applied Photophysics Ltd (Applied Photophysics, North Carolina, US).

To assess the ability of the peptides to displace the binding between PI3K γ and PKA-F5M, steady-state emission spectra of the PI3K γ /PKA-F5M complex in the presence of increasing concentrations of the peptide were acquired. Briefly, 50 nM of recombinant PI3K γ was added to 100 nM F5M-bounded PKA-RII α in a total volume of 100 μL PBS. The concentration of the PI3K γ /PKA-F5M complex was kept constant while gradually titrated with increasing concentrations of the peptides (PI3K γ MP from 0 to 20 μM ; DRI-Pep #20 from 0 to 5 μM). The complex was excited at 490 nm and emission spectra were

recorded in the 500-600 nm spectral range, as described above. The degree of displacement of the PKA-RII α -PI3K γ complex was expressed as the percentage of fluorescence quenching after addition of the peptide.

2.11. Circular dichroism

Circular dichroism (CD) measurements were performed on a Jasco-810 Dichrograph equipped with a Peltier thermoelectric controller (Jasco Inc., Easton, US). The spectra of peptides were recorded in the continuous mode between 260 and 180 nm at 25 °C in 0.1 cm path length quartz cuvette (Hellma GmbH, Müllheim, DE) with a total peptide concentration of 0.2 mg/mL dissolved in 2 mM PBS (0.6 mM KH₂PO₄, 1.6 mM K₂HPO₄), pH 7.4. The CD spectrum in the 190-240 nm range was used to predict the secondary structural content of the peptide using the K2D3 web server ⁴⁷.

2.12. Transmission Electron Microscopy and Dynamic Light Scattering

Self-assembled peptide nanostructures were analyzed by Transmission Electron Microscopy (TEM) analysis. Transmission electron micrographs were obtained with a JEOL 3010-UHR TEM operating at an accelerating voltage of 300.00 kV (JEOL, Tokyo, Japan). TEM samples were prepared by dissolving the peptides at 0.1 mg/mL in water and drying them on a carbon-coated copper grid. The nominal magnification used to record nanostructures were $\times 500000$ and $\times 800000$.

The size distribution profile of the self-assembled peptide was determined by dynamic light scattering (DLS, Malvern Zetasizer, Worcestershire, UK). Samples were prepared at 4 mg/mL in 2 mM PBS (0.6 mM KH₂PO₄, 1.6 mM K₂HPO₄), pH 7.4. Measurements were performed after an equilibration time of 60 s which allowed samples to reach the temperature of 25°C.

2.13. Next Generation Impactor (NGI) studies

The aerodynamic properties of the peptide were assessed by Next Generation Impactor (NGI) (Copley Scientific, Nottingham, UK), according to the Comité Européen de Normalization standard methodology for nebulizer systems. The NGI equipment consisted of seven stages cups (S1-S7), a micro-orifice collector (MOC), an induction port and a vacuum pump simulating inspiration. Three nebulizer devices were tested: one

jet nebulizer –TurboBoy (PARI TurboBOY, PARI GmbH, Starnberg, Germany), and two mesh nebulizers –AeronebGo (Aeroneb® Go, Aerogen Ltd., Galway, Ireland) and – eFlow rapid (PARI eFlow rapid, PARI GmbH, Starnberg, Germany). Briefly, the nebulizer reservoir was filled with 1 mL of a phosphate buffered saline dispersion of the peptide (1 mg/mL). The nebulizer device was connected to the induction port of the NGI and operated with a vacuum pump at a fixed flowrate of 15 L/min. The aerosol was drawn through the impactor for 5 min until dry.

The peptide that remained aerosolized (i.e., inside the nebulizer reservoir, deposited on the seven stages of the NGI and in the induction port) was quantitatively recovered and quantified by High- Performance Liquid Chromatography (HPLC/UV) spectrophotometry.

HPLC/UV involved a Waters Breexe System Liquid Chromatograph equipped with a Waters 717 Plus Autosampler (40 µL injection volume) and a Shimadzu UV–vis HPLC detector online with a computerized workstation. The column used was a Jupiter® C18 widepore (300A, 5 mm x 25 cm), the mobile phase was a mixture of Water 0.1% TFA: Acetonitrile 0.1% TFA 75:25 (v/v) with a flow rate of 1 mL/min, the column temperature was 25 °C and the detection wavelength was 220 nm. Upon emission, the experimental mass median aerodynamic diameter (MMAD_{exp}) and the geometric standard deviation (GSD) were calculated according to the European Pharmacopoeia, by plotting the cumulative mass of peptide retained in each collection stage (expressed as percent of total mass recovered in the impactor) versus the cut-off diameter of the corresponding stage. At the used flow (15 L/min), the cut-off diameters of the NGI stages were 14.10 µm (S1), 8.61 µm (S 2), 5.39 µm (S3), 3.30 µm (S4), 2.08 µm (S5), 1.36 µm (S6), 0.98 µm (S7). The MMAD_{exp} was determined from the graph as the peptide size at which the line crosses the 50% mark; the GSD was defined as:

$$\text{GSD} = (\text{Size X}/\text{Size Y})^{1/2}$$

where size X was the size at which the line crosses the 84% mark and size Y the size at which it crosses the 16% mark.

The emitted dose (ED) was measured as the difference between the total amount initially placed and the amount remaining in the stages. The fine particle fraction (FPF) was calculated by considering the amount of peptide deposited on S3-S6 compared to the

initial amount loaded in the nebulizer chamber, while the respirable fraction (RF) was determined by the total amount recovered from the NGI.

2.14. Peptide mutagenesis

Systematic amino acid substitutions were performed using an in-house Python script. To identify which variant could mimic the characteristics of DRI-Pep #20, we compared the ability of each peptide to adopt the same spatial arrangement and exhibit a similar surface charge distribution. The peptides from the library were subsequently processed using Omega2 (OMEGA, version 4.1.0.2; OpenEye Scientific Software: Santa Fe, NM)^{48,49}, a software that creates a multi-conformer structure database capable of reproducing biologically active conformations. The ROCS software (ROCS, version 3.4.1.2; OpenEye Scientific Software: Santa Fe, NM)⁵⁰ was employed to conduct a shape-based overlay method, in which molecules were aligned through a solid-body optimization process aimed at maximizing the volume overlap between them. Subsequently, the peptides were re-ranked for similarity to DRI-Pep #20 based on electrostatic properties using the EON program (EON, version 2.3.4.2; OpenEye Scientific Software: Santa Fe, NM)⁵¹. The final score assigned to each peptide was based on a dual Tanimoto score, ranging from 0 to 2, where a score of 2 signifies an exact match in both shape and electrostatics between the two molecules. Peptides with the highest scores were considered for further analysis.

2.15. Protein structure prediction

The 3D structure of residues 1-45 of PKA-RII α was predicted using the Iterative Threading ASSEmblY Refinement (I-TASSER) web server⁵², an on-line platform that implements I-TASSER-based algorithms for predictions of protein structure and function. Briefly, starting from the FASTA amino acid sequence I-TASSER ran a three steps simulation, first threading it through a representative PDB structure library to search for possible template folds or supersecondary-structure fragments, using a profile–profile alignment-based threading algorithm. In the second step, the continuous fragments excised from the PDB templates were reassembled into full-length models, while the unaligned regions were built by ab initio modeling. Finally, the structure trajectories were clustered, and the lowest-energy structures selected, and an all-atom model was constructed by REMO41 through optimization of the hydrogen-bonding network. The

five best models obtained by I-TASSER were subsequently evaluated based on their threading template and predicted C-score. The model with the highest C-score of -0.22 and predicted using the NMR structure of PKA-RII α as a threading template (PDB ID 2KYG)⁵³ was selected.

The 3D structure of PI3K γ was downloaded by AlphaFold⁵⁴ and validated by Root-Mean Square Deviation (RMSD) alignment of all the atoms with the cryo-electron microscopy structure of the heterodimeric PI3K γ complex, p110 γ -p101 (PDB ID 7MEZ)⁵⁵.

2.16. Peptide Structure Prediction

The structure of the peptides was predicted with PEP-FOLD3.5⁵⁶, a de novo approach that predicts peptide structures from amino acid sequences. Briefly, starting from the amino acid sequence, first a series of 200 simulations was run, each one sampling a different region of the conformational space using the Generator taboo-sampling 5 (ts5), recommended for peptides longer than 10 amino acids. The output was an archive of clusters of all the models sorted out using the TM score followed by performing the Model Quality assessment using Apollo⁵⁷. The first five models, representing the five best conformation of each cluster with the best scores defined according to the lowest sOPEP energy and the highest TM-score value, were selected and further supported by RMSD. The RMSD of each model was compared to the RMSD of residues 126-150 of the p110 γ structure, both the protein structure predicted by AlphaFold and the crystal structure (PDB ID 7mez, RCSB database). Finally, the best structure of the peptide was validated by visual analysis on PYMOL.

2.17. Docking studies

Docking studies were performed with the High Ambiguity Driven Biomolecular DOCKing (HADDOCK) software. Briefly, starting from the PKA-RII α and peptide structures, the HADDOCK docking ran three consecutive steps, first the molecules were randomly oriented, and a rigid-body search was performed (it0). The output was an archive of 1000 models, among them the top 200 ranked structures were selected based on the energy function and addressed to the semi-flexible simulated annealing stage performed in torsion angle space (it1). In the third stage, the structures were refined in Cartesian space with explicit solvent layer (water) and subjected to a short molecular

dynamic simulation at 300K. During the refinement, both the side chain and backbone of interface residues were progressively allowed to move.

The final models were automatically clustered based on the positional interface ligand RMSD (iL-RMSD) by fitting the conformational changes on the interface of the receptor (PKA-RII α) and on the interface of the smaller partner (the peptides). Finally, the binding poses were assessed by the HADDOCK report and the binding affinity was evaluated by the Optimal Hydrogen Bonding Network. The resulting best binding pose was validated by visual analysis on PYMOL.

2.18. Statistical analysis

Data are presented as scatter plots with bars (means \pm SEM). Prism software (GraphPad Software Inc.) was used for statistical analysis. Raw data were first analyzed to confirm their normal distribution via the Shapiro-Wilk test and then analyzed by unpaired Student's t test, one-way analysis of variance (ANOVA), or two-way ANOVA. Bonferroni correction (one-way and two-way ANOVA) was applied to correct for multiple comparisons. $P < 0.05$ was considered significant.

3. Results

3.1. PI3K γ mimetic peptide (PI3K γ MP) binds selectively PKA-RII α

In order to disrupt the AKAP function of PI3K γ and produce a compartmentalized β_2 -AR/cAMP response, PI3K γ MP was conceived by fusing the cell-penetrating sequence Penetratin-1 (P1) and the PKA-binding motif of PI3K γ (residues 126-150 KATHRSPGQIHLVQRHPPSEESQAF), by means of a glycine (G) linker (Fig. 1a)^{29,30}. First, we sought to elucidate the determinants of the interaction of PI3K γ MP with PKA. Predictions of the tridimensional structure of PI3K γ MP suggested the presence of an α -helix, flanked by an uncoiled region (Fig. 1b). The helical propensity of the peptide was confirmed by circular dichroism analyses showing a double-peak signal, with a maximum at 200 nm which is typical for α -helix structures, and a minimum in the 220–240 nm region which is characteristic for random-coil⁵⁸. As expected, the α -helical content of PI3K γ MP was comparable to the helix pattern found in the PKA-binding motif of PI3K γ (residues 126-150) not fused to the cell-penetrating module (Fig. 1c). *In silico* simulations of the interaction of PI3K γ MP with the AKB domain of PKA-RII α (amino acids 1-45)⁵⁹, revealed that the binding mainly involves hydrophilic amino acids of the PI3K γ MP helical motif. R-22, H-21, H-33 and Q-21 were found to form hydrogen bonds with hydrophilic partners in the PKA-RII α subunit (Fig. 1d and 2a), with a predicted dissociation constant (K_D) of 1.34 μ M (Table 3). In agreement, fast kinetic studies showed the peptide could associate recombinant PKA-RII α with a good affinity, being the equilibrium dissociation constant in the micromolar range, K_D of 2.0 μ M (Fig. 3b). Moreover, these studies showed that PI3K γ MP rapidly associates to PKA-RII α forming a relatively stable complex with the association rate constant (k_{on}) in the order of 10^{-6} M⁻¹s⁻¹ while the moderate dissociation rate (k_{off}) suggesting a certain level of stability of PI3K γ MP in the bound state with PKA-RII α (Fig. 3b). Thus, the binding of PI3K γ MP to PKA-RII α suggested PI3K γ MP as a disruptor of PI3K γ /PKA complex. Indeed, in a displaced-based assay the peptide inhibited the interaction between recombinant PI3K γ and PKA-RII α up to 50%, and with an IC_{50} of 1.5 μ M (Fig. 3d). Notably, the PI3K γ MP showed it was well tolerated 16HBE14o- cells, being the LD_{50} 60-fold higher than the IC_{50} (Fig. 3e). Overall, these data confirms that PI3K γ MP acts as a moderate PI3K γ /PKA disruptor with micromolar affinity for PKA.

3.2. PI3K γ MP overcomes the biobarriers in obstructive airways diseases

Since we have demonstrated that the PI3K γ MP can be topically delivered to the lungs through intratracheal instillation in mice, where it safely boosted airway cAMP up to 24 hours in both tracheas and lungs, without altering cAMP homeostasis in other organs³⁰. Next, we sought to evaluate to what extent PI3K γ MP could effectively target PI3K γ /PKA complex in the lungs, especially in the context of obstructive airways diseases.

Because the efficacy of inhaled therapies may be hindered by biobarriers imposed by diseased lungs, such as a thick layer of protease-rich mucus⁴², we sought to determine the ability of PI3K γ MP to penetrate mucus layers and resist to protease degradation. PI3K γ MP penetrated the phospholipid membrane in the PAMPA system (Fig. 4a) with an apparent permeability (P_{app}) of $5.59 \times 10^{-6} \text{ cm s}^{-1}$ (Fig. 4b). While the addition of pathological CF sputum on top of the phospholipid layer (Fig. 4a) reduced the P_{app} of the peptide ($P_{app} 1.46 \times 10^{-6} \text{ cm s}^{-1}$) (Fig. 4b), this value was comparable to that of propranolol, a standard reference compound known for being high permeable to cell membranes⁴⁴. To better understand the molecular basis of the mucus permeability of PI3K γ MP, we performed Transmission Electron Microscopy (TEM) and Dynamic Light Scattering (DLS) assays. TEM images showed that PI3K γ MP formed irregular aggregates up to 500 nm in size (Fig. 4c), in agreement with the particle diameter of 200-300 nm retrieved by DLS analysis (Fig. 4d). Addition of hexafluoroisopropanol (HFIP), which is responsible for cold denaturation of proteins, reduced the size of aggregates to 10 nm (Fig. 4d). Next, we tested whether PI3K γ MP retained the ability to elevate cAMP in pulmonary cells in the presence of neutrophil elastase, the most abundant protease in the lungs of patients with neutrophilic airway diseases, including but not limited to COPD and CF⁶⁰.

The peptide retained up to 62% of its ability to raise cAMP in 16HBE41o- cells in the presence of 3 $\mu\text{g/ml}$ of recombinant human neutrophil elastase (HNE) (Fig. 4e), a dose which was previously shown to inactivate other therapeutic peptides⁶¹. The cAMP elevating activity of PI3K γ MP was similarly affected by a 10-fold higher concentration of HNE (Fig. 4f), an amount that is typically detected in the lungs of patients with severe bronchiectasis⁶⁰. The relative resistance of PI3K γ MP to degradation was confirmed in the presence of CF sputum, where the peptide retained 52% of its biological activity (Fig. 4g). Taken together, these results provide insights into the ability of PI3K γ MP to

maintain its biological activity in a challenging extracellular environment, marked by a mucus barrier enriched in proteases typical of diseased lungs.

3.3. PI3K γ MP is delivered to the lower respiratory airways

Since PI3K γ MP was originally conceived for inhaled administration³⁰, next we assessed its aerodynamic properties upon nebulization with three different devices commonly used for administering aerosolized compounds to CF patients⁶². One jet nebulizer –TurboBoy– and two mesh nebulizers –AeronebGo and eFlow rapid were used.

To evaluate the ability of the peptide to reach the lower airways, the aerosolized particles of the PI3K γ MP were driven inside the Next Generation Impactor (NGI) passing through seven stages with defined cut-offs diameters (Fig. 5a and Table 1). After aerosolization with the three nebulizers, PI3K γ MP displayed aerodynamic mean dimensions (MMAD: 2-2.99 μ m) compatible with effective delivery to the lower airways (Fig. 5b and Table 2), considered that a particle size of approximately 5 μ m is generally capable of penetrating the lung during inhalation⁶³. Nevertheless, different deposition patterns were observed when the peptide was aerosolized with the different nebulizers (Fig. 5c). Notably, the estimated emitted dose for the two mesh nebulizers was more than 40% and 2-fold higher than that of the jet nebulizer (Fig. 5d and Table 2). Moreover, the respirable fraction (RF), representing the total amount of PI3K γ MP recovered from NGI and thus the amount of peptide that potentially is delivered to the lungs, exceeded 90% (Table 2).

Finally, we verified that PI3K γ MP could retain its biological activity after nebulization. We found that the peptide recovered from Stage 4 after nebulization with eFlow rapid could raise cAMP in 16HBE41o- cells as effectively as the non-nebulized formulation (Fig. 5e). Overall, these data revealed a favourable aerodynamic behaviour of PI3K γ MP positioning the peptide as an ideal candidate for targeting the PI3K γ /PKA complex in the airways for therapeutic purposes. Nevertheless, challenges such as optimizing binding affinity, permeability, stability, and efficacy to deliver intact in the airways and to shield its interactions at the cell target needed to be addressed.

3.4. DRI-Pep #20 as a novel PI3K γ /PKA disruptor with high affinity for PKA.

In parallel to the characterization of PI3K γ MP we embarked on a screening for the identification of novel PI3K γ /PKA disruptors that led to the identification of DRI-Pep

#20. This is a non-naturally occurring peptide, obtained by synthesizing the all-D-retroinverso (DRI) form of a peptide linking the cell penetrating peptide Penetratin 1 (P1) to the non-natural 5 amino acids sequence RHQGK, by means of a glycine (G) linker (Fig. 6a). The incorporation of non-natural D-amino acids in a retro-reversed sequence, aimed to obtain molecules mirroring the structure of the parent L-peptides while exhibiting novel chemical properties, such as increased half-life and resistance to proteolytic degradation, which could potentially enhance their *in vivo* potency⁶⁴.

First, we determined the ability of DRI-Pep #20 to directly bind the PKA regulatory subunit RII α (PKA-RII α), the PKA isoform that we previously demonstrated being specifically bound by PI3K γ ⁶⁵. *In vitro* steady-state fluorescence spectroscopy experiments revealed that the peptide could associate recombinant PKA-RII α with high affinity, being the equilibrium dissociation constant (K_D) in the nanomolar range (76 nM; Fig. 6-c). Further fast kinetic studies showed that DRI-Pep #20 rapidly associates to PKA-RII α forming a relatively stable complex. The association rate constant (K_{on}) in the order of $10^{-6} \text{ M}^{-1}\text{s}^{-1}$ indicated an extremely fast assembly of the DRI-Pep #20/PKA-RII α complex, while the moderate dissociation rate (K_{off}) suggested a certain level of stability in the bound state (Fig. 6d and Table 3). In agreement with the high affinity of DRI-Pep #20 to PKA-RII α , the peptide inhibited the interaction between recombinant PI3K γ and PKA-RII α up to 74%, and with an IC_{50} of 0.16 μM (Fig. 6e-f). Next, we tested whether DRI-Pep #20 could disturb the anchoring of PKA by AKAPs other than PI3K γ . The ability of the peptide to raise cAMP levels in PI3K γ -deficient cells was used as a proxy of its capacity to interfere with other AKAP-based signalosomes³⁰. We found that DRI-Pep #20 failed to raise cAMP in cells that did not express its target PI3K γ , demonstrating that the peptide retained the selectivity for the PI3K γ -directed pool of PKA, despite the high binding affinity for PKA-RII α (Fig. 6g). Overall, these data identify DRI-Pep #20 as a potent and selective disruptor of the PI3K γ /PKA complex.

3.5. DRI-Pep #20 mimics the native interaction between PI3K γ and PKA-RII α .

Next, we sought to elucidate the determinants of the high-affinity interaction of DRI-Pep#20 with PKA-RII α . Predictions of the tridimensional structure of DRI-Pep #20 suggested the presence of an α -helix, flanked by two uncoiled regions (Fig. 7a). The helical propensity of the peptide was confirmed by circular dichroism analyses showing

a double-peak signal, with a maximum at 200 nm which is typical for α -helix structures, and a minimum in the 220–240 nm region which is characteristic for random-coil domains⁵⁸ (Fig. 7b). *In silico* simulations of the binding of DRI-Pep #20 to the typical binding surface for AKAPs (amino acids 1-45 of PKA-RII α)⁵⁹, revealed that 4 out of the 5 amino acids of the RHQGK sequence (R-1, H-2, Q-3 and K-5) could form hydrogen bonds with partners in the PKA-RII α subunit (Fig. 7c, Fig. 8a and Table 4).

Systematic amino acid substitutions within the RHQGK sequence confirmed the importance of positively charged and polar amino acids in position 3 and 4 for the interaction of DRI-Pep #20 with PKA-RII α . Indeed, peptide variants bearing hydrophobic residues in those positions had reduced ability to disrupt the PI3K γ /PKA interaction, and thus to elevate cAMP in human bronchial epithelial cells (16HBE14o-), as compared to the parent sequence (Fig. 9 and Table 4). These observations suggested that a short amino acid sequence enriched in hydrophilic residues could form the backbone for the anchoring of PKA by PI3K γ and prompted us to better characterize the native interaction between the N-terminal domain of PI3K γ , which encompasses the putative PKA-binding motif^{30,65}, and PKA-RII α . *In silico* simulations of the binding between 120-160 PI3K γ and 1-45 PKA-RII α identified a region enriched in hydrophilic amino acids, spanning from K-126 to R-130 (KATHR), that could maximally interact with PKA. K-126, H-129 and R-130 were consistently found at the core of the interaction in all of the possible binding poses between the two proteins (Fig. 10a and Fig. 11a) and were shown to form hydrogen bonds mainly with T-18 and the Q-25 of PKA-RII α (Fig. 10a and Fig. 11b).

Intriguingly, the KATHR sequence phenocopied the complete PKA-binding motif of PI3K γ in raising cAMP in 16HBE14o- cells (Fig. 12 and Table 5), indicating that the core of the interaction between PI3K γ and PKA-RII α could reside within this region. In agreement, structural predictions and molecular docking studies revealed that the KATHR peptide folded in an almost complete α -helical structure (Fig. 10b), allowing the formation of hydrogen bonds between K-126, H-129 and R-130 and partners within 1-45 PKA-RII α (Fig. 10c, Fig. 13 and Table 6).

Taken together, these results demonstrate that the non-natural peptide DRI-Pep #20 acts as a potent PI3K γ /PKA disruptor by mimicking the core of the native interaction of PI3K γ with PKA-RII α .

3.6. DRI-Pep #20 has favorable mucus permeability and protease resistance.

Next, we sought to determine to what extent DRI-Pep #20 could be used for targeting the native PI3K γ /PKA complex in the lungs to modulate cAMP for therapeutic purposes. First, we assessed the suitability for local delivery to the airways. Following intratracheal instillation (Fig. 14a), DRI-Pep #20 induced a dose-dependent increase in cAMP levels in the trachea and in the lungs of treated mice, with an EC₅₀ of 8.06 $\mu\text{g/Kg}$ and 11.78 $\mu\text{g/Kg}$, respectively (Fig. 14b-c). Of note, cardiac cAMP concentrations were unchanged (Fig. 14d), suggesting that the peptide locally increased airway cAMP without systemic effects at the tested dose.

Since the efficacy of inhaled therapies can be hampered by extracellular barriers imposed by diseased lungs, we next sought to determine to what extent DRI-Pep #20 could penetrate mucus layers and resist to protease degradation. DRI-Pep #20 penetrated the phospholipid membrane in the PAMPA system (Fig. 15a) with an apparent permeability (P_{app}) of $1.88 \times 10^{-6} \text{ cm s}^{-1}$ (Fig. 15b). Of note, the addition of pathological CF sputum on top of the phospholipid layer (Fig. 5a) did not significantly affect the P_{app} of the peptide ($P_{\text{app}} 2.55 \times 10^{-6} \text{ cm s}^{-1}$) (Fig. 15b). To verify whether the favorable mucus permeability of DRI-Pep #20 could be ascribed to molecular dimensions compatible with the mesh size of CF mucus⁶⁶, Transmission Electron Microscopy (TEM) and Dynamic Light Scattering (DLS) assays were performed. TEM images showed that DRI-Pep #20 formed irregular aggregates of 5-40 nm in size (Fig. 15c), in agreement with the particle diameter of 10-20 nm retrieved by DLS analysis (Fig. 15d).

Next, we tested the proteolytic resistance of DRI-Pep #20 in pulmonary cells in the presence of neutrophil elastase (HNE). The ability of the peptide to raise cAMP in 16HBE41o- cells was completely unaltered by the presence of 3 $\mu\text{g/ml}$ of HNE (Fig. 5e). Conversely, the cAMP elevating activity of the non-DRI isoform, Pep #20, was reduced by 26% by means of HNE (Fig. 15e). Notably, the activity of the DRI isoform was entirely preserved even in the presence of a 10-fold higher concentration of HNE (Fig. 15f), the amount detected in the lungs of patients with severe bronchiectasis⁶⁰, which was in line with the absence of any predicted cleavage sites by HNE (Fig. 16a). The observed resistance of DRI-Pep #20 to degradation was confirmed in the presence of a more complex biological matrix containing other proteases that could potentially cleave

the peptide (Fig. 16b), that is CF sputum, where the DRI-Pep #20 retained 72% of its biological activity (Fig. 15g).

Taken together, these data demonstrate the potential of DRI-Pep #20 to elevate lung cell cAMP even in the presence of the challenging extracellular environment imposed by diseased lungs, such as a thick layer of mucus enriched in proteases.

3.7. DRI-Pep #20 promotes cAMP-dependent activation of wild-type and F508del-CFTR in human bronchial epithelial cells.

Next, we aimed to assess the extent to which DRI-Pep #20 could effectively restore cAMP levels and consequently reactivate the function of CFTR, a cAMP-dependent chloride channel impaired in a range of respiratory disease, including but not limited to COPD and CF ⁶⁷. First, we assessed the ability of the peptide to stimulate the activity of the wild-type channel in 16HBE141o- cells expressing the halide-sensitive yellow fluorescent protein (HS-YFP) (Fig. 17b), which allows quantifying CFTR activity based on the fluorescence quenching rate elicited by an iodide influx ⁶⁸. DRI-Pep #20 induced a 60% reduction in YFP fluorescence, which was completely prevented by co-application of the CFTR inhibitor, CFTR_{inh-172} (Fig. 17b), demonstrating selective activation of CFTR channels. Dose-response experiments revealed an EC₅₀ of 20 μ M (Fig. 17c) and demonstrated that 25 μ M DRI-Pep #20 was as effective as 10 μ M forskolin, the adenylyl cyclase activator, in triggering CFTR gating in 16HBE141o- cells (Fig. 17d).

Further, we evaluated to what degree DRI-Pep #20 could reinstate the activity of F508del-CFTR in combination with the standard of care, including two CFTR correctors (Elexacaftor/Tezacaftor) and one CFTR potentiator (Ivacaftor), that partially rescue the trafficking and gating defects of the mutant channel, respectively ⁶⁹. In cystic fibrosis bronchial epithelial cells overexpressing the F508del-CFTR mutant and the HS-YFP, Elexacaftor/Tezacaftor/Ivacaftor (ETI) produced a YFP quenching of 50%, which was further decreased down to 25% when DRI-Pep #20 was added together with ETI (Fig. 17e). Hence, these data support the use of DRI-Pep #20 as a single agent or as an-add on to CFTR modulators, to therapeutically stimulate the activity of wild-type and F508del-CFTR, respectively.

4. Discussions

Our results confirm the use of PI3K γ /PKA peptide disruptors as valuable tools for manipulating β_2 -AR/cAMP signaling in the treatment of chronic obstructive airway diseases. The pharmacological actions of PI3K γ /PKA peptide disruptors stem from their ability to displace PKA from the PI3K γ complex, thereby preventing PKA-mediated stimulation of a pool of PDE4 involved in the control of β_2 -AR/cAMP responses in human bronchial smooth muscle, immune and epithelial cells³⁰. Although in the last decade numerous inhibitors of the kinase activity of PI3K γ have been developed, many of which are currently in clinical development for treating neoplastic diseases^{38,39}, PI3K γ MP represents the first compound ever developed to selectively interfere with the anchoring function of PI3K γ ³⁰. Inhalation of peptides is gaining increasing interest for the treatment of different pathological conditions, including but not limited to airway diseases^{70,71,42}. Inhaled peptides offer several advantages over that of classical small molecules, including high target selectivity and enhanced efficacy, as well as limited systemic side effects⁴¹. Nonetheless, clinical efficacy of inhaled therapies, especially of biologics, depends on the ability of the drug to deposit along the airways and to overcome barriers imposed by diseased lungs, especially the mucus⁴². The accumulation of an abnormally thick mucus layer, characterized by high concentrations of proteolytic enzymes, may importantly hamper the delivery of peptides in the airways of patients with obstructive airways diseases⁴².

The present study confirms and extends our previous data indicating that the PI3K γ MP can overcome, at least partially, these obstacles. We demonstrated previously that the PI3K γ MP can be topically delivered to the lungs, where it safely boosts airway cAMP up to 24 hours without altering cAMP homeostasis in other organs where cAMP elevation would not be desirable, such as in the heart³⁰. The present study now provides evidence that, despite being a large molecule (i.e., MW > 5000 g/mol), PI3K γ MP can penetrate the cell membrane and cross the mucus barrier that we reproduced in vitro by exploiting CF patient-derived sputum. Although the permeability of PI3K γ MP is slightly reduced by the presence of the mucus, its behavior is comparable to that of propranolol, a reference compound known for being highly permeable to cell membranes⁴⁴. The reduced permeability of the PI3K γ MP in the presence of a mucus layer could be ascribed to the reduced mesh size (60–300 nm) of the pathological CF mucus⁷² in comparison to

that of physiological mucus (497–503 nm)⁷³. TEM and DLS analyses indicate that the peptide can form two populations of aggregates: one ranging from 200–300 nm, which could freely diffuse through the meshes of CF mucus, and a larger one with aggregates up to 500 nm with reduced permeability⁷³.

On the other side, the ability of the peptide to form aggregates could pose a concern for the nebulization. Inhalable particles should meet specific requirements in order to be effectively deposited in the lower airways, including adequate airways distribution and an appropriate respirable size, namely 1–5 μm , which also depends on the performance of the device used for the delivery^{63,62}. Here we show that, despite the propensity to form aggregates, PI3K γ MP owns aerodynamic mean dimensions (MMAD: 2–2.99 μm) compatible with effective delivery to the lower airways, considered that a particle size of approximately 5 μm is generally capable of penetrating the lung during inhalation⁶³. However, different deposition patterns inside the Next Generation Impactor (NGI) have been observed following nebulization of the PI3K γ MP with the three different devices. Notably, the estimated dose emitted by the two mesh nebulizers resulted more than 40% higher than that of the jet nebulizer (TurboBoy). Moreover, the respirable fraction (RF), representing the total amount of PI3K γ MP recovered from NGI and thus the amount of peptide that potentially is delivered to the lungs, exceeded 90% with the two mesh nebulizers (AeronebGo and eFlow rapid). This high respirable fraction suggests that mesh nebulizers should be favoured over jet nebulizers for therapeutic inhalation of PI3K γ MP. While these data revealed a favourable aerodynamic behaviour of PI3K γ MP positioning the peptide as a good candidate for targeting the PI3K γ /PKA complex in the airways for therapeutic purposes, in parallel we decide to embark on a screening for the identification of novel PI3K γ /PKA disruptors that could be similarly used for the inhalation treatment of airway diseases. This approach led to the identification of a non-natural peptide, named DRI-Pep #20, that functions as a selective and potent disruptor of the PI3K γ /PKA-RII α complex. Our structural predictions and molecular docking studies indicate that DRI-Pep #20 operates similarly to PI3K γ MP and other AKAP disruptor peptides by mimicking the typical α -helical structure through which AKAPs bind PKA⁷⁴. In addition, our results support previous research showing that, within this α -helix, the presence of polar and positively charged amino acids is crucial for the binding between the scaffold and the kinase⁷⁴. In contrast to other AKAP disruptors, DRI-Pep #20 uniquely interferes with the

binding between PKA and PI3K γ , without affecting PKA pools anchored by other AKAPs. This specificity is attributed to our earlier observation that the PKA-anchoring sequence of PI3K γ diverges from that of classical AKAPs^{30,65}. While with PI3K γ MP we previously pinpointed amino acids 126-150 as the PKA-anchoring sequence of PI3K γ , the critical residues for the interaction remained elusive, partly due to the lack of the crystallographic structure of the PI3K γ N-terminal domain. Interestingly, our *in silico* characterization of the high-affinity interaction of DRI-Pep #20 with PKA-RII α sheds light on the native association between PI3K γ and PKA. Our computational modeling demonstrates that the KATHR sequence, encompassing amino acids 126-130 of the N-terminal of PI3K γ , plays a central role in guiding the interaction with PKA. Like DRI-Pep #20, the KATHR peptide can adopt an α -helical conformation, establishing hydrogen bonds with partner amino acids within PKA-RII α , mainly through K-126, H-129 and R-130. Despite structural similarities, DRI-Pep #20 exhibits a significantly higher affinity for PKA compared to the native PKA-docking domain of PI3K γ and the PI3K γ MP, with a K_D value that is 100-fold lower than that obtained with the 126-150 region⁶⁵. Further, fast kinetic studies have demonstrated that, with an association rate constant (K_{on}) in the order of $10^{-6} \text{ M}^{-1} \text{ s}^{-1}$, both PI3K γ MP and DRI-Pep #20 associate extremely fast to PKA-RII α forming a relatively stable complex. In contrast, the DRI-Pep #20 exhibit a higher level of stability in the bound state with PKA-RII α , with a K_{off} value that is 3.6-fold lower than that obtained with PI3K γ MP. This results in a 25% increase in potency of DRI-Pep #20 to inhibit the interaction between recombinant PI3K γ and PKA-RII α compared to PI3K γ MP.

This discrepancy raises questions about why nature selected a PI3K γ sequence with low affinity for PKA. It is plausible that, in physiological conditions, the binding between the two proteins needs to be sufficiently weak to allow PI3K γ to easily leave the complex, thereby interrupting PKA-mediated activation of PDEs, when necessary. This could serve as a protective mechanism against an excessive reduction of cellular cAMP below a critical level.

While the high binding affinity of DRI-Pep #20 to PKA-RII α can be attributed to the numerous hydrogen bonds that this non-natural sequence can form with the kinase, its high proteolytic stability is a direct consequence of the presence of D-amino acids, which are not recognized by proteases⁷⁵. The incorporation of non-natural D-amino acids in a

retro-reversed sequence, as in DRI-Pep #20, aims to obtain molecules with the same structure as the parent L-peptides, but with new chemical properties, such as increased half-life and resistance to proteolytic degradation, which potentially improve their *in vivo* potency⁶⁴. These chemical features, and above all the high stability and target affinity, position DRI-Pep #20 as an ideal candidate for therapeutic cAMP modulation *in vivo*. Obstructive respiratory diseases, where the PI3K γ -PKA complex serves as a central signaling hub to multiple airway cell functions, like smooth muscle relaxation, epithelial ion transport and neutrophil infiltration³⁰, could significantly benefit from a treatment with DRI-Pep #20. We provide evidence that DRI-Pep #20 preserves its biological activity in the presence of human neutrophil elastase and after local delivery in the airways in mice. These observations support the potential use of this peptide for achieving therapeutically relevant cAMP elevation in highly inflamed lungs. This is of particular relevance in a range of airway diseases, including COPD, certain forms of asthma, non-CF bronchiectasis (NCFB), and even in patients with CF who may still experience airway inflammation despite highly effective modulator therapies (HEMT) targeting the basic genetic defect of the disease^{76,77}.

In addition to proteases associated with inflammation, another challenge posed by diseased lungs is the thick mucus layer covering respiratory epithelia⁴². Our assays exploiting patient-derived sputum as a proxy of CF mucus revealed that DRI-Pep #20 is not significantly affected by the barrier activity of mucus. Moreover, in spite of being a relatively large molecule (i.e., MW > 2000 g/mol), DRI-Pep #20 is well below the mesh size of the pathological mucus. TEM and DLS analyses indicate that the peptide can form aggregates of 20 nm in size, which could freely diffuse through the 100-1000 nm meshes of the network of bundled fibers that are typically formed by biopolymers in the CF mucus and that are filled with a low viscosity fluid⁷⁸.

These observations imply that, in diseased lungs, relevant doses of DRI-Pep #20 could reach the underlying epithelial cells wherein targeting the PI3K γ /PKA complex is anticipated to boost CFTR activity³⁰. Our data indicates that in CF bronchial epithelial cells DRI-Pep #20 enhances the effects of the standard combination of CFTR modulators, Elexacaftor/Tezacaftor/Ivacaftor, in rescuing the activity of the most common CFTR mutant, F508del. These findings carry significant clinical implications, especially in light of recent studies demonstrating that CFTR potentiators and correctors only partially

restore the function of mutant channels, achieving up to 60% the wild-type CFTR levels⁷⁹⁻⁸¹. Consequently, CF patients treated with HEMT may still experience residual mucus dysfunction, airway infection and inflammation^{76,77,82} and could significantly benefit from the ability of DRI-Pep #20 to maximize the clinical efficacy of the standard-of-care. In addition, our observation that the peptide itself activates the wild-type form of the CFTR channel supports the prospect of extending the use of DRI-Pep #20 to treat a range of non-genetic conditions characterized by acquired CFTR dysfunction, including COPD, non-atopic asthma, and NCFB⁶⁷.

In summary, our study supports the use of natural and non-natural peptides for manipulating the PI3K γ /PKA complex in the lungs for therapeutic purposes. We demonstrated that these compounds can act locally, providing significant added value over other cAMP elevating agents, i.e. β_2 -adrenergic agonists or classical small molecule PDE4 inhibitors, like roflumilast, that easily diffuse outside the lungs and trigger undesired brain and cardiac effects¹⁸. Additionally, small molecule PDE4 inhibitors lead to indiscriminate inhibition of all the different PDE4 subtypes (PDE4A, B, C and D), potentially determining further side effects. Intriguingly, PI3K γ /PKA peptide disruptors offer the opportunity of blocking selective PDE4 subtypes with a prominent role in the lung, like PDE4B and PDE4D⁸³, with an exquisite isoform and compartment selectivity. On the other hand, differently from β_2 -AR agonists, PI3K γ /PKA disruptors amplify β_2 -AR/cAMP responses through a peculiar mechanism by impinging on cAMP degradation rather than on β_2 -AR activation, avoiding receptor desensitization that, in the long-term, is the major cause of reduced efficacy. Moreover, thanks to the favorable resistance to proteases and ability to penetrate airway mucus, the peptides hereby described hold promise for achieving therapeutic cAMP elevation in obstructive respiratory disorders where mucus accumulation and inflammatory remodeling still result in a highly unmet medical need. While the PI3K γ MP has already completed certified toxicological preclinical studies in rodents and non-rodents, future studies are expected to prove the feasibility and the safety of an inhaled therapy based on a non-natural PI3K γ /PKA disruptor, like DRI-Pep #20.

5. Figures

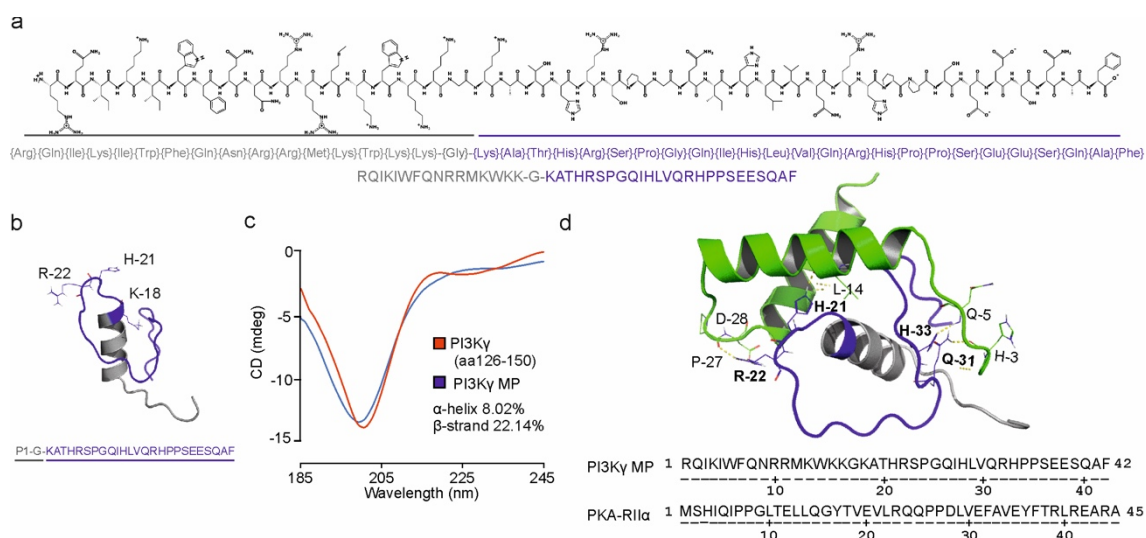


Figure 1. Structural prediction of the binding between PI3K γ MP and PKA-RII α .

a) Chemical structure of PI3K γ MP. The amino acid sequence of PI3K γ MP comprises the cell penetrating peptide Penetratin 1 (P1), a glycine (G) linker and the PKA-binding motif of PI3K γ (residues 126-150: KATHRSPGQIHLVQRHPPSEESQAF). **b)** PI3K γ MP structure prediction by PEP-FOLD3.5. P1-G and residues 126-150 of PI3K γ are shown as cartoons in grey and blue, respectively. R-22, H-21 and K-18 residues are indicated and shown as sticks. **c)** Circular dichroism spectra of PI3K γ MP and PKA-binding motif of PI3K γ showing a peak at 190-220 nm in blue and red, respectively. The percentage of α -helical and β -sheet secondary structures calculated by the K2D3 software are indicated. **d)** Molecular docking simulation of the interaction between PI3K γ MP and PKA by HADDOCK 2.4. The docked pose of PI3K γ MP in complex with residues 1-45 of PKA-RII α (cartoon in green) is shown. The key residues involved in the binding are indicated and shown as sticks, with PI3K γ MP residues in bold. Hydrogen bonds between PI3K γ MP and PKA-RII α are indicated by yellow dashed lines. In **b** and **d**, the structural models were developed using PyMOL.

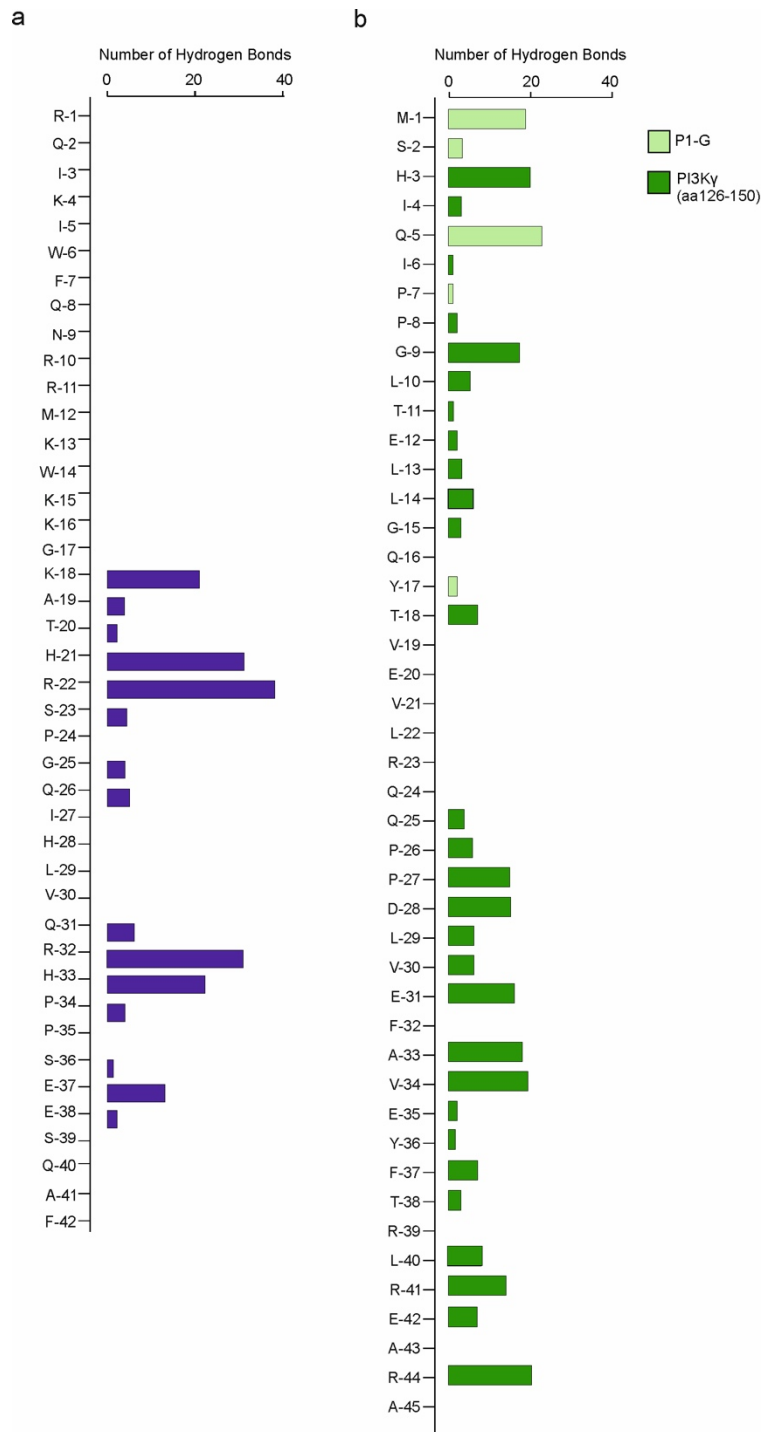


Figure 2. PI3K γ MP/PKA-RII α (1-45) binding analysis by Optimal Hydrogen Bonding Network.

a) Number of hydrogen bonds between PI3K γ MP with partners in the PKA-RII α subunit (1-45 PKA-RII α). **b)** Number of hydrogen bonds between residues 1-45 of PKA-RII α with partners within PI3K γ MP. Hydrogen bonds involving amino acids within the P1-G or the residues 126-150 of the PKA-binding motif of PI3K γ are shown in light green and dark green, respectively.

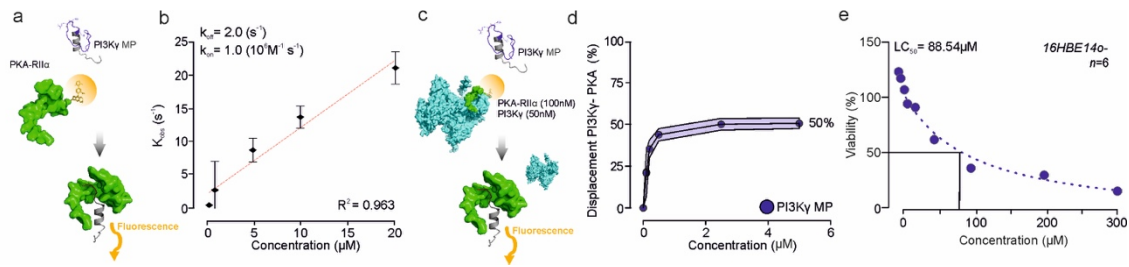


Figure 3. PI3K γ MP displaces the PI3K γ /PKA complex.

a) Schematic representation of the fluorescence spectroscopy assays for the characterization of the interaction between PI3K γ MP and PKA-F5M. **b)** For kinetic analysis, fluorescence spectra of PKA-F5M in the presence of increasing concentrations of PI3K γ MP (0 to 20 μ M) were analyzed and fitted to a single exponential function to obtain the observed rate constant (k_{obs}). The binding of PI3K γ MP to bio-labeled PKA was investigated under *pseudo*-first-order conditions, and the kinetic constants, k_{on} and k_{off} , were determined. **c)** Schematic representation of the displacement assay between PI3K γ MP and the PI3K γ /PKA-F5M complex. **d)** Percentage displacement of the PI3K γ /PKA-R11 α complex by PI3K γ MP, calculated from steady-state emission spectra of the PI3K γ /PKA-F5M complex in the presence of increasing concentrations of PI3K γ MP (0 to 5 μ M). The displacement efficiency was expressed as percentage of the binding between PI3K γ and PKA-F5M relative to that in the absence of PI3K γ MP. **e)** For cytotoxicity analysis, cell viability was evaluated in 16HBE14o- cells treated chronically with increasing concentration of PI3K γ MP (0 to 300 μ M). $n \geq 6$ technical replicates from $N=3$ independent experiments. Nonlinear regression analysis was used to determine the LD₅₀. LD₅₀ was calculated with respect to untreated control cells, whose viability was set to 100%. Throughout, data are means \pm SEM.

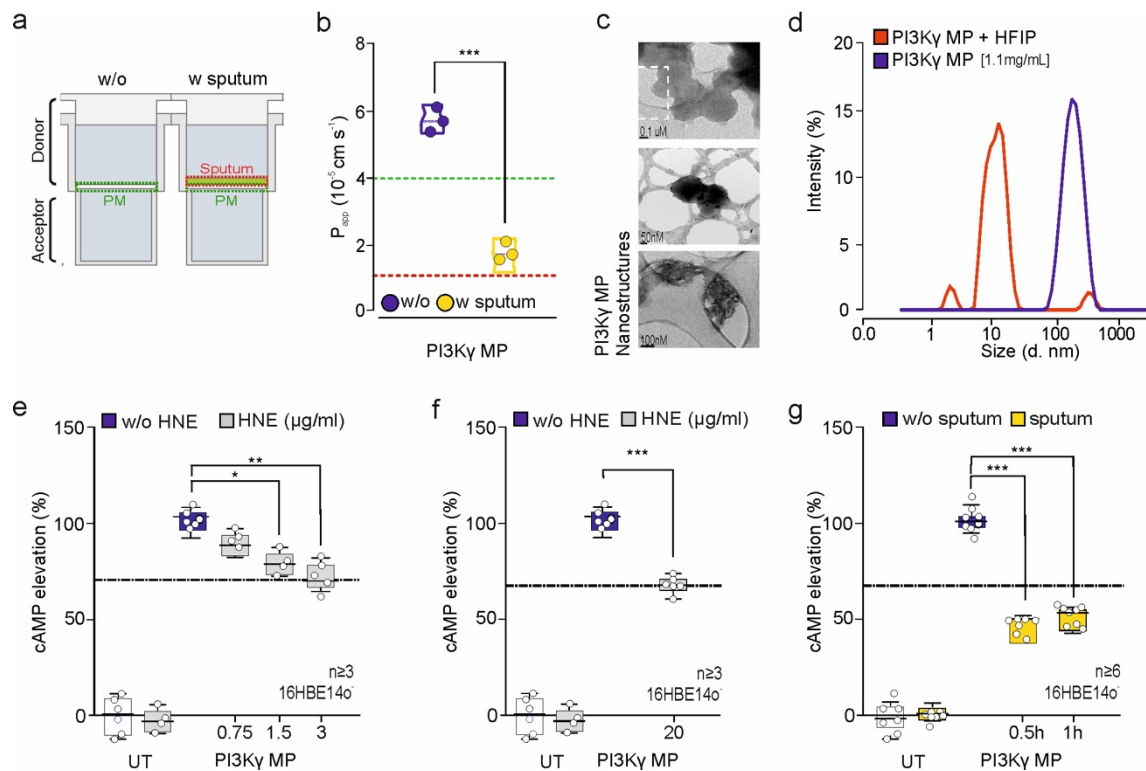


Figure 4. PI3K γ MP can penetrate pathological mucus and resist protease degradation.

a) Schematic representation of the Parallel Artificial Membrane Permeability Assay (PAMPA) with and without deposition of cystic fibrosis (CF) sputum on top of the artificial lipid membrane (PM). **b)** Apparent permeability (P_{app}) measurements of PI3K γ MP (2 mg/mL), in the absence (blue box) and in the presence (yellow box) of CF sputum. The green dashed line indicates the threshold P_{app} for high-medium permeable compounds ($4 \times 10^{-6} \text{ cm s}^{-1}$), while the red dashed line defines the limit for medium-low permeable molecules ($1 \times 10^{-6} \text{ cm s}^{-1}$). **c)** Representative Transmission Electron Microscopy (TEM) images of PI3K γ MP (0.1 mg/mL in water). **d)** Size distribution profile of PI3K γ MP (1.1 mg/mL in 2 mM PBS) in blue and with the addition of hexafluoroisopropanol (HFIP) in red obtained by dynamic light scattering (DLS) analysis. **e-f)** cAMP concentrations in 16HBE14o- cells treated with the PI3K γ MP (25 μM for 30 min) in the absence (blue bars) and in the presence (grey bars) of either 3 $\mu\text{g/ml}$ (**e**) or 20 $\mu\text{g/ml}$ (**f**) human neutrophil elastase (HNE). The amount of cAMP was expressed as percentage of cAMP accumulation elicited by PI3K γ MP without HNE. Dashed lines indicate the amount of cAMP (%) induced by PI3K γ MP with HNE as a reference. $n \geq 3$ technical replicates from $N > 3$ independent experiments. * $P < 0.05$, ** $P < 0.01$ and *** $P < 0.001$ by one-way ANOVA, followed by Bonferroni's post hoc test. **g)** cAMP elevation in 16HBE14o- cells covered with a layer of CF sputum and then treated with 25 μM PI3K γ MP for 30 min and 1 hour. The amount of cAMP was expressed as percentage of cAMP accumulation elicited by PI3K γ MP in the absence of sputum at 30 min. *** $P < 0.001$ versus PI3K γ MP without sputum by two-way ANOVA test, followed by Bonferroni's post-hoc analysis. $n \geq 6$ technical replicates from $N = 3$ independent experiments. Throughout, data are means \pm SEM.

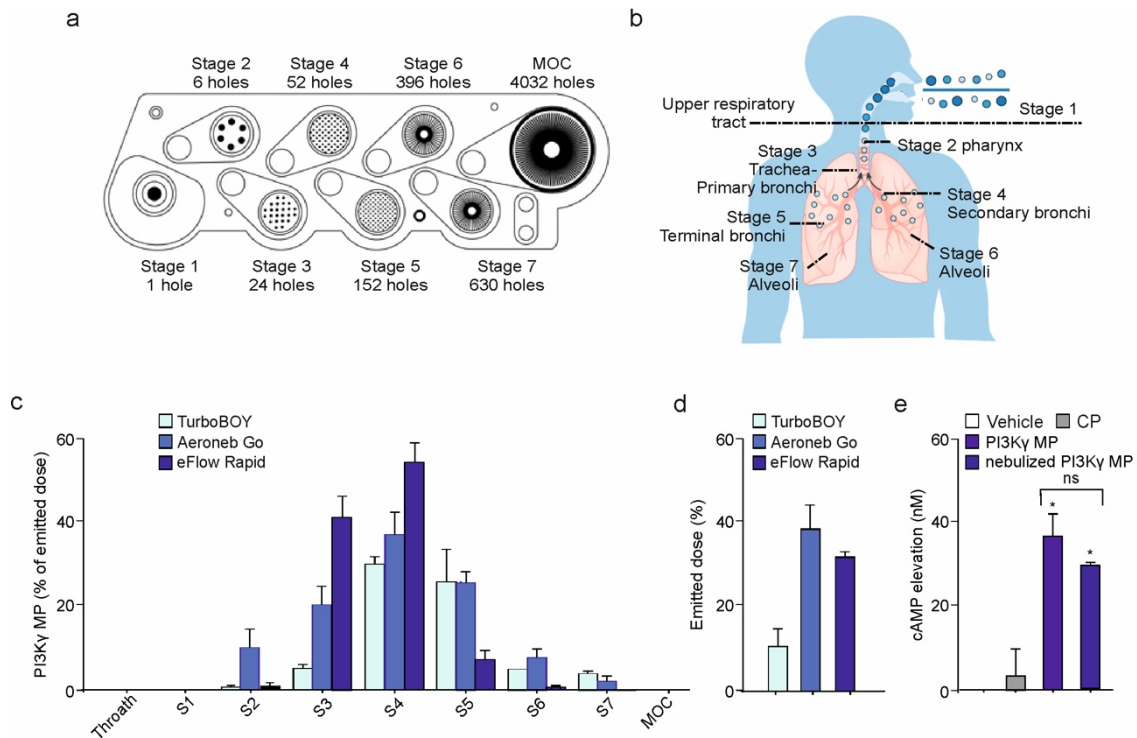


Figure 5. Aerodynamic behaviour of PI3K γ MP

a) Schematic representation of the Next Generation Impactor (NGI) apparatus equipped with seven stages cups (S1-S7) and a micro-orifice collector (MOC). **b)** Dimensional correlation of the different NGI stages with the different regions of the airway respiratory tract. **c-d)** In vitro aerosol performance of PI3K γ MP after nebulization with three devices (one jet nebulizer –TurboBoy- and two mesh nebulizers –AeronebGo and eFlow rapid). In **c)** cumulative mass of PI3K γ MP recovered in the different stages expressed as a function of the cut-off diameter of the NGI and of the emitted dose. In **d)** the emitted dose of PI3K γ MP representing the total mass of peptide emitted from the NGI. This was measured on the difference between the total amount initially placed in the specified nebulizer and the amount that was deposited in the NGI. **e)** cAMP elevation in 16HBE14o- cells treated with the peptide recovered from Stage 4 after nebulization with eFlow rapid. ns: non-significant PI3K γ MP vs nebulized PI3K γ MP by Student's t test. *P<0.05 versus vehicle by one-way ANOVA test, followed by Bonferroni's post-hoc analysis. N=3 independent experiments. Throughout, data are means \pm SEM.

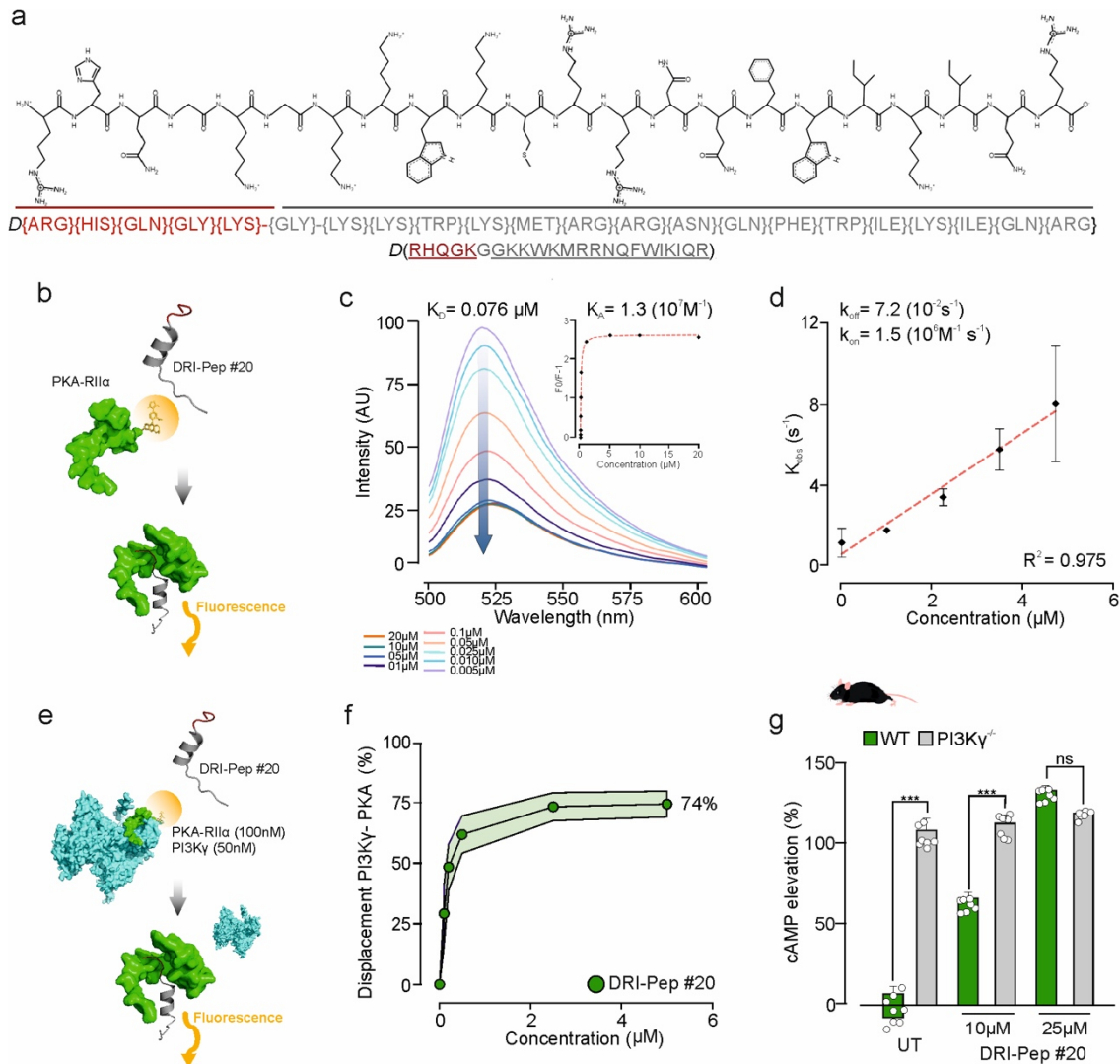


Figure 6. DRI-Pep #20 as a novel PI3K γ /PKA disruptor with high binding affinity for PKA.

a) Chemical structure of DRI-Pep #20. The amino acid sequence of DRI-Pep #20 comprises the cell penetrating peptide Penetratin 1 (P1), a glycine (G) linker and the non-natural sequence RHQGK, wherein each amino acid is a D-amino acid. **b)** Schematic representation of the fluorescence spectroscopy assays for the characterization of the interaction between DRI-Pep #20 and the recombinant fluorescein 5-maleimide-labeled PKA-RII α (PKA-F5M). **c)** Steady-state emission spectra of PKA-F5M in the presence of increasing concentrations of DRI-Pep #20 (0 to 20 μ M). K_D : dissociation constant. AU, arbitrary units. Inset, non-linear fitting of the fluorescence intensity maxima obtained at various concentrations of DRI-Pep #20 for the monitoring of bio-labeled PKA. K_A : association constant. **d)** For kinetic analysis, fluorescence spectra of PKA-F5M in the presence of increasing concentrations of DRI-Pep #20 (0 to 5 μ M) were analyzed and fitted to a single exponential function to obtain the observed rate constant (k_{obs}). The binding of DRI-Pep #20 to bio-labeled PKA was investigated under *pseudo*-first-order conditions, and the kinetic constants, k_{on} and k_{off} , were determined. **e)** Schematic representation of the displacement assay between DRI-Pep #20 and the PI3K γ /PKA-F5M complex. **f)** Percentage displacement of the PI3K γ /PKA-RII α complex by DRI-Pep #20,

calculated from steady-state emission spectra of the PI3K γ /PKA-F5M complex in the presence of increasing concentrations of DRI-Pep #20 (0 to 5 μ M). The displacement efficiency was expressed as percentage of the binding between PI3K γ and PKA-F5M relative to that in the absence of DRI-Pep #20. **g**) cAMP concentrations in peritoneal macrophages from wild-type (WT, in green) and PI3K $\gamma^{-/-}$ mice (in grey) treated with 10-25 μ M DRI-Pep #20 for 30 min. The amount of cAMP was expressed as percentage of cAMP accumulation observed in untreated PI3K $\gamma^{-/-}$ cells. $n \geq 6$ technical replicates from $N > 3$ independent experiments. *** $P < 0.001$ WT versus PI3K $\gamma^{-/-}$ by one-way ANOVA, followed by Bonferroni's post hoc test. Data are means \pm SEM.

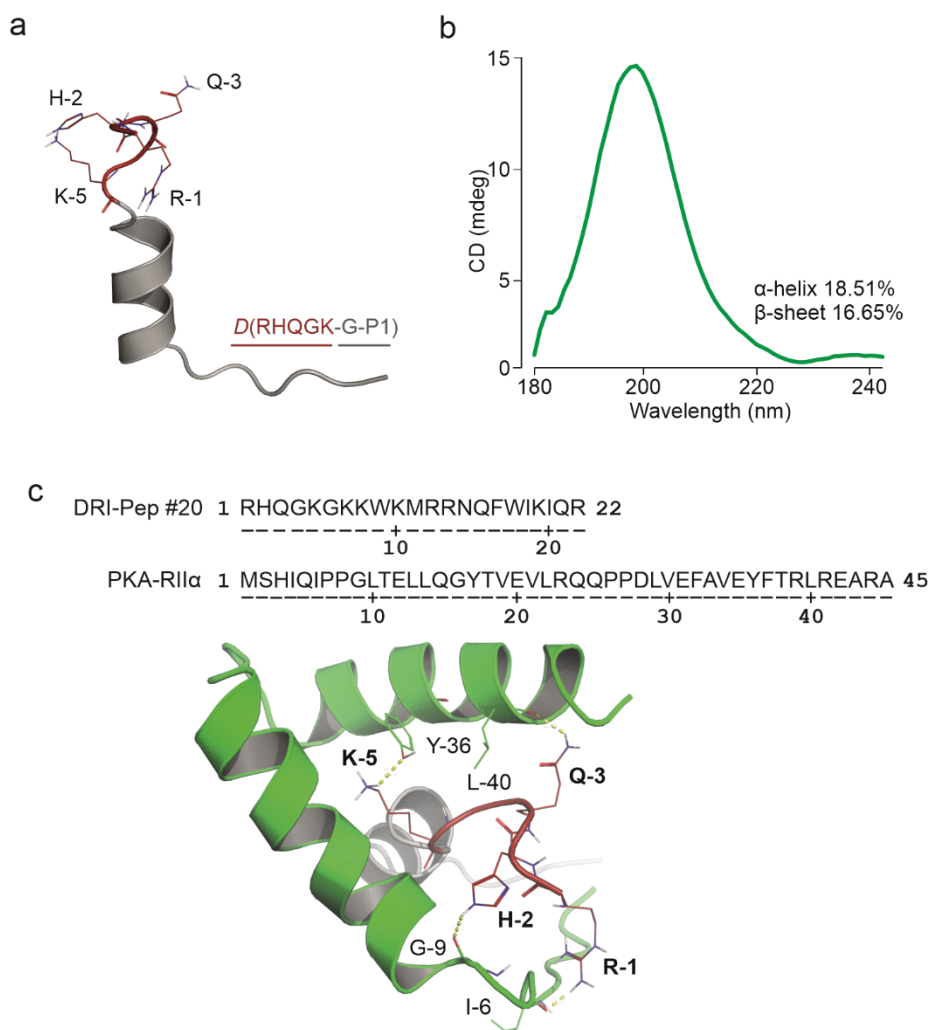


Figure 7. Structural prediction of the binding between DRI-Pep #20 and PKA-RII α .

a) DRI-Pep #20 structure prediction by PEP-FOLD3.5. P1-G and RHQGK domains are shown as cartoons in grey and red, respectively. R-1, H-2, Q-3 and K-5 residues are indicated and shown as sticks. **b)** Circular dichroism spectra of DRI-Pep #20 showing a peak at 190-240 nm. The percentage of α -helical and β -sheet secondary structures calculated by the K2D3 software are indicated. **c)** Molecular docking simulation of the interaction between DRI-Pep #20 and PKA by HADDOCK 2.4. The docked pose of DRI-Pep #20 in complex with residues 1-45 of PKA-RII α (cartoon in green) is shown. The key residues involved in the binding are indicated and shown as sticks, with DRI-Pep #20 residues in bold. Hydrogen bonds between DRI-Pep #20 and PKA-RII α are indicated by yellow dashed lines. In **a** and **c**, the structural models were developed using PyMOL.

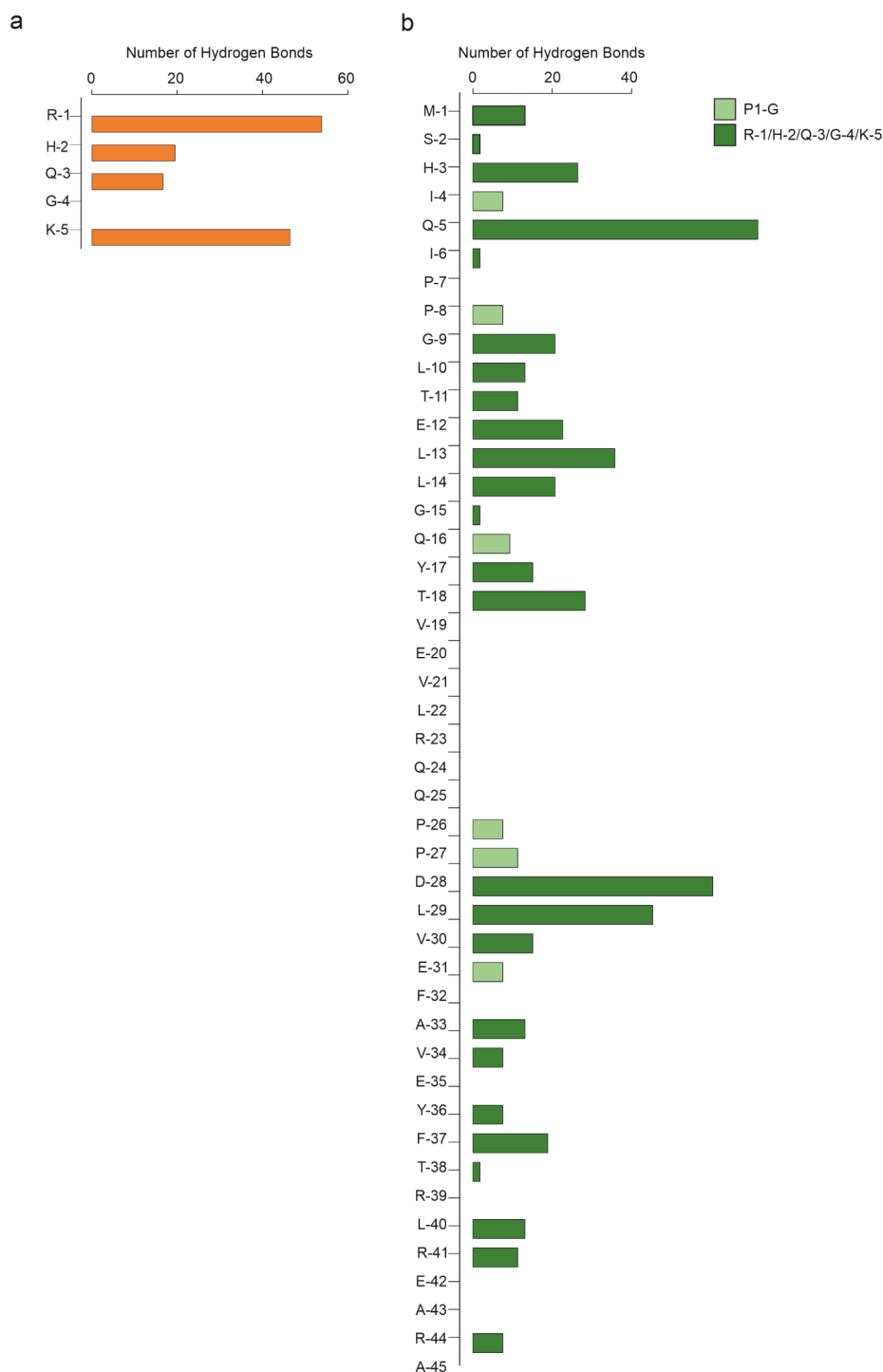


Figure 8. DRI-Pep #20/PKA-RII α (1-45) binding analysis by Optimal Hydrogen Bonding Network.

a) Number of hydrogen bonds between R-1, H-2, Q-3 and K-5 residues of DRI-Pep #20 with partners in the PKA-RII α subunit (1-45 PKA-RII α). **b)** Number of hydrogen bonds between residues 1-45 of PKA-RII α with partners within DRI-Pep #20. Hydrogen bonds involving amino acids within the P1-G or the RHQGK domains of DRI-Pep #20 are shown in light green and dark green, respectively.

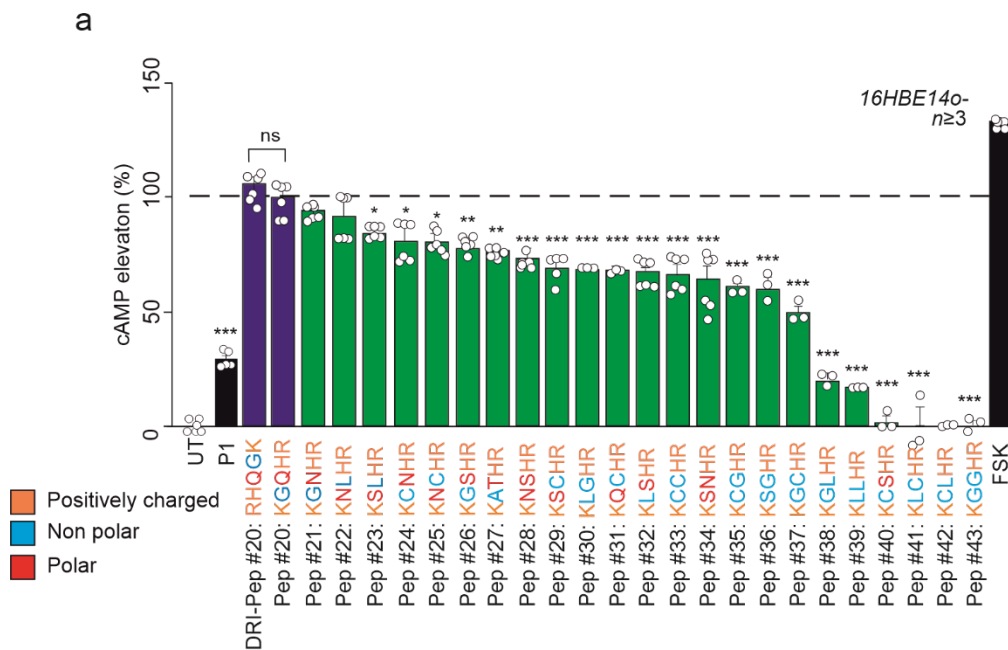


Figure 9. Biological activity (cAMP elevation) of DRI-Pep #20 variants with 2 amino acid substitutions.

a) cAMP concentration in 16HBE14o- cells treated for 30 min with the indicated peptide variants carrying conservative substitutions of Q-3 and G-4 within the DRI-Pep #20 sequence (25 μ M). For screening purposes, non-DRI forms of the peptides were used. Positively charged, non-polar and polar amino acids are shown in orange, blue and red, respectively. The cAMP elevation triggered by each peptide was expressed as percentage of the cAMP accumulation elicited by Pep #20, which is shown as a dashed line. The adenylyl cyclase activator, forskolin (FSK), was used as a positive control (100 nM for 5 min), while P1 was used as a negative control (25 μ M for 30 min). UT: untreated cells. $n \geq 3$ technical replicates from $N=3$ independent experiments. * $P < 0.05$, ** $P < 0.01$, and *** $P < 0.001$ versus Pep #20 by one-way ANOVA, followed by Bonferroni's post hoc test. Data are means \pm SEM.

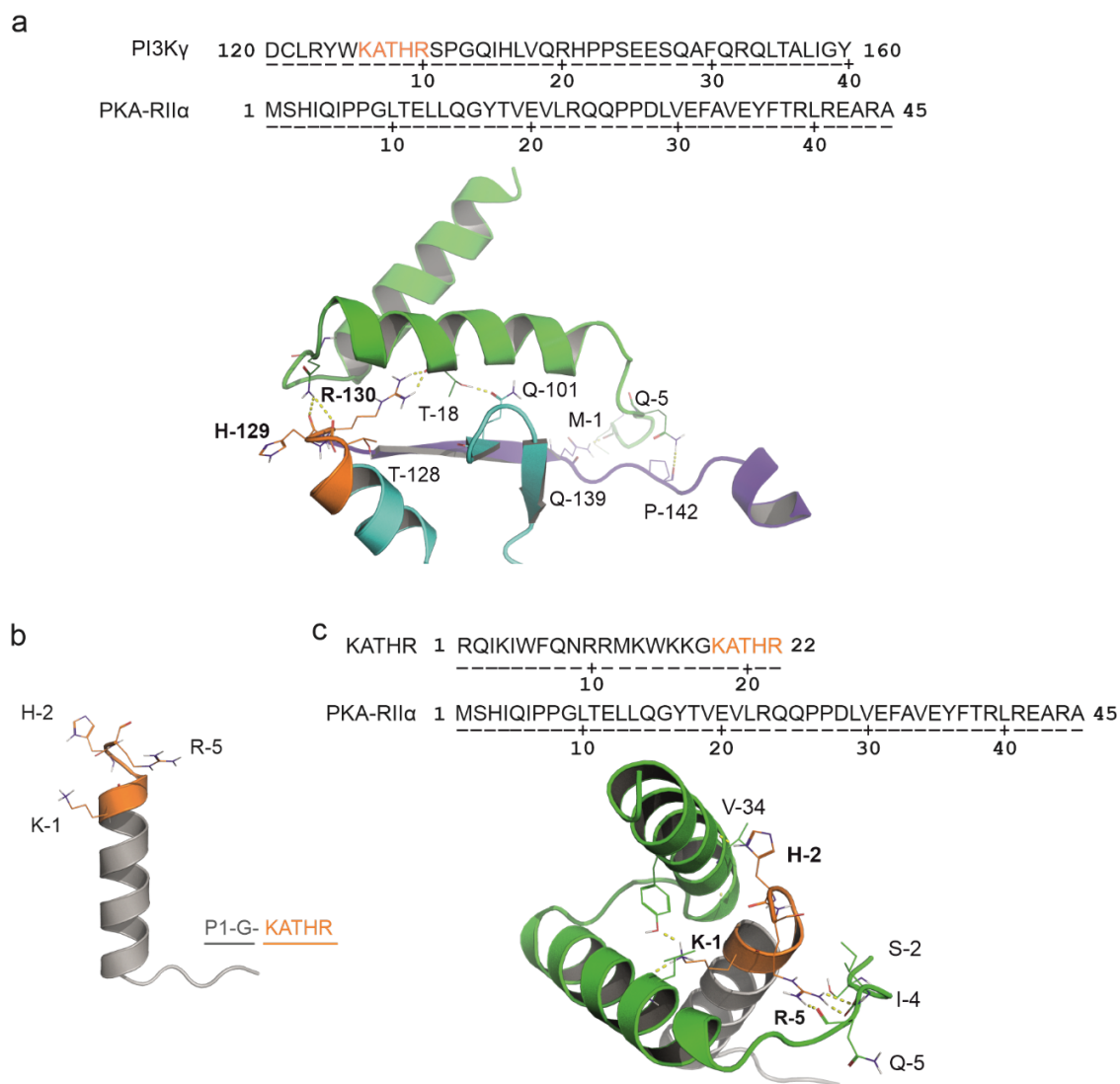


Figure 10. Structural prediction of the native binding between the N-terminal domain of PI3K γ and PKA-RII α .

a) Molecular docking simulation of the interaction between PI3K γ and PKA-RII α by HADDOCK 2.4. The docked pose of residues 120-160 of PI3K γ (cyan cartoon) in complex with residues 1-45 of PKA-RII α (green cartoon) is shown. The amino acids critical for the binding between the two proteins are shown and indicated as sticks, with the residues of PI3K γ in bold. The region of PI3K γ at the core of the interaction (KATHR) is shown in orange. Hydrogen bonds between PI3K γ and PKA-RII α are indicated by yellow dashed lines. **b)** Structural prediction of the KATHR sequence by PEP-FOLD3.5. KATHR and P1-G domains are shown as cartoons in orange and grey, respectively. K-1, H-4 and R-5 residues of PI3K γ are indicated and shown as sticks. **c)** Molecular docking simulation of the interaction between KATHR and PKA by HADDOCK 2.4. The docked pose of KATHR in complex with residues 1-45 of PKA RII α (cartoon in green) is shown. Yellow dashed lines indicate hydrogen bonds between KATHR and 1-45 PKA-RII α . The amino acids critical for the binding are indicated and shown as sticks, with KATHR residues in bold. Throughout, the structural models were developed using PyMOL.

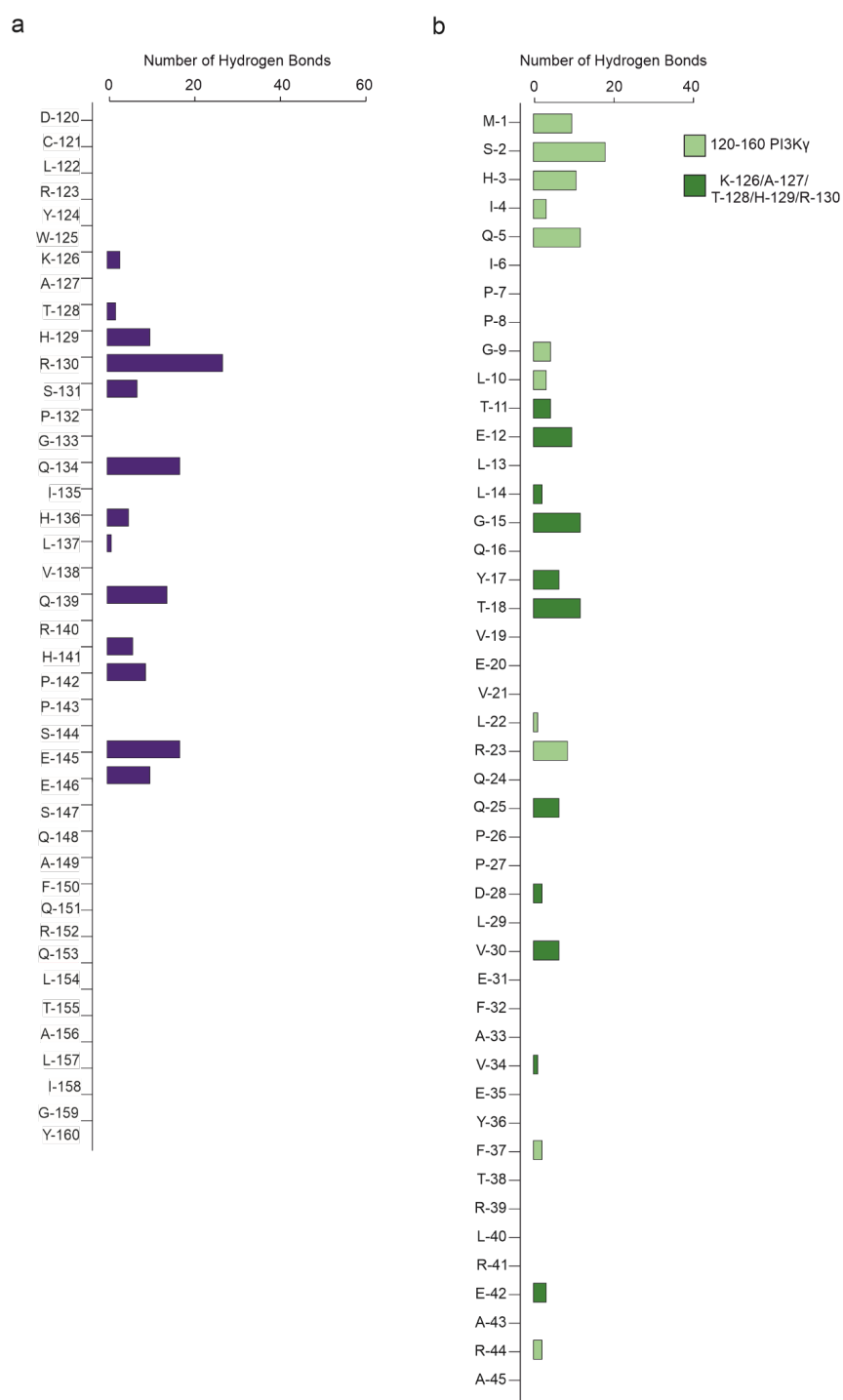


Figure 11. Analysis of the native binding between the N-terminal region of PI3K γ and PKA-RII α by Optimal Hydrogen Bonding Network.

a) Number of hydrogen bonds formed by residues encompassing the putative PKA-binding motif of PI3K γ (120-160 PI3K γ) with partners in the PKA-RII α subunit (1-45 PKA-RII α). **b)** Number of hydrogen bonds between residues 1-45 of PKA-RII α with partners within the 120-160 region of PI3K γ . Hydrogen bonds involving amino acids within the KATHR sequence or the remainder of the 120-160 domain of PI3K γ are shown in dark green and light green, respectively.

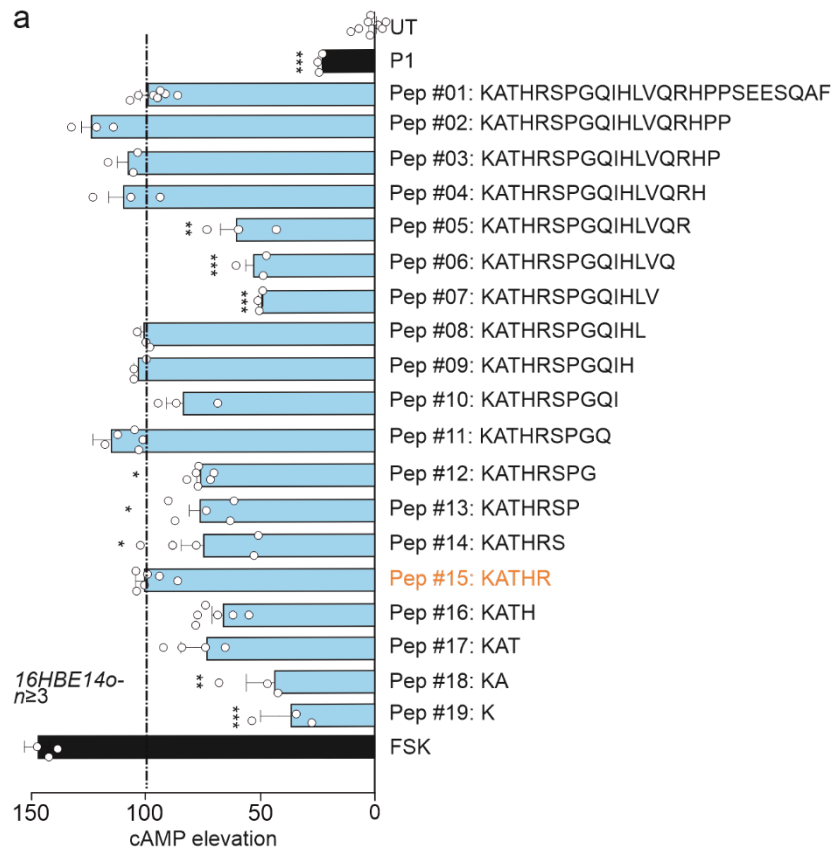


Figure 12. Biological activity (cAMP elevation) of N-terminal PI3K γ peptides progressively truncated at the C-terminus.

a) cAMP concentration in 16HBE14o- cells treated for 30 min with C-terminal truncations of the predicted PKA-binding site of PI3K γ (Pep# 01). Peptides were made permeable to cell membranes by conjugation with Penetratin 1 (P1) through a G linker (not shown) and used at a concentration of 25 μ M. The adenylyl cyclase activator, forskolin (FSK), was used as a positive control (100 nM for 5 min), while P1 was used as a negative control (25 μ M for 30 min). The cAMP elevation induced by each peptide was expressed as percentage of the cAMP accumulation elicited by the predicted full-length PKA-binding sequence of PI3K γ (Pep #01), which is shown as a dashed line. UT: untreated cells. n \geq 3 technical replicates from N=3 independent experiments. *P<0.05, **P<0.01, and ***P<0.001 versus Pep #01 by one-way ANOVA, followed by Bonferroni's post hoc test. Data are means \pm SEM.

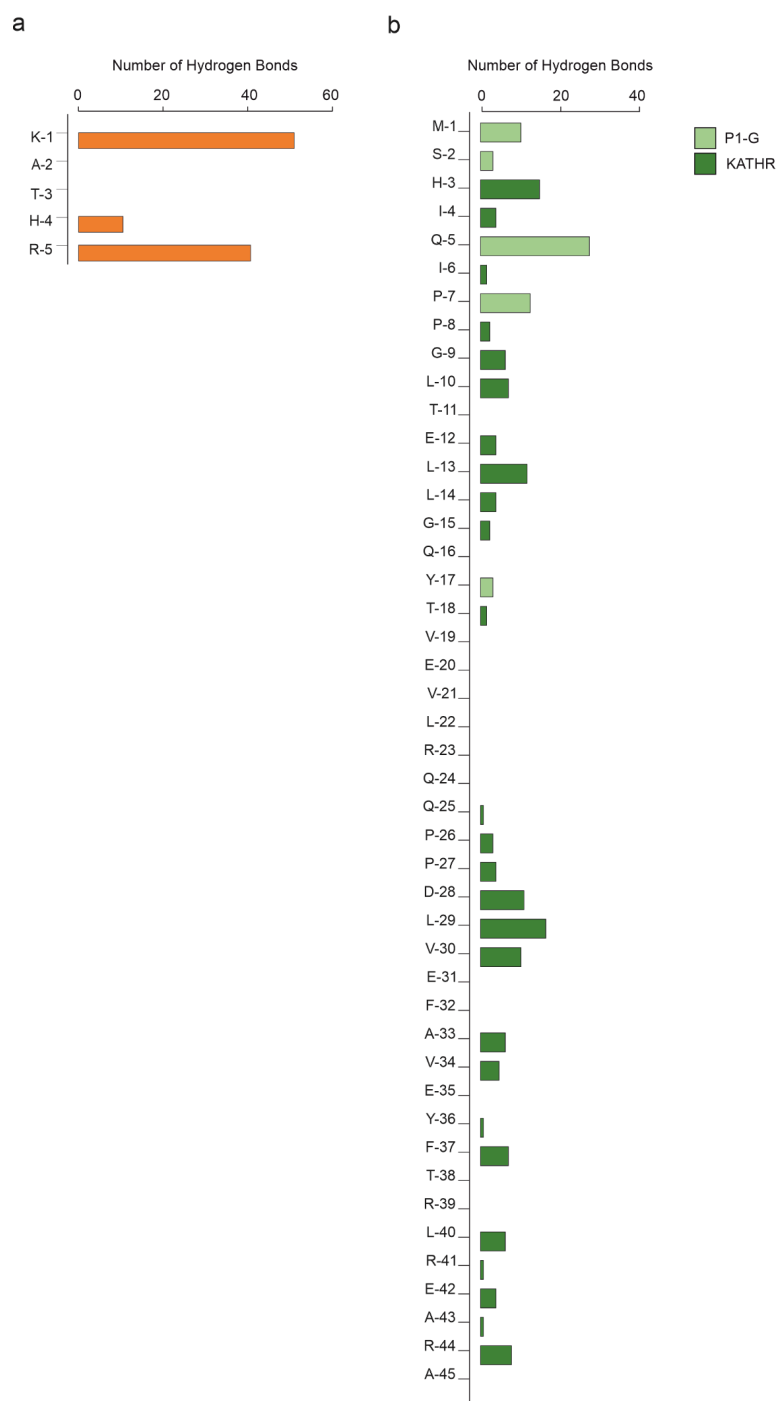


Figure 13. Analysis of the binding between the KATHR peptide and PKA-RII α by Optimal Hydrogen Bonding Network.

a) Number of hydrogen bonds between the KATHR sequence of the N-terminal domain of PI3K γ with partners within 1-45 of PKA-RII α . **b)** Number of hydrogen bonds between residues 1-45 of PKA-RII α with partners within the KATHR sequence. A cell permeable version of the KATHR peptide, linked to Penetratin 1 through a G linker at the N-terminus, was used for the docking. In **b)**, hydrogen bonds involving amino acids within the KATHR sequence, or the P1-G domain of the peptide are shown in green dark and light green, respectively.

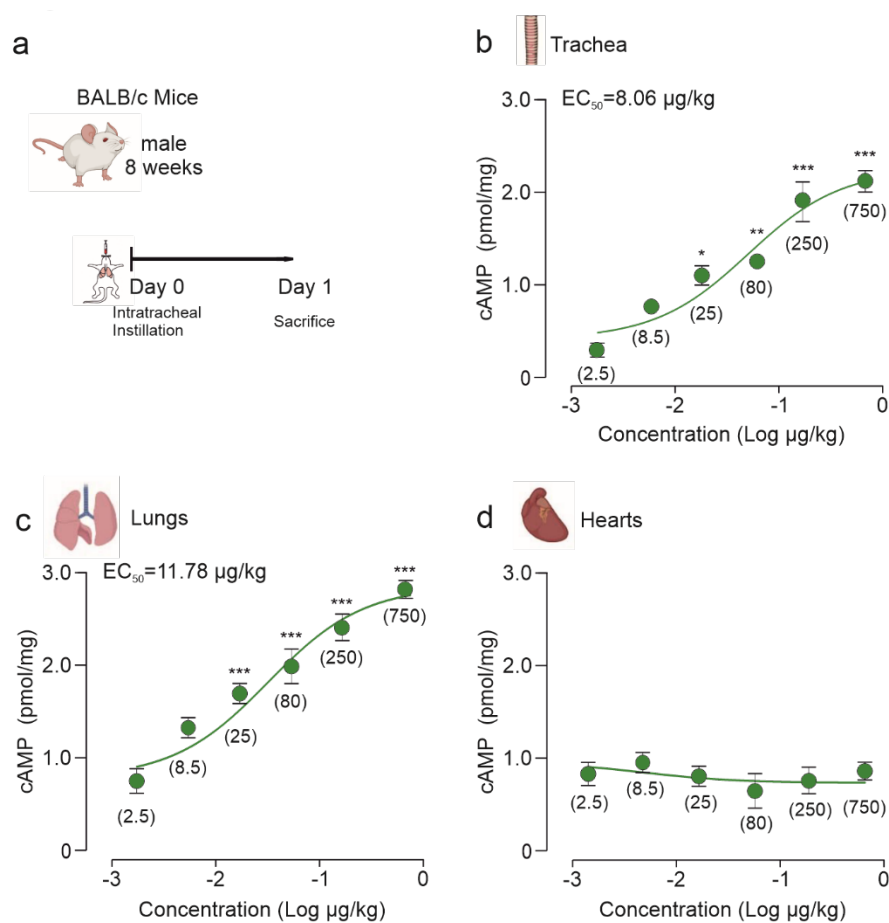


Figure 14. DRI-Pep #20 increases cAMP levels locally in vivo in the airway tract of mice.

a) Schematic representation of the treatment schedule. BALB/c mice received DRI-Pep #20 through intratracheal (i.t.) instillation. **(b-d)** cAMP concentrations in tracheas **(b)**, lungs **(c)** and hearts **(d)** from BALB/c mice 24 hours after i.t. instillation of different doses of DRI-Pep #20 (0 to 750 mg/kg). Values in brackets indicate the dose of DRI-Pep #20 expressed as mg/kg. The number of mice (n) ranged from 3 to 6 per group. EC_{50} , median effective concentration. In **a)** and **b)**, *P < 0.05, **P < 0.01, and ***P < 0.001 by one-way ANOVA, followed by Bonferroni's post hoc test. Throughout, data are means \pm SEM.

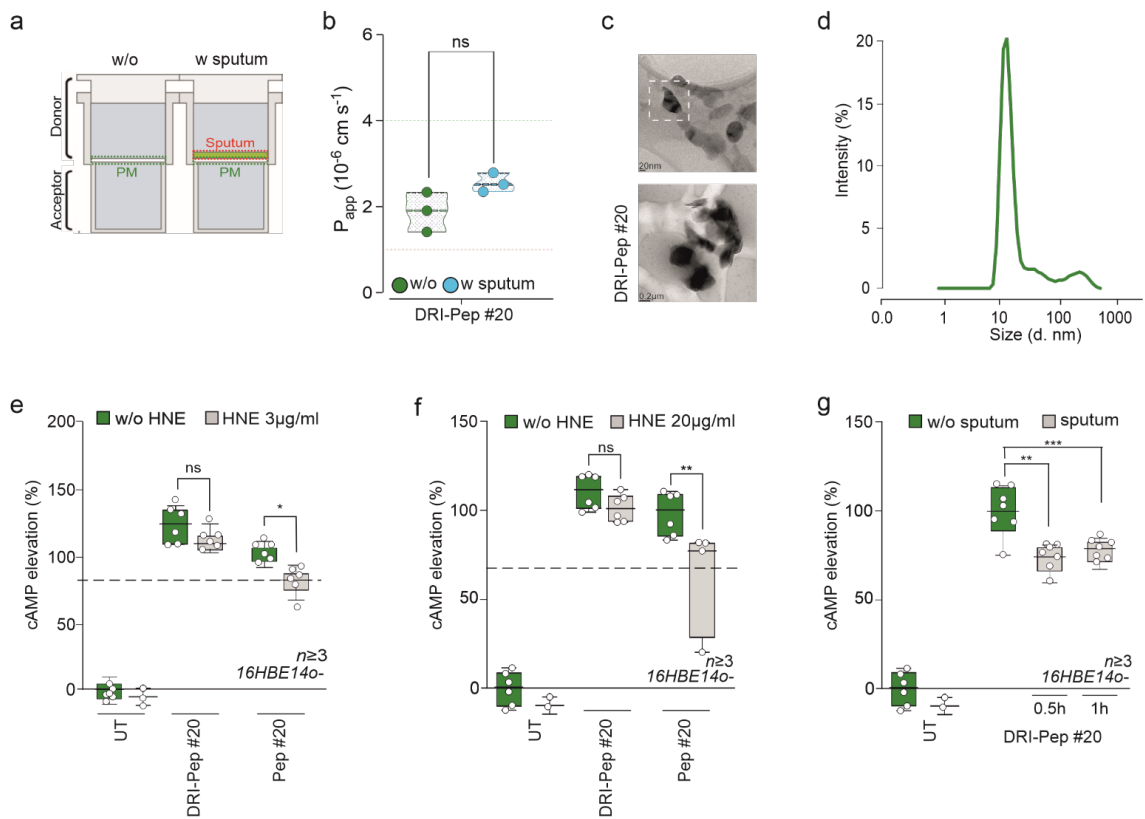


Figure 15. DRI-Pep #20 can penetrate pathological mucus and resist protease degradation.

a) Schematic representation of the Parallel Artificial Membrane Permeability Assay (PAMPA) with and without cystic fibrosis (CF) sputum deposition on top of the artificial lipid membrane (PM). **b)** Apparent permeability (P_{app}) measurements of DRI-Pep #20 (2 mg/mL), in the absence (green box) and in the presence (blue box) of CF sputum. The green dashed line indicates the threshold P_{app} for high-medium permeable compounds ($4 \times 10^{-6} \text{ cm s}^{-1}$), while the red dashed line defines the limit for medium-low permeable molecules ($1 \times 10^{-6} \text{ cm s}^{-1}$). ns: non-significant by Student's t test. **c)** Representative Transmission Electron Microscopy (TEM) images of DRI-Pep #20 (0.1 mg/mL in water). Scale bar: 20 nm. **d)** Size distribution profile of DRI-Pep #20 (4 mg/mL in 2 mM PBS) obtained by dynamic light scattering (DLS) analysis. **e-f)** cAMP concentrations in 16HBE14o- cells treated with the DRI-Pep #20 and Pep #20 (25 μM for 30 min) in the absence (green bars) and in the presence (gray bars) of either 3 $\mu\text{g/ml}$ (**d**) or 20 $\mu\text{g/ml}$ (**e**) human neutrophil elastase (HNE). The amount of cAMP was expressed as percentage of cAMP accumulation elicited by Pep #20 without HNE. Dashed lines indicate the amount of cAMP (%) induced by Pep #20 with HNE as a reference. $n \geq 3$ technical replicates from $N > 3$ independent experiments. * $P < 0.05$ and ** $P < 0.01$ by one-way ANOVA, followed by Bonferroni's post hoc test. ns: non-significant. **g)** cAMP elevation in 16HBE14o- cells covered with a layer of CF sputum and then treated with 25 μM DRI-Pep #20 for 30 min and 1 hour. The amount of cAMP was expressed as percentage of cAMP accumulation elicited by DRI-Pep #20 in the absence of sputum at 30 min. ** $P < 0.01$ and *** $P < 0.001$ versus DRI-Pep #20 without sputum by two-way ANOVA test, followed by Bonferroni's post-hoc analysis. $n \geq 6$ technical replicates from $N > 3$ independent experiments. Throughout, data are means \pm SEM.

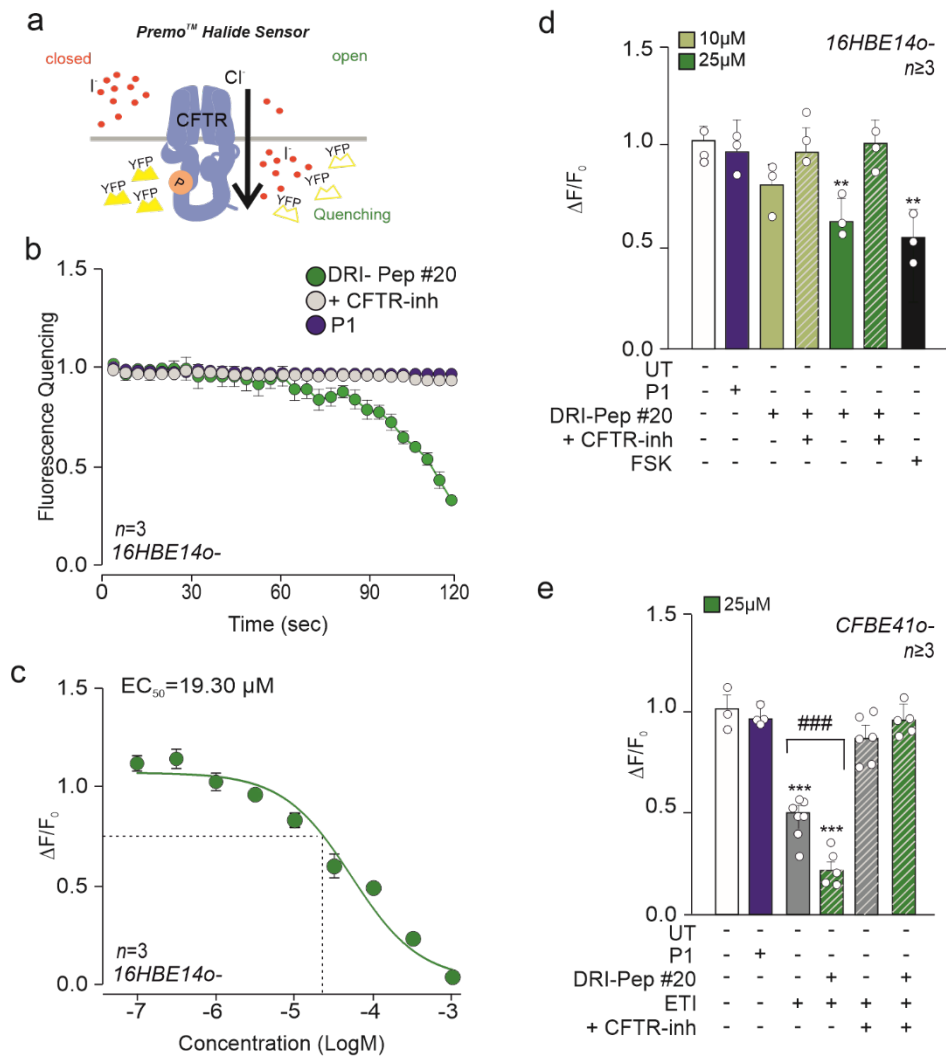


Figure 17. DRI-Pep #20 modulates wild-type and F508del-CFTR activity.

a) Schematic representation of CFTR activity measurement through the Premo™ Halide Sensor assay. **b)** Average fluorescence quenching traces of 16HBE14o- cells expressing the halide-sensitive yellow fluorescent protein (HS-YFP) and treated with either 25 μM DRI-Pep #20 or equimolar amount of the control peptide P1 for 30 min before addition of Premo Halide stimulus buffer. Fluorescence was continuously read (1 point per second) starting at 1 s before addition of the buffer and up to 120 s. The CFTR inhibitor CFTR_{inh}-172 (10 μM for 5 min) was used to evaluate the selective activation of the CFTR channel. **c)** CFTR activity (expressed as the change in fluorescence ΔF/F₀) in response to 30-min stimulation with increasing concentrations of DRI-Pep #20 (31.6 nM to 316 μM) in 16HBE14o- cells expressing HS-YFP. To determine the EC₅₀, nonlinear regression analysis was used. **d)** CFTR activity (expressed as the change in fluorescence ΔF/F₀) in 16HBE14o- cells expressing HS-YFP and treated with 10-25 μM DRI-Pep #20 for 30 min in the absence or in the presence of the CFTR inhibitor CFTR_{inh}-172 (10 μM for 5 min). The adenylyl cyclase activator, forskolin (FSK), was used as a positive control (100 nM for 5 min), while P1 was used as a negative control (25 μM for 30 min). UT: untreated cells. **e)** CFTR activity in F508del-CFTR-CFBE41o- cells expressing HS-YFP and

treated with Elexacaftor/Tezacaftor/Ivacaftor alone (ETI) or together with DRI-Pep #20. Cells were corrected with Elexacaftor (3 μ M) and Tezacaftor (10 μ M) for 24 hours and then exposed acutely to Ivacaftor (1 μ M) for 30 min, alone (ETI) or together with 25 μ M DRI-Pep #20. The CFTR inhibitor CFTR_{inh}-172 was used as in (b). UT: untreated cells. In (b) and (e), $n \geq 3$ technical replicates from $N > 3$ independent experiments. ** $P < 0.01$, and *** $P < 0.001$ versus UT and ### $P < 0.001$ ETI versus ETI plus DRI-Pep #20 by one-way ANOVA, followed by Bonferroni's post hoc test. Throughout, data are means \pm SEM.

5. Tables

Table 1. Next Generation Impactor deposition pattern

<i>NGI Stages</i>	<i>Dimension of Deposited Particles (micron)</i>
Stage 1	14.10
Stage 2	8.61
Stage 3	5.39
Stage 4	3.30
Stage 5	2.08
Stage 6	1.36
Stage 7	0.98

Table 2. Aerosol performance of PI3K γ MP after nebulization with three nebulizer devices (one jet nebulizer –TurboBoy- and two mesh nebulizers –AeronebGo and eFlow rapid)

	TurboBoy	AeronebGo	eFlow rapid
MMAD ($\mu\text{M} \pm \text{SD}$)	2.00 \pm 0.091	2.70 \pm 0.305	2.99 \pm 0.068
GSD ($\pm \text{SD}$)	1.94 \pm 0.308	2.10 \pm 0.234	1.85 \pm 0.013
FPF ($\pm \text{SD}$)	ND	43.2 \pm 11.1	38.9 \pm 1.17
RF ($\pm \text{SD}$)	ND	90.3 \pm 6.08	99.0 \pm 0.75

MMAD= Experimental Mass Mean Aerodynamic Diameter; GSD= Geometric Standard Deviation; FPF = Fine Particle Fraction; RF= Respirable Fraction.

Table 3. Binding energetics and kinetics of the DRI-Pep #20 with PKA-RII α obtained through molecular docking analysis.

	<i>ΔG (kcal mol⁻¹)</i>	<i>K_D (M)</i>	<i>Number of H-bonds</i>
DRI- Pep #20	-102	3.10 E ⁻⁰⁷	7

Table 4. Biological activity (cAMP elevation) of DRI-Pep #20 variants with two amino acid substitutions.

<i>Name</i>	<i>Sequence</i>	<i>cAMP Elevation*</i> (%)
DRI-Pep #20	RHQGK	105.63
Pep #20	KGQHR	100.00
Pep #21	KGNHR	94.75
Pep #22	KNLHR	92.15
Pep #23	KSLHR	88.14
Pep #24	KCNHR	84.65
Pep #25	KNCHR	83.25
Pep #26	KGSHR	79.84
Pep #27	KATHR	78.05
Pep #28	KNSHR	74.89
Pep #29	KSCHR	69.53
Pep #30	KLGHR	69.21
Pep #31	KQCHR	68.69
Pep #32	KLSHR	68.07
Pep #33	KCCHR	66.61
Pep #34	KSNHR	64.91
Pep #35	KCGHR	61.25
Pep #36	KSGHR	60.54
Pep #37	KGCHR	49.99
Pep #38	KGLHR	29.79
Pep #39	KLLHR	19.03
Pep #40	KCSHR	17.03
Pep #41	KLCHR	<0
Pep #42	KCLHR	<0
Pep #43	KGGHR	<0

*The cAMP elevation induced by each peptide was expressed as percentage of the cAMP accumulation elicited by the Pep #20. For screening purposes, non-DRI forms of the peptides conjugated with Penetratin 1 through a G linker were used. Positively charged, non-polar and polar amino acids are shown in orange, blue and red, respectively.

Table 5. Biological activity (cAMP elevation) and energetics/kinetics of the binding of N-terminal PI3K γ peptides progressively truncated at the C-terminus with PKA-RII α .

Name	Sequence	cAMP Elevation* (%)	Number of H-bonds	ΔG (kcal mol ⁻¹)	K_D (M)
Pep #01	KATHRSPGQIHLVQRHPPSEESQAF	100%	7.15	-102.75	1.34 E ⁻⁰⁶
Pep #02	KATHRSPGQIHLVQRHPP	125%	5.5	-97.50	2.62 E ⁻⁰⁶
Pep #03	KATHRSPGQIHLVQRHP	108%	4.45	-101.95	1.21 E ⁻⁰⁶
Pep #04	KATHRSPGQIHLVQRH	110%	5.20	-105.33	8.76 E ⁻⁰⁷
Pep #05	KATHRSPGQIHLVQR	59.6%	5.70	-96.88	2.00 E ⁻⁰⁶
Pep #06	KATHRSPGQIHLVQ	50.5%	3	-90	2.60 E ⁻⁰⁶
Pep #07	KATHRSPGQIHLV	46.8%	5.03	-93.53	2.51 E ⁻⁰⁶
Pep #08	KATHRSPGQIHL	101.3%	5.42	-92.15	1.40 E ⁻⁰⁶
Pep #09	KATHRSPGQIH	104%	4.70	-87.90	1.90 E ⁻⁰⁷
Pep #10	KATHRSPGQI	83.3%	4.68	-92.23	3.85 E ⁻⁰⁶
Pep #11	KATHRSPGQ	116.5%	4.75	-93.50	1.20 E ⁻⁰⁶
Pep #12	KATHRSPG	75.2%	3.53	-83.20	7.10 E ⁻⁰⁶
Pep #13	KATHRSP	75.3%	4.75	-89.08	8.61 E ⁻⁰⁶
Pep #14	KATHRS	73.8%	4.13	-87.53	5.85 E ⁻⁰⁶
Pep #15	KATHR	101%	4.98	-89	2.80 E ⁻⁰⁶
Pep #16	KATH	66.3%	4.75	-78.22	2.55 E ⁻⁰⁵
Pep #17	KAT	74.9%	3.33	-71.22	8.76 E ⁻⁰⁵
Pep #18	KA	42.2%	3.38	-65.33	3.58 E ⁻⁰⁴
Pep #19	K	29.9%	3.98	-67.65	1.65 E ⁻⁰⁴

*The cAMP elevation induced by each peptide was expressed as percentage of the cAMP accumulation elicited by the N-terminal region of PI3K γ containing the PKA-binding motif²¹ (126-150 PI3K γ ; Pep #01). For cell-based assays, peptides were made membrane-permeable by conjugation with Penetratin 1 through a G linker at the N-terminus.

Table 6. Binding energetics and kinetics of the KATHR peptide with PKA-RII α obtained through molecular docking analysis.

	ΔG (kcal mol ⁻¹)	K_D (M)	Number of H-bonds
KATHR	-89	2.80 E ⁻⁰⁶	5

6. References

- 1 Collaborators, G. B. D. C. R. D. Prevalence and attributable health burden of chronic respiratory diseases, 1990-2017: a systematic analysis for the Global Burden of Disease Study 2017. *Lancet Respir Med* **8**, 585-596, doi:10.1016/S2213-2600(20)30105-3 (2020).
- 2 Abozid, H. *et al.* Prevalence of chronic cough, its risk factors and population attributable risk in the Burden of Obstructive Lung Disease (BOLD) study: a multinational cross-sectional study. *EClinicalMedicine* **68**, 102423, doi:10.1016/j.eclinm.2024.102423 (2024).
- 3 Most, J. F. Muco-Obstructive Lung Diseases. *N Engl J Med* **381**, e20, doi:10.1056/NEJMc1907962 (2019).
- 4 Shteinberg, M., Haq, I. J., Polineni, D. & Davies, J. C. Cystic fibrosis. *Lancet* **397**, 2195-2211, doi:10.1016/S0140-6736(20)32542-3 (2021).
- 5 Celli, B. R. & Wedzicha, J. A. Update on Clinical Aspects of Chronic Obstructive Pulmonary Disease. *N Engl J Med* **381**, 1257-1266, doi:10.1056/NEJMra1900500 (2019).
- 6 Billington, C. K., Ojo, O. O., Penn, R. B. & Ito, S. cAMP regulation of airway smooth muscle function. *Pulm Pharmacol Ther* **26**, 112-120, doi:10.1016/j.pupt.2012.05.007 (2013).
- 7 Barnes, P. J. & Hansel, T. T. Prospects for new drugs for chronic obstructive pulmonary disease. *Lancet* **364**, 985-996, doi:10.1016/S0140-6736(04)17025-6 (2004).
- 8 Tavares, L. P. *et al.* Blame the signaling: Role of cAMP for the resolution of inflammation. *Pharmacol Res* **159**, 105030, doi:10.1016/j.phrs.2020.105030 (2020).
- 9 Facchinetti, F. *et al.* Tanimilast, A Novel Inhaled Pde4 Inhibitor for the Treatment of Asthma and Chronic Obstructive Pulmonary Disease. *Front Pharmacol* **12**, 740803, doi:10.3389/fphar.2021.740803 (2021).
- 10 Chin, S., Hung, M. & Bear, C. E. Current insights into the role of PKA phosphorylation in CFTR channel activity and the pharmacological rescue of cystic fibrosis disease-causing mutants. *Cell Mol Life Sci* **74**, 57-66, doi:10.1007/s00018-016-2388-6 (2017).
- 11 Dunican, E. M. *et al.* Mucus Plugs and Emphysema in the Pathophysiology of Airflow Obstruction and Hypoxemia in Smokers. *Am J Respir Crit Care Med* **203**, 957-968, doi:10.1164/rccm.202006-2248OC (2021).
- 12 Boucher, R. C. Muco-Obstructive Lung Diseases. *N Engl J Med* **380**, 1941-1953, doi:10.1056/NEJMra1813799 (2019).

- 13 Crespo-Lessmann, A. *et al.* Association of the CFTR gene with asthma and airway mucus hypersecretion. *PLoS One* **16**, e0251881, doi:10.1371/journal.pone.0251881 (2021).
- 14 Mall, M. A. & Hartl, D. CFTR: cystic fibrosis and beyond. *Eur Respir J* **44**, 1042-1054, doi:10.1183/09031936.00228013 (2014).
- 15 Murabito, A., Bhatt, J. & Ghigo, A. It Takes Two to Tango! Protein-Protein Interactions behind cAMP-Mediated CFTR Regulation. *Int J Mol Sci* **24**, doi:10.3390/ijms241310538 (2023).
- 16 Dodd, J. D., Barry, S. C., Daly, L. E. & Gallagher, C. G. Inhaled beta-agonists improve lung function but not maximal exercise capacity in cystic fibrosis. *J Cyst Fibros* **4**, 101-105, doi:10.1016/j.jcf.2004.11.004 (2005).
- 17 Decramer, M. L., Hanania, N. A., Lotvall, J. O. & Yawn, B. P. The safety of long-acting beta2-agonists in the treatment of stable chronic obstructive pulmonary disease. *Int J Chron Obstruct Pulmon Dis* **8**, 53-64, doi:10.2147/COPD.S39018 (2013).
- 18 Oba, Y. Phosphodiesterase inhibitors in chronic obstructive pulmonary disease. *Am J Respir Crit Care Med* **188**, 1366, doi:10.1164/rccm.201303-0510LE (2013).
- 19 Johnstone, T. B., Agarwal, S. R., Harvey, R. D. & Ostrom, R. S. cAMP Signaling Compartmentation: Adenylyl Cyclases as Anchors of Dynamic Signaling Complexes. *Mol Pharmacol* **93**, 270-276, doi:10.1124/mol.117.110825 (2018).
- 20 Baillie, G. S., Tejada, G. S. & Kelly, M. P. Therapeutic targeting of 3',5'-cyclic nucleotide phosphodiesterases: inhibition and beyond. *Nat Rev Drug Discov* **18**, 770-796, doi:10.1038/s41573-019-0033-4 (2019).
- 21 Zaccolo, M., Zerio, A. & Lobo, M. J. Subcellular Organization of the cAMP Signaling Pathway. *Pharmacol Rev* **73**, 278-309, doi:10.1124/pharmrev.120.000086 (2021).
- 22 Murabito, A., Cnudde, S., Hirsch, E. & Ghigo, A. Potential therapeutic applications of AKAP disrupting peptides. *Clin Sci (Lond)* **134**, 3259-3282, doi:10.1042/CS20201244 (2020).
- 23 Taylor, S. S. *et al.* The Tails of Protein Kinase A. *Mol Pharmacol* **101**, 219-225, doi:10.1124/molpharm.121.000315 (2022).
- 24 Langeberg, L. K. & Scott, J. D. A-kinase-anchoring proteins. *J Cell Sci* **118**, 3217-3220, doi:10.1242/jcs.02416 (2005).
- 25 Welch, E. J., Jones, B. W. & Scott, J. D. Networking with AKAPs: context-dependent regulation of anchored enzymes. *Mol Interv* **10**, 86-97, doi:10.1124/mi.10.2.6 (2010).

- 26 Wang, Y. *et al.* PKA-type I selective constrained peptide disruptors of AKAP complexes. *ACS Chem Biol* **10**, 1502-1510, doi:10.1021/acscchembio.5b00009 (2015).
- 27 Carr, D. W. *et al.* Interaction of the regulatory subunit (RII) of cAMP-dependent protein kinase with RII-anchoring proteins occurs through an amphipathic helix binding motif. *J Biol Chem* **266**, 14188-14192 (1991).
- 28 Diviani, D., Langeberg, L. K., Doxsey, S. J. & Scott, J. D. Pericentrin anchors protein kinase A at the centrosome through a newly identified RII-binding domain. *Curr Biol* **10**, 417-420, doi:10.1016/s0960-9822(00)00422-x (2000).
- 29 Perino, A. *et al.* Integrating cardiac PIP3 and cAMP signaling through a PKA anchoring function of p110gamma. *Mol Cell* **42**, 84-95, doi:10.1016/j.molcel.2011.01.030 (2011).
- 30 Ghigo, A. *et al.* A PI3Kgamma mimetic peptide triggers CFTR gating, bronchodilation, and reduced inflammation in obstructive airway diseases. *Sci Transl Med* **14**, eabl6328, doi:10.1126/scitranslmed.abl6328 (2022).
- 31 Nurnberg, B. & Beer-Hammer, S. Function, Regulation and Biological Roles of PI3Kgamma Variants. *Biomolecules* **9**, doi:10.3390/biom9090427 (2019).
- 32 Fanelli, V. *et al.* Pulmonary-derived phosphoinositide 3-kinase gamma (PI3Kgamma) contributes to ventilator-induced lung injury and edema. *Intensive Care Med* **36**, 1935-1945, doi:10.1007/s00134-010-2018-y (2010).
- 33 Jin, R. *et al.* Phosphoinositide 3-kinase-gamma expression is upregulated in brain microglia and contributes to ischemia-induced microglial activation in acute experimental stroke. *Biochem Biophys Res Commun* **399**, 458-464, doi:10.1016/j.bbrc.2010.07.116 (2010).
- 34 Auger, K. R., Serunian, L. A., Soltoff, S. P., Libby, P. & Cantley, L. C. PDGF-dependent tyrosine phosphorylation stimulates production of novel polyphosphoinositides in intact cells. *Cell* **57**, 167-175, doi:10.1016/0092-8674(89)90182-7 (1989).
- 35 Ghigo, A. *et al.* Phosphoinositide 3-kinase gamma protects against catecholamine-induced ventricular arrhythmia through protein kinase A-mediated regulation of distinct phosphodiesterases. *Circulation* **126**, 2073-2083, doi:10.1161/CIRCULATIONAHA.112.114074 (2012).
- 36 Kennedy, E. J. & Scott, J. D. Selective disruption of the AKAP signaling complexes. *Methods Mol Biol* **1294**, 137-150, doi:10.1007/978-1-4939-2537-7_11 (2015).
- 37 Lukanov, Y., Tanev, A. & Pelev, Z. Significance of a stimulating serum factor in prognosis of the course of delivery. *Folia Med (Plovdiv)* **31**, 40-45 (1989).

- 38 De Henau, O. *et al.* Overcoming resistance to checkpoint blockade therapy by targeting PI3K γ in myeloid cells. *Nature* **539**, 443-447, doi:10.1038/nature20554 (2016).
- 39 Faia, K. *et al.* The phosphoinositide-3 kinase (PI3K)- δ , γ inhibitor, duvelisib shows preclinical synergy with multiple targeted therapies in hematologic malignancies. *PLoS One* **13**, e0200725, doi:10.1371/journal.pone.0200725 (2018).
- 40 Maurice, D. H. *et al.* Advances in targeting cyclic nucleotide phosphodiesterases. *Nat Rev Drug Discov* **13**, 290-314, doi:10.1038/nrd4228 (2014).
- 41 Sala, V., Murabito, A. & Ghigo, A. Inhaled Biologicals for the Treatment of Cystic Fibrosis. *Recent Pat Inflamm Allergy Drug Discov* **13**, 19-26, doi:10.2174/1872213X12666181012101444 (2019).
- 42 d'Angelo, I. *et al.* Improving the efficacy of inhaled drugs in cystic fibrosis: challenges and emerging drug delivery strategies. *Adv Drug Deliv Rev* **75**, 92-111, doi:10.1016/j.addr.2014.05.008 (2014).
- 43 Oriano, M. *et al.* Evaluation of active neutrophil elastase in sputum of bronchiectasis and cystic fibrosis patients: A comparison among different techniques. *Pulm Pharmacol Ther* **59**, 101856, doi:10.1016/j.pupt.2019.101856 (2019).
- 44 Butnarusu, C., Caron, G., Pacheco, D. P., Petrini, P. & Visentin, S. Cystic Fibrosis Mucus Model to Design More Efficient Drug Therapies. *Mol Pharm* **19**, 520-531, doi:10.1021/acs.molpharmaceut.1c00644 (2022).
- 45 Sharifian Gh, M. Recent Experimental Developments in Studying Passive Membrane Transport of Drug Molecules. *Mol Pharm* **18**, 2122-2141, doi:10.1021/acs.molpharmaceut.1c00009 (2021).
- 46 Hermanson, G. T. *Bioconjugate Techniques*. (2008).
- 47 Louis-Jeune, C., Andrade-Navarro, M. A. & Perez-Iratxeta, C. Prediction of protein secondary structure from circular dichroism using theoretically derived spectra. *Proteins* **80**, 374-381, doi:10.1002/prot.23188 (2012).
- 48 Hawkins, P. C. & Nicholls, A. Conformer generation with OMEGA: learning from the data set and the analysis of failures. *J Chem Inf Model* **52**, 2919-2936, doi:10.1021/ci300314k (2012).
- 49 Hawkins, P. C., Skillman, A. G., Warren, G. L., Ellingson, B. A. & Stahl, M. T. Conformer generation with OMEGA: algorithm and validation using high quality structures from the Protein Databank and Cambridge Structural Database. *J Chem Inf Model* **50**, 572-584, doi:10.1021/ci100031x (2010).
- 50 Hawkins, P. C., Skillman, A. G. & Nicholls, A. Comparison of shape-matching and docking as virtual screening tools. *J Med Chem* **50**, 74-82, doi:10.1021/jm0603365 (2007).

- 51 Muchmore, S. W., Souers, A. J. & Akritopoulou-Zanze, I. The use of three-dimensional shape and electrostatic similarity searching in the identification of a melanin-concentrating hormone receptor 1 antagonist. *Chem Biol Drug Des* **67**, 174-176, doi:10.1111/j.1747-0285.2006.00341.x (2006).
- 52 Yang, J. *et al.* The I-TASSER Suite: protein structure and function prediction. *Nat Methods* **12**, 7-8, doi:10.1038/nmeth.3213 (2015).
- 53 Corpora, T. *et al.* Structure of the AML1-ETO NHR3-PKA(RIIalpha) complex and its contribution to AML1-ETO activity. *J Mol Biol* **402**, 560-577, doi:10.1016/j.jmb.2010.08.007 (2010).
- 54 Jumper, J. *et al.* Highly accurate protein structure prediction with AlphaFold. *Nature* **596**, 583-589, doi:10.1038/s41586-021-03819-2 (2021).
- 55 Rathinaswamy, M. K. *et al.* Structure of the phosphoinositide 3-kinase (PI3K) p110gamma-p101 complex reveals molecular mechanism of GPCR activation. *Sci Adv* **7**, doi:10.1126/sciadv.abj4282 (2021).
- 56 Lamiable, A. *et al.* PEP-FOLD3: faster de novo structure prediction for linear peptides in solution and in complex. *Nucleic Acids Res* **44**, W449-454, doi:10.1093/nar/gkw329 (2016).
- 57 Wang, Z., Eickholt, J. & Cheng, J. APOLLO: a quality assessment service for single and multiple protein models. *Bioinformatics* **27**, 1715-1716, doi:10.1093/bioinformatics/btr268 (2011).
- 58 Lopes, J. L., Miles, A. J., Whitmore, L. & Wallace, B. A. Distinct circular dichroism spectroscopic signatures of polyproline II and unordered secondary structures: applications in secondary structure analyses. *Protein Sci* **23**, 1765-1772, doi:10.1002/pro.2558 (2014).
- 59 Omar, M. H. & Scott, J. D. AKAP Signaling Islands: Venues for Precision Pharmacology. *Trends Pharmacol Sci* **41**, 933-946, doi:10.1016/j.tips.2020.09.007 (2020).
- 60 Gramegna, A. *et al.* Neutrophil elastase in bronchiectasis. *Respir Res* **18**, 211, doi:10.1186/s12931-017-0691-x (2017).
- 61 Hobbs, C. A. *et al.* Identification of the SPLUNC1 ENaC-inhibitory domain yields novel strategies to treat sodium hyperabsorption in cystic fibrosis airway epithelial cultures. *Am J Physiol Lung Cell Mol Physiol* **305**, L990-L1001, doi:10.1152/ajplung.00103.2013 (2013).
- 62 Craparo, E. F. *et al.* Sustained-Release Powders Based on Polymer Particles for Pulmonary Delivery of Beclomethasone Dipropionate in the Treatment of Lung Inflammation. *Pharmaceutics* **15**, doi:10.3390/pharmaceutics15041248 (2023).

- 63 Labiris, N. R. & Dolovich, M. B. Pulmonary drug delivery. Part I: physiological factors affecting therapeutic effectiveness of aerosolized medications. *Br J Clin Pharmacol* **56**, 588-599, doi:10.1046/j.1365-2125.2003.01892.x (2003).
- 64 Garton, M. *et al.* Method to generate highly stable D-amino acid analogs of bioactive helical peptides using a mirror image of the entire PDB. *Proc Natl Acad Sci U S A* **115**, 1505-1510, doi:10.1073/pnas.1711837115 (2018).
- 65 Perino, A. *et al.* Integrating Cardiac PIP(3) and cAMP Signaling through a PKA Anchoring Function of p110 γ . *MOLECULAR CELL* **42**, doi:10.1016/j.molcel.2011.01.030 (2011).
- 66 Boegh, M. & Nielsen, H. M. Mucus as a barrier to drug delivery - understanding and mimicking the barrier properties. *Basic Clin Pharmacol Toxicol* **116**, 179-186, doi:10.1111/bcpt.12342 (2015).
- 67 Mall, M. A. *et al.* Cystic fibrosis transmembrane conductance regulator in COPD: a role in respiratory epithelium and beyond. *Eur Respir J* **61**, doi:10.1183/13993003.01307-2022 (2023).
- 68 Parodi, A. *et al.* Journey on VX-809-Based Hybrid Derivatives towards Drug-like F508del-CFTR Correctors: From Molecular Modeling to Chemical Synthesis and Biological Assays. *Pharmaceuticals (Basel)* **15**, doi:10.3390/ph15030274 (2022).
- 69 Mall, M. A., Mayer-Hamblett, N. & Rowe, S. M. Cystic Fibrosis: Emergence of Highly Effective Targeted Therapeutics and Potential Clinical Implications. *Am J Respir Crit Care Med* **201**, 1193-1208, doi:10.1164/rccm.201910-1943SO (2020).
- 70 Alogna, A. *et al.* Lung-to-Heart Nano-in-Micro Peptide Promotes Cardiac Recovery in a Pig Model of Chronic Heart Failure. *J Am Coll Cardiol* **83**, 47-59, doi:10.1016/j.jacc.2023.10.029 (2024).
- 71 Hulot, J. S. & Kupatt, C. Inhalable Therapies for the Heart: Take the "Lung" Way Home? *J Am Coll Cardiol* **83**, 60-62, doi:10.1016/j.jacc.2023.10.028 (2024).
- 72 Suk, J. S. *et al.* The penetration of fresh undiluted sputum expectorated by cystic fibrosis patients by non-adhesive polymer nanoparticles. *Biomaterials* **30**, 2591-2597, doi:10.1016/j.biomaterials.2008.12.076 (2009).
- 73 Yu, T. *et al.* Mucus-Penetrating Nanosuspensions for Enhanced Delivery of Poorly Soluble Drugs to Mucosal Surfaces. *Adv Healthc Mater* **5**, 2745-2750, doi:10.1002/adhm.201600599 (2016).
- 74 Byrne, D. P., Omar, M. H., Kennedy, E. J., Evers, P. A. & Scott, J. D. Biochemical Analysis of AKAP-Anchored PKA Signaling Complexes. *Methods Mol Biol* **2483**, 297-317, doi:10.1007/978-1-0716-2245-2_19 (2022).
- 75 Veine, D. M., Yao, H., Stafford, D. R., Fay, K. S. & Livant, D. L. A D-amino acid containing peptide as a potent, noncovalent inhibitor of $\alpha 5 \beta 1$ integrin in

- human prostate cancer invasion and lung colonization. *Clin Exp Metastasis* **31**, 379-393, doi:10.1007/s10585-013-9634-1 (2014).
- 76 Casey, M. *et al.* Effect of elexacaftor/tezacaftor/ivacaftor on airway and systemic inflammation in cystic fibrosis. *Thorax* **78**, 835-839, doi:10.1136/thorax-2022-219943 (2023).
- 77 Schaupp, L. *et al.* Longitudinal effects of elexacaftor/tezacaftor/ivacaftor on sputum viscoelastic properties, airway infection and inflammation in patients with cystic fibrosis. *Eur Respir J* **62**, doi:10.1183/13993003.02153-2022 (2023).
- 78 Ibrahim, B. M., Park, S., Han, B. & Yeo, Y. A strategy to deliver genes to cystic fibrosis lungs: a battle with environment. *J Control Release* **155**, 289-295, doi:10.1016/j.jconrel.2011.07.039 (2011).
- 79 Capurro, V. *et al.* Partial Rescue of F508del-CFTR Stability and Trafficking Defects by Double Corrector Treatment. *Int J Mol Sci* **22**, doi:10.3390/ijms22105262 (2021).
- 80 Graeber, S. Y. *et al.* Effects of Elexacaftor/Tezacaftor/Ivacaftor Therapy on CFTR Function in Patients with Cystic Fibrosis and One or Two F508del Alleles. *Am J Respir Crit Care Med* **205**, 540-549, doi:10.1164/rccm.202110-2249OC (2022).
- 81 Veit, G. *et al.* Allosteric folding correction of F508del and rare CFTR mutants by elexacaftor-tezacaftor-ivacaftor (Trikafta) combination. *JCI Insight* **5**, doi:10.1172/jci.insight.139983 (2020).
- 82 Nichols, D. P. *et al.* Pharmacologic improvement of CFTR function rapidly decreases sputum pathogen density, but lung infections generally persist. *J Clin Invest* **133**, doi:10.1172/JCI167957 (2023).
- 83 Zuo, H., Cattani-Cavaliere, I., Musheshe, N., Nikolaev, V. O. & Schmidt, M. Phosphodiesterases as therapeutic targets for respiratory diseases. *Pharmacol Ther* **197**, 225-242, doi:10.1016/j.pharmthera.2019.02.002 (2019).

7. Patent and Publications



Ministero delle Imprese e del Made in Italy

Ricevuta di presentazione

per

Brevetto per invenzione industriale



Domanda numero: 102023000025458

Data di presentazione: 29/11/2023

DATI IDENTIFICATIVI DEL DEPOSITO

Ruolo	Mandatario
Depositante	Cristina Freyria Fava
Data di compilazione	29/11/2023
Riferimento depositante	BIT28754-CF/PS
Titolo	Peptidi non naturali che hanno come obiettivo l'attività di scaffold di PI3KY e loro usi terapeutici
Carattere domanda	Ordinaria
Esenzione	NO
Accessibilità al pubblico	NO
Numero rivendicazioni	14
Autorità depositaria	

PRIVACY

Dichiaro di aver letto e compreso l'informativa sul trattamento dei dati personali trasmessi con il presente deposito, resa ai sensi dell'art. 13 del Regolamento (UE) 2016/679 e pubblicata all'interno del presente portale, oltre che sul sito istituzionale della Direzione Generale per la Tutela della Proprieta' Industriale Ufficio Italiano Brevetti e Marchi del Ministero delle Imprese e del Made in Italy

RICHIEDENTE/I

Natura giuridica	Persona giuridica
Denominazione	KITHER BIOTECH S.r.l.
P.IVA/CF	10615040010
Tipo Società	societa' a responsabilita' limitata
Nazione sede legale	Italia
Comune sede legale	Torino (TO)

Indirizzo	Via Nizza
Civico	52
CAP	10126
Telefono	
Fax	
Email	
Pec	
Quota percentuale	100.0%

DOMICILIO ELETTIVO

Cognome/R.sociale	Buzzi, Notaro & Antonielli d'Oulx S.p.A.
Indirizzo	Corso Vittorio Emanuele II, 6
Cap	10123
Nazione	Italia
Comune	Torino (TO)
Telefono	011 - 8392911
Fax	011 - 8392929
Email\PEC	brevetti@pec.bnaturin.eu

MANDATARI/RAPPRESENTANTI

Cognome	Nome
Freyria Fava	Cristina
Bosotti	Luciano
Buzzi	Franco
Buzzi	Filippo
Campogiani	Giovanna
Cesa	Roberta
Crovini	Giorgio
De Bonis	Paolo
Ferrero	Alberto

Frontoni	Stefano
Gallarotti	Franco
Marchitelli	Mauro
Meindl	Tassilo Bertram
Notaro	Gianluca
Notaro	Giancarlo

INVENTORI

Cognome	Nome	Nazione residenza
DELLA SALA	Angela	Italia
SALA	Valentina	Italia
HIRSCH	Emilio	Italia
GHIGO	Alessandra	Italia

CLASSIFICAZIONI

Sezione	Classe	Sottoclasse	Gruppo	Sottogruppo
C	07	K		

NUMERO DOMANDE COLLEGATE

DOCUMENTAZIONE ALLEGATA

Tipo documento	Riserva	Documento
Lettera di Incarico	NO	BIT28754 l.i..pdf.p7m hash: e7f757feec7c52f8d091ff9cd774efae
Rivendicazioni in inglese	NO	BIT28754e riv EN.pdf.p7m hash: 1de8fdb710d04c099bc3de13e53e1faa
Disegni	NO	BIT28754 disegni.pdf.p7m hash: 16ad1cccb208e6f86d40e75569918f13

Sequenza di nucleotidi o aminoacidi	NO	BIT28754.xml hash: 9c11e0332e7439df706441b94924cc0f
Descrizione in inglese	NO	BIT28754e descrizione EN.pdf.p7m hash: 459d3e936796388371862f45648ef01e
Riassunto in Inglese	NO	BIT28754e riassunto EN.pdf.p7m hash: c2b7ab22a4339e242cbe115c321334bd
Riassunto	SI	hash:
Descrizione in italiano*	SI	hash:
Rivendicazioni	SI	hash:

PAGAMENTI

Tipo	Identificativo	Data
Bollo	01211347492033	09/10/2023

DOVUTO

Gli importi indicati non tengono conto delle eventuali esenzioni applicabili

Importo Tasse:	€ 230,00
Importo Imposta Bollo:	€ 16,00

NOTE

Description of the industrial invention with title:

"Non-natural peptides targeting the scaffold activity of PI3K γ and therapeutic uses thereof"

Of: Kither Biotech S.r.l., Italian nationality, Via Nizza, 52 - 10126 Torino

Designated Inventors: Angela DELLA SALA, Valentina SALA, Emilio HIRSCH, Alessandra GHIGO

Filed on: November 29, 2023

* * *

TEXT OF THE DESCRIPTION

FIELD OF THE INVENTION

The present description relates to non-natural peptides targeting the scaffold activity of PI3K γ and their use in the treatment of pathologies of the respiratory apparatus.

BACKGROUND OF THE INVENTION

The 3'-5'-cyclic adenosine monophosphate (cAMP) second messenger controls different cellular functions, including cell growth and differentiation, gene transcription and protein expression. cAMP exerts its function through activation of different effectors, with protein kinase A (PKA) being the most widely characterized. cAMP directly binds the dimer of the regulatory subunits of the PKA holoenzyme, promoting the release of the two catalytic counterparts, which are then free to phosphorylate various substrates. Although different G protein-coupled receptors (GPCR) rely on the same second messenger cAMP for conveying signals within the cell, a tight spatial and temporal regulation of its concentration ensures that activation of a specific GPCR results in the appropriate

cellular response³. This local control of cAMP signals is achieved through multiprotein complexes that sequester within subcellular microdomains enzymes responsible for cAMP generation (adenylyl cyclases) and destruction (phosphodiesterases, PDEs) as well as distinct signal transducers. Key orchestrators of these "signaling islands" are A-kinase anchoring proteins (AKAPs) that, by definition, anchor PKA to its substrates and its regulators in specific cellular compartments¹. Perturbations of this fine control of cAMP compartmentalization underlies different pathologies, including cardiovascular and pulmonary diseases, cancer, neurological disorders, and inflammation. On these grounds, pharmacological manipulation of specific cAMP signalosomes with molecules blocking the interaction of AKAPs with either PKA or other components of the cAMP signaling pathway has been attempted and proven effective in preclinical models^{1, 4}.

Previous work from our group identified the AKAP phosphoinositide 3-kinase γ (PI3K γ) as the orchestrator of a multiprotein complex which is central to smooth muscle contraction, immune cell activation, and epithelial fluid secretion in the airways². In the lungs, PI3K γ -bound PKA activates PDE4, ultimately restricting cAMP responses triggered by stimulation of β_2 -adrenergic receptors, the major GPCR mediating cAMP elevation in the airways. Displacement of the PI3K γ -anchored pool of PKA by a cell-permeable PI3K γ mimetic peptide (PI3K γ MP) inhibits PDE4 and promotes local cAMP elevation, eventually resulting in airway smooth muscle relaxation and reduced neutrophil infiltration in a murine model of asthma. In bronchial epithelial cells, PI3K γ MP

enhances cAMP in the vicinity of the cystic fibrosis transmembrane conductance regulator (CFTR), the ion channel that controls mucus hydration, thereby driving the opening of the wild-type channel, while synergizing with CFTR modulators in reinstating the function of the most prevalent mutant in cystic fibrosis (F508del-CFTR)².

OBJECT AND SUMMARY OF THE INVENTION

An object of the present invention is to provide a potent PI3K γ /PKA disruptor for achieving therapeutic cAMP elevation in chronic respiratory disorders.

According to the invention, the above object is achieved thanks to the products specified in the ensuing claims, which are understood as forming an integral part of the present description.

The present invention concerns a non-naturally occurring peptide targeting PI3K γ with nanomolar affinity for PKA, high resistance to protease degradation and high permeability to the pulmonary mucus barrier able to disrupt the PI3K γ /PKA complex and to trigger cAMP elevation in the airways.

In one embodiment the present invention concerns a non-natural peptide having the ability of inhibiting the A-kinase anchoring function of PI3K γ comprising an amino acid sequence as set forth in SEQ ID No.: 1, wherein each amino acid is a D-amino acid, and wherein the glutamine at position 3 and the glycine at position 4 can be substituted with any amino acid with similar hydrophobicity, hydrophilicity, charge and size, respectively.

In further embodiments, the present invention concerns

the non-natural peptide for use as a medicament, combination products of the non-natural peptide as well as pharmaceutical compositions comprising the same.

BRIEF DESCRIPTION OF THE DRAWINGS

The invention will now be described, by way of example only, with reference to the enclosed figures of drawing, wherein:

- Figure 1. DRI-Pep#20 structure.

a) Chemical structure of DRI-Pep #20. The amino acid sequence of DRI-Pep#20 comprises the cell penetrating peptide penetratin 1 (P1), a glycine (G) linker and the non-natural peptide RHQ GK (SEQ ID No.: 1), wherein each amino acid is a D-amino acid. **b)** Structural prediction of DRI-Pep#20 by PEP-FOLD3.5. The P1-G domain is shown as cartoon in black. The key residues of the RHQ GK domain, R-1, H-2, Q-3 and K-5, are indicated and shown as sticks. **c)** Circular dichroism spectra of DRI-Pep#20 showing a peak at 190-240 nm. The percentage of α -helical and β -sheet secondary structures calculated by the K2D3 software are indicated. **d)** Molecular docking simulation of the interaction between DRI-Pep#20 and PKA by HADDOCK 2.4. The docked pose of DRI-Pep#20 in complex with residues 1-45 of PKA-RII α is shown. The key residues involved in the binding are indicated (DRI-Pep#20 residues are in bold) and shown as sticks. Hydrogen bonds between DRI-Pep#20 and PKA-RII α are indicated by dashed lines. The structural model was developed using PyMOL.

- Figure 2. DRI-Pep #20/PKA-RII α (1-45) binding analysis by Optimal Hydrogen Bonding Network.

a) Number of hydrogen bonds formed by R-1, H-2, Q-3, G-4,

K-5 residues of DRI-Pep#20 with residues 1-45 of PKA-RII α . **b)** Number of hydrogen bonds between residues 1-45 of PKA-RII α with DRI-Pep #20. The interactions between PKA-RII α and either P1-G or RHQGK are shown in grey and black, respectively.

- Figure 3. DRI-Pep#20 binds PKA with high affinity.

a) Schematic representation of the fluorescence spectroscopy assay for the characterization of the interaction between DRI-Pep#20 and the recombinant fluorescein 5-maleimide-labeled PKA-RII α (PKA-F5M). **b)** Steady-state emission spectra of PKA-F5M in the presence of increasing concentrations of DRI-Pep#20 (0 to 20 μ M). K_D : dissociation constant. AU, arbitrary units. Inset, non-linear fitting of the fluorescence intensity maxima obtained at various concentrations of DRI-Pep#20 for the monitoring of bio-labeled PKA. K_A : association constant. **c)** For kinetic analysis, fluorescence spectra of PKA-F5M in the presence of increasing concentrations of DRI-Pep#20 (0 to 5 μ M) were analyzed and fitted to a single exponential function to obtain the observed rate constant (k_{obs}). The binding of DRI-Pep#20 to bio-labeled PKA was investigated under pseudo-first-order conditions, and the kinetic constants, k_{on} and k_{off} , were determined. **d)** Schematic representation of the displacement assay between DRI-Pep#20 and the PI3K γ /PKA-F5M complex. **e)** Percentage displacement of the PI3K γ /PKA-RII α complex by DRI-Pep #20, calculated from steady-state emission spectra of the PI3K γ /PKA-F5M complex in the presence of increasing concentrations of DRI-Pep#20 (0 to 5 μ M). The displacement efficiency was expressed as percentage of the binding between PI3K γ and PKA-F5M in the absence of DRI-Pep #20. **f)** cAMP concentrations in peritoneal macrophages from

wild-type (WT, in black) and PI3K γ ^{-/-} mice (in grey) treated with 10-25 μ M DRI-Pep#20 for 30 min. The amount of cAMP was expressed as percentage of cAMP accumulation observed in untreated PI3K γ ^{-/-} cells. n \geq 6 technical replicates from N $>$ 3 independent experiments. ***P $<$ 0.001 WT versus PI3K γ ^{-/-} by one-way ANOVA, followed by Bonferroni's post hoc test. Data are means \pm SEM.

- Figure 4. Potency and tolerability of DRI-Pep#20 in 16HBE14o- cells.

a) cAMP elevation in 16HBE14o- cells in response to increasing concentrations of DRI-Pep#20 (31.6 nM to 316 mM range) for 30 min. The amount of cAMP was expressed as percentage of cAMP accumulation elicited by 100 mM DRI-Pep #20. n \geq 9 technical replicates from N=3 independent experiments. **b)** Cell viability in 16HBE14o- cells treated with increasing concentration of DRI-Pep#20 (0 to 1000 μ M) for 24 hours. N=3 independent experiments. In **(a)** and **(b)**, the median effective concentration (EC₅₀) and the median lethal dose (LD₅₀) were obtained by nonlinear regression analysis. LD₅₀ was calculated with respect to untreated control cells, whose viability was set to 100%. Throughout, data are means \pm SEM.

- Figure 5. DRI-Pep#20 increases cAMP levels locally in vivo in the airway tract of mice. **a)** Schematic representation of the treatment schedule. BALB/c mice received DRI-Pep#20 through intratracheal (i.t.) instillation. **(b-d)** cAMP concentrations in tracheas **(b)**, lungs **(c)** and hearts **(d)** from BALB/c mice 24 hours after i.t. instillation of different doses of DRI-Pep#20 (0 to 750 mg/kg). Values in brackets indicate the dose of DRI-Pep#20 expressed as mg/kg. The number of mice (n) ranged from 3 to 6 per group. EC₅₀, median effective

concentration. In **a)** and **b)**, *P<0.05, **P<0.01, and ***P<0.001 by one-way ANOVA, followed by Bonferroni's post hoc test. Throughout, data are means ± SEM.

- **Figure 6. DRI-Pep#20 can penetrate pathological mucus and resist protease degradation.** **a)** Schematic representation of the Parallel Artificial Membrane Permeability Assay (PAMPA) with and without deposition of cystic fibrosis (CF) sputum on top of the artificial lipid membrane (PM). **b)** Apparent permeability (P_{app}) measurements of DRI-Pep#20 (2 mg/mL), in the absence and in the presence of CF sputum. The continuous line indicates the threshold P_{app} for high-medium permeable compounds (4×10^{-6} cm s⁻¹), while the dashed line defines the limit for medium-low permeable molecules (1×10^{-6} cm s⁻¹). ns: non-significant by Student's t test. **c)** Representative Transmission Electron Microscopy (TEM) images of DRI-Pep#20 (0.1 mg/mL in water). **d)** Size distribution profile of DRI-Pep#20 obtained by dynamic light scattering (DLS) analysis. **e-f)** cAMP concentrations in 16HBE14o- cells treated with DRI-Pep#20 (25 μM for 30 min) in the absence (black) and in the presence (grey) of either 3 μg/ml (**e**) or 20 μg/ml (**f**) human neutrophil elastase (HNE). n≥6 technical replicates from N>3 independent experiments. *P<0.05 and **P<0.01 by one-way ANOVA, followed by Bonferroni's post hoc test. ns: non-significant. **g)** cAMP elevation in 16HBE14o- cells covered with a layer of CF sputum and then treated with 25 μM DRI-Pep#20 for 30 min and 1 hour. The amount of cAMP was expressed as percentage of cAMP accumulation elicited by DRI-Pep#20 in the absence of sputum at 30 min. **P<0.01 and ***P<0.001 versus DRI-Pep#20 without sputum by two-way ANOVA test, followed by Bonferroni's

post-hoc analysis. $n \geq 6$ technical replicates from $N > 3$ independent experiments. Throughout, data are means \pm SEM.

- **Figure 7. Prediction of protease cleavage sites within DRI-Pep #20.** **a)** Prediction of protease cleavage sites within the DRI-Pep#20 sequence via ExPASy PeptideCutter software. **b)** Prediction of protease cleavage sites within the DRI-Pep#20 sequence via ExPASy PeptideCutter software and the Protease Specificity Prediction Server (PROSPER). The cleavage sites within the P1-G and RHQ GK regions of DRI-Pep#20 are marked with an overbar and in bold, respectively.

- **Figure 8. DRI-Pep#20 reinstates wild-type and F508del-CFTR activity.** **a)** Schematic representation of CFTR activity measurement through the Premo™ Halide Sensor assay. **b)** Average fluorescence quenching traces of 16HBE14o- cells expressing the halide-sensitive yellow fluorescent protein (HS-YFP) and treated with either 25 μ M DRI-Pep#20 or equimolar amount of the control peptide P1 for 30 min before addition of Premo Halide stimulus buffer. Fluorescence was continuously read (1 point per second) starting at 1 s before addition of the buffer and up to 120 s. The CFTR inhibitor CFTR_{inh}-172 (10 μ M for 5 min) was used to evaluate the selective activation of the CFTR channel. **c)** CFTR activity (expressed as the change in fluorescence $\Delta F/F_0$) in response to 30 min stimulation with increasing concentrations of DRI-Pep#20 (31.6 nM to 316 μ M) in 16HBE14o- cells expressing HS-YFP. To determine the median effective concentration (EC_{50}), nonlinear regression analysis was used. **d)** CFTR activity (expressed as the change in fluorescence $\Delta F/F_0$) in 16HBE14o- cells expressing HS-YFP and treated with 10-25 μ M DRI-Pep#20 for 30 min in the absence or in the presence of the CFTR inhibitor CFTR_{inh}-172 (10 μ M for 5

min). The adenylyl cyclase activator, forskolin (FSK), was used as a positive control (100 nM for 5 min), while P1 was used as a negative control (25 μ M for 30 min). UT: untreated cells. **e)** CFTR activity in F508del-CFTR-CFBE41o- cells expressing HS-YFP and treated with elexacaftor/tezacaftor/ivacaftor alone (ETI) or together with DRI-Pep #20. Cells were corrected with elexacaftor (3 μ M) and tezacaftor (10 μ M) for 24 hours and then exposed acutely to ivacaftor (1 μ M) for 30 min, alone (ETI) or together with 25 μ M DRI-Pep #20. The CFTR inhibitor CFTR_{inh}-172 was used as in **(b)**. UT: untreated cells. In **(d)** and **(e)**, $n \geq 3$ technical replicates from $N > 3$ independent experiments. ** $P < 0.01$, and *** $P < 0.001$ versus UT and ### $P < 0.001$ ETI versus ETI plus DRI-Pep#20 by one-way ANOVA, followed by Bonferroni's post hoc test. Throughout, data are means \pm SEM.

DETAILED DESCRIPTION OF THE INVENTION

The invention will now be described in detail, by way of non-limiting examples.

In the following description, numerous specific details are given to provide a thorough understanding of embodiments. The embodiments can be practiced without one or more of the specific details, or with other methods, components, materials, etc. In other instances, well-known structures, materials, or operations are not shown or described in detail to avoid obscuring aspects of the embodiments.

Reference throughout this specification to "one embodiment" or "an embodiment" means that a particular feature, structure, or characteristic described in connection with the embodiment is included in at least one embodiment. Thus, the appearances of the phrases "in one embodiment" or "in an

embodiment" in various places throughout this specification are not necessarily all referring to the same embodiment. Furthermore, the particular features, structures, or characteristics may be combined in any suitable manner in one or more embodiments.

The headings provided herein are for convenience only and do not interpret the scope or meaning of the embodiments.

In one embodiment, the present invention concerns a non-natural peptide having the ability of inhibiting the A-kinase anchoring function of PI3K γ comprising an amino acid sequence as set forth in SEQ ID No.: 1 (RHQ GK), wherein each amino acid is a D-amino acid, and wherein the glutamine at position 3 and the glycine at position 4 can be substituted with any amino acid with similar hydrophobicity, hydrophilicity, charge and size, respectively.

In one embodiment, the glutamine at position 3 can be substituted with asparagine, histidine and serine.

In one embodiment, the glycine at position 4 can be substituted with asparagine, serine and cysteine.

In one embodiment, the non-natural peptide further comprises a cell penetrating peptide.

In one embodiment, the cell penetrating peptide is selected from Penetratin (pAntp - RQIKIWFQNRRMKWKK - SEQ ID No.: 3), HIV TAT peptide (YGRKKRRQRRR - SEQ ID No.: 4), R7 peptide (RRRRRRR - SEQ ID No.: 5), KALA peptide (WEAKLAKALAKALAKHLAKALAKALKACEA - SEQ ID No.: 6), Buforin 2 (TRSSRAGLQFPVGRVHLLRK - SEQ ID No.: 7), MAP (KLALKLALKALKAAKLA-amide - SEQ ID No.: 8), Transportan (GWTLNSAGYLLGKINLKALAALAKKIL-amide - SEQ ID No.: 9), Transportan 10 (AGYLLGKINLKALAALAKKIL-amide - SEQ ID No.: 10),

Pvec (LLIILRRRIRKQAHHSK-amide - SEQ ID No.: 11), MPG peptide (GALFLGWLGAAGSTMGAPKKKRKV-amide - SEQ ID No.: 12).

In one embodiment, the non-natural peptide further comprises a linker conjugating the amino acid sequence of SEQ ID No.: 1 with the cell penetrating peptide sequence.

In one embodiment, the linker is an amino acid linker.

In one embodiment, the linker comprises one or more glycines or one or more amino acids with hydrophobicity, hydrophilicity, charge, and size similar to glycine, e.g., alanine, proline, serine.

In one embodiment, the linker is selected from the following sequences GG, GAG, GPA, GGGS (SEQ ID No.: 13).

In one embodiment, the non-natural peptide comprises from N- to C-term the amino acid sequence of SEQ ID No.: 1, a linker, and a cell penetrating peptide.

In one embodiment, the linker and/or the cell penetrating peptides are made of D-amino acids.

In one embodiment, the non-natural peptide has an amino acid sequence as set forth in SEQ ID No.: 2 (d(RHQGKGGKWKMRNQFWIKIQR) - in the following named DRI-Pep#20).

In one embodiment, the non-natural peptide, preferably the non-natural peptide of SEQ ID No.: 2, contains one or more modifications not altering the primary sequence, including chemical derivatization, e.g., acetylation, deuteration, Fmocylation.

In one embodiment, the present invention concerns the non-natural peptide as disclosed herein for use as a medicament.

In one embodiment, the present invention concerns the non-natural peptide as disclosed herein for use in treating

respiratory diseases, preferably bronco-obstructive diseases.

In one embodiment, the respiratory diseases are selected from allergic asthma, cystic fibrosis (CF), chronic obstructive pulmonary disease (COPD), non-CF bronchiectasis, pulmonary hypertension (PH), and idiopathic pulmonary fibrosis (IPF).

In one embodiment, the non-natural peptide is suitable for administration by inhalation.

In one embodiment, the present invention concerns a product comprising:

i) at least one non-natural peptide as disclosed herein, and

ii) at least one potentiator of the cystic fibrosis transmembrane conductance regulator (CFTR) and/or at least one corrector of the cystic fibrosis transmembrane conductance regulator (CFTR) as a combined preparation for sequential, simultaneous or separate use in treating a respiratory disease.

In one embodiment, the respiratory disease is a bronco-obstructive disease.

In one embodiment, the respiratory disease is cystic fibrosis.

In one embodiment, the potentiator of the cystic fibrosis transmembrane conductance regulator (CFTR) is selected from Ivacaftor or VX-770 (N-(2,4-Di-tert-butyl-5-hydroxyphenyl)-1,4-dihydro-4-oxoquinoline-3-carboxamide), Navocaftor or ABBV-3067 ([5-[3-amino-5-[4-(trifluoromethoxy)phenyl]sulfonylpyridin-2-yl]-1,3,4-oxadiazol-2-yl]methanol) and Deutivacaftor or D9-ivacaftor (N-[2-tert-butyl-4-[1,1,1,3,3,3-hexadeuterio-2-(trideuteriomethyl)propan-2-yl]-5-hydroxyphenyl]-4-oxo-1H-quinoline-3-carboxamide).

In one embodiment, the corrector of the cystic fibrosis transmembrane conductance regulator (CFTR) is selected from Lumacaftor or VX-809 (3-(6-(1-(2,2-difluorobenzo[d][1,3]dioxol-5-yl)cyclopropanecarboxamido)-3-methylpyridin-2-yl)benzoic acid), Tezacaftor or VX-661 (1-(2,2-difluoro-1,3-benzodioxol-5-yl)-N-[1-[(2R)-2,3-dihydroxypropyl]-6-fluoro-2-(1-hydroxy-2-methylpropan-2-yl)indol-5-yl]cyclopropane-1-carboxamide), Elaxacaftor or VX-445 (N-(1,3-dimethylpyrazol-4-yl)sulfonyl-6-[3-(3,3,3-trifluoro-2,2-dimethylpropoxy)pyrazol-1-yl]-2-[(4S)-2,2,4-trimethylpyrrolidin-1-yl]pyridine-3-carboxamide), Galicaftor or ABBV-2222 (4-[(2R,4R)-4-[[1-(2,2-difluoro-1,3-benzodioxol-5-yl)cyclopropanecarbonyl]amino]-7-(difluoromethoxy)-3,4-dihydro-2H-chromen-2-yl]benzoic acid) and Vanzacaftor ((3Z,14S)-8-[3-(2-dispiro[2.0.24.13]heptan-7-ylethoxy)pyrazol-1-yl]-12,12-dimethyl-2,2-dioxo-2λ6-thia-3,9,11,18,23-pentazatetracyclo[17.3.1.111,14.05,10]tetracos-1(22),3,5(10),6,8,19(23),20-heptaen-4-olate).

In one embodiment, the present invention concerns a pharmaceutical composition comprising at least one non-natural peptide as disclosed herein and a pharmaceutically acceptable vehicle.

In one embodiment, the pharmaceutically acceptable vehicle is selected among phosphate buffered saline, saline, hypertonic saline, water.

In one embodiment, the pharmaceutical composition comprises at least one excipient.

In one embodiment, the pharmaceutical composition comprises at least one excipient selected among NaCl, HCl, NaOH, EDTA, Polysorbate 20, Polysorbate 80, Citric acid, Na citrate, K phosphate, Na phosphate, Na bicarbonate, Ascorbic

acid, Lactose, Glucose, Mannitol, Trehalose, Sucrose, Mg stearate, Glutathione, Vitamin E, Cyclodextrin, DPPC, DSPC, DMPC, Leucine, Isoleucine, Methionine, Histidine, Glycine, Poloxamer, Chitosan, Trimethylchitosan, PLGA, PEG.

The unexpectedly high resistance to degradation and potency of DRI-Pep#20 renders this compound the ideal candidate for therapeutic cAMP modulation, especially for the treatment of chronic respiratory diseases, being the PI3K γ -PKA signaling hub central to multiple functions of airway cells, like smooth muscle relaxation, epithelial ion transport and neutrophil infiltration². Our observations that DRI-Pep#20 can be efficiently delivered locally in the airways, and that its biological activity is completely preserved in the presence of human neutrophil elastase, support the possibility of using this peptide to ensure therapeutically relevant cAMP elevation in highly inflamed lungs. This is relevant for patients with COPD, non-CF bronchiectasis and certain forms of asthma, but also the lethal genetic disease CF, since airway inflammation is not eliminated in these patients, despite the introduction of highly effective modulator therapies (HEMT) targeting the basic genetic defect of the disease^{17, 18}.

In addition to inflammation-related proteases, another barrier imposed by diseased lungs that may hamper the bioavailability of inhaled therapeutics is the thick mucus layer covering the respiratory epithelia⁷, especially in CF individuals, as well as in patients with COPD, non-CF bronchiectasis and asthma. Our cell-based assays using patient-derived sputum as a proxy of CF mucus reveal a good mucus permeability of DRI-Pep #20, which likely stems from its molecular dimensions being compatible with that of the meshes

of the pathological mucus. TEM and DLS analysis indicate that the peptide can form aggregates of 200 nm in size, which could freely diffuse through the 100-1000 nm meshes of the network of bundled fibers that are typically formed by biopolymers of the CF mucus and that are filled with a low viscosity fluid¹⁹.

In virtue of its ability to efficiently penetrate mucus layers, DRI-Pep#20 can be exploited to achieve therapeutic cAMP elevation in CF bronchial epithelial cells, specifically in PI3K γ -directed subcellular compartments, which we previously show to positively affect CFTR activity and maximize the effect of HEMT². This is supported by our data showing that DRI-Pep#20 doubles the effects of the gold-standard combination of CFTR modulators, elexacaftor/tezacaftor/ivacaftor in rescuing the activity of the most common CFTR mutant, F508del. These findings have important clinical implications in light of recent studies showing that CFTR potentiators and correctors restore only partially the function of mutant channels, up to 60% of the levels of the wild-type CFTR²⁰⁻²², with consequent residual disease in CF patients treated with HEMT^{17, 18, 23}. Thus, DRI-Pep#20 offers the possibility of significantly increasing the efficacy of the standard of care for CF patients.

In conclusion, DRI-Pep#20 can be used for achieving therapeutic cAMP elevation locally in the lungs, in chronic respiratory disorders with high unmet medical need, such as the lethal genetic disease CF.

Results

DRI-Pep#20 structure and biological properties.

The chemical structure of DRI-Pep#20 is shown in Fig. 1a (d(RHQGKGGKWKMRNQFWIKIQR) - SEQ ID No.: 2). Predictions of

the tridimensional structure of the peptide suggested the presence of an α -helix, flanked by two uncoiled regions (Fig. 1b). The presence of α -helix structures (18.51%) was confirmed by circular dichroism analyses showing a double-peak signal, with a maximum at 200 nm which is typical for α -helix structures, and a minimum in the 220-240 nm region which is characteristic for random-coil regions⁶ (Fig. 1c). In silico simulations of the binding of DRI-Pep#20 to amino acids 1-45 of PKA-RII α , the typical binding surface for AKAPs, revealed that the kinase could form hydrogen bonds with the RHQ GK sequence, mainly involving the arginine and the lysine in position 1 and 5, respectively, and to a lesser extent histidine 2 and glutamine 3 (Fig. 1d, Fig. 2 and Table 1).

Table 1. Binding energetics and kinetics of DRI-Pep#20 obtained through molecular docking analysis.

	ΔG (kcal mol ⁻¹)	K_D (M)	Number of H-bonds
DRI-Pep #20	-102	3.10 E ⁻⁰⁷	7

The high affinity of the DRI-Pep#20 for PKA was further corroborated by in vitro experiments showing that the peptide associated recombinant PKA-RII α with a dissociation constant (K_D) in the nanomolar range (76 nM; Fig. 3a-b). Furthermore, stopped-flow fluorescence assays revealed that the binding of DRI-Pep#20 to PKA-RII α was extremely fast, with a K_{on} of 10⁻⁶ s, while the dissociation process was significantly slow, being the K_{off} 10⁻² s (Fig. 3c and Table 2).

Table 2. Binding kinetics of the interaction between DRI-

Pep#20 and PKA-RII α .

	<i>Steady- state experiment</i>	<i>Kinetic experiment</i>
k_{on} (10^6 M $^{-1}$ s $^{-1}$)	-	1.5
k_{off} (10^{-2} s $^{-1}$)	-	7.2
K_A (10^7 M $^{-1}$)	1.3	2.0
K_D (10^{-8} M)	7.6	4.9

In agreement with the high affinity of DRI-Pep#20 to PKA-RII α , the peptide displaced the binding between recombinant PI3K γ and PKA-RII α with an efficiency as high as 74% (Fig. 3d-e). Notably, despite the elevated binding affinity to PKA-RII α , DRI-Pep#20 retained the selectivity for the PI3K γ -bound pool of PKA since the peptide failed to increase cAMP in cells devoid of PI3K γ (Fig. 3f).

Dose-response experiments showed that DRI-Pep#20 increased cAMP levels in 16HBE14o- cells with an EC₅₀ of 15 μ M (Fig. 4a) and it was well tolerated, being the LD₅₀ 10-fold higher than the EC₅₀ (Fig. 4b).

Overall, these results identify DRI-Pep#20 as a selective PI3K γ /PKA-RII α peptide disruptor with high affinity to PKA-RII α .

DRI-Pep#20 has good mucus permeability and protease resistance

Next, we sought to determine to what extent DRI-Pep#20 could be used for modulating cAMP in the lungs for therapeutic purposes. First, we assessed the suitability for local delivery to the airways. Following intratracheal instillation (Fig. 5a), DRI-Pep#20 induced a dose-dependent increase in cAMP levels in the trachea and in the lungs, with an EC₅₀ of 8.06 μ g/Kg and

11.78 $\mu\text{g}/\text{Kg}$, respectively (Fig. 5b-c). Of note, cardiac cAMP metabolism was unchanged (Fig. 5d), suggesting that the peptide increased cAMP locally in the lungs without systemic effects.

Because the efficacy of inhaled therapies can be hampered by extracellular barriers imposed by diseased lungs, such as a thick layer of protease-rich mucus⁷, we next sought to determine to what extent DRI-Pep#20 could penetrate mucus layers and resist to protease degradation. DRI-Pep#20 penetrated the phospholipid membrane of the PAMPA system (Fig. 6a) with an apparent permeability (P_{app}) of $1.88 \times 10^{-6} \text{ cm s}^{-1}$ (Fig. 6b). Of note, the addition of pathological CF sputum on top of the phospholipid layer (Fig. 6a) did not significantly affect the P_{app} of the peptide ($P_{\text{app}} 2.55 \times 10^{-6} \text{ cm s}^{-1}$) (Fig. 6b). To verify whether the good mucus permeability of DRI-Pep#20 could be ascribed to molecular dimensions compatible with the mesh size of CF mucus⁸, Transmission Electron Microscopy (TEM) and Dynamic Light Scattering (DLS) assays were performed. TEM images show that DRI-Pep#20 formed irregular aggregates of 5-40 nm in size (Fig. 6c), which was in agreement with the particle diameter of 10-20 nm retrieved by DLS analysis (Fig. 6d).

Next, we tested whether DRI-Pep#20 retained the ability to elevate cAMP in pulmonary cells in the presence of neutrophil elastase, the most abundant protease in the lungs of patients with neutrophilic airway diseases, like COPD and CF⁹. The ability of the peptide to raise cAMP in 16HBE41o-cells was completely unaltered by the presence of 3 $\mu\text{g}/\text{ml}$ of recombinant human neutrophil elastase (HNE) (Fig. 6e), a dose which was previously shown to inactivate other therapeutic peptides¹⁰. Notably, the activity of the DRI-Pep#20 was

completely preserved even in the presence of a 10-fold higher concentration of HNE (Fig. 6f), an amount that is typically detected in the lungs of patients with severe bronchiectasis⁹, which was in agreement with the absence of any predicted cleavage sites by HNE (Fig. 7a). The good resistance of DRI-Pep#20 to degradation was confirmed in the presence of a more complex biological matrix containing other proteases that could potentially cleave the peptide (Fig. 7b), that is CF sputum, where the DRI-Pep#20 retained 72% of its biological activity (Fig. 6g).

Taken together, these data demonstrate the ability of DRI-Pep#20 to elevate lung cell cAMP in the presence of a hostile extracellular environment composed of a mucus barrier enriched in proteases, which is typical of diseased lungs.

DRI-Pep#20 promotes cAMP-dependent activation of wild-type and F508del-CFTR in human bronchial epithelial cells

Next, we aimed to assess the extent to which DRI-Pep#20 could effectively restore cAMP levels and consequently reactivate the activity of CFTR, a cAMP-dependent chloride channel impaired in a range of respiratory disease, primarily including CF¹¹. First, we assessed the ability of the peptide to stimulate the activity of the wild-type channel in 16HBE141o- cells expressing the halide-sensitive yellow fluorescent protein (HS-YFP) (Fig. 8b), which allows quantifying CFTR activity based on the fluorescence quenching rate elicited by an iodide influx¹². DRI-Pep#20 induced a 60% reduction in YFP fluorescence, which was completely prevented by co-application of the CFTR inhibitor, CFTR_{inh}-172 (Fig. 8b), demonstrating selective activation of CFTR channels. Dose-

response experiments revealed an EC₅₀ of 20 μM (Fig. 8c) and demonstrated that 25 μM DRI-Pep#20 was as effective as 10 μM forskolin, the adenylyl cyclase activator, in triggering CFTR gating in 16HBE141o- cells (Fig. 8d).

Next, we assessed to what extent DRI-Pep#20 could reinstate the activity of F508del-CFTR in combination with the standard of care for CF, including two CFTR correctors (Elexacaftor/Tezacaftor) and one CFTR potentiator (Ivacaftor), that partially rescue the trafficking and gating defects of the mutant channel, respectively¹³. In CF bronchial epithelial cells overexpressing the F508del-CFTR mutant and the HS-YFP, Elexacaftor/Tezacaftor/Ivacaftor (ETI) reduced YFP fluorescence of 50%, which was further decreased down to 25% when DRI-Pep#20 was added together with ETI (Fig. 8e).

Hence, these data support the use of DRI-Pep#20 as a single agent or as an-add on to CFTR modulators, to therapeutically stimulate the activity of wild-type and F508del CFTR, respectively.

Material and Methods

Peptides and reagents

Peptides were synthesized by GenScript (Piscataway, NJ) at >95% purity.

Recombinant human PKA regulatory subunit RIIα (PKA-RIIα) and PI3Kγ catalytic subunit (p110γ) were purchased by Biaffin GmbH & Co KG (product code: PK-PKA-R2A025, Kassel, DE) and Origene Technologies (TP307790, Rockville, US), respectively.

Human neutrophil elastase was purchased from Sigma-Aldrich (CAS 9004-06-2, Sigma-Aldrich, Saint Louis, MO) and reconstituted in 50 mM sodium acetate, pH 5.5, with 200 mM

NaCl. VX-809 (Lumacaftor), VX-770 (Ivacaftor), VX-661 (Tezacaftor) and VX-445 (Elexacaftor) were purchased from MedChemExpress LLC (Princeton, USA). Forskolin and CFTR_{inh}-172 were purchased from Sigma-Aldrich (CAS 66575-29-9, Sigma-Aldrich, Saint Louis, MO).

Cell lines

Immortalized human bronchial epithelial cells expressing wild-type CFTR (16HBE14o-) or F508del-CFTR (CFBE41o-) were purchased from Sigma-Aldrich (16HBE14o-, product code: CAS SCC150, CFBE41o-, product code: CAS SCC151, Sigma-Aldrich, Saint Louis, MO). Cells were grown in Minimum Essential Medium (MEM) supplemented with 10% FBS, 5 mM L-Glutamine, 100 U/ml penicillin and 100 µg/ml streptomycin (Thermo Fisher Scientific, Waltham, MA) on culture dishes pre-coated with human fibronectin (1 mg/ml; Sigma-Aldrich, Saint Louis, MO), bovine collagen I (3 mg/ml; Sigma-Aldrich, Saint Louis, MO) and bovine serum albumin (0.1%; Sigma-Aldrich, Saint Louis, MO) diluted in LHC-8 basal medium (Invitrogen, Waltham, MA). Cells up to passage 15 were used for experiments. All cells were cultured at 37°C and under a 5% CO₂ atmosphere.

Animals

PI3K γ -deficient mice (PI3K γ ^{-/-}) were described previously². Mutant mice were back-crossed with C57Bl/6j mice for 15 generations to inbreed the genetic background and C57Bl/6j were used as controls (WT). Mice used in all experiments were 8 to 12 weeks of age. Mice were group-housed, provided free-access to standard chow and water in a controlled facility providing a 12-hour light/dark cycle and were used according to

institutional animal welfare guidelines and legislation, approved by the local Animal Ethics Committee. All animal experiments were approved by the animal ethical committee of the University of Torino and by the Italian Ministry of Health (Authorization n°757/2016-PR) and the obligations of Legislative Decrees No. 206 of April 12, 2001, and No. 224 of July 8, 2003 have been met.

Isolation of murine peritoneal macrophages

Peritoneal macrophages were prepared from 8- to 12-week-old wild-type (WT) and PI3K $\gamma^{-/-}$ mice, as described previously ². Briefly, cells were collected from euthanized animals by peritoneal lavage with 5 mL of PBS, supplemented with 5 mM EDTA. Cells were centrifuged for 3 min at 300 g and the pellet was resuspended in culture media including Roswell Park Memorial Institute (RPMI) media, 100 U/ml penicillin and 100 μ g/ml streptomycin, and 10% heat-inactivated FBS (Thermo Fisher Scientific, Waltham, MA). Macrophages were seeded in 96-well plates (1×10^6 cells/well) and maintained at 37°C with 5% CO₂ for at least 16/18 h before treatment with the peptide and cAMP quantification.

cAMP measurements

From cells: cAMP content was measured in 16HBE14o- cells at the indicated time points after treatment with the indicated doses of peptides using the Promega cAMP-Glo™ Assay kit (Promega, Milano, IT), according to the manufacturer's protocol.

From tissues: lungs, tracheas and hearts were collected from euthanized mice 24 h after intratracheal instillation of

different doses of the peptide (0 to 750 mg/kg in a final volume of 50 μ l of PBS). Snap-frozen tissues were powdered in liquid nitrogen and extracted with cold 6% trichloroacetic acid. Samples were sonicated for 10 sec, incubated at 4°C under gentle agitation for 10 min and then centrifuged at 13000 rpm at 4°C for 10 min. Supernatants were washed four times with five volumes of water saturated with diethyl ether and lyophilized. cAMP content was detected with Cyclic AMP ELISA Kit (Cayman Chemical, Michigan, USA), according to the manufacturer's protocol.

Cell viability assay

Human bronchial epithelial cells (16HBE14o-) were seeded in 96-well plates (2×10^4 cells/well) and incubated for at least 16/18 hours at 37°C with 5% CO₂ before experiments. Non-adherent cells were eliminated by washing with PBS and cells were then stimulated with 8 different doses of the indicated peptide (0 μ M - 1 mM range) for 24h. ATP levels were evaluated as an indicator of viable cells using the Cell Titer-Glo® Luminescent Cell Viability Assay (Promega, Milano, IT), according to the manufacturer's protocol. The lethal dose (LD₅₀) was calculated with respect to untreated control cells, whose viability was set to 100%.

CFTR activity measurements

CFTR-mediated anion transport was measured by using the Premo™ Halide Sensor (Thermo Fisher Scientific, Waltham, MA) which allows assessing CFTR activity by measuring the rate of YFP fluorescence quenching caused by iodide/chloride exchange across the plasma membrane. Briefly, the halide-sensitive

yellow fluorescent protein (HS-YFP) was expressed in 16HBE14o- and F508del-CFTR-CFBE41o- cells through the BacMam technology, according to the manufacturer's protocol. Cells expressing the HS-YFP were cultured on 96-well plates and treated with the indicated peptides/compounds for the indicated time. Fluorescence was evaluated in a plate reader immediately after addition of 150 μ l of Halide stimulus buffer (an NaI-containing solution) leading to a final NaI concentration in the wells of 75 mM. Fluorescence was continuously read (1 point per second) starting at 1 s before Halide stimulus buffer addition and up to 120 s. CFTR activity was expressed as $\Delta F/F_0$ where ΔF was obtained by subtracting the background fluorescence (fluorescence of cells not expressing HS-YFP) to the fluorescence measured at the specific time point after addition of NaI. ΔF was then normalized to the initial fluorescence F_0 (fluorescence of HS-YFP-expressing cells immediately after addition of NaI) to obtain a measure of relative fluorescence $\Delta F/F_0$.

CF sputum samples

Spontaneous expectorated sputum samples from CF patients in stable clinical conditions were collected at the Bronchiectasis and Cystic Fibrosis Programs of the Respiratory Department of Fondazione IRCCS Ca' Granda Ospedale Maggiore Policlinico in Milan (Italy) and processed as previously described²⁵. The patients signed an express, free and informed, consent to the collection and use of their biological samples. Briefly, samples were processed getting first rid of saliva, sputum plugs were then selected and weighted. Samples were diluted 8X in PBS, vortexed until sputum dissolution and

centrifuged for 15min at 3000g. Supernatants were recovered and stored at -80 °C, thawed overnight at 4 °C, and all subsequent experiments were undertaken within 24h from thawing. Neutrophil elastase was quantified as described previously (31626976) and sputum samples containing 20 µg/mL of active neutrophil elastase were used to assess the activity of peptides in 16HBE14o- cells in the presence of CF sputum. Briefly, cells were seeded in 96-well plates (2*10⁴ cells/well) and incubated for at least 16/18 h at 37°C with 5% CO₂ before experiments. Subsequently, peptides were diluted in PBS at a final concentration of 25 µM and a PBS: sputum mixture (1:1) was added on the top of adherent cells (100 µl/well) and cAMP levels were quantified at the indicated time points using the Promega cAMP-Glo™ Assay kit (Promega, Milano, IT), according to the manufacturer's protocol.

PAMPA assay

To assess the permeability of peptides through a CF sputum layer, a parallel artificial membrane permeability system (PAMPA) (Corning Gentest Pre-coated PAMPA, 353015, USA plates) that allows to measure the ability of drugs to diffuse from a donor compartment, through an artificial membrane, into an acceptor compartment, was used as described previously²⁶. The bottom wells of the PAMPA system ("acceptor" wells) were filled with 300 µL of PBS (10mM, 150 mM NaCl, pH 7.4), while "donor" wells were filled with 200 µL of the peptide solution (2 mg/mL in 10mM PBS, 150 mM NaCl, pH 7.4), in the absence or in the presence of CF sputum. In the latter case, 40 µL of CF sputum was first deposited over the PAMPA membrane, and the peptide

solution was subsequently added over the CF sputum layer. Afterwards, the two wells were coupled and incubated for 5 h at RT. At the end of the incubation, the plates were splitted and the amount of peptide diffused into the acceptor well was quantified by fluorescence spectroscopy using a Horiba Jobin Yvon Fluorolog 3 TCSPC fluorimeter (Horiba, Kyoto, Japan) equipped with a 450-W xenon lamp and a R928 photomultiplier (Hamamatsu Photonics, Hamamatsu, Japan). Excitation was performed at 280nm while emission was recorded the wavelength region 290-500 nm (maximum of emission at 362 nm). Excitation and emission slits were set at 4 and 5 nm, respectively. The concentration of the peptide was calculated using a 6-points calibration curve. The apparent permeability coefficient (P_{app}) was expressed according to this relationship:

$$P_{app} = \frac{dQ/dt}{C_0 \times A}$$

derived from Fick's law for steady-state conditions²⁷, where dQ is the quantity of peptide expressed as moles permeated into the acceptor compartment at time t (18000 sec), C_0 is the initial concentration of the peptide in the donor well, and A is the area of the well membrane (0.3 cm²).

PKA-RII α bioconjugation and fluorescence spectroscopy

Recombinant PKA-RII α was bio-conjugated to fluorescein 5-maleimide (F5M), as described previously²⁸ using 75 μ g of PKA-RII α and a 50-fold excess of F5M. After bioconjugation, the derivative was immediately purified using a Sephadex® G-25 desalting column and phosphate-buffered saline solution (PBS) (20 mM, 150 mM NaCl, pH 7.2) as eluent. To evaluate F5M labelling efficiency, the dye/protein ratio (D/P) of the

conjugates was determined by the absorption spectra of the labelled proteins in PBS (20 mM, 150 mM NaCl, pH 7.2), according to the following equation:

$$\frac{D}{P} = \frac{A_{max} e_{prot}}{(A_{280} - cA_{max}) e_{dye}}$$

where A_{280} is the absorption of the conjugate at 280 nm; A_{max} is the absorption of the conjugate at the absorption maximum of the corresponding F5M; c is a correction factor (which must be used to normalize the A_{280} signal because fluorescent dyes (i.e. F5M) also absorb at 280 nm and equals the A_{280} of the dye divided by the A_{max} of the dye ($c = 0.29$); e_{prot} ($25,169 \text{ M}^{-1}\text{cm}^{-1}$) and e_{dye} ($63,096 \text{ M}^{-1} \text{ cm}^{-1}$) are the molar extinction coefficients of PKA and F5M, respectively. PKA-RII α presents six cysteine residues, and the final D/P value was 0.2.

UV-visible absorption spectra were measured with a UH5300 spectrophotometer (Hitachi, Tokyo, Japan) at RT, using 1 cm pathway length quartz cuvette. Fluorescence emission spectra in steady-state mode were acquired at RT using a Jobin Yvon Fluorolog 3 TCSPC fluorimeter (Horiba, Kyoto, Japan) equipped with a 450-W Xenon lamp and a R928 photomultiplier (Hamamatsu Photonics, Hamamatsu, Japan). Steady-state fluorescence spectra were recorded in the 500-600 nm range. The excitation wavelength was set on 490 nm and the excitation and emission slits were set on 2 and 4, respectively. Equilibrium binding constants (K_D and K_A) were obtained from steady-state data.

Fluorescence kinetics were measured using an Applied Photophysics SX20 stopped-flow spectrophotometer (Applied Photophysics, North Carolina, US) fitted with a 495 nm cut-off filter between the cell and the fluorescence detector and equipped with a thermostat bath set at $25 \pm 0.2^\circ\text{C}$. Association

and dissociation rate constants (k_{on} and k_{off}) were calculated from stopped-flow kinetics data. Data acquisition, visualization and analysis were performed with Pro-Data software from Applied Photophysics Ltd (Applied Photophysics, North Carolina, US).

To assess the ability of DRI-Pep#20 to displace the binding between PI3K γ and PKA-F5M, steady-state emission spectra of the PI3K γ /PKA-F5M complex in the presence of increasing concentrations of the peptide were acquired. Briefly, 50 nM of recombinant PI3K γ was added to 100 nM F5M-bound PKA-R11 α in a total volume of 100 μ L PBS. The concentration of the PI3K γ /PKA-F5M complex was kept constant while gradually titrated with increasing concentrations of the peptide from 0 to 5 μ M. The complex was excited at 490 nm and emission spectra were recorded in the 500-600 nm spectral range, as described above. The degree of displacement of the PKA-R11 α -PI3K γ complex was expressed as the percentage of fluorescence quenching after addition of the peptide.

Circular dichroism

Circular dichroism (CD) measurements were performed on a Jasco-810 Dichrograph equipped with a Peltier thermoelectric controller (Jasco Inc., Easton, US). The spectra of peptides were recorded in the continuous mode between 260 and 180 nm at 25 °C in 0.1 cm path length quartz cuvette (Hellma GmbH, Müllheim, DE) with a total peptide concentration of 0.2 mg/mL dissolved in 2 mM PBS (0.6 mM KH₂PO₄, 1.6 mM K₂HPO₄), pH 7.4. The CD spectrum in the 190-240 nm range was used to predict the secondary structural content of the peptide using the K2D3

web server²⁹.

Transmission Electron Microscopy (TEM) and Dynamic Light Scattering (DLS)

Self-assembled peptide nanostructures were analyzed by Transmission Electron Microscopy (TEM) analysis. Transmission electron micrographs were obtained with a JEOL 3010-UHR TEM operating at an accelerating voltage of 300.00 kV (JEOL, Tokyo, Japan). TEM samples were prepared by dissolving the peptides at 0.1 mg/mL in water and drying them on a carbon-coated copper grid. The nominal magnification used to record nanostructures were $\times 500000$ and $\times 800000$.

The size distribution profile of the self-assembled peptide was determined by dynamic light scattering (DLS, Malvern Zetasizer, Worcestershire, UK). Samples were prepared at 4 mg/mL in 2 mM PBS (0.6 mM KH_2PO_4 , 1.6 mM K_2HPO_4), pH 7.4. Measurements were performed after an equilibration time of 60 s which allowed samples to reach the temperature of 25°C.

PKA-RII α structure prediction

The 3D structure of residues 1-45 of PKA-RII α (SEQ ID No.: 14 - MSHIQIPPGLTELLQGYTVEVLRQPPDLVEFAVEYFTRLREARA) was predicted using the Iterative Threading ASSEmblY Refinement (I-TASSER) web server³⁰, an on-line platform that implements I-TASSER-based algorithms for predictions of protein structure and function. Briefly, starting from the FASTA amino acid sequence I-TASSER ran a three steps simulation, first threading it through a representative PDB structure library to search for possible template folds or supersecondary-structure

fragments, using a profile-profile alignment-based threading algorithm. In the second step, the continuous fragments excised from the PDB templates were reassembled into full-length models, while the unaligned regions were built by ab initio modeling. Finally, the structure trajectories were clustered, and the lowest-energy structures selected, and an all-atom model was constructed by REMO41 through optimization of the hydrogen-bonding network. The five best models obtained by I-TASSER were subsequently evaluated based on their threading template and predicted C-score. The model with the highest C-score of -0.22 and predicted using the NMR structure of PKA-RIIa as a threading template (PDB ID 2KYG)³¹ was selected.

DRI-Pep#20 Structure Prediction

The structure of DRI-Pep#20 was predicted with PEP-FOLD3.5³⁴, a de novo approach that predicts peptide structures from amino acid sequences. Briefly, starting from the amino acid sequence, first a series of 200 simulations was run, each one sampling a different region of the conformational space using the Generator taboo-sampling 5 (ts5), recommended for peptides longer than 10 amino acids. The output was an archive of clusters of all the models sorted out using the TM score followed by performing the Model Quality assessment using Apollo³⁵. The first five models, representing the five best conformation of each cluster with the best scores defined according to the lowest soPEP energy and the highest TM-score value, were selected and further supported by RMSD. Finally, the best structure of the peptide was validated by visual analysis on PYMOL.

PKA-RII α -DRI-Pep#20 docking

PKA-RII α -DRI-Pep#20 docking studies were performed with the High Ambiguity Driven Biomolecular DOCKing (HADDOCK) software. Within the HADDOCK process, the residues 1-45 of PKA-RII α were selected as the active residues and enforced to be part of the interface by applying ambiguous interaction restraints. Briefly, starting from the PKA-RII α and the DRI-Pep#20 structure, the HADDOCK docking ran three consecutive steps, first the molecules were randomly oriented, and a rigid-body search was performed (it0). The output was an archive of 1000 models, among them the top 200 ranked structures were selected based on the energy function and addressed to the semi-flexible simulated annealing stage performed in torsion angle space (it1). In the third stage, the structures were refined in Cartesian space with explicit solvent layer (water) and subjected to a short molecular dynamic simulation at 300K. During the refinement, both the side chain and backbone of interface residues were progressively allowed to move.

The final models were automatically clustered based on the positional interface ligand RMSD (iL-RMSD) by fitting the conformational changes on the interface of the receptor (PKA-RII α) and on the interface of the smaller partner (the peptides). Finally, the protein-peptide binding poses were assessed by the HADDOCK report and the binding affinity was evaluated by the Optimal Hydrogen Bonding Network. The resulting best binding pose was validated by visual analysis on PYMOL.

Statistical analysis

Data are presented as scatter plots with bars (means \pm SEM). Prism software (GraphPad Software Inc.) was used for statistical analysis. Raw data were first analyzed to confirm their normal distribution via the Shapiro-Wilk test and then analyzed by unpaired Student's t test, one-way analysis of variance (ANOVA), or two-way ANOVA. Bonferroni correction (one-way and two-way ANOVA) was applied to correct for multiple comparisons. $P < 0.05$ was considered significant.

References

1. Omar, M. H.; Scott, J. D., AKAP Signaling Islands: Venues for Precision Pharmacology. *Trends Pharmacol Sci* **2020**, *41* (12), 933-946.
2. Ghigo, A.; Murabito, A.; Sala, V.; Pisano, A. R.; Bertolini, S.; Gianotti, A.; Caci, E.; Montresor, A.; Premchandrar, A.; Pirozzi, F.; Ren, K.; Della Sala, A.; Mergiotti, M.; Richter, W.; de Poel, E.; Matthey, M.; Caldrrer, S.; Cardone, R. A.; Civiletti, F.; Costamagna, A.; Quinney, N. L.; Butnarasu, C.; Visentin, S.; Ruggiero, M. R.; Baroni, S.; Crich, S. G.; Ramel, D.; Laffargue, M.; Tocchetti, C. G.; Levi, R.; Conti, M.; Lu, X. Y.; Melotti, P.; Sorio, C.; De Rose, V.; Facchinetti, F.; Fanelli, V.; Wenzel, D.; Fleischmann, B. K.; Mall, M. A.; Beekman, J.; Laudanna, C.; Gentzsch, M.; Lukacs, G. L.; Pedemonte, N.; Hirsch, E., A PI3Kgamma mimetic peptide triggers CFTR gating, bronchodilation, and reduced inflammation in obstructive airway diseases. *Sci Transl Med* **2022**, *14* (638), eabl6328.
3. Zaccolo, M.; Zerio, A.; Lobo, M. J., Subcellular Organization of the cAMP Signaling Pathway. *Pharmacol Rev* **2021**, *73* (1), 278-309.
4. Murabito, A.; Cnudde, S.; Hirsch, E.; Ghigo, A., Potential therapeutic applications of AKAP disrupting peptides. *CLINICAL SCIENCE* **2020**, *134* (24).
5. Perino, A.; Ghigo, A.; Ferrero, E.; Morello, F.; Santulli, G.; Baillie, G.; Damilano, F.; Dunlop, A.; Pawson, C.; Walser, R.; Levi, R.; Altruda, F.; Silengo, L.; Langeberg, L.; Neubauer, G.; Heymans, S.; Lembo, G.; Wymann, M.; Wetzker, R.; Houslay, M.; Iaccarino, G.; Scott, J.; Hirsch, E., Integrating Cardiac PIP(3) and cAMP Signaling through a PKA Anchoring Function of p110 γ . *MOLECULAR CELL* **2011**, *42*.
6. Lopes, J. L.; Miles, A. J.; Whitmore, L.; Wallace, B. A., Distinct circular dichroism spectroscopic signatures of polyproline II and unordered secondary structures: applications in secondary structure analyses. *Protein Sci* **2014**, *23* (12), 1765-72.
7. d'Angelo, I.; Conte, C.; La Rotonda, M. I.; Miro, A.; Quaglia, F.; Ungaro, F., Improving the efficacy of inhaled drugs in cystic fibrosis: challenges and emerging drug delivery strategies. *Adv Drug Deliv Rev* **2014**, *75*, 92-111.
8. Boegh, M.; Nielsen, H. M., Mucus as a barrier to drug delivery - understanding and mimicking the barrier properties. *Basic Clin Pharmacol Toxicol* **2015**, *116* (3), 179-86.
9. Gramegna, A.; Amati, F.; Terranova, L.; Sotgiu, G.; Tarsia, P.; Miglietta, D.; Calderazzo, M. A.; Aliberti, S.; Blasi, F., Neutrophil elastase in bronchiectasis. *Respir Res* **2017**, *18* (1), 211.
10. Hobbs, C. A.; Blanchard, M. G.; Alijevic, O.; Tan, C. D.; Kellenberger, S.; Bencharit, S.; Cao, R.; Kesimer, M.; Walton, W. G.; Henderson, A. G.; Redinbo, M. R.; Stutts, M. J.;

Tarran, R., Identification of the SPLUNC1 ENaC-inhibitory domain yields novel strategies to treat sodium hyperabsorption in cystic fibrosis airway epithelial cultures. *Am J Physiol Lung Cell Mol Physiol* **2013**, 305 (12), L990-L1001.

11. Mall, M. A.; Criner, G. J.; Miravittles, M.; Rowe, S. M.; Vogelmeier, C. F.; Rowlands, D. J.; Schoenberger, M.; Altman, P., Cystic fibrosis transmembrane conductance regulator in COPD: a role in respiratory epithelium and beyond. *Eur Respir J* **2023**, 61 (4).

12. Parodi, A.; Righetti, G.; Pesce, E.; Salis, A.; Tomati, V.; Pastorino, C.; Tasso, B.; Benvenuti, M.; Damonte, G.; Pedemonte, N.; Cichero, E.; Millo, E., Journey on VX-809-Based Hybrid Derivatives towards Drug-like F508del-CFTR Correctors: From Molecular Modeling to Chemical Synthesis and Biological Assays. *Pharmaceuticals (Basel)* **2022**, 15 (3).

13. Mall, M. A.; Mayer-Hamblett, N.; Rowe, S. M., Cystic Fibrosis: Emergence of Highly Effective Targeted Therapeutics and Potential Clinical Implications. *Am J Respir Crit Care Med* **2020**, 201 (10), 1193-1208.

14. Byrne, D. P.; Omar, M. H.; Kennedy, E. J.; Eyers, P. A.; Scott, J. D., Biochemical Analysis of AKAP-Anchored PKA Signaling Complexes. *Methods Mol Biol* **2022**, 2483, 297-317.

15. Garton, M.; Nim, S.; Stone, T. A.; Wang, K. E.; Deber, C. M.; Kim, P. M., Method to generate highly stable D-amino acid analogs of bioactive helical peptides using a mirror image of the entire PDB. *Proceedings of the National Academy of Sciences of the United States of America* **2018**, 115 (7), 1505-1510.

16. Veine, D. M.; Yao, H.; Stafford, D. R.; Fay, K. S.; Livant, D. L., A D-amino acid containing peptide as a potent, noncovalent inhibitor of alpha5beta1 integrin in human prostate cancer invasion and lung colonization. *Clin Exp Metastasis* **2014**, 31 (4), 379-93.

17. Casey, M.; Gabillard-Lefort, C.; McElvaney, O. F.; McElvaney, O. J.; Carroll, T.; Heeney, R. C.; Gunaratnam, C.; Reeves, E. P.; Murphy, M. P.; McElvaney, N. G., Effect of elexacaftor/tezacaftor/ivacaftor on airway and systemic inflammation in cystic fibrosis. *Thorax* **2023**, 78 (8), 835-839.

18. Schaupp, L.; Addante, A.; Voller, M.; Fentker, K.; Kuppe, A.; Bardua, M.; Duerr, J.; Piehler, L.; Rohmel, J.; Thee, S.; Kirchner, M.; Ziehm, M.; Lauster, D.; Haag, R.; Gradzielski, M.; Stahl, M.; Mertins, P.; Boutin, S.; Graeber, S. Y.; Mall, M. A., Longitudinal effects of elexacaftor/tezacaftor/ivacaftor on sputum viscoelastic properties, airway infection and inflammation in patients with cystic fibrosis. *Eur Respir J* **2023**, 62 (2).

19. Ibrahim, B. M.; Park, S.; Han, B.; Yeo, Y., A strategy to deliver genes to cystic fibrosis lungs: a battle with environment. *J Control Release* **2011**, 155 (2), 289-95.

20. Capurro, V.; Tomati, V.; Sondo, E.; Renda, M.;

Borrelli, A.; Pastorino, C.; Guidone, D.; Venturini, A.; Giraudo, A.; Mandrup Bertozzi, S.; Musante, I.; Bertozzi, F.; Bandiera, T.; Zara, F.; Galietta, L. J. V.; Pedemonte, N., Partial Rescue of F508del-CFTR Stability and Trafficking Defects by Double Corrector Treatment. *International journal of molecular sciences* **2021**, *22* (10).

21. Graeber, S. Y.; Vitzthum, C.; Pallenberg, S. T.; Naehrlich, L.; Stahl, M.; Rohrbach, A.; Drescher, M.; Minso, R.; Ringshausen, F. C.; Rueckes-Nilges, C.; Klajda, J.; Berges, J.; Yu, Y.; Scheuermann, H.; Hirtz, S.; Sommerburg, O.; Dittrich, A. M.; Tummler, B.; Mall, M. A., Effects of Elexacaftor/Tezacaftor/Ivacaftor Therapy on CFTR Function in Patients with Cystic Fibrosis and One or Two F508del Alleles. *Am J Respir Crit Care Med* **2022**, *205* (5), 540-549.

22. Veit, G.; Roldan, A.; Hancock, M. A.; Da Fonte, D. F.; Xu, H.; Hussein, M.; Frenkiel, S.; Matouk, E.; Velkov, T.; Lukacs, G. L., Allosteric folding correction of F508del and rare CFTR mutants by elexacaftor-tezacaftor-ivacaftor (Trikafta) combination. *JCI insight* **2020**, *5* (18).

23. Nichols, D. P.; Morgan, S. J.; Skalland, M.; Vo, A. T.; Van Dalfsen, J. M.; Singh, S. B.; Ni, W.; Hoffman, L. R.; McGeer, K.; Heltshe, S. L.; Clancy, J. P.; Rowe, S. M.; Jorth, P.; Singh, P. K.; Group, P. R.-M. S., Pharmacologic improvement of CFTR function rapidly decreases sputum pathogen density, but lung infections generally persist. *The Journal of clinical investigation* **2023**, *133* (10).

24. Uppalapati, M.; Lee, D. J.; Mandal, K.; Li, H.; Miranda, L. P.; Lowitz, J.; Kenney, J.; Adams, J. J.; Ault-Riche, D.; Kent, S. B.; Sidhu, S. S., A Potent d-Protein Antagonist of VEGF-A is Nonimmunogenic, Metabolically Stable, and Longer-Circulating in Vivo. *ACS chemical biology* **2016**, *11* (4), 1058-65.

25. Oriano, M.; Terranova, L.; Sotgiu, G.; Sadari, L.; Bellofiore, A.; Retucci, M.; Marotta, C.; Gramegna, A.; Miglietta, D.; Carnini, C.; Marchisio, P.; Chalmers, J. D.; Aliberti, S.; Blasi, F., Evaluation of active neutrophil elastase in sputum of bronchiectasis and cystic fibrosis patients: A comparison among different techniques. *Pulm Pharmacol Ther* **2019**, *59*, 101856.

26. Butnarasu, C.; Caron, G.; Pacheco, D. P.; Petrini, P.; Visentin, S., Cystic Fibrosis Mucus Model to Design More Efficient Drug Therapies. *Mol Pharm* **2022**, *19* (2), 520-531.

27. Sharifian Gh, M., Recent Experimental Developments in Studying Passive Membrane Transport of Drug Molecules. *Mol Pharm* **2021**, *18* (6), 2122-2141.

28. Hermanson, G. T., *Bioconjugate Techniques*. 2008.

29. Louis-Jeune, C.; Andrade-Navarro, M. A.; Perez-Iratxeta, C., Prediction of protein secondary structure from circular dichroism using theoretically derived spectra. *Proteins* **2012**, *80* (2), 374-81.

30. Yang, J.; Yan, R.; Roy, A.; Xu, D.; Poisson, J.; Zhang, Y., The I-TASSER Suite: protein structure and function prediction. *Nat Methods* **2015**, *12* (1), 7-8.
31. Corpora, T.; Roudaia, L.; Oo, Z. M.; Chen, W.; Manuylova, E.; Cai, X.; Chen, M. J.; Cierpicki, T.; Speck, N. A.; Bushweller, J. H., Structure of the AML1-ETO NHR3-PKA(RIIalpha) complex and its contribution to AML1-ETO activity. *J Mol Biol* **2010**, *402* (3), 560-77.
32. Jumper, J.; Evans, R.; Pritzel, A.; Green, T.; Figurnov, M.; Ronneberger, O.; Tunyasuvunakool, K.; Bates, R.; Zidek, A.; Potapenko, A.; Bridgland, A.; Meyer, C.; Kohl, S. A. A.; Ballard, A. J.; Cowie, A.; Romera-Paredes, B.; Nikolov, S.; Jain, R.; Adler, J.; Back, T.; Petersen, S.; Reiman, D.; Clancy, E.; Zielinski, M.; Steinegger, M.; Pacholska, M.; Berghammer, T.; Bodenstein, S.; Silver, D.; Vinyals, O.; Senior, A. W.; Kavukcuoglu, K.; Kohli, P.; Hassabis, D., Highly accurate protein structure prediction with AlphaFold. *Nature* **2021**, *596* (7873), 583-589.
33. Rathinaswamy, M. K.; Dalwadi, U.; Fleming, K. D.; Adams, C.; Stariha, J. T. B.; Pardon, E.; Baek, M.; Vadas, O.; DiMaio, F.; Steyaert, J.; Hansen, S. D.; Yip, C. K.; Burke, J. E., Structure of the phosphoinositide 3-kinase (PI3K) p110gamma-p101 complex reveals molecular mechanism of GPCR activation. *Sci Adv* **2021**, *7* (35).
34. Lamiable, A.; Thevenet, P.; Rey, J.; Vavrusa, M.; Derreumaux, P.; Tuffery, P., PEP-FOLD3: faster de novo structure prediction for linear peptides in solution and in complex. *Nucleic acids research* **2016**, *44* (W1), W449-54.
35. Wang, Z.; Eickholt, J.; Cheng, J., APOLLO: a quality assessment service for single and multiple protein models. *Bioinformatics* **2011**, *27* (12), 1715-6.

CLAIMS

1. A non-natural peptide having the ability of inhibiting the A-kinase anchoring function of PI3K γ comprising an amino acid sequence as set forth in SEQ ID No.: 1, wherein each amino acid is a D-amino acid, and wherein the glutamine at position 3 and the glycine at position 4 can be substituted with any amino acid with similar hydrophobicity, hydrophilicity, charge and size, respectively.

2. The non-natural peptide according to claim 1, wherein the peptide further comprises a cell penetrating peptide.

3. The non-natural peptide according to claim 2, wherein the cell penetrating peptide is selected from Penetratin (pAntp), HIV TAT peptide, R7 peptide, KALA peptide, Buforin 2, MAP, Transportan, Transportan 10, pVEC, MPG peptide.

4. The non-natural peptide according to claim 2 or claim 3, wherein the peptide further comprises a linker conjugating the amino acid sequence of SEQ ID No.: 1 with the cell penetrating peptide.

5. The non-natural peptide according to claim 4, wherein the linker is an amino acid linker comprising one or more glycine amino acids and/or one or more amino acids with hydrophobicity, hydrophilicity, charge, and size similar to glycine.

6. The non-natural peptide according to any one of the

preceding claims having an amino acid sequence as set forth in SEQ ID No.: 2.

7. The non-natural peptide according to any one of the preceding claims for use as a medicament.

8. The non-natural peptide according to any one of the preceding claims for use in treating respiratory diseases, preferably broncho-obstructive diseases.

9. The non-natural peptide for use according to claim 8, wherein the respiratory diseases are selected from allergic asthma, cystic fibrosis, chronic obstructive pulmonary disease, non-cystic fibrosis bronchiectasis, pulmonary hypertension, and idiopathic pulmonary fibrosis.

10. The non-natural peptide for use according to any one of claims 7 to 9, wherein the non-natural peptide is suitable for administration by inhalation.

11. A product comprising:

i) at least one non-natural peptide according to any one of claims 1 to 6, and

ii) at least one potentiator of the cystic fibrosis transmembrane conductance regulator (CFTR) and/or at least one corrector of the cystic fibrosis transmembrane conductance regulator (CFTR) as a combined preparation for sequential, simultaneous or separate use in treating respiratory diseases.

12. Product according to claim 11, wherein the potentiator

of the cystic fibrosis transmembrane conductance regulator (CFTR) is selected from Ivacaftor, Navocaftor and Deutivacaftor.

13. Product according to claim 11 or claim 12, wherein the corrector of the cystic fibrosis transmembrane conductance regulator (CFTR) is selected from Lumacaftor, Tezacaftor, Elaxacaftor, Galicaftor and Vanzacaftor.

14. A pharmaceutical composition comprising at least one non-natural peptide according to any one of claims 1 to 6 and a pharmaceutically acceptable vehicle.

Abstract

A non-natural peptide having the ability of inhibiting the A-kinase anchoring function of PI3K γ comprising an amino acid sequence as set forth in SEQ ID No.: 1, wherein each amino acid is a D-amino acid, therapeutic uses and composition thereof.

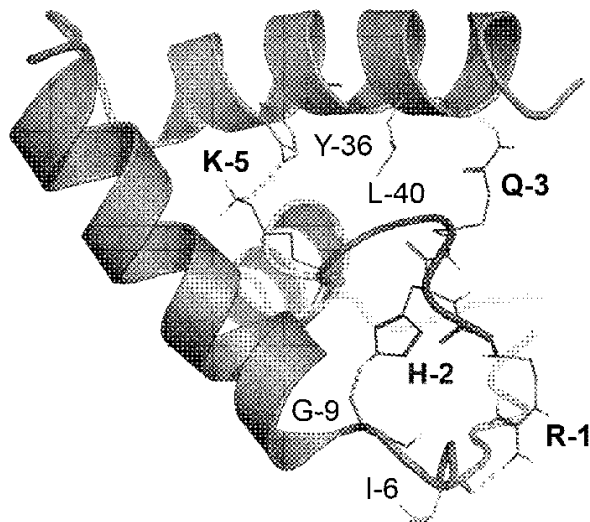
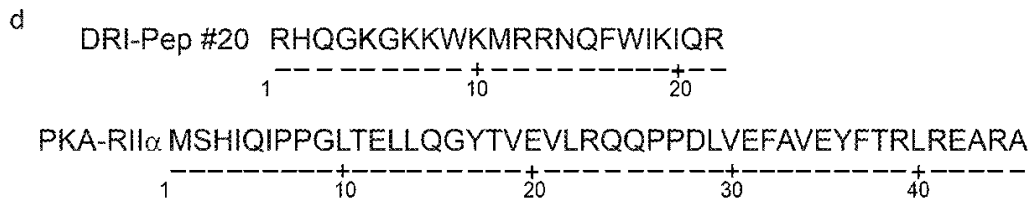
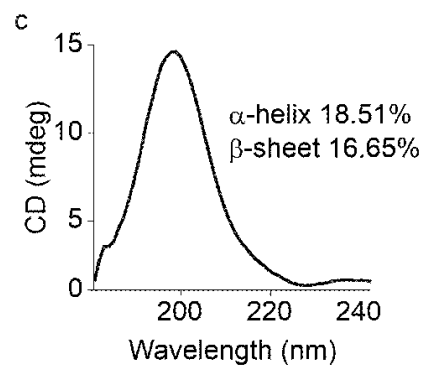
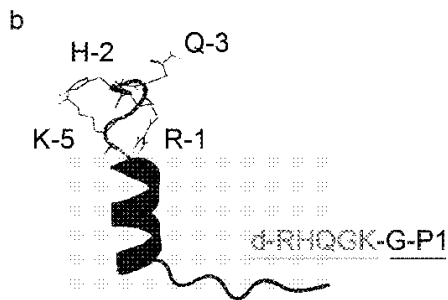
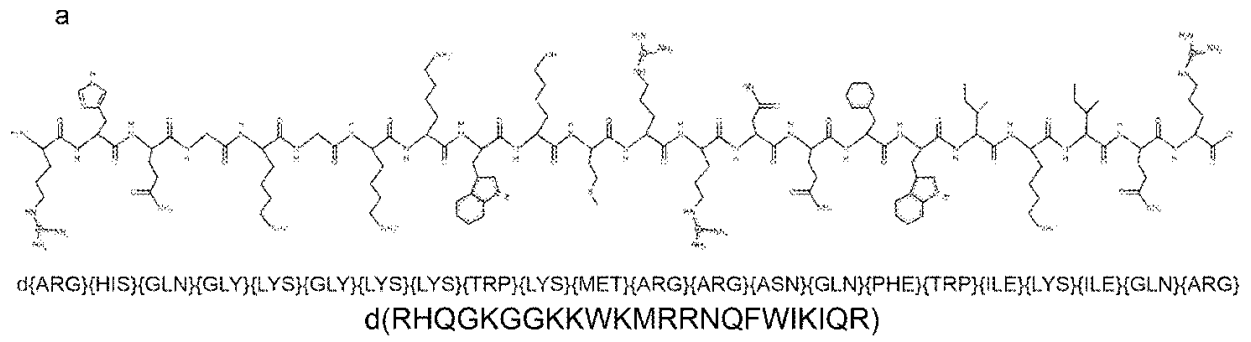


Figure 1

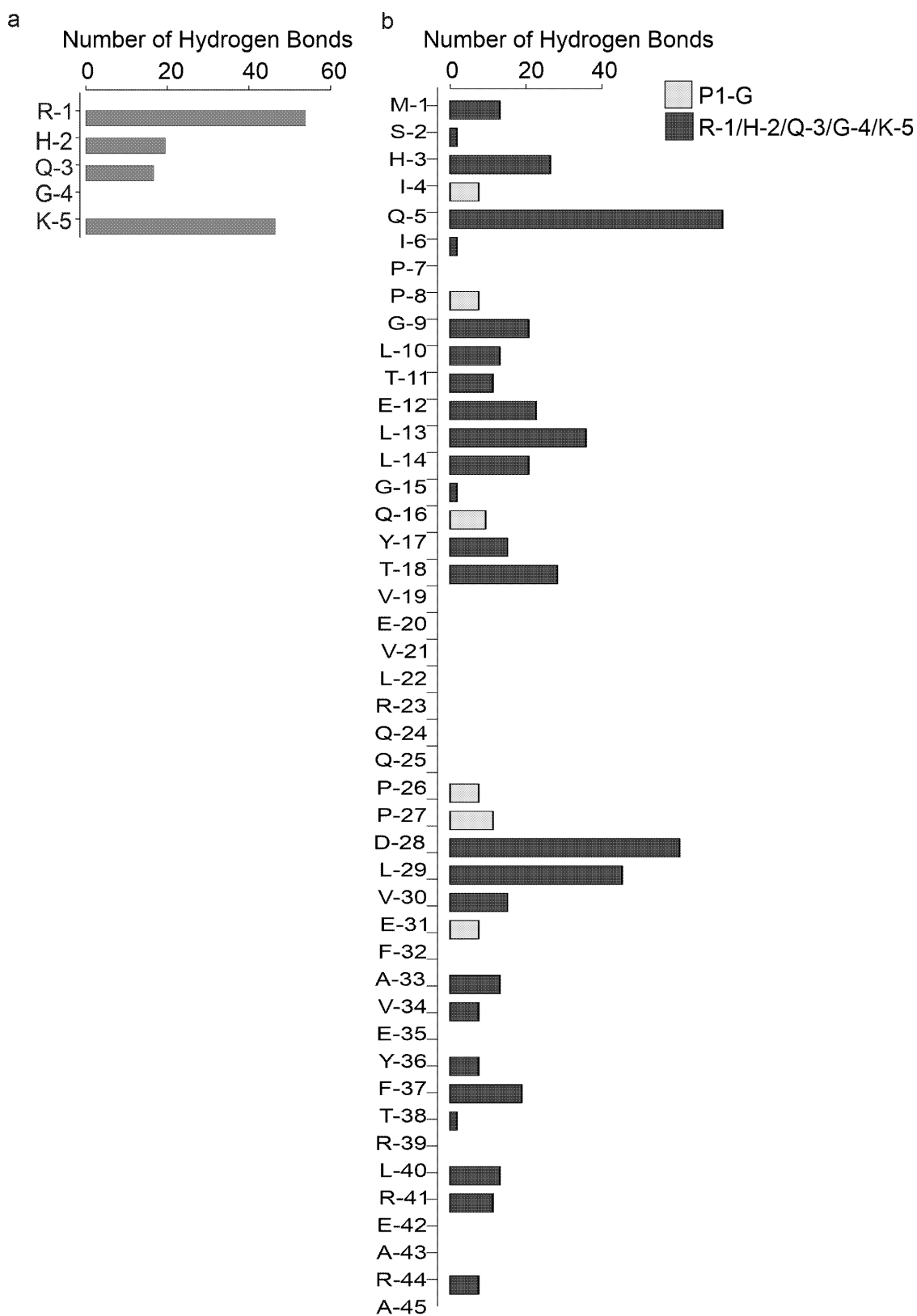


Figure 2

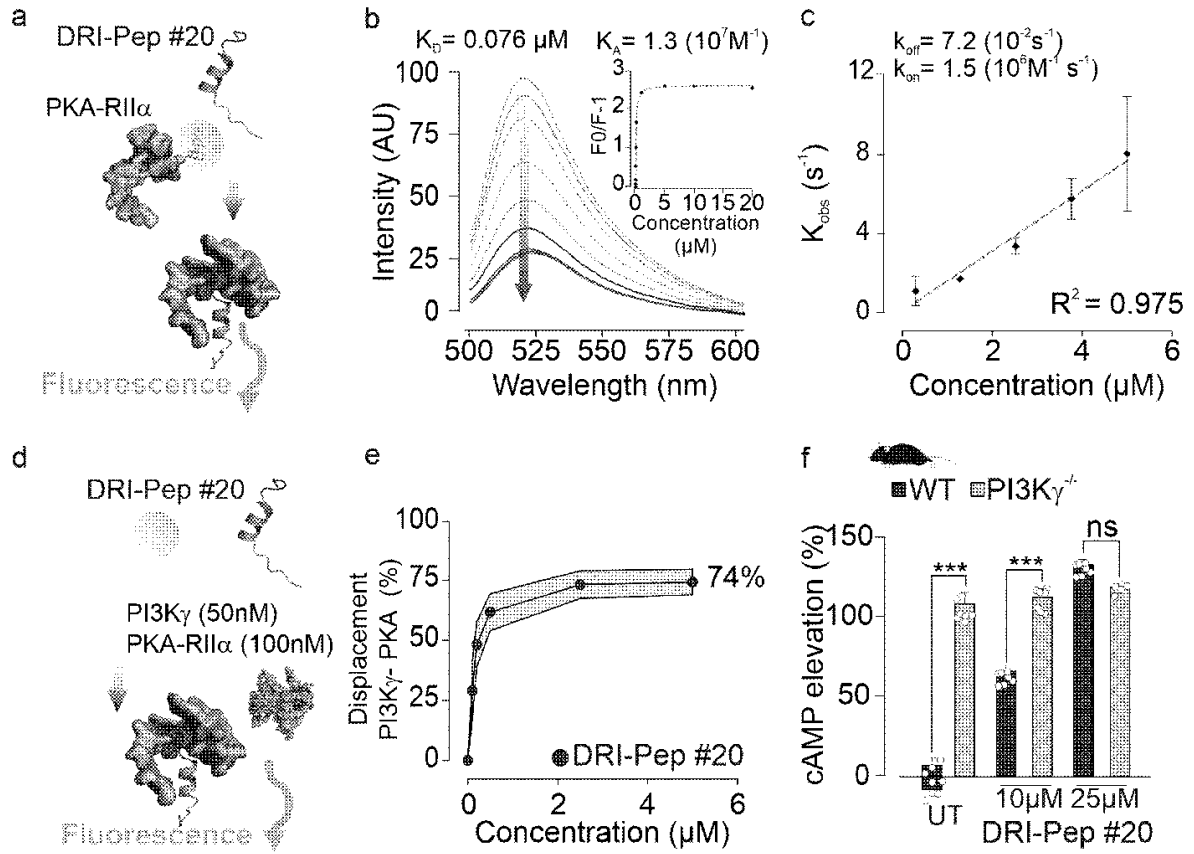


Figure 3

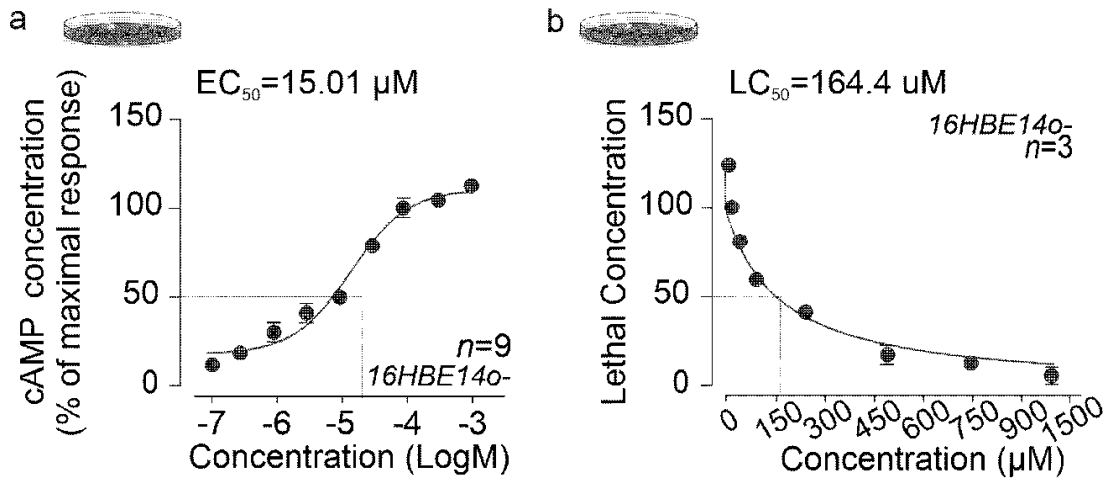


Figure 4

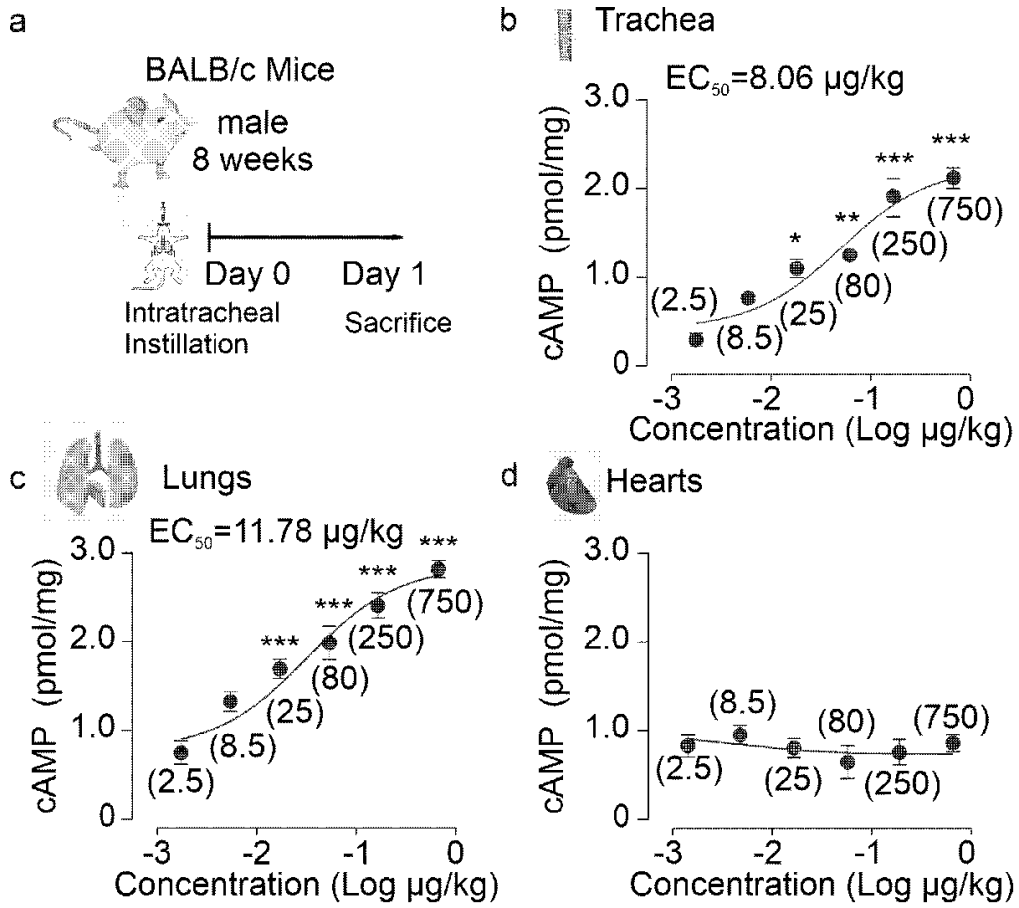


Figure 5

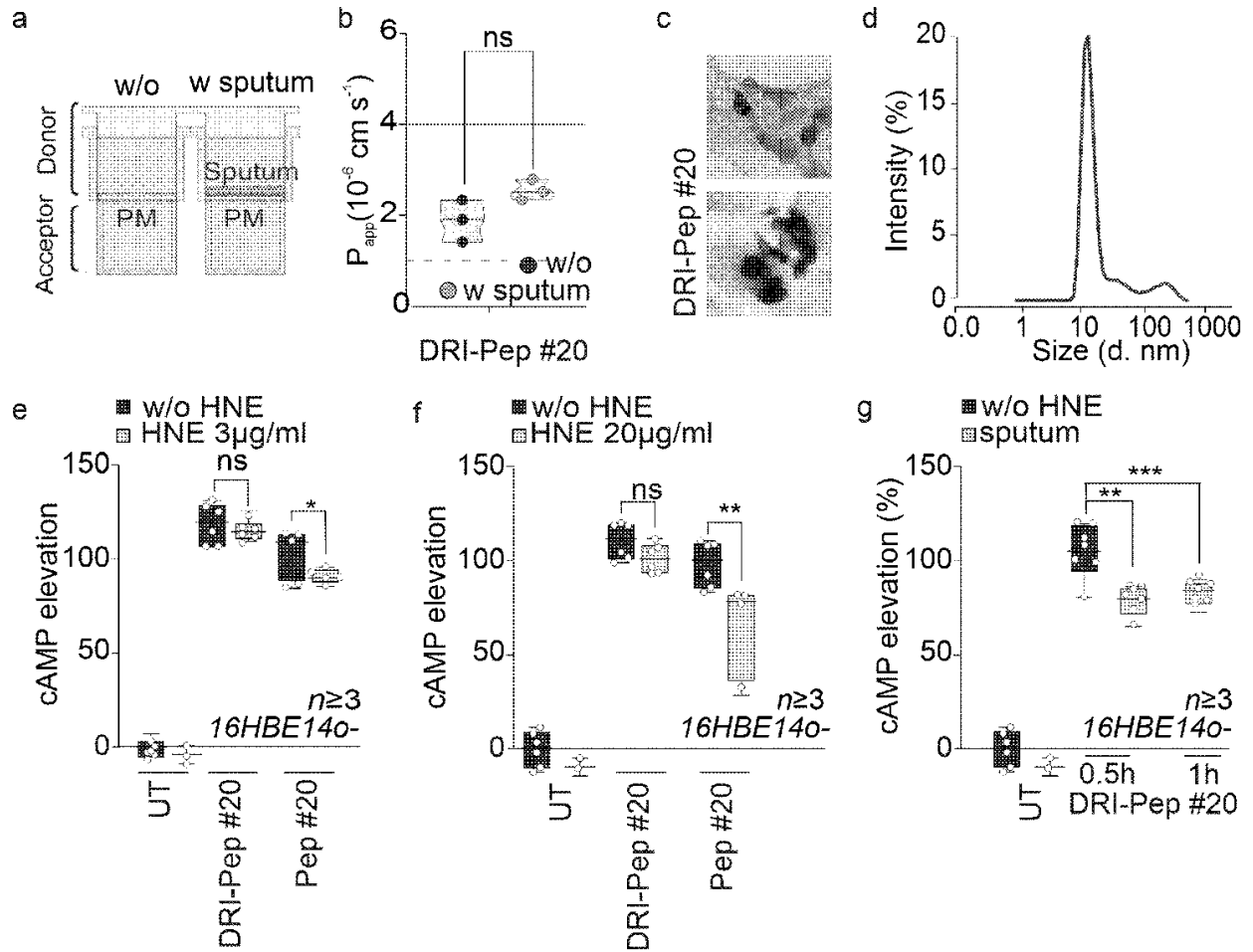


Figure 6

a

Expasy		PeptideCutter	
Peptide	Name of enzyme	No. of cleavages	Positions of cleavage sites
DRI-Pep #20	Neutrophil elastase	/	/
DRI-Pep #20	RHQGKGKKWKMRRNQFWIKIQR		
		1	10 22

b

Expasy		PROSPER Protease specificity prediction server	
Peptide	Name of enzyme	No. of cleavages	Positions of cleavage sites
DRI-Pep #20	Trypsin (Try)	9	1-5-7-8-10-12-13-19-22
	Arg-C Proteinase (ArgC)	4	1-12-13-22
	Serine protease	1	20
	Metallo protease	2	10-19
	Cysteine protease	/	/
	Aspartic protease	/	/
DRI-Pep #20	RHQGKGKKWKMRRNQFWIKIQR		
	ArgC-TRY TRY	1	10 22

Figure 7

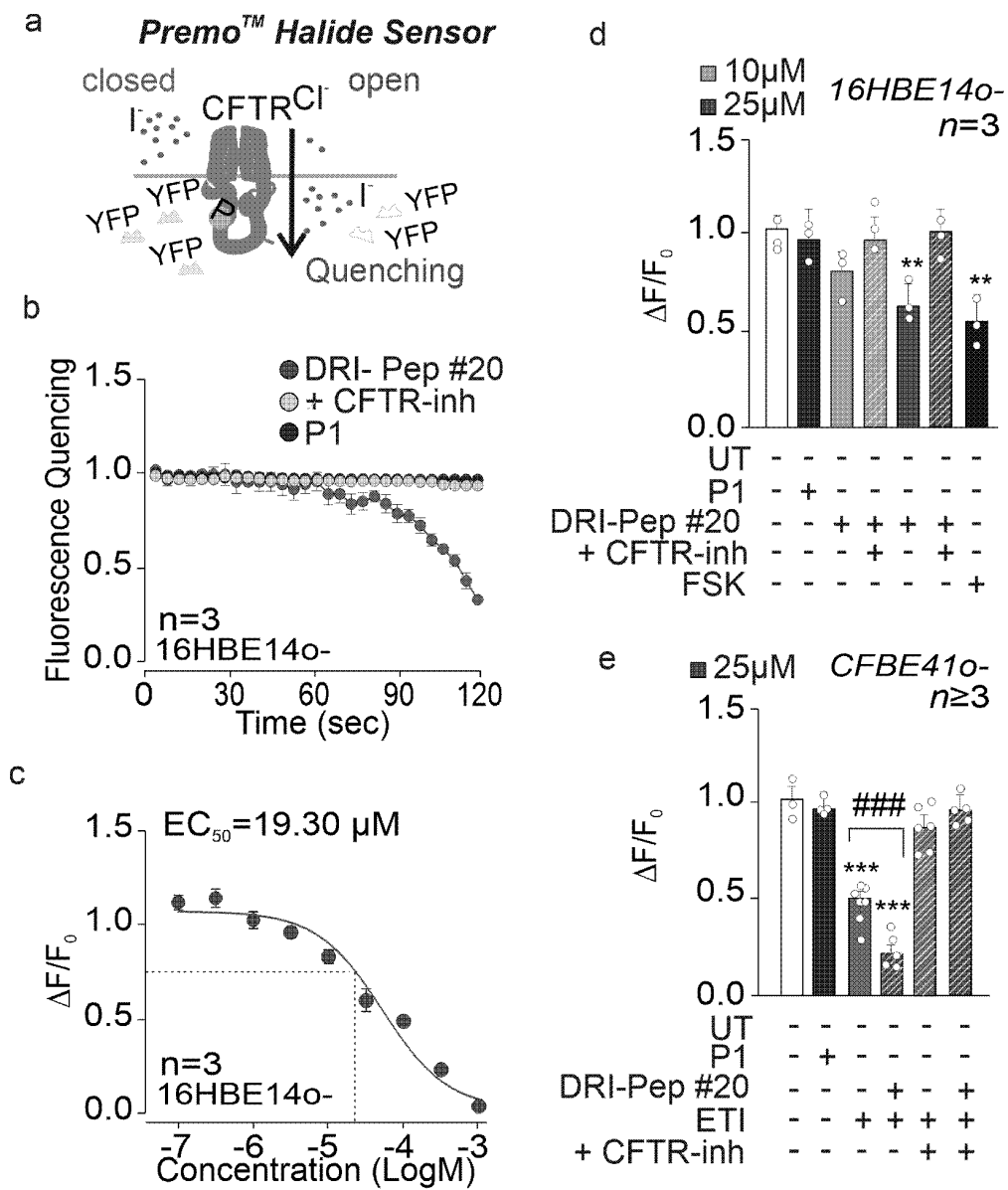


Figure 8

Cellular and Molecular Life Sciences

A Non-natural Peptide Targeting the A-kinase Anchoring Function of PI3Kg for Therapeutic cAMP Modulation in Pulmonary Cells

--Manuscript Draft--

Manuscript Number:													
Full Title:	A Non-natural Peptide Targeting the A-kinase Anchoring Function of PI3Kg for Therapeutic cAMP Modulation in Pulmonary Cells												
Article Type:	Original Article												
Corresponding Author:	Alessandra Ghigo Universita degli Studi di Torino ITALY												
Corresponding Author Secondary Information:													
Corresponding Author's Institution:	Universita degli Studi di Torino												
Corresponding Author's Secondary Institution:													
First Author:	Angela Della Sala												
First Author Secondary Information:													
Order of Authors:	Angela Della Sala Laura Tasca Cosmin Butnarusu Valentina Sala Giulia Prono Alessandra Murabito Enrico Millo Leonardo Terranova Francesco Blasi Andrea Gramegna Stefano Aliberti Alberto Massarotti Sonja Visentin Emilio Hirsch Alessandra Ghigo												
Order of Authors Secondary Information:													
Funding Information:	<table border="1" style="width: 100%;"> <tr> <td>Fondazione Cariplo (2018-0498)</td> <td>Dr. Emilio Hirsch</td> </tr> <tr> <td>Roche Italia (Bando Roche per la Ricerca 2019)</td> <td>Dr. Alessandra Ghigo</td> </tr> <tr> <td>Compagnia di San Paolo (CSTO161109)</td> <td>Dr. Emilio Hirsch</td> </tr> <tr> <td>Fondazione Telethon (GGP20079)</td> <td>Dr. Alessandra Ghigo</td> </tr> <tr> <td>Ministero della Salute (RC 2023/260-01)</td> <td>Dr. Francesco Blasi</td> </tr> <tr> <td>Regione Lombardia (18563 Capitolo 13.01.1)</td> <td>Dr. Francesco Blasi</td> </tr> </table>	Fondazione Cariplo (2018-0498)	Dr. Emilio Hirsch	Roche Italia (Bando Roche per la Ricerca 2019)	Dr. Alessandra Ghigo	Compagnia di San Paolo (CSTO161109)	Dr. Emilio Hirsch	Fondazione Telethon (GGP20079)	Dr. Alessandra Ghigo	Ministero della Salute (RC 2023/260-01)	Dr. Francesco Blasi	Regione Lombardia (18563 Capitolo 13.01.1)	Dr. Francesco Blasi
Fondazione Cariplo (2018-0498)	Dr. Emilio Hirsch												
Roche Italia (Bando Roche per la Ricerca 2019)	Dr. Alessandra Ghigo												
Compagnia di San Paolo (CSTO161109)	Dr. Emilio Hirsch												
Fondazione Telethon (GGP20079)	Dr. Alessandra Ghigo												
Ministero della Salute (RC 2023/260-01)	Dr. Francesco Blasi												
Regione Lombardia (18563 Capitolo 13.01.1)	Dr. Francesco Blasi												

	Ministero dell'Istruzione, dell'Università e della Ricerca (PRIN 2022 - 2022WHSCCL3)	Dr. Stefano Aliberti
Abstract:	<p>A-kinase anchoring proteins (AKAPs) are key orchestrators of cyclic AMP (cAMP) signaling that act by recruiting protein kinase A (PKA) in proximity of its substrates and regulators to specific subcellular compartments. Modulation of AKAPs function offers the opportunity to achieve compartment-restricted modulation of the cAMP/PKA axis, paving the way to new targeted treatments. For instance, blocking the AKAP activity of PI3Kg improves lung function by inducing cAMP-mediated bronchorelaxation, ion transport and anti-inflammatory responses. Here, we report the generation of a non-natural peptide, DRI-Pep #20, optimized to disrupt the AKAP function of PI3Kg. DRI-Pep #20 mimicked the native interaction between the N-terminal domain of PI3Kg and PKA, demonstrating nanomolar affinity for PKA, high resistance to protease degradation and high permeability to the pulmonary mucus barrier. DRI-Pep #20 triggered cAMP elevation both in vivo in the airway tract of mice upon intratracheal administration, and in vitro in bronchial epithelial cells of cystic fibrosis (CF) patients. In CF cells, DRI-Pep #20 rescued the defective function of the cAMP-operated channel cystic fibrosis conductance regulator (CFTR), by boosting the efficacy of approved CFTR modulators. Overall, this study unveils DRI-Pep #20 as a potent PI3Kg/PKA disruptor for achieving therapeutic cAMP elevation in chronic respiratory disorders.</p>	
Suggested Reviewers:	<p>Kjetil Tasken kjetil.tasken@medisin.uio.no</p> <p>Enno Klussmann enno.klussmann@mdc-berlin.de</p> <p>John Scott scottjd@uw.edu</p>	
Opposed Reviewers:	Manuela Zaccolo	

[Click here to view linked References](#)

1 **A Non-natural Peptide Targeting the A-kinase Anchoring Function of**
2 **PI3K γ for Therapeutic cAMP Modulation in Pulmonary Cells**

3
4 Angela Della Sala¹, Laura Tasca^{1,2}, Cosmin Butnarusu¹, Valentina Sala^{1,2}, Giulia Prono¹, Alessandra
5 Murabito¹, Enrico Millo³, Leonardo Terranova⁴, Francesco Blasi^{4,5}, Andrea Gramegna^{4,5}, Stefano
6 Aliberti⁶, Alberto Massarotti⁷, Sonja Visentin¹, Emilio Hirsch^{1,2}, Alessandra Ghigo^{1,2}
7
8

9
10 ¹Department of Molecular Biotechnology and Health Sciences, Molecular Biotechnology Center “Guido Tarone”, University
of Torino, 10126, Torino, Italy.

11 ²Kither Biotech Srl, 10126, Torino, Italy.

12 ³Department of Experimental Medicine, Section of Biochemistry, University of Genova, 16132, Genova, Italy

13 ⁴Internal Medicine Department, Respiratory Unit and Cystic Fibrosis Center, Fondazione IRCCS Ca' Granda Ospedale
14 Maggiore Policlinico, 20122, Milan, Italy

15 ⁵Department of Pathophysiology and Transplantation, University of Milan, 20122 Milan, Italy

16 ⁶Humanitas University, IRCCS Humanitas Research Hospital, Respiratory Unit, 20089, Milan, Italy

17 ⁷Department of Pharmaceutical Science, University of Piemonte Orientale ", 28100, Novara, Italy.
18

19
20 Correspondence to: Alessandra Ghigo, PhD, University of Torino, Department of Molecular
21 Biotechnology and Health Sciences, Via Nizza 52, 10126, Torino, Italy, Email alessandra.ghigo@unito.it
22
23
24
25
26
27
28
29
30
31
32
33
34
35
36
37
38
39
40
41
42
43
44
45
46
47
48
49
50
51
52
53
54
55
56
57
58
59
60
61
62
63
64
65

Abstract

A-kinase anchoring proteins (AKAPs) are key orchestrators of cyclic AMP (cAMP) signaling that act by recruiting protein kinase A (PKA) in proximity of its substrates and regulators to specific subcellular compartments. Modulation of AKAPs function offers the opportunity to achieve compartment-restricted modulation of the cAMP/PKA axis, paving the way to new targeted treatments. For instance, blocking the AKAP activity of PI3K γ improves lung function by inducing cAMP-mediated bronchorelaxation, ion transport and anti-inflammatory responses. Here, we report the generation of a non-natural peptide, DRI-Pep #20, optimized to disrupt the AKAP function of PI3K γ . DRI-Pep #20 mimicked the native interaction between the N-terminal domain of PI3K γ and PKA, demonstrating nanomolar affinity for PKA, high resistance to protease degradation and high permeability to the pulmonary mucus barrier. DRI-Pep #20 triggered cAMP elevation both *in vivo* in the airway tract of mice upon intratracheal administration, and *in vitro* in bronchial epithelial cells of cystic fibrosis (CF) patients. In CF cells, DRI-Pep #20 rescued the defective function of the cAMP-operated channel cystic fibrosis conductance regulator (CFTR), by boosting the efficacy of approved CFTR modulators. Overall, this study unveils DRI-Pep #20 as a potent PI3K γ /PKA disruptor for achieving therapeutic cAMP elevation in chronic respiratory disorders.

Keywords

AKAP, PKA, PI3K γ , peptide, cAMP, respiratory diseases

Abbreviations

AKAPs: A-kinase anchoring proteins	I-TASSER: Iterative Threading ASSEMBly Refinement
ANOVA: Analysis of Variance	IC ₅₀ : Half-maximal inhibitory concentration
ATP: Adenosine Triphosphate	Ivacaftor: VX-770
COPD: Chronic Obstructive Pulmonary Disease	K _D : Dissociation constant
cAMP: 3'-5'-cyclic adenosine monophosphate	K _{on} : Association rate constant
CF: Cystic Fibrosis	K _{off} : Dissociation rate constant
CFTR: Cystic Fibrosis Transmembrane Conductance Regulator	Lumacaftor: VX-809
DLS: Dynamic Light Scattering	LD ₅₀ : Lethal Dose 50%
ETI: Elexacaftor/ Tezacaftor/ Ivacaftor	Penetratin 1: P1
GPCR: G protein-coupled receptor	PI3K γ : Phosphoinositide 3-kinase gamma
HADDOCK: High Ambiguity Driven Biomolecular DOCKing	PKA: Protein Kinase A
HEMT: Highly Effective Modulator Therapies	RMSD: Root-Mean Square Deviation
HS-YFP: halide-sensitive yellow fluorescent protein	SEM: Standard Error of the Mean
	Tezacaftor: VX-661
	TEM: Transmission Electron Microscopy

Introduction

The 3'-5'-cyclic adenosine monophosphate (cAMP) second messenger controls different cellular processes, including cell growth and differentiation, gene transcription and protein expression. cAMP exerts its function through the activation of different effectors, with protein kinase A (PKA) being the most widely characterized. cAMP directly binds the dimer of the regulatory subunits of the PKA holoenzyme, promoting the release of the two catalytic counterparts, which are then free to phosphorylate various substrates. Although different G protein-coupled receptors (GPCR) rely on the same second messenger cAMP for conveying signals within the cell, a tight spatial and temporal regulation of its concentration ensures that activation of a specific GPCR results in the appropriate cellular response [1]. This local control of cAMP signals is achieved through multiprotein complexes that sequester enzymes responsible for cAMP generation (adenylyl cyclases) and destruction (phosphodiesterases, PDEs), as well as distinct signal transducers, in specific cellular locations. Key orchestrators of these "signaling islands" are A-kinase anchoring proteins (AKAPs) that, by definition, anchor PKA and its substrates and regulators

1 to definite subcellular compartments [2]. Perturbations of this fine control of cAMP compartmentalization
2 underlies different pathologies, including cardiovascular and pulmonary diseases, cancer, neurological
3 disorders, and inflammation. On these grounds, pharmacological manipulation of specific cAMP
4 signalosomes with molecules blocking the interaction of AKAPs with either PKA or other components of
5 the cAMP signaling pathway has been attempted and proven effective in preclinical models [2, 3].

6 Previous work identified the AKAP phosphoinositide 3-kinase γ (PI3K γ) as the core of a multiprotein
7 complex which is central to smooth muscle contraction, immune cell activation, and epithelial fluid
8 secretion in the airways [4]. In the lungs, PI3K γ -bound PKA activates PDE4, ultimately restricting cAMP
9 responses triggered by stimulation of β_2 -adrenergic receptors, the major GPCR mediating cAMP elevation
10 in the airways. In agreement, inhibition of the PI3K γ /PKA interaction promotes local cAMP elevation,
11 eventually resulting in airway smooth muscle relaxation and reduced neutrophil infiltration in a murine
12 model of asthma. In bronchial epithelial cells, targeting the PI3K γ AKAP function enhances cAMP in the
13 vicinity of the cystic fibrosis transmembrane conductance regulator (CFTR), the ion channel that regulates
14 mucus hydration, thereby driving the opening of the wild-type channel, while synergizing with CFTR
15 modulators in reinstating the function of F508del-CFTR, the most prevalent mutant in cystic fibrosis (CF)
16 [4].

17 Here, we report the design of a non-naturally occurring peptide, named DRI-Pep #20, that acted as a
18 potent disruptor of the PI3K γ /PKA complex by mimicking the core of the native interaction of PI3K γ with
19 PKA, and that was characterized by nanomolar affinity for PKA, high resistance to protease degradation
20 and high permeability to the pulmonary mucus barrier. Peptide-based inhibition of the PI3K γ /PKA
21 interaction triggered cAMP elevation both *in vitro* in bronchial epithelial cells and *in vivo* in the airway
22 tract of mice after intratracheal administration. Finally, the cAMP elevation elicited by DRI-Pep #20
23 rescued the defective function of the cAMP-operated channel CFTR in *in vitro* models of CF.
24

25 **Material and Methods**

26 **Peptides and reagents**

27 Peptides were synthesized by GenScript (Piscataway, NJ) at >95% purity. The sequences of all peptides
28 are listed in Tables S2 and S3.

29 Recombinant human PKA regulatory subunit RII α (PKA-RII α) and PI3K γ catalytic subunit (p110 γ) were
30 purchased by BIAFFIN GmbH & Co KG (Kassel, DE) and Origene Technologies (TP307790, Rockville,
31 US), respectively.

32 Human neutrophil elastase was purchased from Sigma-Aldrich (CAS 9004-06-2, Sigma-Aldrich, Saint
33 Louis, MO) and reconstituted in 50 mM sodium acetate, pH 5.5, with 200 mM NaCl. VX-809
34 (Lumacaftor), VX-770 (Ivacaftor), VX-661 (Tezacaftor) and VX-445 (Elexacaftor) were purchased from
35 MedChemExpress LLC (Princeton, USA). Forskolin and CFTR_{inh}-172 were purchased from Sigma-
36 Aldrich (CAS 66575-29-9, Sigma-Aldrich, Saint Louis, MO).
37

38 **Cell lines**

39 Immortalized normal human bronchial epithelial cells (16HBE14o-) were kindly provided by Dr.
40 Gruenert (University of California San Francisco, San Francisco, CA). Cystic fibrosis bronchial epithelial
41 (CFBE41o-) cells stably expressing F508del-CFTR (F508del-CFTR-CFBE41o-) were kindly provided
42 by L. Fu from the UAB Research Foundation (Birmingham, AL). Cells were grown in Minimum Essential
43 Medium (MEM) supplemented with 10% FBS, 5 mM L-Glutamine, 100 U/ml penicillin and 100 μ g/ml
44 streptomycin (Thermo Fisher Scientific, Waltham, MA) on culture dishes pre-coated with human
45 fibronectin (1 mg/ml; Sigma-Aldrich, Saint Louis, MO), bovine collagen I (3 mg/ml; Sigma- Aldrich,
46 Saint Louis, MO) and bovine serum albumin (0.1%; Sigma-Aldrich, Saint Louis, MO) diluted in LHC-8
47 basal medium (Invitrogen, Waltham, MA). Cells up to passage 15 were used for experiments. All cells
48 were cultured at 37°C and under a 5% CO₂ atmosphere.
49

50 **Animals**

1 PI3K γ -deficient mice (PI3K γ ^{-/-}) were described previously [4]. Mutant mice were back-crossed with
2 C57Bl/6j mice for 15 generations to inbreed the genetic background and C57Bl/6j were used as controls
3 (WT). Mice used in all experiments were 8 to 12 weeks of age. Mice were group-housed, provided free-
4 access to standard chow and water in a controlled facility providing a 12-hour light/dark cycle and were
5 used according to institutional animal welfare guidelines and legislation, approved by the local Animal
6 Ethics Committee. All animal experiments were approved by the animal ethical committee of the
7 University of Torino and by the Italian Ministry of Health (Authorization n°757/2016-PR).
8
9

10 **Isolation of murine peritoneal macrophages**

11 Peritoneal macrophages were prepared from 8- to 12-week- old wild-type (WT) and PI3K γ ^{-/-} mice, as
12 described previously [4]. Briefly, cells were collected from euthanized animals by peritoneal lavage with
13 5 mL of PBS, supplemented with 5 mM EDTA. Cells were centrifuged for 3 min at 300 g and the pellet
14 was resuspended in culture media including Roswell Park Memorial Institute (RPMI) media, 100 U/ml
15 penicillin and 100 μ g/ml streptomycin, and 10% heat-inactivated FBS (Thermo Fisher Scientific,
16 Waltham, MA). Macrophages were seeded in 96-well plates (1*10⁶ cells/well) and maintained at 37°C
17 with 5% CO₂ for at least 16/18 h before treatment with the peptide and cAMP quantification.
18
19
20
21

22 **cAMP measurements**

23 From cells: cAMP content was measured in 16HBE14o- cells at the indicated time points after treatment
24 with the indicated doses of peptides using the Promega cAMP-Glo™ Assay kit (Promega, Milano, IT),
25 according to the manufacturer's protocol.
26

27 From tissues: lungs, tracheas and hearts were collected from euthanized mice 24 h after intratracheal
28 instillation of different doses of the peptide (0 to 750 mg/kg in a final volume of 50 μ l of PBS). Snap-
29 frozen tissues were powdered in liquid nitrogen and extracted with cold 6% trichloroacetic acid. Samples
30 were sonicated for 10 sec, incubated at 4°C under gentle agitation for 10 min and then centrifuged at
31 13000 rpm at 4°C for 10 min. Supernatants were washed four times with five volumes of water saturated
32 with diethyl ether and lyophilized. cAMP content was detected with Cyclic AMP ELISA Kit (Cayman
33 Chemical, Michigan, USA), according to the manufacturer's protocol.
34
35

36 **Cell viability assay**

37 Human bronchial epithelial cells (16HBE14o-) were seeded in 96-well plates (2*10⁴ cells/well) and
38 incubated for at least 16/18 hours at 37°C with 5% CO₂ before experiments. Non-adherent cells were
39 eliminated by washing with PBS and cells were then stimulated with 8 different doses of the indicated
40 peptide (0 μ M – 1 mM range) for 24h. ATP levels were evaluated as an indicator of viable cells using the
41 Cell Titer-Glo® Luminescent Cell Viability Assay (Promega, Milano, IT), according to the
42 manufacturer's protocol. The lethal dose (LD₅₀) was calculated with respect to untreated control cells,
43 whose viability was set to 100%.
44
45
46

47 **CFTR activity measurements**

48 CFTR-mediated anion transport was measured by using the Premo™ Halide Sensor (Thermo Fisher
49 Scientific, Waltham, MA) which allows assessment of CFTR activity by measuring the rate of YFP
50 fluorescence quenching caused by iodide/chloride exchange across the plasma membrane. Briefly, the
51 halide-sensitive yellow fluorescent protein (HS-YFP) was expressed in 16HBE14o- and F508del-CFTR-
52 CFBE41o- cells through the BacMam technology, according to the manufacturer's protocol. Cells
53 expressing the HS-YFP were cultured on 96-well plates and treated with the indicated
54 peptides/compounds for the indicated time. Fluorescence was evaluated in a plate reader immediately
55 after addition of 150 μ l of Halide stimulus buffer (an NaI-containing solution) leading to a final NaI
56 concentration in the wells of 75 mM. Fluorescence was continuously read (1 point per second) starting at
57 1 s before Halide stimulus buffer addition and up to 120 s. CFTR activity was expressed as $\Delta F/F_0$ where
58 ΔF was obtained by subtracting the background fluorescence (fluorescence of cells not expressing HS-
59 YFP) to the fluorescence measured at the specific time point after addition of NaI. ΔF was then normalized
60
61
62
63
64
65

1 to the initial fluorescence F_0 (fluorescence of HS-YFP-expressing cells immediately after addition of NaI)
2 to obtain a measure of relative fluorescence $\Delta F/F_0$.
3
4

5 **CF sputum samples**

6 Spontaneous expectorated sputum samples from CF patients in stable clinical conditions were collected
7 at the Bronchiectasis and Cystic Fibrosis Programs of the Respiratory Department of Fondazione IRCCS
8 Ca' Granda Ospedale Maggiore Policlinico in Milan (Italy) and processed as previously described [5].
9 The study protocol was approved by local institutional review boards (594_2016bis) and all participants
10 provided written informed consent to the collection and use of their biological samples. Briefly, samples
11 were first processed by eliminating saliva, then sputum plugs were selected and weighted. Samples were
12 diluted 8X in PBS, vortexed until sputum dissolution and centrifuged for 15 min at 3000 g. Supernatants
13 were recovered and stored at -80°C , thawed overnight at 4°C , and all subsequent experiments were
14 undertaken within 24h from thawing. Neutrophil elastase was quantified as described previously [5] and
15 sputum samples containing $20\ \mu\text{g}/\text{mL}$ of active neutrophil elastase were used to assess the activity of
16 peptides in 16HBE14o- cells in the presence of CF sputum. Briefly, cells were seeded in 96-well plates
17 (2×10^4 cells/well) and incubated for at least 16/18 h at 37°C with 5% CO_2 before experiments.
18 Subsequently, peptides were diluted in PBS at a final concentration of $25\ \mu\text{M}$ and a PBS:sputum mixture
19 (1:1) was added on the top of adherent cells ($100\ \mu\text{l}/\text{well}$). cAMP levels were quantified at the indicated
20 time points using the Promega cAMP-Glo™ Assay kit (Promega, Milano, IT), according to the
21 manufacturer's protocol.
22
23
24
25
26

27 **PAMPA assay**

28 To assess the permeability of peptides through a CF sputum layer, a parallel artificial membrane
29 permeability system (PAMPA) (Corning Gentest Pre-coated PAMPA, 353015, USA plates) that allows
30 to measure the ability of drugs to diffuse from a donor compartment, through an artificial membrane, into
31 an acceptor compartment, was used as described previously [6]. The bottom wells of the PAMPA system
32 ("acceptor" wells) were filled with $300\ \mu\text{L}$ of PBS (10mM , $150\ \text{mM}$ NaCl, pH 7.4), while "donor" wells
33 were filled with $200\ \mu\text{L}$ of the peptide solution ($2\ \text{mg}/\text{mL}$ in 10mM PBS, $150\ \text{mM}$ NaCl, pH 7.4), in the
34 absence or presence of CF sputum. In the latter case, $40\ \mu\text{L}$ of CF sputum was first deposited over the
35 PAMPA membrane, and the peptide solution was subsequently added over the CF sputum layer.
36 Afterwards, the two wells were coupled and incubated for 5h at RT. At the end of the incubation, the
37 plates were split, and the amount of peptide diffused into the acceptor well was quantified by fluorescence
38 spectroscopy using a Horiba Jobin Yvon Fluorolog 3 TCSPC fluorimeter (Horiba, Kyoto, Japan) equipped
39 with a 450-W xenon lamp and a R928 photomultiplier (Hamamatsu Photonics, Hamamatsu, Japan).
40 Excitation was performed at 280nm while emission was recorded in the spectral region of $290\text{-}500\ \text{nm}$
41 (maximum of emission at $362\ \text{nm}$). Excitation and emission slits were set at 4 and 5 nm, respectively. The
42 concentration of the peptide was calculated using a 6-points calibration curve. The apparent permeability
43 coefficient (P_{app}) was expressed according to this relationship:
44
45
46
47

$$48 \quad P_{\text{app}} = \frac{dQ/dt}{C_0 \times A}$$

49 derived from Fick's law for steady-state conditions[7], where dQ is the quantity of drug expressed as
50 moles permeated into the acceptor compartment at time t ($18000\ \text{sec}$), C_0 is the initial concentration of
51 the peptide in the donor well, and A is the area of the well membrane ($0.3\ \text{cm}^2$).
52
53

54 **PKA-RII α bioconjugation and fluorescence spectroscopy**

55 Recombinant PKA-RII α was bio-conjugated to fluorescein 5-maleimide (F5M), as described previously
56 [8], using $75\ \mu\text{g}$ of PKA-RII α and a 50-fold excess of F5M. After bioconjugation, the derivative was
57 immediately purified using a Sephadex® G-25 desalting column and phosphate-buffered saline solution
58 (PBS) ($20\ \text{mM}$, $150\ \text{mM}$ NaCl, pH 7.2) as eluent. To evaluate F5M labelling efficiency, the dye/protein
59 ratio (D/P) of the conjugates was determined by the absorption spectra of the labelled proteins in PBS ($20\ \text{mM}$,
60 $150\ \text{mM}$ NaCl, pH 7.2), according to the following equation:
61
62
63
64
65

$$\frac{D}{P} = \frac{A_{max} e_{prot}}{(A_{280} - cA_{max}) e_{dye}}$$

where A_{280} is the absorption of the conjugate at 280 nm; A_{max} is the absorption of the conjugate at the absorption maximum of the corresponding F5M; c is a correction factor ($c = 0.29$); e_{prot} ($25,169 \text{ M}^{-1}\text{cm}^{-1}$) and e_{dye} ($63,096 \text{ M}^{-1}\text{cm}^{-1}$) are the molar extinction coefficients of PKA and F5M, respectively. PKA-RII α presents six cysteine residues, and the final D/P value was 0.2.

UV-visible absorption spectra were measured with a UH5300 spectrophotometer (Hitachi, Tokyo, Japan) at RT, using 1 cm pathway length quartz cuvette. Fluorescence emission spectra in steady-state mode were acquired at RT using a Jobin Yvon Fluorolog 3 TCSPC fluorimeter (Horiba, Kyoto, Japan) equipped with a 450-W Xenon lamp and a R928 photomultiplier (Hamamatsu Photonics, Hamamatsu, Japan). Steady-state fluorescence spectra were recorded in the 500-600 nm range. The excitation wavelength was set on 490 nm and the excitation and emission slits were set on 2 and 4, respectively. Equilibrium binding constants (K_D and K_A) were obtained from steady-state data.

Fluorescence kinetics were measured using an Applied Photophysics SX20 stopped-flow spectrophotometer (Applied Photophysics, North Carolina, US) fitted with a 495 nm cut-off filter between the cell and the fluorescence detector, and equipped with a thermostat bath set at $25 \pm 0.2^\circ\text{C}$. Association and dissociation rate constants (k_{on} and k_{off}) were calculated from stopped-flow kinetics data. Data acquisition, visualization and analysis were performed with Pro-Data software from Applied Photophysics Ltd (Applied Photophysics, North Carolina, US).

To assess the ability of DRI-Pep #20 to displace the binding between PI3K γ and PKA-F5M, steady-state emission spectra of the PI3K γ /PKA-F5M complex in the presence of increasing concentrations of the peptide were acquired. Briefly, 50 nM of recombinant PI3K γ was added to 100 nM F5M-bounded PKA-RII α in a total volume of 100 μL PBS. The concentration of the PI3K γ /PKA-F5M complex was kept constant while gradually titrated with increasing concentrations of the peptide from 0 to 5 μM . The complex was excited at 490 nm and emission spectra were recorded in the 500-600 nm spectral range, as described above. The degree of displacement of the PKA-RII α -PI3K γ complex was expressed as the percentage of fluorescence quenching after addition of the peptide.

Circular dichroism

Circular dichroism (CD) measurements were performed on a Jasco-810 Dichrograph equipped with a Peltier thermoelectric controller (Jasco Inc., Easton, US). The spectra of peptides were recorded in the continuous mode between 260 and 180 nm at 25°C in 0.1 cm path length quartz cuvette (Hellma GmbH, Müllheim, DE) with a total peptide concentration of 0.2 mg/mL dissolved in 2 mM PBS (0.6 mM KH_2PO_4 , 1.6 mM K_2HPO_4), pH 7.4. The CD spectrum in the 190-240 nm range was used to predict the secondary structural content of the peptide using the K2D3 web server [9].

Transmission Electron Microscopy (TEM) and Dynamic Light Scattering (DLS)

Self-assembled peptide nanostructures were analyzed by Transmission Electron Microscopy (TEM) analysis. Transmission electron micrographs were obtained with a JEOL 3010-UHR TEM operating at an accelerating voltage of 300.00 kV (JEOL, Tokyo, Japan). TEM samples were prepared by dissolving the peptides at 0.1 mg/mL in water and drying them on a carbon-coated copper grid. The nominal magnification used to record nanostructures were $\times 500000$ and $\times 800000$.

The size distribution profile of the self-assembled peptide was determined by dynamic light scattering (DLS, Malvern Zetasizer, Worcestershire, UK). Samples were prepared at 4 mg/mL in 2 mM PBS (0.6 mM KH_2PO_4 , 1.6 mM K_2HPO_4), pH 7.4. Measurements were performed after an equilibration time of 60 s which allowed samples to reach the temperature of 25°C .

Peptide mutagenesis

Systematic amino acid substitutions were performed using an in-house Python script. To identify which variant could mimic the characteristics of DRI-Pep #20, we compared the ability of each peptide to adopt

1 the same spatial arrangement and exhibit a similar surface charge distribution. The peptides from the
2 library were subsequently processed using Omega2 (OMEGA, version 4.1.0.2; OpenEye Scientific
3 Software: Santa Fe, NM) [10, 11], a software that creates a multi-conformer structure database capable of
4 reproducing biologically active conformations. The ROCS software (ROCS, version 3.4.1.2; OpenEye
5 Scientific Software: Santa Fe, NM) [12] was employed to conduct a shape-based overlay method, in which
6 molecules were aligned through a solid-body optimization process aimed at maximizing the volume
7 overlap between them. Subsequently, the peptides were re-ranked for similarity to DRI-Pep #20 based on
8 electrostatic properties using the EON program (EON, version 2.3.4.2; OpenEye Scientific Software:
9 Santa Fe, NM) [13]. The final score assigned to each peptide was based on a dual Tanimoto score, ranging
10 from 0 to 2, where a score of 2 signifies an exact match in both shape and electrostatics between the two
11 molecules. Peptides with the highest scores were considered for further analysis.
12
13
14

15 **Protein structure prediction**

16 The 3D structure of residues 1-45 of PKA-RII α was predicted using the Iterative Threading ASSEmbly
17 Refinement (I-TASSER) web server [14], an on-line platform that implements I-TASSER-based
18 algorithms for predictions of protein structure and function. Briefly, starting from the FASTA amino acid
19 sequence I-TASSER ran a three steps simulation, first threading it through a representative PDB structure
20 library to search for possible template folds or supersecondary-structure fragments, using a profile-profile
21 alignment-based threading algorithm. In the second step, the continuous fragments excised from the PDB
22 templates were reassembled into full-length models, while the unaligned regions were built by ab initio
23 modeling. Finally, the structure trajectories were clustered, and the lowest-energy structures selected, and
24 an all-atom model was constructed by REMO41 through optimization of the hydrogen-bonding network.
25 The five best models obtained by I-TASSER were subsequently evaluated based on their threading
26 template and predicted C-score. The model with the highest C-score of -0.22 and predicted using the NMR
27 structure of PKA-RII α as a threading template (PDB ID 2KYG) [15] was selected.

28 The 3D structure of PI3K γ was downloaded by AlphaFold [16] and validated by Root-Mean Square
29 Deviation (RMSD) alignment of all the atoms with the cryo-electron microscopy structure of the
30 heterodimeric PI3K γ complex, p110 γ -p101 (PDB ID 7MEZ) [17].
31
32
33
34
35

36 **Peptide Structure Prediction**

37 The structure of the peptides was predicted with PEP-FOLD3.5 [18], a de novo approach that predicts
38 peptide structures from amino acid sequences. Briefly, starting from the amino acid sequence, first a series
39 of 200 simulations was run, each one sampling a different region of the conformational space using the
40 Generator taboo-sampling 5 (ts5), recommended for peptides longer than 10 amino acids. The output was
41 an archive of clusters of all the models sorted out using the TM score followed by performing the Model
42 Quality assessment using Apollo [19]. The first five models, representing the five best conformation of
43 each cluster with the best scores defined according to the lowest sOPEP energy and the highest TM-score
44 value, were selected and further supported by RMSD. The RMDS of each model was compared to the
45 RMDS of residues 126-150 of the p110 γ structure, both the protein structure predicted by AlphaFold and
46 the crystal structure (PDB ID 7mez, RCSB database). Finally, the best structure of the peptide was
47 validated by visual analysis on PYMOL.
48
49
50
51

52 **Docking studies**

53 Docking studies were performed with the High Ambiguity Driven Biomolecular DOCKing (HADDOCK)
54 software. Briefly, starting from the PKA-RII α and peptide structures, the HADDOCK docking ran three
55 consecutive steps, first the molecules were randomly oriented, and a rigid-body search was performed
56 (it0). The output was an archive of 1000 models, among them the top 200 ranked structures were selected
57 based on the energy function and addressed to the semi-flexible simulated annealing stage performed in
58 torsion angle space (it1). In the third stage, the structures were refined in Cartesian space with explicit
59
60
61
62
63
64
65

1 solvent layer (water) and subjected to a short molecular dynamic simulation at 300K. During the
2 refinement, both the side chain and backbone of interface residues were progressively allowed to move.
3 The final models were automatically clustered based on the positional interface ligand RMSD (iL-RMSD)
4 by fitting the conformational changes on the interface of the receptor (PKA-RII α) and on the interface of
5 the smaller partner (the peptides). Finally, the binding poses were assessed by the HADDOCK report and
6 the binding affinity was evaluated by the Optimal Hydrogen Bonding Network. The resulting best binding
7 pose was validated by visual analysis on PYMOL.
8
9

10 **Statistical analysis**

11 Data are presented as scatter plots with bars (means \pm SEM). Prism software (GraphPad Software Inc.)
12 was used for statistical analysis. Raw data were first analyzed to confirm their normal distribution via the
13 Shapiro-Wilk test and then analyzed by unpaired Student's t test, one-way analysis of variance (ANOVA),
14 or two-way ANOVA. Bonferroni correction (one-way and two-way ANOVA) was applied to correct for
15 multiple comparisons. $P < 0.05$ was considered significant.
16
17
18

19 **Results**

20 **DRI-Pep #20 is a PI3K γ /PKA disruptor with high binding affinity for PKA.**

21 DRI-Pep #20 was obtained by synthesizing the all-D-retroinverso (DRI) form of a peptide linking the cell
22 penetrating peptide Penetratin 1 (P1) to the non-natural 5 amino acids sequence RHQGK, by means of a
23 glycine (G) linker (Fig. 1a). First, we determined the ability of DRI-Pep #20 to directly bind the PKA
24 regulatory subunit RII α (PKA-RII α), the PKA isoform that we previously demonstrated being specifically
25 bound by PI3K γ [20]. *In vitro* steady-state fluorescence spectroscopy experiments revealed that the
26 peptide could associate recombinant PKA-RII α with high affinity, being the equilibrium dissociation
27 constant (K_D) in the nanomolar range (76 nM; Fig. 1b-c). Further fast kinetic studies showed that DRI-
28 Pep #20 rapidly associates to PKA-RII α forming a relatively stable complex. The association rate constant
29 (K_{on}) in the order of $10^{-6} \text{ M}^{-1} \text{ s}^{-1}$ indicated a quick assembly of the DRI-Pep #20/PKA-RII α complex, while
30 the moderate dissociation rate (K_{off}) suggested a certain level of stability in the bound state (Fig. 1d and
31 Table 1). In agreement with the high affinity of DRI-Pep #20 to PKA-RII α , the peptide inhibited the
32 interaction between recombinant PI3K γ and PKA-RII α up to 74%, and with an IC_{50} of 0.16 μM (Fig. 1e-
33 f). Next, we tested whether DRI-Pep #20 could disturb the anchoring of PKA by AKAPs other than PI3K γ .
34 The ability of the peptide to raise cAMP levels in PI3K γ -deficient cells was used as a proxy of its capacity
35 to interfere with other AKAP-based signalosomes [4]. We found that DRI-Pep #20 failed to raise cAMP
36 in cells that did not express its target PI3K γ , demonstrating that the peptide retained the selectivity for the
37 PI3K γ -directed pool of PKA, despite the high binding affinity for PKA-RII α (Fig. 1g). Overall, these data
38 identify DRI-Pep #20 as a potent and selective disruptor of the PI3K γ /PKA complex.
39
40
41
42
43
44

45 **DRI-Pep #20 mimics the native interaction between PI3K γ and PKA-RII α .**

46 Next, we sought to elucidate the determinants of the high-affinity interaction of DRI-Pep#20 with PKA-
47 RII α . Predictions of the tridimensional structure of DRI-Pep #20 suggested the presence of an α -helix,
48 flanked by two uncoiled regions (Fig. 2a). The helical propensity of the peptide was confirmed by circular
49 dichroism analyses showing a double-peak signal, with a maximum at 200 nm which is typical for α -helix
50 structures, and a minimum in the 220–240 nm region which is characteristic for random-coil domains [21]
51 (Fig. 2b). *In silico* simulations of the binding of DRI-Pep #20 to the typical binding surface for AKAPs
52 (amino acids 1–45 of PKA-RII α) [2], revealed that 4 out of the 5 amino acids of the RHQGK sequence
53 (R-1, H-2, Q-3 and K-5) could form hydrogen bonds with partners in the PKA-RII α subunit (Fig. 2c, Fig.
54 S1a and Table S1). Systematic amino acid substitutions within the RHQGK sequence confirmed the
55 importance of positively charged and polar amino acids in position 3 and 4 for the interaction of DRI-Pep
56 #20 with PKA-RII α . Indeed, peptide variants bearing hydrophobic residues in those positions had reduced
57 ability to disrupt the PI3K γ /PKA interaction, and thus to elevate cAMP in human bronchial epithelial cells
58 (16HBE14o-), as compared to the parent sequence (Fig. S2a and Table S2). These observations suggested
59
60
61
62
63
64
65

1 that a short amino acid sequence enriched in hydrophilic residues could form the backbone for the
2 anchoring of PKA by PI3K γ and prompted us to better characterize the native interaction between the N-
3 terminal domain of PI3K γ , which encompasses the putative PKA-binding motif [4, 20], and PKA-RII α .
4 *In silico* simulations of the binding between 120-160 PI3K γ and 1-45 PKA-RII α identified a region
5 enriched in hydrophilic amino acids, spanning from K-126 to R-130 (KATHR), that could maximally
6 interact with PKA. K-126, H-129 and R-130 were consistently found at the core of the interaction in all
7 of the possible binding poses between the two proteins (Fig. 3a and Fig. S3a) and were shown to form
8 hydrogen bonds mainly with T-18 and the Q-25 of PKA-RII α (Fig. 3a and Fig. S3b). Intriguingly, the
9 KATHR sequence phenocopied the complete PKA-binding motif of PI3K γ in raising cAMP in
10 16HBE14o- cells (Fig. S4a and Table S3), indicating that the core of the interaction between PI3K γ and
11 PKA-RII α could reside within this region. In agreement, structural predictions and molecular docking
12 studies revealed that the KATHR peptide folded in an almost complete α -helical structure (Fig. 3b),
13 allowing the formation of hydrogen bonds between K-126, H-129 and R-130 and partners within 1-45
14 PKA-RII α (Fig. 3c, Fig. S5 and Table S4).
15 Taken together, these results demonstrate that the non-natural peptide DRI-Pep #20 acts as a potent
16 PI3K γ /PKA disruptor by mimicking the core of the native interaction of PI3K γ with PKA-RII α .
17
18
19
20
21

22 **DRI-Pep #20 has favorable mucus permeability and protease resistance.**

23 Next, we sought to determine to what extent DRI-Pep #20 could be used for targeting the native
24 PI3K γ /PKA complex in the lungs to modulate cAMP for therapeutic purposes. First, we assessed the
25 suitability for local delivery to the airways. Following intratracheal instillation (Fig. 4a), DRI-Pep #20
26 induced a dose-dependent increase in cAMP levels in the trachea and in the lungs of treated mice, with
27 an EC₅₀ of 8.06 μ g/Kg and 11.78 μ g/Kg, respectively (Fig. 4b-c). Of note, cardiac cAMP concentrations
28 were unchanged (Fig. 4d), suggesting that the peptide locally increased airway cAMP without systemic
29 effects at the tested dose.
30

31 Since the efficacy of inhaled therapies can be hampered by extracellular barriers imposed by diseased
32 lungs, including a thick layer of protease-rich mucus [22], we next sought to determine to what extent
33 DRI-Pep #20 could penetrate mucus layers and resist to protease degradation. DRI-Pep #20 penetrated
34 the phospholipid membrane in the PAMPA system (Fig. 5a) with an apparent permeability (P_{app}) of 1.88
35 $\times 10^{-6}$ cm s⁻¹ (Fig. 5b). Of note, the addition of pathological CF sputum on top of the phospholipid layer
36 (Fig. 5a) did not significantly affect the P_{app} of the peptide (P_{app} 2.55×10^{-6} cm s⁻¹) (Fig. 5b). To verify
37 whether the favorable mucus permeability of DRI-Pep #20 could be ascribed to molecular dimensions
38 compatible with the mesh size of CF mucus [23], Transmission Electron Microscopy (TEM) and Dynamic
39 Light Scattering (DLS) assays were performed. TEM images showed that DRI-Pep #20 formed irregular
40 aggregates of 5-40 nm in size (Fig. 5c), in agreement with the particle diameter of 10-20 nm retrieved by
41 DLS analysis (Fig. 5d).
42

43 Next, we tested whether DRI-Pep #20 retained the ability to elevate cAMP in pulmonary cells in the
44 presence of neutrophil elastase, the most abundant protease in the lungs of patients with neutrophilic
45 airway diseases, including but not limited to chronic obstructive pulmonary disease (COPD) and CF [24].
46 The ability of the peptide to raise cAMP in 16HBE41o- cells was completely unaltered by the presence
47 of 3 μ g/ml of recombinant human neutrophil elastase (HNE) (Fig. 5e), a dose which was previously shown
48 to inactivate other therapeutic peptides [25]. Conversely, the cAMP elevating activity of the non-DRI
49 isoform, Pep #20, was reduced by 26% by means of HNE (Fig. 5e). Notably, the activity of the DRI
50 isoform was entirely preserved even in the presence of a 10-fold higher concentration of HNE (Fig. 5f),
51 an amount that is typically detected in the lungs of patients with severe bronchiectasis [24], which was in
52 line with the absence of any predicted cleavage sites by HNE (Fig. S4a). The observed resistance of DRI-
53 Pep #20 to degradation was confirmed in the presence of a more complex biological matrix containing
54 other proteases that could potentially cleave the peptide (Fig. S4b), that is CF sputum, where the DRI-Pep
55 #20 retained 72% of its biological activity (Fig. 5g).
56
57
58
59
60
61
62
63
64
65

1 Taken together, these data demonstrate the ability of DRI-Pep #20 to elevate lung cell cAMP in the
2 presence of a hostile extracellular environment composed of a mucus barrier enriched in proteases, which
3 is typical of diseased lungs.
4

5 **DRI-Pep #20 promotes cAMP-dependent activation of wild-type and F508del-CFTR in human** 6 **bronchial epithelial cells.**

7
8 Next, we aimed to assess the extent to which DRI-Pep #20 could effectively restore cAMP levels and
9 consequently reactivate the function of CFTR, a cAMP-dependent chloride channel impaired in a range
10 of respiratory disease, including but not limited to COPD and CF [26]. First, we assessed the ability of
11 the peptide to stimulate the activity of the wild-type channel in 16HBE141o- cells expressing the halide-
12 sensitive yellow fluorescent protein (HS-YFP) (Fig. 6b), which allows quantifying CFTR activity based
13 on the fluorescence quenching rate elicited by an iodide influx [27]. DRI-Pep #20 induced a 60%
14 reduction in YFP fluorescence, which was completely prevented by co-application of the CFTR inhibitor,
15 CFTR_{inh-172} (Fig. 6b), demonstrating selective activation of CFTR channels. Dose-response experiments
16 revealed an EC₅₀ of 20 μ M (Fig. 6c) and demonstrated that 25 μ M DRI-Pep #20 was as effective as 10
17 μ M forskolin, the adenylyl cyclase activator, in triggering CFTR gating in 16HBE141o- cells (Fig. 6d).
18 Further, we evaluated to what degree DRI-Pep #20 could reinstate the activity of F508del-CFTR in
19 combination with the standard of care, including two CFTR correctors (Elexacaftor/Tezacaftor) and one
20 CFTR potentiator (Ivacaftor), that partially rescue the trafficking and gating defects of the mutant channel,
21 respectively [28]. In cystic fibrosis bronchial epithelial cells overexpressing the F508del-CFTR mutant
22 and the HS-YFP, Elexacaftor/Tezacaftor/Ivacaftor (ETI) produced a YFP quenching of 50%, which was
23 further decreased down to 25% when DRI-Pep #20 was added together with ETI (Fig. 6e).
24 Hence, these data support the use of DRI-Pep #20 as a single agent or as an-add on to CFTR modulators,
25 to therapeutically stimulate the activity of wild-type and F508del-CFTR, respectively.
26
27
28
29
30
31

32 **Discussion**

33 Our study identifies a non-natural peptide that functions as a selective and potent disruptor of the
34 PI3K γ /PKA-RII α complex. This peptide, named DRI-Pep #20, serves as an effective tool to study PKA
35 anchoring and manipulate cAMP/PKA signaling for therapeutic purposes.
36 Our structural predictions and molecular docking studies indicate that DRI-Pep #20 operates similarly to
37 other AKAP disruptor peptides by mimicking the typical α -helical structure through which AKAPs bind
38 PKA [29]. In addition, our results support previous research showing that, within this α -helix, the presence
39 of polar and positively charged amino acids is crucial for the binding between the scaffold and the kinase
40 [29]. In contrast to other AKAP disruptors, DRI-Pep #20 uniquely interferes with the binding between
41 PKA and PI3K γ , without affecting PKA pools anchored by other AKAPs. This specificity is attributed to
42 our earlier observation that the PKA-anchoring sequence of PI3K γ diverges from that of classical AKAPs
43 [4, 20]. While our previous report pinpointed amino acids 126-150 as the PKA-anchoring sequence of
44 PI3K γ [4, 20], the critical residues for the interaction remained elusive, partly due to the lack of the
45 crystallographic structure of the PI3K γ N-terminal domain. In this study, our *in silico* characterization of
46 the high-affinity interaction of DRI-Pep #20 with PKA-RII α sheds light on the native association between
47 PI3K γ and PKA. Our computational modeling demonstrates that the KATHR sequence, encompassing
48 amino acids 126-130 of the N-terminal of PI3K γ , plays a central role in guiding the interaction with PKA.
49 Like DRI-Pep #20, the KATHR peptide can adopt an α -helical conformation, establishing hydrogen bonds
50 with partner amino acids within PKA-RII α , mainly through K-126, H-129 and R-130. Despite structural
51 similarities, DRI-Pep #20 exhibits a significantly higher affinity for PKA compared to the native PKA-
52 docking domain of PI3K γ , with a K_D value that is 100 folds lower than that obtained with the 126-150
53 region [20]. This discrepancy raises questions about why nature selected a PI3K γ sequence with low
54 affinity for PKA. It is plausible that, in physiological conditions, the binding between the two proteins
55 needs to be sufficiently weak to allow PI3K γ to easily leave the complex, thereby interrupting PKA-
56
57
58
59
60
61
62
63
64
65

1 mediated activation of PDEs, when necessary. This could serve as a protective mechanism against an
2 excessive reduction of cellular cAMP below a critical level.

3 While the high binding affinity of DRI-Pep #20 to PKA-RII α can be attributed to the numerous hydrogen
4 bonds that this non-natural sequence can form with the kinase, its high proteolytic stability is a direct
5 consequence of the presence of D-amino acids, which are not recognized by proteases [30]. The
6 incorporation of non-natural D-amino acids in a retro-reversed sequence, as in DRI-Pep #20, aims to
7 obtain molecules with the same structure as the parent L-peptides, but with new chemical properties, such
8 as increased half-life and resistance to proteolytic degradation, which potentially improve their *in vivo*
9 potency [31]. These chemical features, and above all the high stability and target affinity, position DRI-
10 Pep #20 as an ideal candidate for therapeutic cAMP modulation *in vivo*. Chronic respiratory diseases,
11 where the PI3K γ -PKA complex serves as a central signaling hub to multiple airway cell functions, like
12 smooth muscle relaxation, epithelial ion transport and neutrophil infiltration [4], could significantly
13 benefit from a treatment with DRI-Pep #20. We provide evidence that DRI-Pep #20 preserves its
14 biological activity in the presence of human neutrophil elastase and after local delivery in the airways in
15 mice. These observations support the potential use of this peptide for achieving therapeutically relevant
16 cAMP elevation in highly inflamed lungs. This is of particular relevance in a range of airway diseases,
17 including COPD, certain forms of asthma, non-CF bronchiectasis (NCFB), and even in patients with CF
18 who may still experience airway inflammation despite highly effective modulator therapies (HEMT)
19 targeting the basic genetic defect of the disease [32, 33].

20 In addition to proteases associated with inflammation, another challenge posed by diseased lungs is the
21 thick mucus layer covering respiratory epithelia [22]. Especially in patients with CF and NCFB, mucus
22 may reduce the bioavailability of inhaled therapeutics decreasing their overall efficacy. Our assays
23 exploiting patient-derived sputum as a proxy of CF mucus revealed that DRI-Pep #20 is not significantly
24 affected by the barrier activity of mucus. Moreover, in spite of being a relatively large molecule (i.e., MW
25 > 2000 g/mol), DRI-Pep #20 is well below the mesh size of the pathological mucus. TEM and DLS
26 analyses indicate that the peptide can form aggregates of 20 nm in size, which could freely diffuse through
27 the 100-1000 nm meshes of the network of bundled fibers that are typically formed by biopolymers in the
28 CF mucus and that are filled with a low viscosity fluid [34].

29 These observations imply that, in diseased lungs, relevant doses of DRI-Pep #20 could reach the
30 underlying epithelial cells wherein targeting the PI3K γ /PKA complex is anticipated to boost CFTR
31 activity [4]. Our data indicates that in CF bronchial epithelial cells DRI-Pep #20 enhances the effects of
32 the standard combination of CFTR modulators, Elexacaftor/Tezacaftor/Ivacaftor, in rescuing the activity
33 of the most common CFTR mutant, F508del. These findings carry significant clinical implications,
34 especially in light of recent studies demonstrating that CFTR potentiators and correctors only partially
35 restore the function of mutant channels, achieving up to 60% the wild-type CFTR levels [35-37].
36 Consequently, CF patients treated with HEMT may still experience residual mucus dysfunction, airway
37 infection and inflammation [32, 33, 38] and could significantly benefit from the ability of DRI-Pep #20
38 to maximize the clinical efficacy of the standard-of-care. In addition, our observation that the peptide
39 itself activates the wild-type form of the CFTR channel supports the prospect of extending the use of DRI-
40 Pep #20 to treat a range of non-genetic conditions characterized by acquired CFTR dysfunction, including
41 COPD, non-atopic asthma, and NCFB [26].

42 In summary, our study identified a non-natural peptide that targets the AKAP function of PI3K γ , with
43 unprecedented target binding affinity and potency. Due to its resistance to proteases and its ability to
44 penetrate airway mucus, DRI-Pep #20 holds promise for achieving therapeutic cAMP elevation in chronic
45 respiratory disorders where mucus accumulation and inflammatory remodeling still result in a highly
46 unmet medical need. Although DRI peptides have been shown to be well tolerated and therapeutically
47 effective in clinical trials [39], further preclinical testing in rodents and non-rodents is necessary to
48 establish the feasibility of an inhaled therapy based on DRI-Pep #20 for human use.

61 References

1. Zaccolo, M., A. Zerio and M.J. Lobo, *Subcellular Organization of the cAMP Signaling Pathway*. *Pharmacol Rev*, (2021). 73: 278-309.10.1124/pharmrev.120.000086
2. Omar, M.H. and J.D. Scott, *AKAP Signaling Islands: Venues for Precision Pharmacology*. *Trends Pharmacol Sci*, (2020). 41: 933-946.10.1016/j.tips.2020.09.007
3. Murabito, A., S. Cnudde, E. Hirsch and A. Ghigo, *Potential therapeutic applications of AKAP disrupting peptides*. *CLINICAL SCIENCE*, (2020). 134.10.1042/cs20201244
4. Ghigo, A., A. Murabito, V. Sala, A.R. Pisano, S. Bertolini, A. Gianotti, E. Caci, A. Montresor, A. Premchandrar, F. Pirozzi, K. Ren, A. Della Sala, M. Mergioti, W. Richter, E. de Poel, M. Matthey, S. Calderr, R.A. Cardone, F. Civiletti, et al., *A PI3Kgamma mimetic peptide triggers CFTR gating, bronchodilation, and reduced inflammation in obstructive airway diseases*. *Sci Transl Med*, (2022). 14: eabl6328.10.1126/scitranslmed.abl6328
5. Oriano, M., L. Terranova, G. Sotgiu, L. Saderi, A. Bellofiore, M. Retucci, C. Marotta, A. Gramegna, D. Miglietta, C. Carnini, P. Marchisio, J.D. Chalmers, S. Aliberti, and F. Blasi, *Evaluation of active neutrophil elastase in sputum of bronchiectasis and cystic fibrosis patients: A comparison among different techniques*. *Pulm Pharmacol Ther*, (2019). 59: 101856.10.1016/j.pupt.2019.101856
6. Butnarusu, C., G. Caron, D.P. Pacheco, P. Petrini and S. Visentin, *Cystic Fibrosis Mucus Model to Design More Efficient Drug Therapies*. *Mol Pharm*, (2022). 19: 520-531.10.1021/acs.molpharmaceut.1c00644
7. Sharifian Gh, M., *Recent Experimental Developments in Studying Passive Membrane Transport of Drug Molecules*. *Mol Pharm*, (2021). 18: 2122-2141.10.1021/acs.molpharmaceut.1c00009
8. Hermanson, G.T., *Bioconjugate Techniques*. 2008.
9. Louis-Jeune, C., M.A. Andrade-Navarro and C. Perez-Iratxeta, *Prediction of protein secondary structure from circular dichroism using theoretically derived spectra*. *Proteins*, (2012). 80: 374-81.10.1002/prot.23188
10. Hawkins, P.C. and A. Nicholls, *Conformer generation with OMEGA: learning from the data set and the analysis of failures*. *J Chem Inf Model*, (2012). 52: 2919-36.10.1021/ci300314k
11. Hawkins, P.C., A.G. Skillman, G.L. Warren, B.A. Ellingson and M.T. Stahl, *Conformer generation with OMEGA: algorithm and validation using high quality structures from the Protein Databank and Cambridge Structural Database*. *J Chem Inf Model*, (2010). 50: 572-84.10.1021/ci100031x
12. Hawkins, P.C., A.G. Skillman and A. Nicholls, *Comparison of shape-matching and docking as virtual screening tools*. *J Med Chem*, (2007). 50: 74-82.10.1021/jm0603365
13. Muchmore, S.W., A.J. Souers and I. Akritopoulou-Zanze, *The use of three-dimensional shape and electrostatic similarity searching in the identification of a melanin-concentrating hormone receptor 1 antagonist*. *Chem Biol Drug Des*, (2006). 67: 174-6.10.1111/j.1747-0285.2006.00341.x
14. Yang, J., R. Yan, A. Roy, D. Xu, J. Poisson and Y. Zhang, *The I-TASSER Suite: protein structure and function prediction*. *Nat Methods*, (2015). 12: 7-8.10.1038/nmeth.3213
15. Corpora, T., L. Roudaia, Z.M. Oo, W. Chen, E. Manuylova, X. Cai, M.J. Chen, T. Cierpicki, N.A. Speck, and J.H. Bushweller, *Structure of the AML1-ETO NHR3-PKA(RIIalpha) complex and its contribution to AML1-ETO activity*. *J Mol Biol*, (2010). 402: 560-77.10.1016/j.jmb.2010.08.007
16. Jumper, J., R. Evans, A. Pritzel, T. Green, M. Figurnov, O. Ronneberger, K. Tunyasuvunakool, R. Bates, A. Zidek, A. Potapenko, A. Bridgland, C. Meyer, S.A.A. Kohl, A.J. Ballard, A. Cowie, B. Romera-Paredes, S. Nikolov, R. Jain, J. Adler, et al., *Highly accurate protein structure prediction with AlphaFold*. *Nature*, (2021). 596: 583-589.10.1038/s41586-021-03819-2
17. Rathinaswamy, M.K., U. Dalwadi, K.D. Fleming, C. Adams, J.T.B. Stariha, E. Pardon, M. Baek, O. Vadas, F. DiMaio, J. Steyaert, S.D. Hansen, C.K. Yip, and J.E. Burke, *Structure of the phosphoinositide 3-kinase (PI3K) p110gamma-p101 complex reveals molecular mechanism of GPCR activation*. *Sci Adv*, (2021). 7.10.1126/sciadv.abj4282

- 1 18. Lamiable, A., P. Thevenet, J. Rey, M. Vavrusa, P. Derreumaux and P. Tuffery, *PEP-FOLD3: faster de novo structure prediction for linear peptides in solution and in complex*. Nucleic Acids Res, (2016). 44: W449-54.10.1093/nar/gkw329
- 2
- 3
- 4
- 5 19. Wang, Z., J. Eickholt and J. Cheng, *APOLLO: a quality assessment service for single and multiple protein models*. Bioinformatics, (2011). 27: 1715-6.10.1093/bioinformatics/btr268
- 6
- 7 20. Perino, A., A. Ghigo, E. Ferrero, F. Morello, G. Santulli, G. Baillie, F. Damilano, A. Dunlop, C. Pawson, R. Walser, R. Levi, F. Altruda, L. Silengo, L. Langeberg, G. Neubauer, S. Heymans, G. Lembo, M. Wymann, R. Wetzker, et al., *Integrating Cardiac PIP(3) and cAMP Signaling through a PKA Anchoring Function of p110 γ* . MOLECULAR CELL, (2011). 42.10.1016/j.molcel.2011.01.030
- 8
- 9
- 10
- 11
- 12
- 13 21. Lopes, J.L., A.J. Miles, L. Whitmore and B.A. Wallace, *Distinct circular dichroism spectroscopic signatures of polyproline II and unordered secondary structures: applications in secondary structure analyses*. Protein Sci, (2014). 23: 1765-72.10.1002/pro.2558
- 14
- 15
- 16 22. d'Angelo, I., C. Conte, M.I. La Rotonda, A. Miro, F. Quaglia and F. Ungaro, *Improving the efficacy of inhaled drugs in cystic fibrosis: challenges and emerging drug delivery strategies*. Adv Drug Deliv Rev, (2014). 75: 92-111.10.1016/j.addr.2014.05.008
- 17
- 18
- 19
- 20
- 21 23. Boegh, M. and H.M. Nielsen, *Mucus as a barrier to drug delivery - understanding and mimicking the barrier properties*. Basic Clin Pharmacol Toxicol, (2015). 116: 179-86.10.1111/bcpt.12342
- 22
- 23 24. Gramegna, A., F. Amati, L. Terranova, G. Sotgiu, P. Tarsia, D. Miglietta, M.A. Calderazzo, S. Aliberti, and F. Blasi, *Neutrophil elastase in bronchiectasis*. Respir Res, (2017). 18: 211.10.1186/s12931-017-0691-x
- 24
- 25
- 26 25. Hobbs, C.A., M.G. Blanchard, O. Alijevic, C.D. Tan, S. Kellenberger, S. Bencharit, R. Cao, M. Kesimer, W.G. Walton, A.G. Henderson, M.R. Redinbo, M.J. Stutts, and R. Tarran, *Identification of the SPLUNC1 ENaC-inhibitory domain yields novel strategies to treat sodium hyperabsorption in cystic fibrosis airway epithelial cultures*. Am J Physiol Lung Cell Mol Physiol, (2013). 305: L990-L1001.10.1152/ajplung.00103.2013
- 27
- 28
- 29
- 30
- 31 26. Mall, M.A., G.J. Criner, M. Miravittles, S.M. Rowe, C.F. Vogelmeier, D.J. Rowlands, M. Schoenberger, and P. Altman, *Cystic fibrosis transmembrane conductance regulator in COPD: a role in respiratory epithelium and beyond*. Eur Respir J, (2023). 61.10.1183/13993003.01307-2022
- 32
- 33
- 34
- 35
- 36
- 37 27. Parodi, A., G. Righetti, E. Pesce, A. Salis, V. Tomati, C. Pastorino, B. Tasso, M. Benvenuti, G. Damonte, N. Pedemonte, E. Cichero, and E. Millo, *Journey on VX-809-Based Hybrid Derivatives towards Drug-like F508del-CFTR Correctors: From Molecular Modeling to Chemical Synthesis and Biological Assays*. Pharmaceuticals (Basel), (2022). 15.10.3390/ph15030274
- 38
- 39
- 40
- 41 28. Mall, M.A., N. Mayer-Hamblett and S.M. Rowe, *Cystic Fibrosis: Emergence of Highly Effective Targeted Therapeutics and Potential Clinical Implications*. Am J Respir Crit Care Med, (2020). 201: 1193-1208.10.1164/rccm.201910-1943SO
- 42
- 43
- 44
- 45
- 46 29. Byrne, D.P., M.H. Omar, E.J. Kennedy, P.A. Eyers and J.D. Scott, *Biochemical Analysis of AKAP-Anchored PKA Signaling Complexes*. Methods Mol Biol, (2022). 2483: 297-317.10.1007/978-1-0716-2245-2_19
- 47
- 48
- 49
- 50 30. Veine, D.M., H. Yao, D.R. Stafford, K.S. Fay and D.L. Livant, *A D-amino acid containing peptide as a potent, noncovalent inhibitor of alpha5beta1 integrin in human prostate cancer invasion and lung colonization*. Clin Exp Metastasis, (2014). 31: 379-93.10.1007/s10585-013-9634-1
- 51
- 52
- 53 31. Garton, M., S. Nim, T.A. Stone, K.E. Wang, C.M. Deber and P.M. Kim, *Method to generate highly stable D-amino acid analogs of bioactive helical peptides using a mirror image of the entire PDB*. Proc Natl Acad Sci U S A, (2018). 115: 1505-1510.10.1073/pnas.1711837115
- 54
- 55
- 56
- 57 32. Casey, M., C. Gabillard-Lefort, O.F. McElvaney, O.J. McElvaney, T. Carroll, R.C. Heeney, C. Gunaratnam, E.P. Reeves, M.P. Murphy, and N.G. McElvaney, *Effect of elexacaftor/tezacaftor/ivacaftor on airway and systemic inflammation in cystic fibrosis*. Thorax, (2023). 78: 835-839.10.1136/thorax-2022-219943
- 58
- 59
- 60
- 61
- 62
- 63
- 64
- 65

- 1 33. Schaupp, L., A. Addante, M. Voller, K. Fentker, A. Kuppe, M. Bardua, J. Duerr, L. Piehler, J.
2 Rohmel, S. Thee, M. Kirchner, M. Ziehm, D. Lauster, R. Haag, M. Gradzielski, M. Stahl, P.
3 Mertins, S. Boutin, S.Y. Graeber, et al., *Longitudinal effects of elexacaftor/tezacaftor/ivacaftor on*
4 *sputum viscoelastic properties, airway infection and inflammation in patients with cystic fibrosis.*
5 *Eur Respir J*, (2023). 62.10.1183/13993003.02153-2022
6
7 34. Ibrahim, B.M., S. Park, B. Han and Y. Yeo, *A strategy to deliver genes to cystic fibrosis lungs: a*
8 *battle with environment.* *J Control Release*, (2011). 155: 289-95.10.1016/j.jconrel.2011.07.039
9
10 35. Capurro, V., V. Tomati, E. Sondo, M. Renda, A. Borrelli, C. Pastorino, D. Guidone, A. Venturini,
11 A. Giraud, S. Mandrup Bertozzi, I. Musante, F. Bertozzi, T. Bandiera, F. Zara, L.J.V. Galiotta,
12 and N. Pedemonte, *Partial Rescue of F508del-CFTR Stability and Trafficking Defects by Double*
13 *Corrector Treatment.* *Int J Mol Sci*, (2021). 22.10.3390/ijms22105262
14
15 36. Graeber, S.Y., C. Vitzthum, S.T. Pallenberg, L. Naehrlich, M. Stahl, A. Rohrbach, M. Drescher,
16 R. Minso, F.C. Ringshausen, C. Rueckes-Nilges, J. Klajda, J. Berges, Y. Yu, H. Scheuermann, S.
17 Hirtz, O. Sommerburg, A.M. Dittrich, B. Tummler, and M.A. Mall, *Effects of*
18 *Elexacaftor/Tezacaftor/Ivacaftor Therapy on CFTR Function in Patients with Cystic Fibrosis and*
19 *One or Two F508del Alleles.* *Am J Respir Crit Care Med*, (2022). 205: 540-
20 549.10.1164/rccm.202110-2249OC
21
22 37. Veit, G., A. Roldan, M.A. Hancock, D.F. Da Fonte, H. Xu, M. Hussein, S. Frenkiel, E. Matouk,
23 T. Velkov, and G.L. Lukacs, *Allosteric folding correction of F508del and rare CFTR mutants by*
24 *elexacaftor-tezacaftor-ivacaftor (Trikafta) combination.* *JCI Insight*, (2020).
25 5.10.1172/jci.insight.139983
26
27 38. Nichols, D.P., S.J. Morgan, M. Skalland, A.T. Vo, J.M. Van Daltsen, S.B. Singh, W. Ni, L.R.
28 Hoffman, K. McGeer, S.L. Heltshe, J.P. Clancy, S.M. Rowe, P. Jorth, P.K. Singh, and P.R.-M.S.
29 Group, *Pharmacologic improvement of CFTR function rapidly decreases sputum pathogen*
30 *density, but lung infections generally persist.* *J Clin Invest*, (2023). 133.10.1172/JCI167957
31
32 39. Wang, L., N. Wang, W. Zhang, X. Cheng, Z. Yan, G. Shao, X. Wang, R. Wang, and C. Fu,
33 *Therapeutic peptides: current applications and future directions.* *Signal Transduct Target Ther*,
34 (2022). 7: 48.10.1038/s41392-022-00904-4
35
36

37 **Statements and Declarations**

38 **Funding**

39 This work was supported by research grants from Cariplo Foundation (#2018-0498 to E.H.), Roche
40 Foundation (Bando Roche per la Ricerca 2019 to A.G.), Compagnia di San Paolo (CSTO161109 to E.H.),
41 Telethon Foundation (GGP20079 to A.G.), Research Grant Ministero della Salute, Italy (RC 2023/260-
42 01 to F.B.), Fondazione IRCCS Ca' Granda Ospedale Maggiore Policlinico Milano, Regione Lombardia
43 Cystic Fibrosis Funding 2022 (Cod. 18563 Capitolo 13.01.1 to F.B.) and PRIN 2022 (2022WHSC3 to
44 S.A., F.B. and E.H.).
45
46
47

48 **Competing Interests**

49 Alessandra Ghigo and Emilio Hirsch are cofounders and shareholders of Kither Biotech Srl. Valentina
50 Sala and Laura Tasca are employees of Kither Biotech Srl. All other authors report no conflict.
51
52

53 **Author Contributions**

54 Alessandra Ghigo and Angela Della Sala conceived and designed the overall study. Angela Della Sala
55 carried out the core of the experiments and analyzed the data. Laura Tasca performed structure prediction
56 and docking studies. Cosmin Stefan Butnarusu measured peptides binding kinetic constants and
57 permeability in PAMPA assays. Alberto Massarotti designed DRI-Pep #20 peptide variants. Valentina
58 Sala, Giulia Prono, Alessandra Murabito, Enrico Millo, Leonardo Terranova, Francesco Blasi, Andrea
59 Gramegna, Stefano Aliberti, Sonja Visentin, Emilio Hirsch provided advice on the interpretation of data.
60
61
62
63
64
65

1 Angela Della Sala and Alessandra Ghigo wrote the manuscript with input from coauthors. All authors
2 reviewed and approved the final manuscript.
3

4 **Data Availability**

5 All data associated with this study are available in the paper or the Supplementary Information.
6
7

8 **Ethics approval**

9 All animal experiments conducted in this study were approved by the animal ethical committee of the
10 University of Torino and by the Italian Ministry of Health (Authorization n°757/2016-PR). Spontaneous
11 expectorated sputum samples from CF patients in stable clinical conditions were collected at the
12 Bronchiectasis and Cystic Fibrosis Programs of the Respiratory Department of Fondazione IRCCS Ca'
13 Granda Ospedale Maggiore Policlinico in Milan (Italy). The patients signed an express, free and informed,
14 consent to the collection and use of their biological samples. The study protocol was approved by local
15 institutional review boards (594_2016bis).
16
17
18
19

20 **Tables**

21 **Table 1. Binding kinetics of the interaction between DRI-Pep #20 and PKA-RII α .**

	<i>Steady- state experiment</i>	<i>Kinetic experiment</i>
k_{on} ($10^6 M^{-1} s^{-1}$)	-	1.5
k_{off} ($10^{-2} s^{-1}$)	-	7.2
K_A ($10^7 M^{-1}$)	1.3	2.0
K_D ($10^{-8} M$)	7.6	4.9

22 **Figures**

23
24
25
26
27
28
29
30
31
32
33
34
35
36
37
38
39
40
41
42
43
44
45
46
47
48
49
50
51
52
53
54
55
56
57
58
59
60
61
62
63
64
65

Figure 1

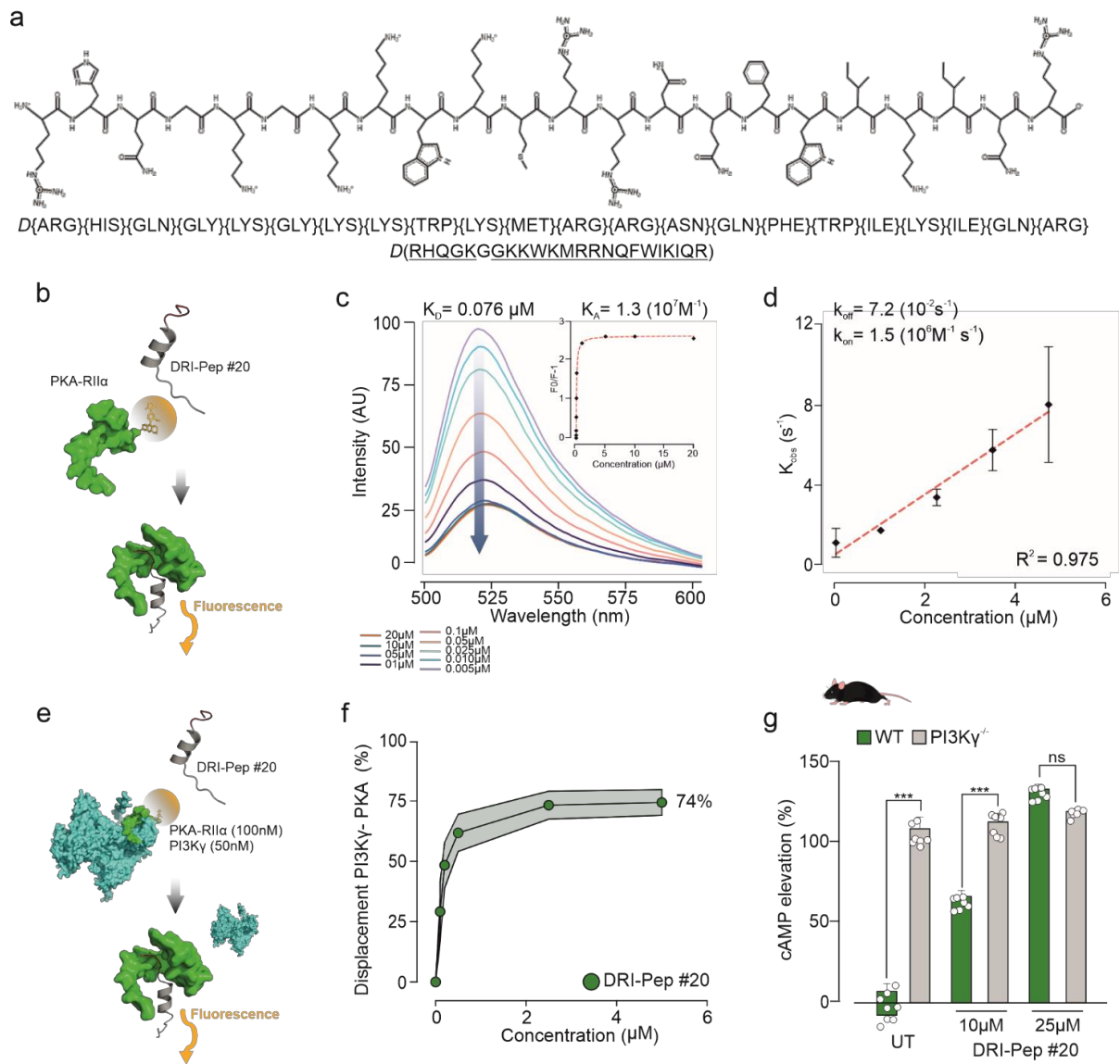


Figure 2

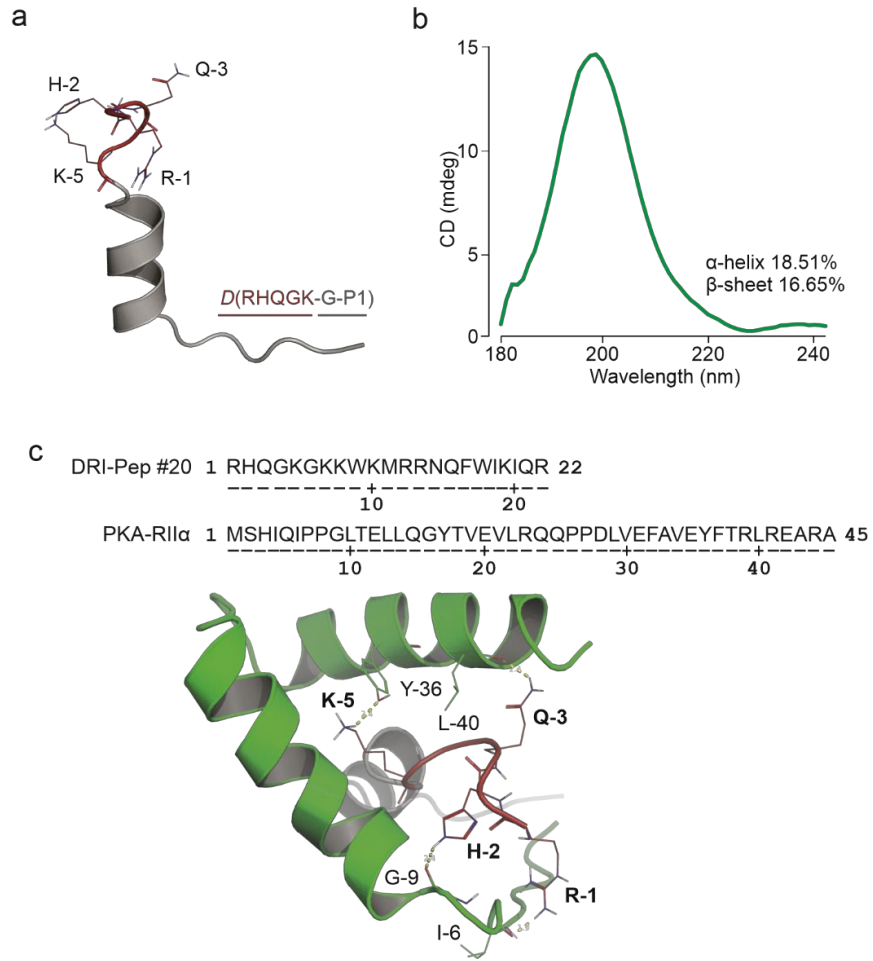
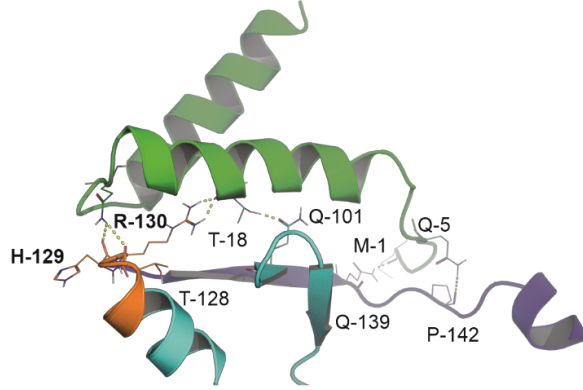


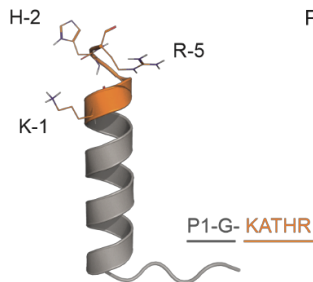
Figure 3

a

PI3K γ 120 DCLRYW**KATHR**SPGQIHLVQRHPPSEESQAFQRQLTALIGY 160
 PKA-RII α 1 MSHIQIPPGLTELLQGYTVEVLRQQPPDLVEFAVEYFTRLREARA 45

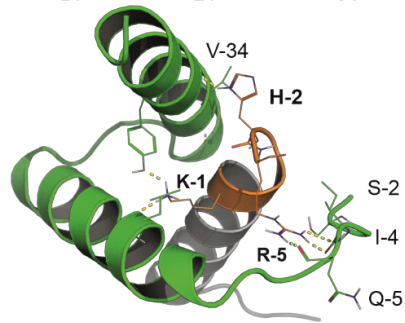


b



c

KATHR 1 RQIKIWFQNRRMKWKK**KATHR** 22
 PKA-RII α 1 MSHIQIPPGLTELLQGYTVEVLRQQPPDLVEFAVEYFTRLREARA 45



1
2
3
4
5
6
7
8
9
10
11
12
13
14
15
16
17
18
19
20
21
22
23
24
25
26
27
28
29
30
31
32
33
34
35
36
37
38
39
40
41
42
43
44
45
46
47
48
49
50
51
52
53
54
55
56
57
58
59
60
61
62
63
64
65

Figure 4

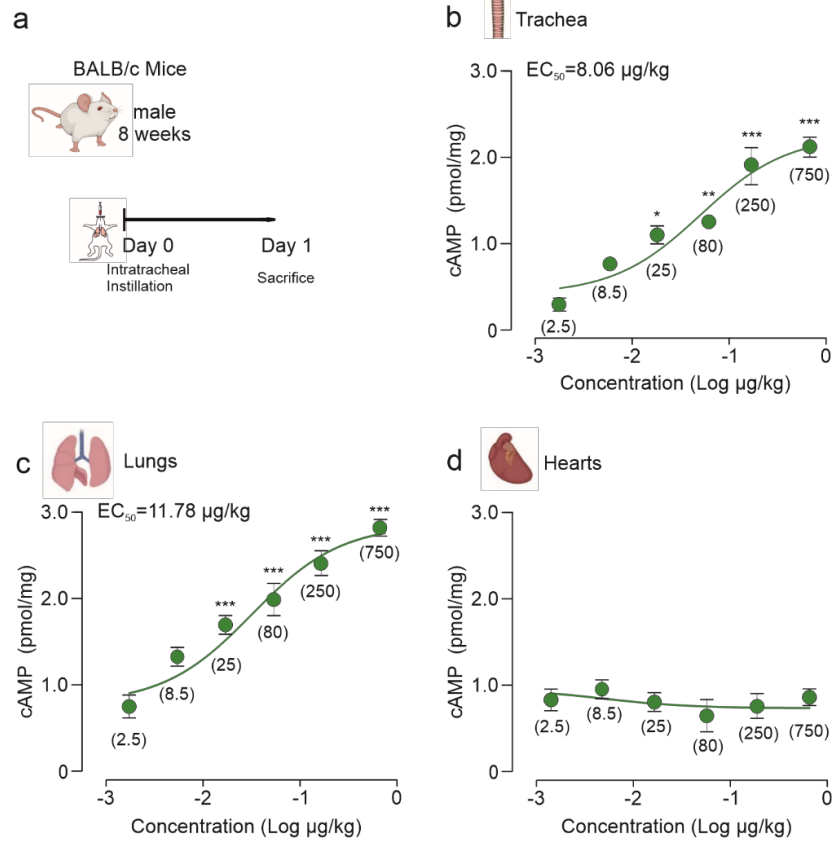


Figure 5

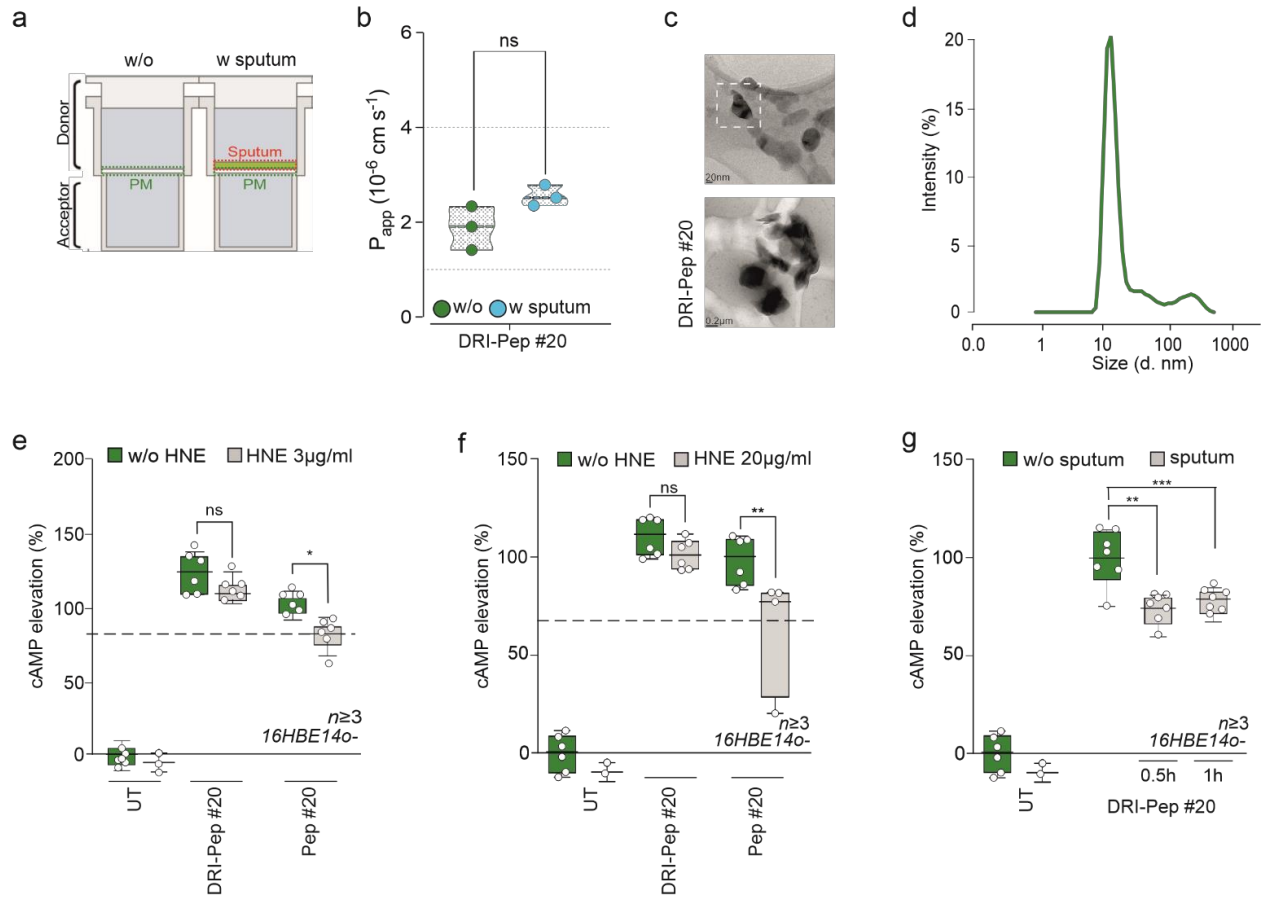
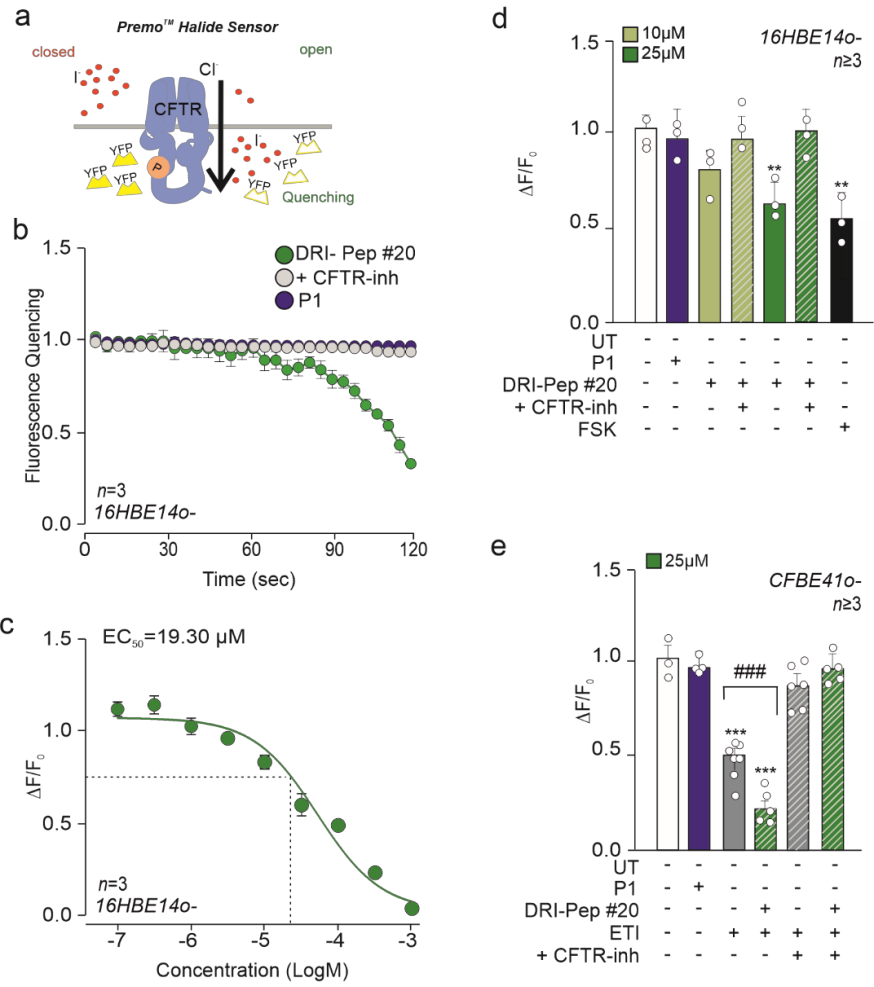


Figure 6



Legends

Figure 1. DRI-Pep #20 is a potent PI3K γ /PKA disruptor peptide.

a) Chemical structure of DRI-Pep #20. The amino acid sequence of DRI-Pep #20 comprises the cell penetrating peptide Penetratin 1 (P1), a glycine (G) linker and the non-natural sequence RHQGK, wherein each amino acid is a D-amino acid. **b)** Schematic representation of the fluorescence spectroscopy assays for the characterization of the interaction between DRI-Pep #20 and the recombinant fluorescein 5-maleimide-labeled PKA-RII α (PKA-F5M). **c)** Steady-state emission spectra of PKA-F5M in the presence of increasing concentrations of DRI-Pep #20 (0 to 20 μ M). K_D : dissociation constant. AU, arbitrary units. Inset, non-linear fitting of the fluorescence intensity maxima obtained at various concentrations of DRI-Pep #20 for the monitoring of bio-labeled PKA. K_A : association constant. **d)** For kinetic analysis, fluorescence spectra of PKA-F5M in the presence of increasing concentrations of DRI-Pep #20 (0 to 5 μ M) were analyzed and fitted to a single exponential function to obtain the observed rate constant (k_{obs}). The binding of DRI-Pep #20 to bio-labeled PKA was investigated under *pseudo*-first-order conditions, and the kinetic constants, k_{on} and k_{off} , were determined. **e)** Schematic representation of the displacement assay between DRI-Pep #20 and the PI3K γ /PKA-F5M complex. **f)** Percentage displacement of the PI3K γ /PKA-RII α complex by DRI-Pep #20, calculated from steady-state emission spectra of the PI3K γ /PKA-F5M complex in the presence of increasing concentrations of DRI-Pep #20 (0 to 5 μ M). The displacement efficiency was expressed as percentage of the binding between PI3K γ and PKA-F5M relative to that in the absence of DRI-Pep #20. **g)** cAMP concentrations in peritoneal macrophages from wild-type (WT, in green) and PI3K $\gamma^{-/-}$ mice (in grey) treated with 10-25 μ M DRI-Pep #20 for 30 min. The amount of cAMP was expressed as percentage of cAMP accumulation observed in untreated PI3K $\gamma^{-/-}$ cells. $n \geq 6$ technical replicates from $N > 3$ independent experiments. *** $P < 0.001$ WT versus PI3K $\gamma^{-/-}$ by one-way ANOVA, followed by Bonferroni's post hoc test. Data are means \pm SEM.

Figure 2. Structural prediction of the binding between DRI-Pep #20 and PKA-RII α .

a) DRI-Pep #20 structure prediction by PEP-FOLD3.5. P1-G and RHQGK domains are shown as cartoons in grey and red, respectively. R-1, H-2, Q-3 and K-5 residues are indicated and shown as sticks. **b)** Circular dichroism spectra of DRI-Pep #20 showing a peak at 190-240 nm. The percentage of α -helical and β -sheet secondary structures calculated by the K2D3 software are indicated. **c)** Molecular docking simulation of the interaction between DRI-Pep #20 and PKA by HADDOCK 2.4. The docked pose of DRI-Pep #20 in complex with residues 1-45 of PKA-RII α (cartoon in green) is shown. The key residues involved in the binding are indicated and shown as sticks, with DRI-Pep #20 residues in bold. Hydrogen bonds between DRI-Pep #20 and PKA-RII α are indicated by yellow dashed lines. In **a** and **c**, the structural models were developed using PyMOL.

Figure 3. Structural prediction of the native binding between the N-terminal domain of PI3K γ and PKA-RII α .

a) Molecular docking simulation of the interaction between PI3K γ and PKA-RII α by HADDOCK 2.4. The docked pose of residues 120-160 of PI3K γ (cyan cartoon) in complex with residues 1-45 of PKA-RII α (green cartoon) is shown. The amino acids critical for the binding between the two proteins are shown and indicated as sticks, with the residues of PI3K γ in bold. The region of PI3K γ at the core of the interaction (KATHR) is shown in orange. Hydrogen bonds between PI3K γ and PKA-RII α are indicated by yellow dashed lines. **b)** Structural prediction of the KATHR sequence by PEP-FOLD3.5. KATHR and P1-G domains are shown as cartoons in orange and grey, respectively. K-1, H-4 and R-5 residues of PI3K γ are indicated and shown as sticks. **c)** Molecular docking simulation of the interaction between KATHR and PKA by HADDOCK 2.4. The docked pose of KATHR in complex with residues 1-45 of PKA RII α (cartoon in green) is shown. Yellow dashed lines indicate hydrogen bonds between KATHR and 1-45 PKA-RII α . The amino acids critical for the binding are indicated and shown as sticks, with KATHR residues in bold. Throughout, the structural models were developed using PyMOL.

1
2 **Figure 4. DRI-Pep #20 increases cAMP levels locally *in vivo* in the airway tract of mice.**

3 **a)** Schematic representation of the treatment schedule. BALB/c mice received DRI-Pep #20 through
4 intratracheal (i.t.) instillation. **(b-d)** cAMP concentrations in tracheas **(b)**, lungs **(c)** and hearts **(d)** from
5 BALB/c mice 24 hours after i.t. instillation of different doses of DRI-Pep #20 (0 to 750 mg/kg). Values
6 in brackets indicate the dose of DRI-Pep #20 expressed as mg/kg. The number of mice (n) ranged from 3
7 to 6 per group. EC₅₀, median effective concentration. In **a)** and **b)**, *P < 0.05, **P < 0.01, and ***P <
8 0.001 by one-way ANOVA, followed by Bonferroni's post hoc test. Throughout, data are means ± SEM.
9
10
11

12 **Figure 5. DRI-Pep #20 can penetrate pathological mucus and resist protease degradation.**

13 **a)** Schematic representation of the Parallel Artificial Membrane Permeability Assay (PAMPA) with and
14 without cystic fibrosis (CF) sputum deposition on top of the artificial lipid membrane (PM). **b)** Apparent
15 permeability (P_{app}) measurements of DRI-Pep #20 (2 mg/mL), in the absence (green box) and in the
16 presence (blue box) of CF sputum. The green dashed line indicates the threshold P_{app} for high-medium
17 permeable compounds (4×10^{-6} cm s⁻¹), while the red dashed line defines the limit for medium-low
18 permeable molecules (1×10^{-6} cm s⁻¹). ns: non-significant by Student's t test. **c)** Representative
19 Transmission Electron Microscopy (TEM) images of DRI-Pep #20 (0.1 mg/mL in water). Scale bar: 20
20 nm. **d)** Size distribution profile of DRI-Pep #20 (4 mg/mL in 2 mM PBS) obtained by dynamic light
21 scattering (DLS) analysis. **e-f)** cAMP concentrations in 16HBE14o- cells treated with the DRI-Pep #20
22 and Pep #20 (25 μM for 30 min) in the absence (green bars) and in the presence (gray bars) of either 3
23 μg/ml **(d)** or 20 μg/ml **(e)** human neutrophil elastase (HNE). The amount of cAMP was expressed as
24 percentage of cAMP accumulation elicited by Pep #20 without HNE. Dashed lines indicate the amount
25 of cAMP (%) induced by Pep #20 with HNE as a reference. n ≥ 6 technical replicates from N > 3
26 independent experiments. *P < 0.05 and **P < 0.01 by one-way ANOVA, followed by Bonferroni's post
27 hoc test. ns: non-significant. **g)** cAMP elevation in 16HBE14o- cells covered with a layer of CF sputum
28 and then treated with 25 μM DRI-Pep #20 for 30 min and 1 hour. The amount of cAMP was expressed as
29 percentage of cAMP accumulation elicited by DRI-Pep #20 in the absence of sputum at 30 min. **P < 0.01
30 and ***P < 0.001 versus DRI-Pep #20 without sputum by two-way ANOVA test, followed by Bonferroni's
31 post-hoc analysis. n ≥ 6 technical replicates from N > 3 independent experiments. Throughout, data are
32 means ± SEM.
33
34
35
36
37
38
39

40 **Figure 6. DRI-Pep #20 modulates wild-type and F508del-CFTR activity.**

41 **a)** Schematic representation of CFTR activity measurement through the Premo™ Halide Sensor assay. **b)**
42 Average fluorescence quenching traces of 16HBE14o- cells expressing the halide-sensitive yellow
43 fluorescent protein (HS-YFP) and treated with either 25 μM DRI-Pep #20 or equimolar amount of the
44 control peptide P1 for 30 min before addition of Premo Halide stimulus buffer. Fluorescence was
45 continuously read (1 point per second) starting at 1 s before addition of the buffer and up to 120 s. The
46 CFTR inhibitor CFTR_{inh}-172 (10 μM for 5 min) was used to evaluate the selective activation of the CFTR
47 channel. **c)** CFTR activity (expressed as the change in fluorescence ΔF/F₀) in response to 30-min
48 stimulation with increasing concentrations of DRI-Pep #20 (31.6 nM to 316 mM) in 16HBE14o- cells
49 expressing HS-YFP. To determine the EC₅₀, nonlinear regression analysis was used. **d)** CFTR activity
50 (expressed as the change in fluorescence ΔF/F₀) in 16HBE14o- cells expressing HS-YFP and treated with
51 10-25 μM DRI-Pep #20 for 30 min in the absence or in the presence of the CFTR inhibitor CFTR_{inh}-172
52 (10 μM for 5 min). The adenylyl cyclase activator, forskolin (FSK), was used as a positive control (100
53 nM for 5 min), while P1 was used as a negative control (25 μM for 30 min). UT: untreated cells. **e)** CFTR
54 activity in F508del-CFTR-CFBE41o- cells expressing HS-YFP and treated with
55 Elexacaftor/Tezacaftor/Ivacaftor alone (ETI) or together with DRI-Pep #20. Cells were corrected with
56 Elexacaftor (3 μM) and Tezacaftor (10 μM) for 24 hours and then exposed acutely to Ivacaftor (1 μM)
57 for 30 min, alone (ETI) or together with 25 μM DRI-Pep #20. The CFTR inhibitor CFTR_{inh}-172 was used
58 as in **(b)**. UT: untreated cells. In **(b)** and **(e)**, n ≥ 3 technical replicates from N > 3 independent experiments.
59
60
61
62
63
64
65

LUNG DISEASE

A PI3K γ mimetic peptide triggers CFTR gating, bronchodilation, and reduced inflammation in obstructive airway diseases

Alessandra Ghigo^{1,2,*†}, Alessandra Murabito^{1†}, Valentina Sala^{1,2}, Anna Rita Pisano³, Serena Bertolini³, Ambra Gianotti⁴, Emanuela Caci⁴, Alessio Montresor^{5,6}, Aiswarya Premchandrar⁷, Flora Pirozzi^{1,8}, Kai Ren¹, Angela Della Sala¹, Marco Mergioti¹, Wito Richter⁹, Eyleen de Poel¹⁰, Michaela Matthey¹¹, Sara Caldrea^{5,6,†}, Rosa A. Cardone¹², Federica Civiletti¹³, Andrea Costamagna¹³, Nancy L. Quinney¹⁴, Cosmin Butnaru¹, Sonja Visentin¹, Maria Rosaria Ruggiero¹, Simona Baroni¹, Simonetta Geninatti Crich¹, Damien Ramel¹⁵, Muriel Laffargue¹⁵, Carlo G. Tocchetti^{8,16,17}, Renzo Levi¹⁸, Marco Conti¹⁹, Xiao-Yun Lu²⁰, Paola Melotti²¹, Claudio Sorio^{5,6}, Virginia De Rose¹, Fabrizio Facchinetti³, Vito Fanelli¹³, Daniela Wenzel^{11,22}, Bernd K. Fleischmann²², Marcus A. Mall^{23,24}, Jeffrey Beekman¹⁰, Carlo Laudanna^{5,6}, Martina Gentsch^{14,25}, Gergely L. Lukacs⁷, Nicoletta Pedemonte⁴, Emilio Hirsch^{1,2,*}

Cyclic adenosine 3',5'-monophosphate (cAMP)-elevating agents, such as β_2 -adrenergic receptor (β_2 -AR) agonists and phosphodiesterase (PDE) inhibitors, remain a mainstay in the treatment of obstructive respiratory diseases, conditions characterized by airway constriction, inflammation, and mucus hypersecretion. However, their clinical use is limited by unwanted side effects because of unrestricted cAMP elevation in the airways and in distant organs. Here, we identified the A-kinase anchoring protein phosphoinositide 3-kinase γ (PI3K γ) as a critical regulator of a discrete cAMP signaling microdomain activated by β_2 -ARs in airway structural and inflammatory cells. Displacement of the PI3K γ -anchored pool of protein kinase A (PKA) by an inhaled, cell-permeable, PI3K γ mimetic peptide (PI3K γ MP) inhibited a pool of subcortical PDE4B and PDE4D and safely increased cAMP in the lungs, leading to airway smooth muscle relaxation and reduced neutrophil infiltration in a murine model of asthma. In human bronchial epithelial cells, PI3K γ MP induced unexpected cAMP and PKA elevations restricted to the vicinity of the cystic fibrosis transmembrane conductance regulator (CFTR), the ion channel controlling mucus hydration that is mutated in cystic fibrosis (CF). PI3K γ MP promoted the phosphorylation of wild-type CFTR on serine-737, triggering channel gating, and rescued the function of F508del-CFTR, the most prevalent CF mutant, by enhancing the effects of existing CFTR modulators. These results unveil PI3K γ as the regulator of a β_2 -AR/cAMP microdomain central to smooth muscle contraction, immune cell activation, and epithelial fluid secretion in the airways, suggesting the use of a PI3K γ MP for compartment-restricted, therapeutic cAMP elevation in chronic obstructive respiratory diseases.

INTRODUCTION

Obstructive airway diseases, including asthma, chronic obstructive pulmonary disease (COPD) and the genetic disorder cystic fibrosis (CF), represent a major health burden worldwide. Over the next decade, prevalence of asthma and COPD is predicted to rise in developing countries (1) and so is the number of patients with CF requiring

long-term care, because survival is progressively improving due to better treatments and intensive follow-up (2). Despite the diversity in etiology, pathogenetic mechanisms, and clinical manifestations, these conditions share common features such as chronic airway inflammation, mucus hypersecretion, and airflow obstruction due to airway hyperreactivity and/or mucus plugging (1, 2). Conventional

¹Department of Molecular Biotechnology and Health Sciences, Molecular Biotechnology Center, University of Torino, 10126 Torino, Italy. ²Kither Biotech Srl, 10126, Torino, Italy. ³Chiesi Farmaceutici S.p.A., Corporate Pre-Clinical R&D, 43122 Parma, Italy. ⁴UOC Genetica Medica, IRCCS Istituto Giannina Gaslini, 16147 Genova, Italy. ⁵Division of General Pathology, Department of Medicine, University of Verona School of Medicine, 37134 Verona, Italy. ⁶Cystic Fibrosis Translational Research Laboratory "Daniele Lissandrini," Department of Medicine, University of Verona School of Medicine, 37134 Verona, Italy. ⁷Department of Physiology, McGill University, Montréal, Quebec H3G 1Y6, Canada. ⁸Department of Translational Medical Sciences, Federico II University, 80131 Naples, Italy. ⁹Department of Biochemistry and Molecular Biology, University of South Alabama College of Medicine Mobile, AL 36688, USA. ¹⁰Department of Pediatric Pulmonology, Wilhelmina Children's Hospital, University Medical Center Utrecht, 3584 EA Utrecht, Netherlands. ¹¹Department of Systems Physiology, Medical Faculty, Ruhr University Bochum, 44801 Bochum, Germany. ¹²Department of Biosciences, Biotechnologies, and Biopharmaceutics, University of Bari, 70126 Bari, Italy. ¹³Department of Anesthesia and Critical Care Medicine, University of Torino, Azienda Ospedaliera Città della Salute e della Scienza di Torino, 10126 Torino, Italy. ¹⁴Marsico Lung Institute/Cystic Fibrosis Research Center, University of North Carolina, Chapel Hill, NC 27599, USA. ¹⁵Institute of Metabolic and Cardiovascular Diseases, Paul Sabatier University, 31432 Toulouse, France. ¹⁶Interdepartmental Center of Clinical and Translational Research (CIRCET), Federico II University, 80131 Naples, Italy. ¹⁷Interdepartmental Hypertension Research Center (CIRIAPA), Federico II University, 80131 Naples, Italy. ¹⁸Department of Life Sciences and Systems Biology, University of Torino, 10123 Torino, Italy. ¹⁹Department of Obstetrics, Gynecology, and Reproductive Sciences, University of California San Francisco, San Francisco, CA 94143, USA. ²⁰School of Life Science and Technology, Xi'an Jiaotong University, 710049 Xi'an Shaanxi, P.R. China. ²¹Cystic Fibrosis Center, Azienda Ospedaliera Universitaria Integrata di Verona, 37126 Verona, Italy. ²²Institute of Physiology I, Life and Brain Center, Medical Faculty, University of Bonn, 53127 Bonn, Germany. ²³Department of Pediatric Respiratory Medicine, Immunology, and Critical Care Medicine, Charité-Universitätsmedizin Berlin, 10117 Berlin, Germany. ²⁴German Center for Lung Research (DZL), associated partner, 10117 Berlin, Germany. ²⁵Department of Pediatric Pulmonology, University of North Carolina, Chapel Hill, NC 27599, USA. *Corresponding author. Email: alessandra.ghigo@unito.it (A.G.); emilio.hirsch@unito.it (E.H.)

†These authors contributed equally to this work.

‡Present address: Department of Infectious, Tropical Diseases and Microbiology, IRCCS Sacro Cuore Don Calabria Hospital, 37024 Negrar, Italy.

medications, especially for asthma, include inhaled corticosteroids and β_2 -adrenergic receptor (β_2 -AR) agonists, which reduce airway inflammation and reverse airway constriction, respectively (1). Whereas the primary effect of β_2 -AR agonists is relaxation of airway smooth muscle, these drugs can also engage this receptor in infiltrating leukocytes, eventually contributing to the resolution of inflammation through the cyclic adenosine 3',5'-monophosphate (cAMP) pathway (3). Furthermore, β_2 -AR agonists are potent inducers of the CF transmembrane conductance regulator (CFTR) (4), the epithelial anion channel that drives airway surface fluid hydration. CFTR dysfunction is a major cause of mucus hyperconcentration that leads to impaired mucociliary clearance and mucus plugging not only in patients with the genetic disorder CF (2) but also in COPD (5) and asthma (6). Although β_2 -AR agonists could be beneficial in these chronic obstructive diseases, their efficacy is still limited, primarily because of tachyphylaxis and adverse events, such as tachyarrhythmias, stemming from systemic drug exposure. Similarly, inhibition of cAMP breakdown by drugs targeting phosphodiesterase 4 (PDE4) (7), the major cAMP-hydrolyzing enzyme in the airways, is clinically effective but exhibits unwanted side effects, such as emesis, diarrhea, and weight loss, likely due to systemic PDE4 blockade (8). Thus, safer approaches for the manipulation of the β_2 -AR/cAMP signaling axis for the treatment of chronic airway diseases are desirable.

Previous work from our group identified phosphoinositide 3-kinase γ (PI3K γ) as a negative regulator of β_2 -AR/cAMP signaling in the heart. In this tissue, PI3K γ serves as an A-kinase anchoring protein (AKAP) that tethers protein kinase A (PKA) to PDE3 and PDE4, favoring their PKA-mediated phosphorylation and activation. This mechanism of localized PDE stimulation eventually allows restricting β_2 -AR/cAMP responses to discrete subcellular compartments (9, 10). Accordingly, disruption of the scaffold but not the kinase activity of PI3K γ results in β_2 -AR/cAMP signaling amplification in cardiomyocytes (9). Because PI3K γ is also found in pulmonary cells (11), we speculated that PI3K γ could contribute to the compartmentalization of β_2 -AR/cAMP responses in the lungs and that pharmacological targeting of PI3K γ scaffold activity could achieve therapeutic cAMP elevation in the airways.

Here, we described a cell-permeable PI3K γ -derived mimetic peptide (PI3K γ MP) that, by interrupting the interaction between PI3K γ and PKA, inhibited PI3K γ -associated PDE4B and PDE4D and, in turn, enhanced β_2 -AR/cAMP responses in human bronchial smooth muscle, epithelial, and immune cells. Intratracheal instillation of PI3K γ MP limited bronchoconstriction and lung neutrophil infiltration in a mouse model of asthma. In human airway epithelial cells, PI3K γ MP promoted gating of wild-type (wt) CFTR and restored the function of the most prevalent CFTR mutant in CF (F508del) by potentiating the effects of approved CFTR modulators.

RESULTS

A PI3K γ MP enhances airway β_2 -AR/cAMP signaling

To assess the role of PI3K γ scaffold activity in the regulation of airway cAMP, we compared PI3K γ knockout mice (PI3K $\gamma^{-/-}$), lacking both the anchoring and the catalytic function of the p110 γ subunit of PI3K γ , with animals expressing a kinase-inactive p110 γ that retains the scaffold activity [PI3K γ kinase-dead (PI3K $\gamma^{KD/KD}$)] (9). The amount of cAMP was twofold higher in PI3K $\gamma^{-/-}$ than in wt (PI3K $\gamma^{+/+}$) and PI3K $\gamma^{KD/KD}$ tracheas (Fig. 1A), suggesting a kinase-

independent control of airway cAMP by PI3K γ . Similar to previous findings in the heart (9), the increased cAMP concentration detected in PI3K $\gamma^{-/-}$ tracheas correlated with reduced activity of PDE4B and PDE4D, whereas their function was normal in PI3K $\gamma^{KD/KD}$ tissues (Fig. 1B). Modulation of PDE4B and PDE4D by PI3K γ was also detected in isolated murine tracheal smooth muscle cells (mTSMCs) (Fig. 1C), where PI3K γ was found to be highly abundant (Fig. 1D). As shown in Fig. 1D, the canonical p110 γ doublet was detectable in peripheral blood mononuclear cells and tracheas, whereas mTSMCs and human bronchial smooth muscle cells (hBSMCs) displayed the low-molecular weight isoform only. These PI3K γ forms were found to organize multiprotein complexes containing both PDEs and their activator PKA (Fig. 1, E and F). Down-regulation of the *PIK3CG* gene (encoding p110 γ) in hBSMCs increased β_2 -AR-activated cAMP responses by 30% (Fig. 1G), thus supporting a PI3K γ kinase-independent activation of PDE4, restraining airway cAMP downstream of β_2 -ARs.

These findings prompted us to design a molecule interfering with the scaffold function of PI3K γ and enhancing β_2 -AR/cAMP signaling in the airways. To disrupt the PKA-anchoring function of PI3K γ in vivo, a peptide encompassing the PKA-binding motif of PI3K γ (10) was fused to the cell-penetrating sequence penetratin-1 (P1) (Fig. 2A) (12). A fluorescein isothiocyanate (FITC)-labeled version of this PI3K γ MP was detectable in hBSMCs within 30 min of administration (Fig. 2A). PI3K γ MP associated the recombinant RII α subunit of PKA with a dissociation constant of 7.5 μ M (Fig. 2B) and dose-dependently disrupted the PKA-RII/p110 γ interaction (Fig. 2C). Conversely, PI3K γ MP did not alter C5a-mediated Akt phosphorylation (fig. S1A), indicating that it did not interfere with the kinase function of PI3K γ (9). In line with the ability to disturb PKA/p110 γ association, PI3K γ MP reduced PDE4B and PDE4D activity by 30% in primary wt mTSMCs, whereas no significant effect of the peptide was observed in PI3K γ -deficient cells ($P > 0.9999$) (Fig. 2D). Similarly, PI3K γ MP failed to increase cAMP in PI3K $\gamma^{-/-}$ macrophages (fig. S1B), confirming that PI3K γ MP specifically inhibited PI3K γ -associated PDEs but not PDEs anchored to other AKAPs (7). In hBSMCs, PI3K γ MP, but not a control peptide (CP) containing P1 only, increased β_2 -AR-evoked cAMP responses by 35% (Fig. 2E). Furthermore, PI3K γ MP induced cAMP elevation in human airway epithelial cells (16HBE14o-) with a maximal effective concentration of 21.66 μ M (Fig. 2F), whereas a CP containing P1 fused to a scrambled sequence of the PKA-binding site of p110 γ failed to affect cAMP abundance (fig. S1C).

To assess whether PI3K γ MP could enhance airway β_2 -AR/cAMP signaling in vivo, the peptide was instilled intratracheally in mice and found to induce a dose-dependent increase in cAMP, with 80 μ g/kg as the lowest dose eliciting a significant increase in cAMP concentration in both tracheas ($P < 0.0001$) and lungs ($P = 0.0288$) (Fig. 3A). Mice receiving FITC-labeled PI3K γ MP (80 μ g/kg) showed fluorescence in the airways as soon as 30 min after a single intratracheal administration (fig. S2A) when the amount of cAMP was already 30% higher than in tissues from animals receiving either saline or CP (fig. S2B). Moreover, PI3K γ MP persisted in the airways up to 24 hours after a single-dose instillation (Fig. 3B) when maximal cAMP accumulation was detected (Fig. 3C). Direct intrapulmonary application prevented PI3K γ MP from diffusing outside of the respiratory tract and from altering cAMP homeostasis in the heart (Fig. 3, A to C). No systemic side effects were observed after chronic exposure to PI3K γ MP, as evidenced by histopathological examination

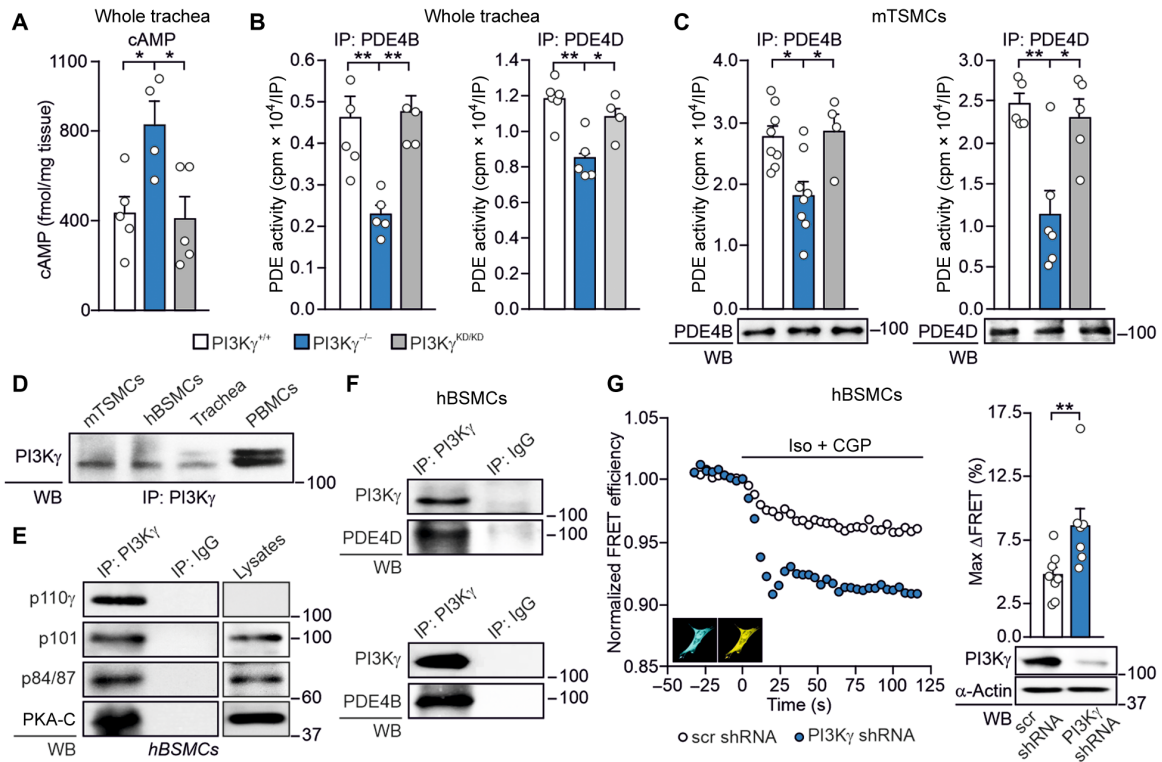


Fig. 1. PI3K γ decreases airway cAMP through kinase-dependent activation of PDE4B and PDE4D. (A) cAMP concentration in tracheas from PI3K $\gamma^{+/+}$ ($n = 5$), PI3K $\gamma^{KD/KD}$ ($n = 5$), and PI3K $\gamma^{-/-}$ ($n = 4$) mice. (B) Phosphodiesterase activity in PDE4B and PDE4D immunoprecipitates from PI3K $\gamma^{+/+}$ ($n = 5$ and $n = 6$), PI3K $\gamma^{KD/KD}$ ($n = 4$ and $n = 4$), and PI3K $\gamma^{-/-}$ ($n = 5$ and $n = 5$) tracheas. (C) Phosphodiesterase activity in PDE4B and PDE4D IP from PI3K $\gamma^{+/+}$ ($n = 8$ and $n = 5$), PI3K $\gamma^{KD/KD}$ ($n = 4$ and $n = 5$), and PI3K $\gamma^{-/-}$ ($n = 6$ and $n = 5$) independent cultures of murine tracheal smooth muscle cells (mTSMCs). Western blots (WBs) of representative IPs are shown. (D) Western blot of PI3K γ expression in mTSMCs, human bronchial smooth muscle cells (hBSMCs), and murine trachea. Peripheral blood mononuclear cells (PBMCs) are used as positive control. (E) Coimmunoprecipitation of PI3K γ catalytic subunit (p110 γ) with its relative adaptors (p101 and p84/87) and PKA catalytic subunit (PKA-C) in hBSMCs. (F) Coimmunoprecipitation of PI3K γ with PDE4B and PDE4D in hBSMCs. Immunoglobulin G (IgG) immunoprecipitation was used as control. In (D) to (F), representative Western blot images of $n = 4$ independent experiments are shown. (G) Representative fluorescence resonance energy transfer (FRET) (left) traces and (right) maximal FRET changes (max Δ FRET) of hBSMCs transfected with a FRET-based sensor for cytosolic cAMP (Epac2-cAMPs), together with either a short hairpin RNA (shRNA) against the *PI3K3CG* gene encoding PI3K γ (PI3K γ shRNA; $n = 7$) or a scrambled shRNA (scr shRNA; $n = 9$) vector. β_2 -ARs were selectively activated by isoproterenol (Iso; 100 nM for 15 s) and the β_1 -AR-selective antagonist CGP-20712A (CGP; 100 nM). Insets: Representative cyan and yellow fluorescence protein images of hBSMCs expressing Epac2-cAMPs. n indicates the number of cells analyzed in $n = 3$ independent experiments. Representative Western blot of PI3K γ expression in hBSMCs 48 hours after transfection with the PI3K γ shRNA and scr shRNA is shown below the graph. In (A) to (C), * $P < 0.05$ and ** $P < 0.01$ by one-way ANOVA, followed by Bonferroni's post hoc test. In (G), ** $P < 0.01$ by Mann-Whitney test. Throughout, data are means \pm SEM.

of major organs (fig. S3A), body weight monitoring (fig. S3B), blood biochemical tests, and cardiac function analysis (tables S1 and S2). Furthermore, negligible immunogenicity was observed only after repeated systemic administration of the peptide in the presence of adjuvants (fig. S3C), whereas PI3K γ MP did not elicit any antibody response when applied locally (fig. S3D). Thus, inhalation of PI3K γ MP might be safely used to boost airway β_2 -AR/cAMP signaling in vivo.

PI3K γ MP induces airway relaxation in a mouse model of asthma

Next, we assessed ex vivo in mouse tracheal rings if the PI3K γ scaffold activity affected cAMP-dependent airway smooth muscle relaxation. Acetylcholine-induced contraction was lower in PI3K $\gamma^{-/-}$ tracheas than in PI3K $\gamma^{+/+}$ controls, whereas PI3K $\gamma^{KD/KD}$ rings exhibited normal tone (Fig. 4A). Similarly, carbachol-dependent contractility was 35% lower in PI3K $\gamma^{-/-}$ than in PI3K $\gamma^{+/+}$ and PI3K $\gamma^{KD/KD}$ samples

(Fig. 4B). Next, PI3K $\gamma^{+/+}$ and PI3K $\gamma^{-/-}$ rings were pretreated with the selective PDE4 inhibitor roflumilast before exposure to carbachol. PDE4 inhibition decreased the contraction of PI3K $\gamma^{+/+}$ rings to the values observed in PI3K $\gamma^{-/-}$ samples where the inhibitor was ineffective (Fig. 4C), thus confirming that the decreased contraction of PI3K $\gamma^{-/-}$ airways is causally linked to a reduction in PDE4 activity.

We then determined whether PI3K γ MP could phenocopy the reduced contractility observed in PI3K $\gamma^{-/-}$ airways. Lung resistance was assessed in healthy wt mice pretreated with an aerosol of PI3K γ MP, CP, or saline before exposure to increasing doses of the contracting agent methacholine (MCh). MCh triggered a dose-dependent increase in airway resistance that was lower in mice treated with PI3K γ MP than in animals exposed to CP (Fig. 4D). Next, we tested the ability of the peptide to promote airway relaxation in ovalbumin (OVA)-sensitized mice, a well-established model of asthma. Single-dose inhalation of PI3K γ MP significantly increased the amount of cAMP in lungs ($P = 0.0065$) and tracheas ($P = 0.0137$) (Fig. 4E) and

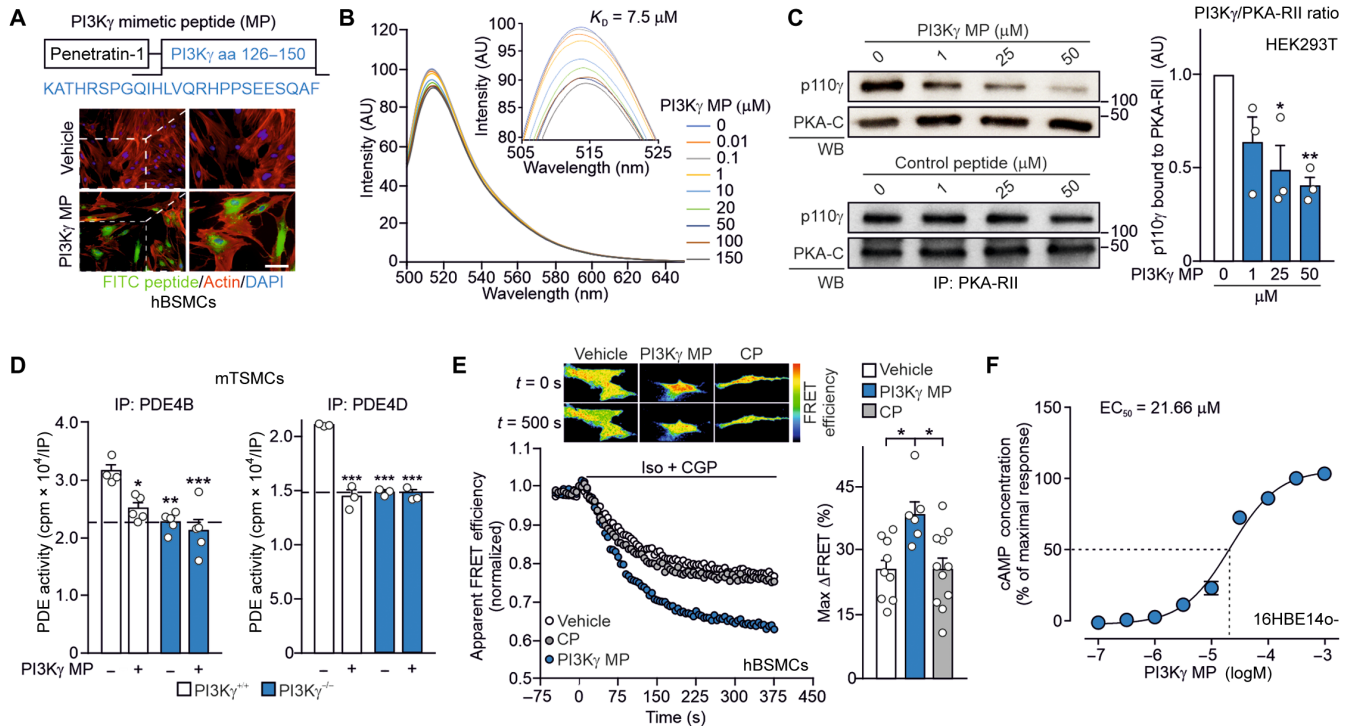


Fig. 2. PI3K γ MP enhances airway β_2 -AR/cAMP signaling in vitro. (A) Top: Schematic representation of the cell-permeable PI3K γ MP. The 126–150 region of PI3K γ was fused to the cell-penetrating peptide penetratin-1 (P1). Bottom: Intracellular fluorescence of hBSMCs after 1-hour incubation with a FITC-labeled version of PI3K γ MP (50 μ M) or vehicle. Scale bar, 10 μ m. aa, amino acid; DAPI, 4',6-diamidino-2-phenylindole. (B) Steady-state emission spectra of recombinant fluorescein 5-maleimide-labeled PKA-R11 (PKA-F5M) in the presence of increasing concentrations of PI3K γ MP (0 to 150 μ M), revealing a dissociation constant for PI3K γ MP/PKA-R11 interaction of 7.5 μ M. AU, arbitrary units. (C) Coimmunoprecipitation of the catalytic subunit of PI3K γ (p110 γ) and PKA-R11 from human embryonic kidney 293T (HEK293T) cells expressing p110 γ and exposed to increasing doses of PI3K γ MP for 2 hours. Representative immunoblots (left) and relative quantification (right) of $n = 3$ independent experiments are shown. (D) PDE4B and PDE4D activity in PI3K $\gamma^{+/+}$ and PI3K $\gamma^{-/-}$ mTSMCs treated with either vehicle or PI3K γ MP (50 μ M) for 30 min. For PDE4B IP, PI3K $\gamma^{+/+}$ + vehicle, $n = 4$; PI3K $\gamma^{+/+}$ + PI3K γ MP, $n = 5$; PI3K $\gamma^{-/-}$ + vehicle, $n = 5$; and PI3K $\gamma^{-/-}$ + PI3K γ MP, $n = 5$ independent cultures. For PDE4D IP, $n = 3$ independent cultures in all groups. (E) Representative FRET traces (left) and maximal FRET changes (right) in hBSMCs expressing the indicator of cAMP using Epac (ICUE3) cAMP FRET sensor and pretreated for 30 min with vehicle ($n = 9$), 50 μ M PI3K γ MP ($n = 6$), or equimolar control peptide (CP) ($n = 11$) before activation of β_2 -adrenergic receptors (β_2 -ARs) with isoproterenol and the β_1 -AR antagonist CGP-20712A (Iso + CGP) (100 nM each). Insets show representative intensity-modulated pseudocolor images at $t = 0$ and 500 s after the addition of Iso + CGP. n indicates the number of cells analyzed in $n = 3$ independent experiments. (F) cAMP elevation in human bronchial epithelial (HBE) cells (16HBE140-) in response to increasing concentrations of PI3K γ MP (31.6 nM to 316 μ M range) for 30 min. The amount of cAMP was expressed as percentage of cAMP accumulation elicited by 100 μ M PI3K γ MP. $N = 6$ independent experiments. In (C) to (E), * $P < 0.05$, ** $P < 0.01$, and *** $P < 0.001$ by one-way ANOVA, followed by Bonferroni's post hoc test. In (F), nonlinear regression analysis was used. Throughout, data are means \pm SEM.

reduced MCh-induced bronchoconstriction, as evidenced by measurements of both tidal volume (Fig. 4F) and lung resistance (Fig. 4G). Thus, PI3K γ MP could alleviate bronchoconstriction associated with asthma via elevation of cAMP.

PI3K γ MP limits neutrophilic inflammation in a mouse model of asthma

Because cAMP-elevating agents have anti-inflammatory actions (3), we tested whether PI3K γ MP could relieve airway inflammation in OVA-sensitized mice. Peribronchial inflammation and mucin production were dampened in animals repeatedly exposed to PI3K γ MP (Fig. 5, A and B). Moreover, a significantly lower number of neutrophils was detected in the bronchoalveolar lavage fluid of PI3K γ MP-treated mice than in controls ($P = 0.0437$) (Fig. 5C), indicating that PI3K γ MP inhibits the neutrophilic inflammation associated with asthma. PI3K γ MP also inhibited chemoattractant-induced adhesion of human neutrophils to intercellular adhesion molecule-1 (ICAM-1) and ICAM-2 (fig. S4, A and B) by reducing lymphocyte

function-associated antigen 1 (LFA-1) activation (fig. S4C). PKA inhibition rescued neutrophil adhesion to ICAM-1, ICAM-2, and fibrinogen (Fig. 5, D to F) in the presence of PI3K γ MP, indicating that the impaired adhesion was dependent on PKA hyperactivation. In line with ICAM-1 controlling neutrophil recruitment to the airways, PI3K γ MP significantly reduced neutrophil chemotaxis to *N*-formyl-Met-Leu-Phe (*f*MLP) ($P < 0.0001$) via PKA activation (Fig. 5G) and the consequent inhibition of RhoA-mediated (Fig. 5H) LFA-1 triggering (13). Thus, PI3K γ MP could limit neutrophilic inflammation in asthma by dampening neutrophil adhesion and transmigration.

PI3K γ MP promotes cAMP-dependent activation of CFTR and chloride efflux in airway epithelial cells

Next, we tested whether PI3K γ MP could promote chloride (Cl⁻) secretion via the cAMP-gated CFTR channel. PI3K γ was enriched at the apical membrane of 16HBE140- cells (fig. S5A) and coimmunoprecipitated with CFTR (fig. S5B). Fluorescence resonance energy transfer (FRET) analysis showed that, in response to forskolin (Fsk),

Downloaded from https://www.science.org on January 28, 2024

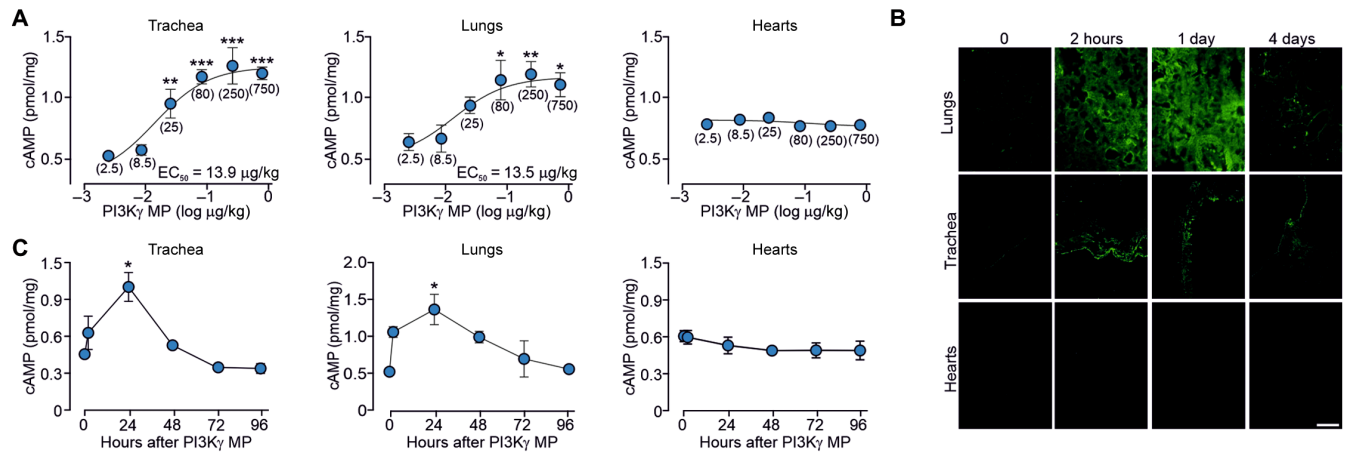


Fig. 3. PI3K γ MP elevates airway cAMP abundance in vivo in mice. (A) cAMP concentrations in tissues from BALB/c mice 24 hours after intratracheal instillation of different doses of PI3K γ MP (0 to 750 μ g/kg). Values in brackets indicate the dose of PI3K γ MP expressed as μ g/kg. The number of mice (n) ranged from three to nine per group. EC₅₀, median effective concentration. (B) Tissue distribution of a FITC-labeled version of PI3K γ MP at indicated time points after intratracheal instillation of 0.08 mg/kg (1.5 μ g) in BALB/c mice. Representative images of $n = 3$ experiments are shown. Scale bar, 50 μ m. (C) Amount of cAMP in tissues from mice treated as in (B). The number of mice (n) ranged from three to six per group. In (A), * $P < 0.05$, ** $P < 0.01$, and *** $P < 0.001$ by one-way ANOVA, followed by Bonferroni's post hoc test. In (C), * $P < 0.05$ by Kruskal-Wallis test, followed by Dunn's multiple comparison test. Throughout, data are means \pm SEM.

PI3K γ MP induced threefold higher subcortical membrane cAMP concentration than either CP or saline (Fig. 6A) while not affecting cytosolic cAMP responses (Fig. 6A).

To test whether PI3K γ MP could trigger CFTR gating, PKA-mediated phosphorylation of the channel was assessed by Western blot and found to be fivefold higher in 16HBE14o- cells treated with PI3K γ MP than in cells exposed to either vehicle or CP (Fig. 6B). PI3K γ MP increased CFTR phosphorylation to a similar extent as rolipram, implying that PI3K γ MP affects the PDE4-mediated regulation of CFTR (14). To further characterize the CFTR phosphorylation elicited by PI3K γ MP, the phospho-occupancy of known PKA sites in the regulatory domain of the channel was analyzed by liquid chromatography-coupled tandem mass spectrometry in CF human bronchial epithelial (HBE) cells expressing a wt CFTR (wt-CFTR-CFBE41o-) (15), treated with PI3K γ MP, CP, Fsk, or vehicle. Whereas Fsk-mediated adenylyl cyclase activation triggered the phosphorylation of most PKA sites, PI3K γ MP selectively increased the phospho-occupancy of S737 and, to a lesser extent, of S753 (Fig. 6C and fig. S6, A to C). In agreement with mass spectrometry results, the CFTR phosphorylation elicited by PI3K γ MP was completely abolished in cells expressing a CFTR mutant where the serine was replaced by alanine (Fig. 6D).

Because phosphorylation of S737 can lead to a ~25% increase in the open probability of CFTR (16), we anticipated that PI3K γ MP could activate Cl⁻ secretion. Measurement of short-circuit currents (I_{SC}) showed that acute application of PI3K γ MP to polarized wt-CFTR-CFBE41o- monolayers induced a dose-dependent increase in CFTR conductance (fig. S7A), reaching up to either 30 or 45% of the maximal channel activation when applied either alone or in association with nanomolar doses of Fsk, respectively (fig. S7, A to C). Addition of the adenylyl cyclase inhibitor SQ22536 and the PKA blocker H89 after treatment with PI3K γ MP inhibited the increase in CFTR conductance elicited by the peptide (fig. S7D), confirming that PI3K γ MP activated CFTR through PKA.

I_{SC} measurements in primary HBE cells showed that PI3K γ MP, but not CP, induced a dose-dependent increase in CFTR currents

(Fig. 6E). No further elevation in I_{SC} was observed when rolipram was added to PI3K γ MP (Fig. 6E), confirming that the peptide inhibited the PDE4 pool associated to CFTR regulation (14). Boosting cAMP production with Fsk produced an additional increment of I_{SC} that was blocked by the CFTR inhibitor 172 (CFTR_{inh}-172) (Fig. 6E). Similarly, the nonhydrolysable cAMP analog CPT-cAMP further increased I_{SC} in addition to PI3K γ MP (fig. S8, A and B) but blocked the effect of the peptide on CFTR currents when applied as a pre-treatment (fig. S8, A to C), providing further evidence that PI3K γ MP activated the channel through cAMP and PKA.

Primary HBE cells express other cAMP/PKA-dependent ion channels and transporters that can indirectly influence CFTR activity by increasing the electrochemical driving force (17). In the presence of CFTR_{inh}-172, PI3K γ MP retained the ability to induce a transient increase in I_{SC} (fig. S8D), indicating the opening of Ca²⁺-activated Cl⁻ channels (CaCCs). Furthermore, the current decreased to baseline after application of clotrimazole (fig. S8D), an inhibitor of basolateral Ca²⁺-activated K⁺ channels, and bumetanide, an inhibitor of the Na-K-Cl cotransporter NKCC1 (fig. S8D), suggesting that the peptide could also promote luminal Cl⁻ secretion indirectly via these channels. To further evaluate the direct action of PI3K γ MP on CFTR currents, Ca²⁺ stores were first depleted with thapsigargin (fig. S8, E and F), and then, CaCCs were blocked using either a general CaCC inhibitor (fig. S8E) or an inhibitor targeting TMEM16A (fig. S8F), the major CaCC isoform in HBE cells. Without functional CaCCs, PI3K γ MP elicited a response that was fully abolished by CFTR_{inh}-172, confirming a direct activation of CFTR (fig. S8E). This observation was corroborated in rectal organoids, where CaCCs are not consistently expressed, and organoid swelling in response to Fsk [Fsk-induced swelling (FIS)] is CFTR dependent (18). PI3K γ MP potentiated by twofold the swelling of wt organoids elicited by a low dose of Fsk (2 μ M) priming cAMP production (Fig. 6F). As CFTR activation triggers water secretion, essential for proper mucus hydration and clearance (2), PI3K γ MP, but not CP, decreased intracellular water residence time, indicative of rapid water efflux, in cells expressing

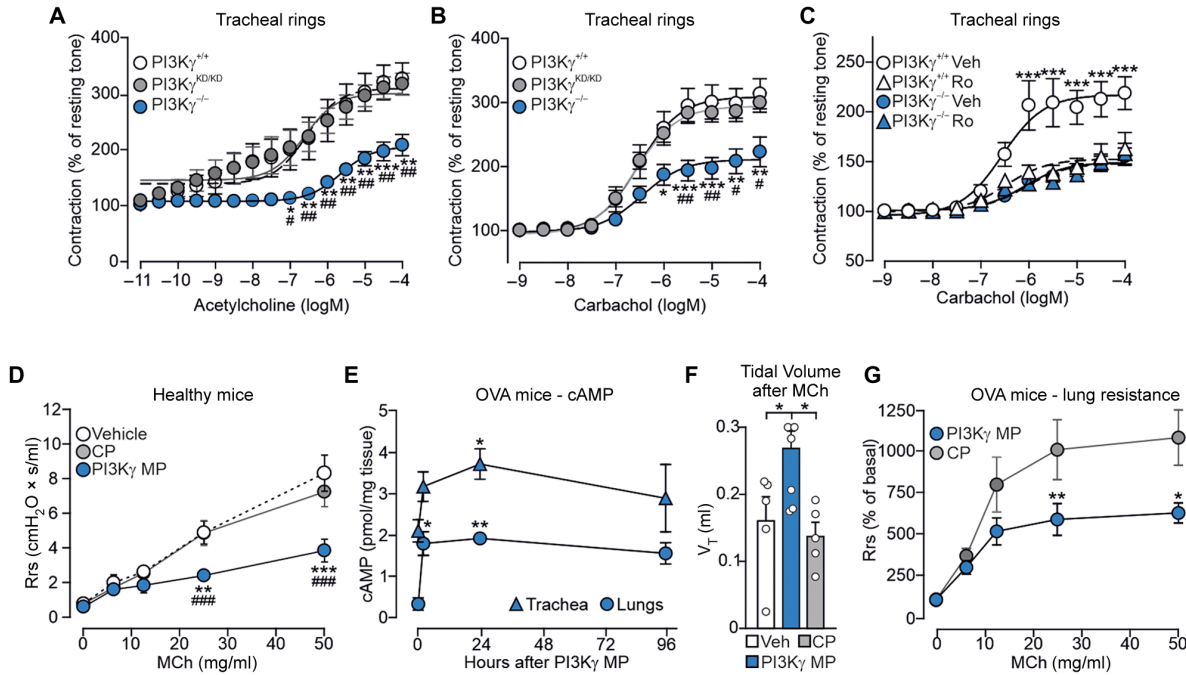


Fig. 4. PI3K γ MP promotes airway relaxation ex vivo and in vivo in a mouse model of asthma. (A and B) Cumulative contractile response of PI3K $\gamma^{+/+}$, PI3K $\gamma^{KD/KD}$, and PI3K $\gamma^{-/-}$ tracheal rings to increasing concentrations of acetylcholine (A) and carbachol (B). The developed tension is expressed as a percentage of the resting tone. In (A), PI3K $\gamma^{+/+}$, $n = 7$; PI3K $\gamma^{KD/KD}$, $n = 6$; and PI3K $\gamma^{-/-}$, $n = 5$ mice. In (B), PI3K $\gamma^{+/+}$, $n = 9$; PI3K $\gamma^{KD/KD}$, $n = 6$; and PI3K $\gamma^{-/-}$, $n = 5$ mice. (C) Cumulative contractile response to carbachol of PI3K $\gamma^{+/+}$ and PI3K $\gamma^{-/-}$ tracheal rings pretreated with either vehicle (Veh) or the PDE4 inhibitor roflumilast (Ro) (10 μ M) for 30 min. PI3K $\gamma^{+/+}$ + vehicle, $n = 10$; PI3K $\gamma^{+/+}$ + Ro, $n = 5$; PI3K $\gamma^{-/-}$ + vehicle, $n = 13$, and PI3K $\gamma^{-/-}$ + Ro, $n = 9$ mice. (D) Average lung resistance in healthy mice treated with vehicle ($n = 4$), 1.5 μ g of PI3K γ MP ($n = 4$), or equimolar amount of control peptide (CP) ($n = 5$) directly before exposure to increasing doses of the bronchoconstrictor methacholine (MCh). (E) cAMP concentrations in lungs and tracheas of ovalbumin (OVA)-sensitized mice at the indicated time points after intratracheal administration of PI3K γ MP (15 μ g). The number of mice (n) ranged from three to eight per group. (F) Tidal volume (V_T) of OVA-sensitized mice pretreated with Veh ($n = 5$), PI3K γ MP (15 μ g; $n = 6$), and CP (equimolar amounts; $n = 5$) and exposed to MCh (500 μ g/kg). (G) Average lung resistance (expressed as % of basal) in OVA-sensitized mice treated with 15 μ g of PI3K γ MP ($n = 9$) or equimolar amount of CP ($n = 10$) 30 min before MCh challenge. In (A) and (B), $*P < 0.05$, $**P < 0.01$, and $***P < 0.001$ versus PI3K $\gamma^{+/+}$ and $\#P < 0.05$ and $\#\#\#P < 0.01$ versus PI3K $\gamma^{KD/KD}$ by two-way ANOVA, followed by Bonferroni's multiple comparisons test. In (C), $**P < 0.01$ and $***P < 0.001$ for PI3K $\gamma^{+/+}$ + vehicle versus all other groups by two-way ANOVA, followed by Bonferroni's multiple comparisons test. In (D), $**P < 0.01$ and $***P < 0.001$ versus vehicle and $\#\#\#P < 0.001$ versus CP by two-way ANOVA, followed by Bonferroni's post hoc test. In (E) and (F), $*P < 0.05$ and $**P < 0.01$ by one-way ANOVA, followed by Bonferroni's post hoc test. In (G), $*P < 0.05$ and $**P < 0.01$ between groups by two-way ANOVA, followed by Bonferroni's post hoc test. Throughout, data are means \pm SEM.

wt-CFTR (Fig. 6G). Hence, PI3K γ MP could induce Cl $^-$ and consequent water secretion in bronchial epithelial cells through a cAMP-dependent mechanism, coordinating direct CFTR gating with the elevation of the electrochemical driving force.

PI3K γ MP enhances the therapeutic effects of CFTR modulators in CF in vitro models

Next, we tested whether PI3K γ MP could rescue the function of the most common CF-causing CFTR mutant (F508del-CFTR). F508del-CFTR exhibits multiple molecular defects that require the combined use of correctors (VX-809/lumacaftor, VX-661/tezacaftor, or VX-445/elexacaftor) and a potentiator (VX-770/ivacaftor) to restore the plasma membrane localization and channel gating, respectively (2). In the presence of the corrector VX-809, PI3K γ MP enhanced subcortical cAMP concentrations by 35% in F508del-CFTR-CFBE41o- cells (Fig. 7A). Furthermore, primary HBE cells from a patient homozygous for the F508del mutation, treated with the first-generation combination of VX-809 and VX-770, showed a fivefold increase in I_{SC} when PI3K γ MP was given after acute administration of VX-770 (Fig. 7B). Similar results were obtained in

F508del/F508del HBE cells from a second donor, with the exception that in these cells, PI3K γ MP, added in addition to VX-770, stimulated a biphasic response, with a first I_{SC} peak that indicated CaCC activation, followed by a plateau phase corresponding to CFTR $_{inh-172}$ -sensitive CFTR-mediated currents (Fig. 7C and fig. S9, A to D). In agreement with a coordinated action of the peptide on CFTR currents and the electrochemical driving force, I_{SC} was completely abolished by sequential application of CFTR $_{inh-172}$, clotrimazole, and bumetanide (fig. S9, A to C). The synergy between the CFTR potentiator VX-770 and PI3K γ MP was further supported by FIS assays in intestinal organoids. The effect of the peptide was first assessed in organoids derived from compound heterozygotes bearing the F508del allele and the residual function mutation D1152H. After correction with VX-809, organoid size was increased by 50% in the group pretreated with PI3K γ MP before stimulation with VX-770 and Fsk (Fig. 7D), and CFTR $_{inh-172}$ prevented this effect (Fig. 7D). In F508del/F508del organoids under chronic treatment with VX-809 and VX-770, where their interaction reduces correction efficacy (19), PI3K γ MP dose-dependently increased organoid size up to 6.5-fold the volume of controls (Fig. 7E). The maximal synergy between the

Downloaded from https://www.science.org on January 28, 2024

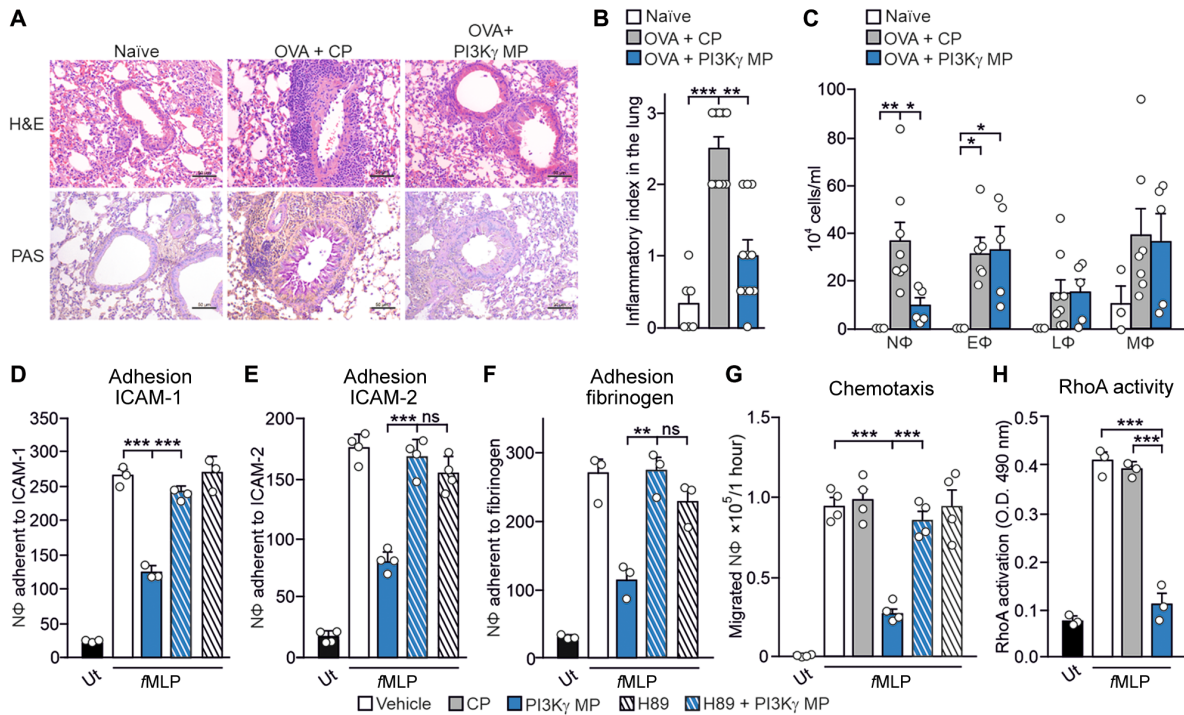


Fig. 5. PI3K γ MP limits neutrophilic lung inflammation in asthmatic mice. (A) Representative images of hematoxylin-eosin (H&E) (top) and periodic acid-Schiff's reagent (PAS) (bottom) staining of lung sections of naïve and OVA-sensitized mice, pretreated with PI3K γ MP (25 μ g) or CP (equimolar amount), before each intranasal OVA administration (days 14, 25, 26, and 27 of the OVA-sensitization protocol). Scale bars, 50 μ m. (B) Semiquantitative analysis of peribronchial inflammation in lung sections as shown in (A). Naïve, $n = 6$; OVA + CP, $n = 8$; and OVA + PI3K γ MP, $n = 5$ mice. (C) Number of neutrophils (N Φ), eosinophils (E Φ), lymphocytes (L Φ), and macrophages (M Φ) in the bronchoalveolar lavage fluid of mice treated as in (A). Naïve, $n = 3$; OVA + CP, $n = 8$; and OVA + PI3K γ MP, $n = 5$ animals. (D to F) fMLP-induced adhesion to ICAM-1 (D), ICAM-2 (E), and fibrinogen (F) of human neutrophils pretreated or not with the PKA inhibitor H89 (200 nM for 30 min) before exposure to vehicle or PI3K γ MP (50 μ M for 1 hour). Static adhesion was induced with 25 nM fMLP for 1 min. Average numbers of adherent cells/0.2 mm² are shown. In (D) and (F), $n = 3$ in all groups; in (E), $n = 4$ in all groups. (G) fMLP-triggered chemotaxis of human neutrophils treated with vehicle, CP (50 μ M), or PI3K γ MP (50 μ M) for 1 hour, without or with pretreatment with the PKA inhibitor H89 (200 nM for 30 min). $n = 4$ in all groups. (H) fMLP-induced RhoA activity in human neutrophils treated with vehicle, CP (50 μ M), or PI3K γ MP (50 μ M). $n = 3$ in all groups. In (B), $^{***}P < 0.01$ and $^{****}P < 0.001$ by Kruskal-Wallis test, followed by Dunn's multiple comparison test. In (C) to (H), $^{*}P < 0.05$, $^{**}P < 0.01$, and $^{***}P < 0.001$ by one-way ANOVA, followed by Bonferroni's post hoc test. O.D., optical density. ns, not significant; Ut, untreated.

peptide and CFTR modulators was observed at a low nonsaturating dose of Fsk (0.051 μ M), which was expected to minimally increase the amount of cAMP and which was almost ineffective in inducing swelling in the control VX-770 + VX-809 group.

Last, we assessed the ability of PI3K γ MP to enhance the therapeutic effects of the recent triple combination elexacaftor/tezacaftor/ivacaftor (ETI) (VX-445 + VX-661 + VX-770) in F508del/F508del HBE cells from two different donors with CF. VX-770-mediated Cl⁻ currents were 40% higher in cells treated chronically with VX-661 + VX-445 together with PI3K γ MP than in controls exposed to correctors alone (Fig. 8, A to C, and fig. S9E). In both cases, CPT-cAMP further increased Cl⁻ currents, which were inhibited by CFTR_{inh}-172, further demonstrating that Cl⁻ secretion was CFTR dependent. These data thus suggest the use of PI3K γ MP to increase the efficacy of CFTR modulators and to provide bronchodilator and anti-inflammatory activities, potentially beneficial to CF and other diseases like COPD and asthma.

DISCUSSION

Our results establish that targeting the PKA-anchoring function of PI3K γ with an MP allows therapeutic manipulation of β_2 -AR/cAMP

signaling in multiple cell types participating to the pathogenesis of chronic obstructive airway diseases (fig. S10). These findings are consistent with a model where PI3K γ acts as a scaffold protein for PKA (AKAP) in a complex containing the PKA-dependent phosphodiesterase PDE4 (7). The pharmacological actions of PI3K γ MP stem from its ability to displace PKA from the PI3K γ complex, thereby preventing PKA-mediated stimulation of a pool of PDE4 that is responsible for lowering the amount of cAMP close to neighboring distinct PKA-containing complexes, including those regulating CFTR gating (14).

Our finding that PI3K γ MP fails to increase cAMP in PI3K γ -deficient cells demonstrates that the peptide inhibits uniquely PI3K γ -dependent PDEs and does so without disturbing other AKAP-PKA complexes. This is supported by our previous findings showing that the PKA-binding sequence of the peptide diverges from that of classical AKAPs (10).

Although the AKAP function of PI3K γ has been previously linked to cAMP modulation in the heart (9, 10) and in vascular smooth muscles (20), the role and the pathophysiological relevance of PI3K γ noncatalytic activity outside the cardiovascular system has remained elusive. The present study identified the scaffold function

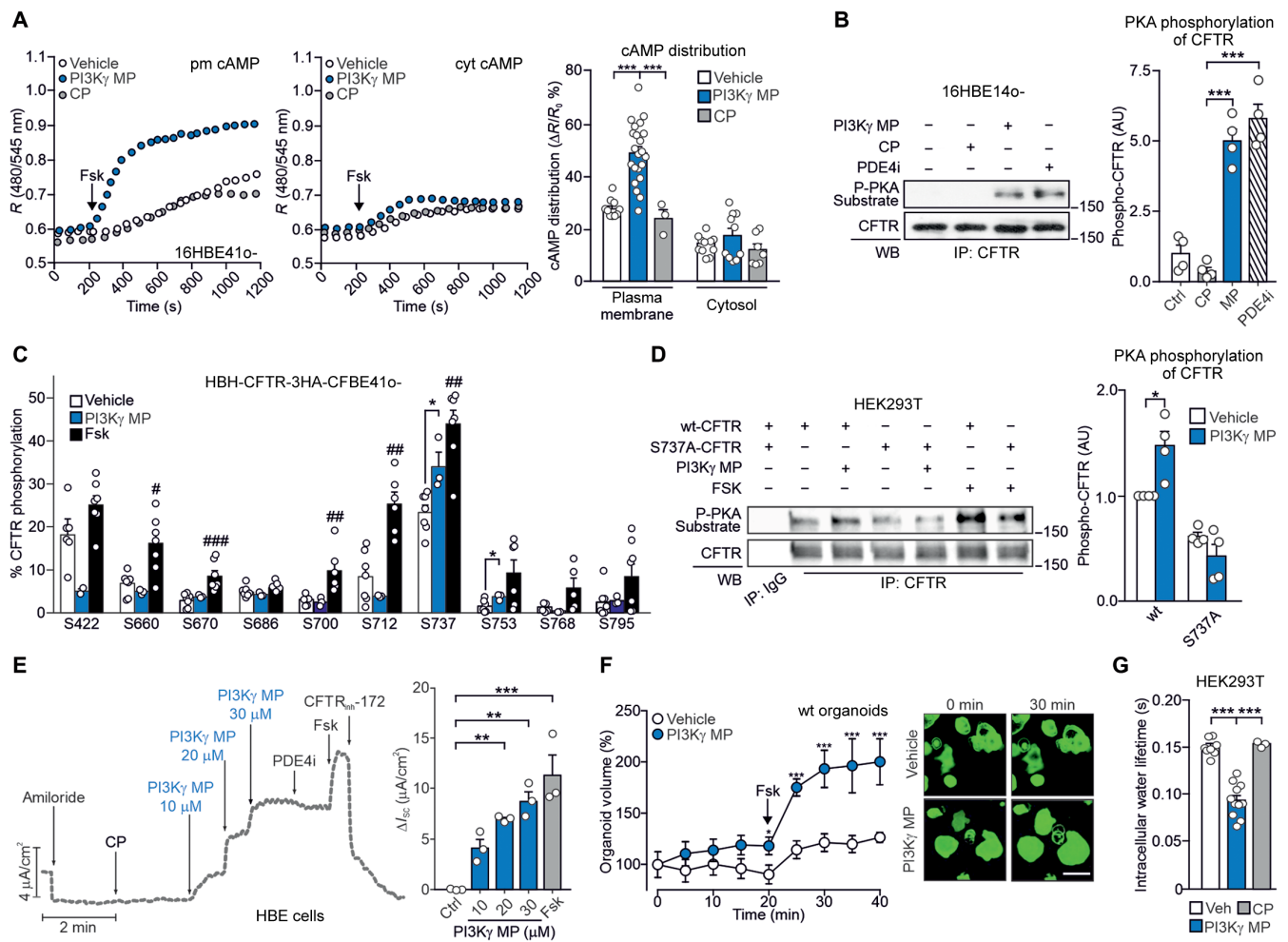


Fig. 6. PI3K γ MP promotes cAMP-dependent gating of CFTR. (A) Representative FRET traces (left) and maximal FRET changes (right) in HBE cells (16HBE140o) expressing the FRET probe for either plasma membrane (pm cAMP) or cytosolic cAMP (cyt cAMP). Cells were preincubated with vehicle, PI3K γ MP (25 μ M), or control peptide (CP) (25 μ M) before treatment with 1 μ M forskolin (Fsk). R is the normalized 480 nm/545 nm emission ratio calculated at indicated time points. n indicates the number of cells from $n = 3$ independent experiments. vehicle, $n = 10$ and $n = 12$; PI3K γ MP, $n = 22$ and $n = 11$; and CP $n = 3$ and $n = 7$ for pm cAMP and cyt cAMP, respectively. (B) Representative Western blot (left) and relative quantification (right) of PKA-mediated phosphorylation of CFTR in 16HBE140o cells treated with vehicle, CP (25 μ M), PI3K γ MP (25 μ M), and the PDE4 inhibitor rolipram (PDE4i) (10 μ M) for 30 min. CFTR was immunoprecipitated, and PKA-dependent phosphorylation was detected in IP pellets by immunoblotting with a PKA substrate antibody. $n = 4$ independent experiments. (C) Relative phosphorylation (%) or phospho-occupancy of identified PKA sites of CFTR in wt-CFTR-CFBE41o-expressing HBH-CFTR-3HA treated with vehicle [dimethyl sulfoxide (DMSO); $n = 7$], PI3K γ MP (25 μ M for 1 hour, $n = 3$), and Fsk (10 μ M for 10 min, $n = 7$). n is the number of biological replicates from $n = 3$ independent experiments. The phospho-occupancy or the percent of relative phosphorylation of each site was calculated as a ratio of all phosphorylated and unphosphorylated peptides that contained a given phosphorylation site [% phosphorylation of site A = (area of peptides phosphorylated at site A/sum of areas of all peptides carrying site A) as described in Materials and Methods]. Representative fragmentation spectra from each identified phosphorylation site and representative chromatograms from S737-containing peptides in their unphosphorylated and phosphorylated form are provided in fig. S6. (D) Representative Western blot (left) and relative quantification (right) of PKA-mediated phosphorylation of CFTR in HEK293T cells expressing either wt- or S737A-CFTR and exposed to vehicle, PI3K γ MP (25 μ M, 1 hour), or Fsk (10 μ M, 10 min). $n = 4$ independent experiments. (E) Left: Representative trace of short-circuit currents (I_{sc}) measured in Ussing chambers in primary normal HBE cells cultured at the air-liquid interface (ALI). The following treatments were applied at the indicated times: epithelial sodium channel inhibitor amiloride (10 μ M), CP (30 μ M), PI3K γ MP (10 to 30 μ M), PDE4i inhibitor rolipram (PDE4i) (10 μ M), Fsk (10 μ M), and CFTR inhibitor 172 (CFTR_{inh}-172) (20 μ M). Right: Average current variations in response to the indicated treatments. $n = 3$ biological replicates from the same donor. (F) Normalized swelling curves (left) and representative confocal images (right) of Fsk-stimulated calcein green-labeled wt organoids pre-incubated with PI3K γ MP (25 μ M) or vehicle for 20 min. Fsk was used at 2 μ M. Scale bar, 100 μ m. Vehicle, $n = 25$ and PI3K γ MP, $n = 28$ organoids from $n = 3$ independent experiments. (G) Water residence time (τ_{in}) determined by ¹H nuclear magnetic resonance relaxometry (as described in the Supplementary Materials) in HEK293T cells transfected with wt-CFTR and treated with vehicle (DMSO; $n = 8$), CP (25 μ M; $n = 3$), and PI3K γ MP (25 μ M; $n = 11$). n indicates the number of biological replicates in $n = 3$ independent experiments. In (A), (B), (D), (E), and (G), * $P < 0.05$, ** $P < 0.01$, and *** $P < 0.001$ by one-way ANOVA, followed by Bonferroni's post hoc test. In (C), unpaired t tests, followed by Holm-Sidak's multiple comparisons test were performed on each phosphorylation site between two different treatment conditions. # $P < 0.05$, ## $P < 0.01$, and ### $P < 0.001$ Fsk versus vehicle and * $P < 0.05$ PI3K γ MP versus vehicle. (F) * $P < 0.05$ and *** $P < 0.001$ by two-way ANOVA followed by Bonferroni's multiple comparisons test. Throughout, data are means \pm SEM.

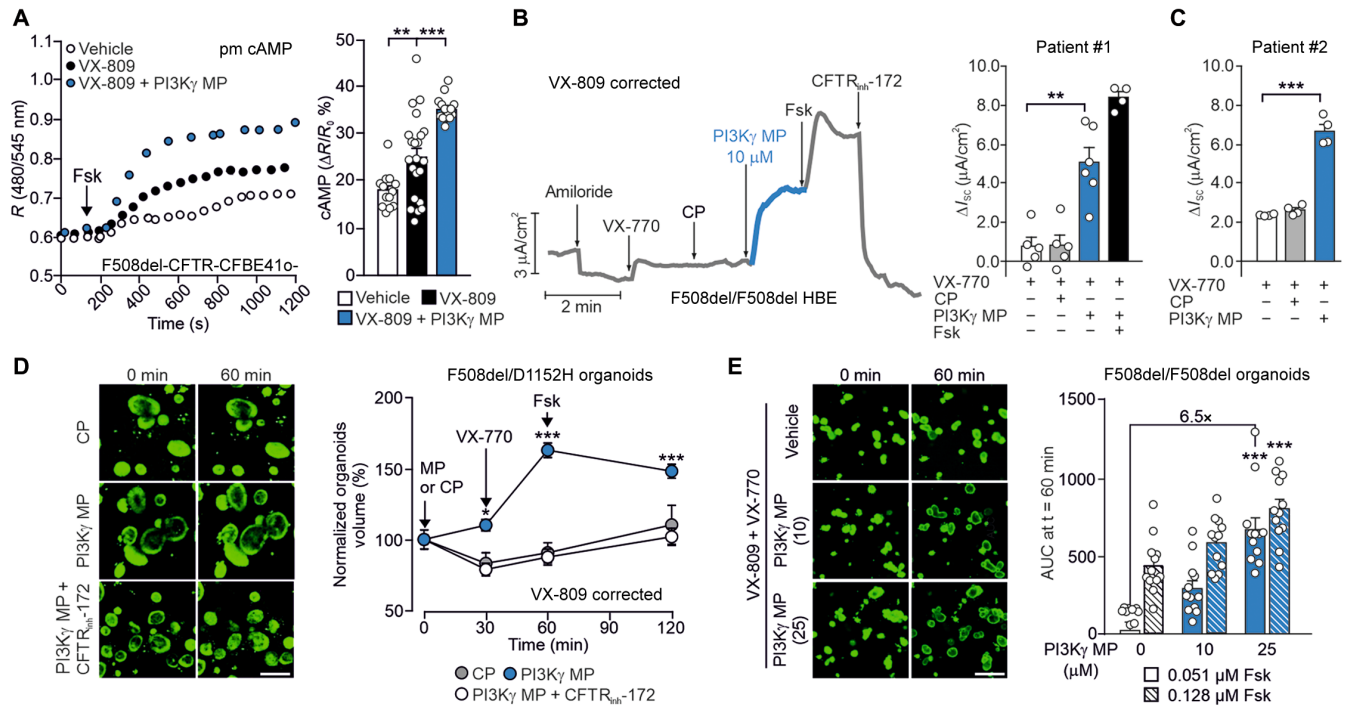


Fig. 7. PI3K γ MP potentiates the therapeutic effects of CFTR modulators in CF in vitro models. (A) Representative FRET traces (left) and maximal FRET changes (right) in CFBE41o- cells overexpressing F508del-CFTR and the plasma membrane-targeted FRET probe for cAMP (pm cAMP). Cells were preincubated with vehicle, the CFTR corrector VX-809 (5 μ M) alone, or together with PI3K γ MP (25 μ M) before treatment with 1 μ M Fsk. *R* is the normalized 480 nm/545 nm emission ratio calculated at indicated time points. Vehicle, *n* = 12; VX-809, *n* = 22; and VX-809 + PI3K γ MP, *n* = 16, where *n* is the number of cells from *n* = 3 independent experiments. (B) Left: Representative trace of short-circuit currents (*I*_{sc}) in primary HBE cells from a donor with CF (patient #1) homozygous for the F508del mutation (F508del/F508del HBE) and grown at the ALI. Cells were corrected with VX-809 for 48 hours (5 μ M) and then exposed to the following drugs at the indicated times: amiloride (100 μ M), CP (10 μ M), PI3K γ MP (10 μ M), Fsk (10 μ M), VX-770 (1 μ M), and CFTR_{inh}-172 (10 μ M). Right: Average total current variation in response to VX-770 (1 μ M), CP (10 μ M), PI3K γ MP (10 μ M), and Fsk (10 μ M) of *n* = 4 technical replicates of the same donor. (C) Average total current variation in response to VX-770 (1 μ M), CP (25 μ M), and PI3K γ MP (25 μ M) in F508del/F508del HBE cells from a second donor with CF (patient #2) grown at ALI and precorrected with VX-809 for 48 hours (5 μ M). *n* = 4 technical replicates of the same donor. Representative *I*_{sc} traces are provided in fig. S9 (A to C). (D) Representative confocal images and quantification of Fsk-induced swelling (FIS) of calcein green-labeled rectal organoids from a patient carrying compound CF F508del and D1152H mutations (F508del/D1152H). Organoids were corrected with VX-809 (3 μ M) for 24 hours, incubated with calcein green (3 μ M) for 30 min, and exposed to either PI3K γ MP or CP (both 25 μ M) for 30 min before stimulation with Fsk (2 μ M). Organoid response was measured as a percentage change in volume at different time points after addition of Fsk (*t* = 30, *t* = 60, and *t* = 120 min) compared to the volume at *t* = 0. *n* = 15 to 34 organoids from one donor in *n* = 2 independent experiments. Scale bar, 200 μ m. (E) FIS responses (right) and representative confocal images (left) of calcein green-labeled rectal organoids from a CF patient homozygous for the F508del mutation (F508del/F508del). Organoids were preincubated with the CFTR corrector VX-809 (3 μ M) and the CFTR potentiator VX-770 (3 μ M) for 24 hours before exposure to two different concentrations of Fsk (0.51 and 0.128 μ M) and PI3K γ MP (10 and 5 μ M). The peptide was added to the organoids together with Fsk. Organoid response was measured as area under the curve of relative size increase of organoids after 60 min Fsk stimulation, *t* = 0 min: baseline of 100%. *n* = 12 organoids per group analyzed in *n* = 2 independent cultures from *n* = 2 different donors. Scale bar, 200 μ m. In (A) to (C), ****P* < 0.01 and *****P* < 0.001 by one-way ANOVA, followed by Bonferroni's post hoc test. In (D), **P* < 0.05 and *****P* < 0.001 by two-way ANOVA, followed by Bonferroni's post hoc test. In (E), *****P* < 0.001 by Kruskal-Wallis test, followed by Dunn's multiple comparisons test. Throughout, data are means \pm SEM.

of PI3K γ as a key negative regulator of a discrete cAMP/PKA microdomain in different cell subsets of the airways, including epithelial, smooth muscle, and immune cells. Like in cardiomyocytes (9), in airway cells PI3K γ -mediated reduction of cAMP is spatially confined to compartments that contain β_2 -ARs, key pharmacological targets for respiratory diseases. Although the effects of PI3K γ MP might be attained with the use of β_2 -AR agonists, these drugs suffer from efficacy and tolerability concerns linked to tachyphylaxis and unwanted pharmacological effects outside the lungs. Unlike β_2 -AR agonists, PI3K γ MP acts through a distinct mechanism with at least two advantages. First, PI3K γ MP amplifies β_2 -AR/cAMP responses by impinging on cAMP degradation rather than on β_2 -AR activation, thus avoiding receptor desensitization, which, in the long run, is a

major cause of reduced efficacy. Second, being an inhaled peptide of 5 kDa, PI3K γ MP boosts lung cAMP without reaching other tissues where cAMP elevation would not be desirable, such as in the heart (9).

In addition, the local action of the peptide provides an added value over other cAMP-elevating agents, such as the classical small-molecule PDE4 inhibitors, like roflumilast, that easily diffuse outside the lungs and trigger undesired brain and cardiac effects (8). In addition, small-molecule PDE4 inhibitors lead to indiscriminate inhibition of all four different PDE4 subtypes (PDE4A, PDE4B, PDE4C, and PDE4D), potentially causing further side effects. PI3K γ MP blocked selective PDE4 subtypes with a prominent role in the lungs, such as PDE4B and PDE4D (21), with high isoform and compartment selectivity.

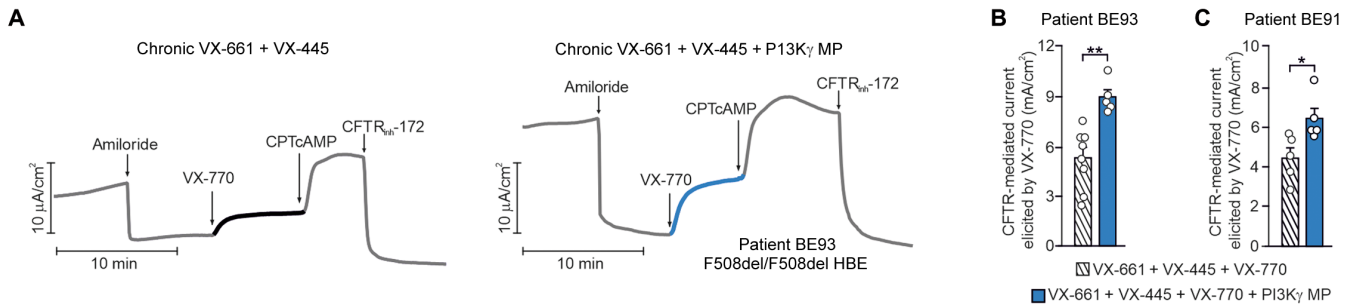


Fig. 8. PI3K γ MP enhances the effect of ETI in primary F508del/F508del HBE cells. (A) Representative traces of I_{sc} in primary HBE from a donor with CF (patient BE93) homozygous for the F508del mutation (F508del/F508del HBE) and grown at the ALI. Cells were corrected for 24 hours with VX-661 and VX-445 alone (10 μ M + 3 μ M) or together with PI3K γ MP (10 μ M) before exposure at the indicated time to the following drugs: amiloride (100 μ M), VX-770 (1 μ M), CPTcAMP (100 μ M), and CFTR_{inh}-172 (10 μ M). (B) Average total current variation in response to VX-770 (1 μ M) from $n = 5$ to 8 technical replicates of donor BE93. (C) Average total current variation in response to VX-770 (1 μ M) from $n = 5$ technical replicates of a second F508del/F508del donor (patient BE91). Representative I_{sc} traces are provided in fig. S9E. Throughout, * $P < 0.05$ and ** $P < 0.001$ and by Student's t test. Data are means \pm SEM.

Consistent with the prorelaxing action of cAMP, PI3K γ MP demonstrated prominent bronchodilator effects in vivo in healthy and asthmatic mice, which could be explained by enhanced β_2 -AR/cAMP signaling, secondary to PDE4 inhibition in airway smooth muscle cells. Although the bronchorelaxant action of β_2 -AR agonists, such as salbutamol and formoterol, is well established, conflicting findings have been reported for PDE4 inhibitors (21). Our observation that roflumilast blunts PI3K γ -dependent contractility of tracheal rings confirms a role for PDE4 in regulating airway smooth muscle tone. This view agrees with previous reports of reduced airway smooth muscle contractility in *Pde4d* knockout mice (22) and of enhanced β_2 -AR-stimulated cAMP accumulation in *PDE4D5* knockdown human smooth muscle cells (23).

PDE4 is also enriched in immune cells, and PDE4 inhibitors have demonstrated anti-inflammatory properties (7, 21). The finding that PI3K γ MP specifically inhibited neutrophil recruitment suggests that this peptide might be effective in hard-to-treat chronic airway disease subtypes with neutrophilic inflammation, such as corticosteroid-insensitive neutrophilic asthma (24), as well as COPD and CF (2, 25). Similar to standard anti-inflammatory drugs, such as inhaled corticosteroids, PI3K γ MP might increase the risk of respiratory infections, requiring antibiotic therapy. This is particularly relevant to patients with CF who already suffer from infections causing lung function decline and, ultimately, mortality (2). A limitation of our study is that the effects of PI3K γ MP were not tested in infection models. Hence, although genetic and pharmacologic PDE4 inhibition appear safe in pulmonary infections (26), future studies are required to define whether PI3K γ MP affects host defense.

Another effect of targeting PDE4 is the cAMP/PKA-dependent gating of the CFTR channel, increasing airway surface liquid and facilitating mucus clearance (27). CFTR functional defects and mucus stasis can be observed in patients with COPD and certain forms of asthma (28) but are critical in CF (2). Previous reports identified PDE4D as a negative regulator of the cAMP/PKA-dependent activation of wt-CFTR in bronchial epithelial cells, highlighting the potential of PDE4 inhibitors to stimulate the channel (14, 29). Our study pinpoints PI3K γ as a key AKAP orchestrating cAMP-mediated signal transduction in a microdomain involving β_2 -ARs, PDE4D, and CFTR. Accordingly, whereas a generalized cAMP elevation induced by Fsk correlated with the phosphorylation of most of CFTR

phospho-sites, PI3K γ MP triggered local cAMP elevation, resulting in the selective phosphorylation of S737. Although S737 phosphorylation might have contrasting effects on CFTR gating (16, 30), this likely depends on contextual modifications of other phosphorylation sites (31), and our observations indicate that PI3K γ MP-mediated phosphorylation of S737 triggers the same activity observed after reintroduction of S737 in a PKA-insensitive CFTR mutant (16). PI3K γ MP contributes to Cl⁻ secretion not only through a direct action on CFTR but also by engaging Ca²⁺-activated Cl⁻ channels and basolateral, clotrimazole-sensitive Ca²⁺-activated K⁺ channels increasing the electrochemical driving force (17). Hence, PI3K γ MP coordinates different mechanisms culminating in Cl⁻ secretion, provided that sufficient functional CFTR is appropriately located at the plasma membrane.

In CF, the most common CFTR mutation (F508del) leads to the intracellular retention of the channel (2). The function of F508del-CFTR can be improved by the combined administration of correctors and potentiators, which enable the plasma membrane exposure and facilitate PKA-dependent gating of the mutant channel, respectively (2, 32). In agreement, the efficacy of the potentiator VX-770 depends on concomitant cAMP/PKA phosphorylation of the channel (33). Although Fsk has been extensively used to elevate cAMP in the preclinical testing of all CFTR modulators, PI3K γ MP ensured a more physiological and compartment-restricted increase in cAMP in the vicinity of CFTR that maximized the action of all combinations, including both lumacaftor/ivacaftor and ETI. Despite the improvement in lung function achieved with ETI (2), rescue of CFTR activity does not reach more than 60% of physiological values (34, 35). Our observation that the peptide can almost double the gating of the F508del-CFTR mutant after correction and potentiation with ETI suggests that enhancing PKA-mediated CFTR phosphorylation might represent an avenue for reinstating F508del-CFTR activity close to 100% of wt function, a condition potentially matching that of healthy carriers of CF mutations (34). Our initial preclinical toxicology studies in mice have shown that the inhaled PI3K γ MP remains confined in the lungs and is tolerable, but additional investigations in other animal models are awaited to corroborate the ability of the aerosolized peptide to overcome the mucus barrier imposed by CF (36). Nonetheless, treatment with ETI is associated with a substantial improvement in mucus mobilization (37) and could thus facilitate the combined action of PI3K γ MP.

Together, this study highlights the therapeutic potential of increasing cAMP concentrations in a compartmentalized manner. With its pharmacological properties, PI3K γ MP might be useful for the treatment of airway diseases including asthma and COPD, where cAMP-elevating agents with broncho-relaxant properties are highly desirable. In addition, by inhibiting PDE4, PI3K γ MP may exert a selective activity on neutrophil adhesion and pulmonary recruitment. Last, PI3K γ MP might be used in CF where, despite the success of currently approved modulators, treatments allowing patients a normal life span are still lacking.

MATERIALS AND METHODS

Study design

We tested the hypothesis that targeting the scaffold function of PI3K γ could trigger local cAMP elevation in the lungs and could reduce airway smooth constriction, pulmonary inflammation, and mucus stasis in chronic respiratory diseases without incurring unwanted systemic side effects. We devised a cell-penetrating peptide disturbing the AKAP function of PI3K γ (PI3K γ MP), and we tested its ability to induce compartmentalized cAMP responses in vitro in hBSMCs and epithelial (16HBE14o-) cells, as well as in vivo after intratracheal instillation in mice. Bronchodilator and anti-inflammatory activities of PI3K γ MP were studied in vivo in a mouse model of asthma (OVA-sensitized mice). Effects on CFTR activity were studied in primary HBE cells and intestinal organoids from healthy controls and donors with CF through I_{sc} measurements and FIS assays, respectively.

The sample size for each experiment is included in the figure legends. For mouse studies, females and males of 8 to 12 weeks of age were used and randomly assigned to the experimental groups. Experiments were approved by the animal ethical committee of the University of Torino and by the Italian Ministry of Health (authorization no. 757/2016-PR). The number of mice in each group was determined by power calculations based on previous experience with the model system and is defined in the respective figure legends. For in vitro experiments using immortalized cell lines, at least three independent experiments were performed. For in vitro studies in cells and organoids derived from human subjects, the results of at least $n = 2$ independent cultures from $n = 2$ different donors are provided. Informed consent was obtained from all participating subjects, and all studies were ethically approved. All experiments were conducted by blinded researchers. When outliers were identified, they were excluded from analysis if justified based on confirmed technical failure in parameter acquisition. Further details can be found in relevant sections within the Supplementary Materials and Methods.

Animals

PI3K γ -deficient mice (PI3K $\gamma^{-/-}$) and knock-in mice with catalytically inactive PI3K γ (PI3K $\gamma^{KD/KD}$) were described previously (38, 39). Mutant mice were back-crossed with C57Bl/6j mice for 15 generations to inbreed the genetic background, and C57Bl/6j mice were used as controls (PI3K $\gamma^{+/+}$). For asthma studies, wt BALB/c females were used. Mice used in all experiments were 8 to 12 weeks of age. Mice were group-housed, provided free access to standard chow and water in a controlled facility providing a 12-hour light/12-hour dark cycle, and were used according to institutional animal welfare guidelines and legislation, approved by the local Animal Ethics

Committee. All animal experiments were approved by the animal ethical committee of the University of Torino and by the Italian Ministry of Health (authorization no. 757/2016-PR).

Human material

Approval for primary bronchial epithelial cells and organoids cultures was obtained by the different local ethics committees (University of California San Francisco, Istituto Giannina Gaslini, the University of North Carolina at Chapel Hill, University of Verona, and University Medical Center Utrecht), and informed consent was obtained from all participating subjects.

Statistical analysis

Prism software (GraphPad Software Inc.) was used for statistical analysis. Data are presented as scatter plots with bars (means \pm SEM). Raw data were first analyzed to confirm their normal distribution via the Shapiro-Wilk test and then analyzed by unpaired Student's t test, one-way analysis of variance (ANOVA), or two-way ANOVA. Bonferroni correction (one-way and two-way ANOVA) was applied to correct for multiple comparisons. In the absence of a normal distribution, nonparametric Kruskal-Wallis or Mann-Whitney tests were used, followed by Dunn's correction for multiple comparisons if appropriate. $P < 0.05$ was considered significant.

SUPPLEMENTARY MATERIALS

www.science.org/doi/10.1126/scitranslmed.abl6328

Materials and Methods

Figs. S1 to S10

Tables S1 and S2

Data files S1 and S2

MDAR reproducibility checklist

References (40–60)

[View/request a protocol for this paper from Bio-protocol](#)

REFERENCES AND NOTES

1. B. R. Celli, J. A. Wedzicha, Update on clinical aspects of chronic obstructive pulmonary disease. *N. Engl. J. Med.* **381**, 1257–1266 (2019).
2. M. Shteinberg, I. J. Haq, D. Polineni, J. C. Davies, Cystic fibrosis. *Lancet* **397**, 2195–2211 (2021).
3. P. J. Barnes, New drugs for asthma. *Nat. Rev. Drug Discov.* **3**, 831–844 (2004).
4. L. A. Vijftigschild, G. Berkers, J. F. Dekkers, D. D. Zomer-van Ommen, E. Matthes, E. Kruisselbrink, A. Vonk, C. E. Hensen, S. Heida-Michel, M. Geerdink, H. M. Janssens, E. A. van de Graaf, I. Bronsveld, K. M. de Winter-de Groot, C. J. Majoer, H. G. Heijerman, H. R. de Jonge, J. W. Hanrahan, C. K. van der Ent, J. M. Beekman, β 2-Adrenergic receptor agonists activate CFTR in intestinal organoids and subjects with cystic fibrosis. *Eur. Respir. J.* **48**, 768–779 (2016).
5. E. M. Dunican, B. M. Elicker, T. Henry, D. S. Gierada, M. L. Schiebler, W. Anderson, I. Barjaktarevic, R. G. Barr, E. R. Bleecker, R. C. Boucher, R. Bowler, S. A. Christenson, A. Comellas, C. B. Cooper, D. Couper, G. J. Criner, M. Dransfield, C. M. Doerschuk, M. B. Drummond, N. N. Hansel, M. K. Han, A. T. Hastie, E. A. Hoffman, J. A. Krishnan, S. C. Lazarus, F. J. Martinez, C. E. McCulloch, W. K. O'Neal, V. E. Ortega, R. Paine III, S. Peters, J. D. Schroeder, P. G. Woodruff, J. V. Fahy, Mucus plugs and emphysema in the pathophysiology of airflow obstruction and hypoxemia in smokers. *Am. J. Respir. Crit. Care Med.* **203**, 957–968 (2021).
6. E. M. Dunican, B. M. Elicker, D. S. Gierada, S. K. Nagle, M. L. Schiebler, J. D. Newell, W. W. Raymond, M. E. Lachowicz-Scroggins, S. Di Maio, E. A. Hoffman, M. Castro, S. B. Fain, N. N. Jarjour, E. Israel, B. D. Levy, S. C. Erzurum, S. E. Wenzel, D. A. Meyers, E. R. Bleecker, B. R. Phillips, D. T. Mauger, E. D. Gordon, P. G. Woodruff, M. C. Peters, J. V. Fahy; National Heart Lung and Blood Institute (NHLBI) Severe Asthma Research Program, Mucus plugs in patients with asthma linked to eosinophilia and airflow obstruction. *J. Clin. Invest.* **128**, 997–1009 (2018).
7. D. H. Maurice, H. Ke, F. Ahmad, Y. Wang, J. Chung, V. C. Manganiello, Advances in targeting cyclic nucleotide phosphodiesterases. *Nat. Rev. Drug Discov.* **13**, 290–314 (2014).

8. Y. Oba, Phosphodiesterase inhibitors in chronic obstructive pulmonary disease. *Am. J. Respir. Crit. Care Med.* **188**, 1366 (2013).
9. A. Ghigo, A. Perino, H. Mehel, A. Zahradnikova Jr., F. Morello, J. Leroy, V. O. Nikolaev, F. Damilano, J. Cimino, E. De Luca, W. Richter, R. Westenbroek, W. A. Catterall, J. Zhang, C. Yan, M. Conti, A. M. Gomez, G. Vandecasteele, E. Hirsch, R. Fischmeister, Phosphoinositide 3-kinase γ protects against catecholamine-induced ventricular arrhythmia through protein kinase A-mediated regulation of distinct phosphodiesterases. *Circulation* **126**, 2073–2083 (2012).
10. A. Perino, A. Ghigo, E. Ferrero, F. Morello, G. Santulli, G. S. Baillie, F. Damilano, A. J. Dunlop, C. Pawson, R. Walser, R. Levi, F. Altruda, L. Silengo, L. K. Langeberg, G. Neubauer, S. Heymans, G. Lembo, M. P. Wymann, R. Wetzker, M. D. Houslay, G. Iaccarino, J. D. Scott, E. Hirsch, Integrating cardiac PIP3 and cAMP signaling through a PKA anchoring function of p110 γ . *Mol. Cell* **42**, 84–95 (2011).
11. V. Fanelli, V. Puntorieri, B. Assenzio, E. L. Martin, V. Elia, M. Bosco, L. Delsedime, L. Del Sorbo, A. Ferrari, S. Italiano, A. Ghigo, A. S. Slutsky, E. Hirsch, V. M. Ranieri, Pulmonary-derived phosphoinositide 3-kinase gamma (PI3K γ) contributes to ventilator-induced lung injury and edema. *Intensive Care Med.* **36**, 1935–1945 (2010).
12. G. Guidotti, L. Brambilla, D. Rossi, Cell-penetrating peptides: From basic research to clinics. *Trends Pharmacol. Sci.* **38**, 406–424 (2017).
13. C. Laudanna, J. J. Campbell, E. C. Butcher, Elevation of intracellular cAMP inhibits RhoA activation and integrin-dependent leukocyte adhesion induced by chemoattractants. *J. Biol. Chem.* **272**, 24141–24144 (1997).
14. E. Blanchard, L. Zlock, A. Lao, D. Mika, W. Namkung, M. Xie, C. Scheitrum, D. C. Gruenert, A. S. Verkman, W. E. Finkbeiner, M. Conti, W. Richter, Anchored PDE4 regulates chloride conductance in wild-type and Δ F508-CFTR human airway epithelia. *FASEB J.* **28**, 791–801 (2014).
15. A. Schnur, A. Premchand, M. Bagdany, G. L. Lukacs, Phosphorylation-dependent modulation of CFTR macromolecular signalling complex activity by cigarette smoke condensate in airway epithelia. *Sci. Rep.* **9**, 12706 (2019).
16. T. Hegeudus, A. Aleksandrov, A. Mengos, L. Cui, T. J. Jensen, J. R. Riordan, Role of individual R domain phosphorylation sites in CFTR regulation by protein kinase A. *Biochim. Biophys. Acta* **1788**, 1341–1349 (2009).
17. S. L. Martin, V. Saint-Criq, T. C. Hwang, L. Csanady, Ion channels as targets to treat cystic fibrosis lung disease. *J. Cyst. Fibros.* **17**, S22–S27 (2018).
18. J. F. Dekkers, C. L. Wiegerinck, H. R. de Jonge, I. Bronsveld, H. M. Janssens, K. M. de Winter-de Groot, A. M. Brandsma, N. W. de Jong, M. J. Bijvelds, B. J. Scholte, E. E. Nieuwenhuis, S. van den Brink, H. Clevers, C. K. van der Ent, S. Middendorp, J. M. Beekman, A functional CFTR assay using primary cystic fibrosis intestinal organoids. *Nat. Med.* **19**, 939–945 (2013).
19. D. M. Cholon, N. L. Quinney, M. L. Fulcher, C. R. Esther Jr., J. Das, N. V. Dokholyan, S. H. Randell, R. C. Boucher, M. Gentszsch, Potentiator ivacaftor abrogates pharmacological correction of Δ F508 CFTR in cystic fibrosis. *Sci. Transl. Med.* **6**, 246ra96 (2014).
20. A. Lupieri, R. Blaise, A. Ghigo, N. Smirnova, M. K. Sarthou, N. Malet, I. Limon, P. Vincent, E. Hirsch, S. Gayral, D. Ramel, M. Laffargue, A non-catalytic function of PI3K γ drives smooth muscle cell proliferation after arterial damage. *J. Cell Sci.* **133**, jcs245969 (2020).
21. H. Zuo, I. Cattani-Cavaliere, N. Musheshe, V. O. Nikolaev, M. Schmidt, Phosphodiesterases as therapeutic targets for respiratory diseases. *Pharmacol. Ther.* **197**, 225–242 (2019).
22. C. Mehats, S. L. Jin, J. Wahlstrom, E. Law, D. T. Umetsu, M. Conti, PDE4D plays a critical role in the control of airway smooth muscle contraction. *FASEB J.* **17**, 1831–1841 (2003).
23. C. K. Billington, I. R. Le Jeune, K. W. Young, I. P. Hall, A major functional role for phosphodiesterase 4D5 in human airway smooth muscle cells. *Am. J. Respir. Cell Mol. Biol.* **38**, 1–7 (2008).
24. A. Ray, J. K. Kolls, Neutrophilic inflammation in asthma and association with disease severity. *Trends Immunol.* **38**, 942–954 (2017).
25. A. Butler, G. M. Walton, E. Sapey, Neutrophilic inflammation in the pathogenesis of chronic obstructive pulmonary disease. *COPD* **15**, 392–404 (2018).
26. L. Abou Saleh, A. Boyd, I. V. Aragon, A. Koloteva, D. Spadafora, W. Mneimneh, R. A. Barrington, W. Richter, Ablation of PDE4B protects from *Pseudomonas aeruginosa*-induced acute lung injury in mice by ameliorating the cytoskeleton and associated hypothermia. *FASEB J.* **35**, e21797 (2021).
27. M. J. Turner, K. Abbott-Banner, D. Y. Thomas, J. W. Hanrahan, Cyclic nucleotide phosphodiesterase inhibitors as therapeutic interventions for cystic fibrosis. *Pharmacol. Ther.* **224**, 107826 (2021).
28. S. D. Patel, T. R. Bono, S. M. Rowe, G. M. Solomon, CFTR targeted therapies: Recent advances in cystic fibrosis and possibilities in other diseases of the airways. *Eur. Respir. Rev.* **29**, 190068 (2020).
29. M. J. Turner, Y. Luo, D. Y. Thomas, J. W. Hanrahan, The dual phosphodiesterase 3/4 inhibitor RPL554 stimulates rare class III and IV CFTR mutants. *Am. J. Physiol. Lung Cell. Mol. Physiol.* **318**, L908–L920 (2020).
30. H. Vais, R. Zhang, W. W. Reenstra, Dibasic phosphorylation sites in the R domain of CFTR have stimulatory and inhibitory effects on channel activation. *Am. J. Physiol. Cell Physiol.* **287**, C737–C745 (2004).
31. O. Baldursson, H. A. Berger, M. J. Welsh, Contribution of R domain phosphoserines to the function of CFTR studied in Fischer rat thyroid epithelia. *Am. J. Physiol. Lung Cell. Mol. Physiol.* **279**, L835–L841 (2000).
32. S. Chin, M. Hung, C. E. Bear, Current insights into the role of PKA phosphorylation in CFTR channel activity and the pharmacological rescue of cystic fibrosis disease-causing mutants. *Cell. Mol. Life Sci.* **74**, 57–66 (2017).
33. P. D. Eckford, C. Li, M. Ramjessingh, C. E. Bear, Cystic fibrosis transmembrane conductance regulator (CFTR) potentiator VX-770 (ivacaftor) opens the defective channel gate of mutant CFTR in a phosphorylation-dependent but ATP-independent manner. *J. Biol. Chem.* **287**, 36639–36649 (2012).
34. M. A. Mall, N. Mayer-Hamblett, S. M. Rowe, Cystic fibrosis: Emergence of highly effective targeted therapeutics and potential clinical implications. *Am. J. Respir. Crit. Care Med.* **201**, 1193–1208 (2020).
35. G. Veit, A. Roldan, M. A. Hancock, D. F. Da Fonte, H. Xu, M. Hussein, S. Frenkiel, E. Matouk, T. Velkov, G. L. Lukacs, Allosteric folding correction of F508del and rare CFTR mutants by elxacaftor-tezacaftor-ivacaftor (Trikafta) combination. *JCI Insight* **5**, e139983 (2020).
36. I. d'Angelo, C. Conte, M. I. La Rotonda, A. Miro, F. Quaglia, F. Ungaro, Improving the efficacy of inhaled drugs in cystic fibrosis: Challenges and emerging drug delivery strategies. *Adv. Drug Deliv. Rev.* **75**, 92–111 (2014).
37. C. B. Morrison, K. M. Shaffer, K. C. Araba, M. R. Markovetz, J. A. Wykoff, N. L. Quinney, S. Hao, M. F. Delion, A. L. Flen, L. C. Morton, J. Liao, D. B. Hill, M. L. Drumm, W. K. O'Neal, M. Kesimer, M. Gentszsch, C. Ehre, Treatment of cystic fibrosis airway cells with CFTR modulators reverses aberrant mucus properties via hydration. *Eur. Respir. J.* **2100185** (2022).
38. E. Hirsch, V. L. Katanaev, C. Garlanda, O. Azzolino, L. Pirola, L. Silengo, S. Sozzani, A. Mantovani, F. Altruda, M. P. Wymann, Central role for G protein-coupled phosphoinositide 3-kinase gamma in inflammation. *Science* **287**, 1049–1053 (2000).
39. E. Patrucco, A. Notta, L. Barberis, G. Selvetella, A. Maffei, M. Brancaccio, S. Marengo, G. Russo, O. Azzolino, S. D. Rybalkin, L. Silengo, F. Altruda, R. Wetzker, M. P. Wymann, G. Lembo, E. Hirsch, PI3Kgamma modulates the cardiac response to chronic pressure overload by distinct kinase-dependent and -independent effects. *Cell* **118**, 375–387 (2004).
40. L. M. DiPilato, J. Zhang, The role of membrane microdomains in shaping beta2-adrenergic receptor-mediated cAMP dynamics. *Mol. Biosyst.* **5**, 832–837 (2009).
41. A. Terrin, G. Di Benedetto, V. Pertegato, Y. F. Cheung, G. Baillie, M. J. Lynch, N. Elvassore, A. Prinz, F. W. Herberg, M. D. Houslay, M. Zaccolo, PGE(1) stimulation of HEK293 cells generates multiple contiguous domains with different [cAMP]: Role of compartmentalized phosphodiesterases. *J. Cell Biol.* **175**, 441–451 (2006).
42. B. Ponsioen, J. Zhao, J. Riedl, F. Zwartkruis, G. van der Krogt, M. Zaccolo, W. H. Moolenaar, J. L. Bos, K. Jalink, Detecting cAMP-induced Epac activation by fluorescence resonance energy transfer: Epac as a novel cAMP indicator. *EMBO Rep.* **5**, 1176–1180 (2004).
43. W. J. Thompson, M. M. Appleman, Characterization of cyclic nucleotide phosphodiesterases of rat tissues. *J. Biol. Chem.* **246**, 3145–3150 (1971).
44. G. Di Benedetto, A. Zoccarato, V. Lissandron, A. Terrin, X. Li, M. D. Houslay, G. S. Baillie, M. Zaccolo, Protein kinase A type I and type II define distinct intracellular signaling compartments. *Circ. Res.* **103**, 836–844 (2008).
45. R. A. Cardone, A. Bagorda, A. Bellizzi, G. Busco, L. Guerra, A. Paradiso, V. Casavola, M. Zaccolo, S. J. Reshkin, Protein kinase A gating of a pseudopodial-located RhoA/ROCK/p38/NHE1 signal module regulates invasion in breast cancer cell lines. *Mol. Biol. Cell* **16**, 3117–3127 (2005).
46. K. L. Holmes, L. M. Lantz, W. Russ, Conjugation of fluorochromes to monoclonal antibodies. *Curr. Protoc. Cytom.* **Chapter 4**, Unit 4.2 (2001).
47. G. T. Hermanson, *Bioconjugate Techniques* (2008).
48. D. W. McGraw, S. L. Forbes, L. A. Kramer, D. P. Witte, C. N. Fortner, R. J. Paul, S. B. Liggett, Transgenic overexpression of β 2-adrenergic receptors in airway smooth muscle alters myocyte function and ablates bronchial hyperreactivity. *J. Biol. Chem.* **274**, 32241–32247 (1999).
49. M. Matthey, R. Roberts, A. Seidinger, A. Simon, R. Schroder, M. Kuschak, S. Annala, G. M. Konig, C. E. Muller, I. P. Hall, E. Kostenis, B. K. Fleischmann, D. Wenzel, Targeted inhibition of G $_q$ signaling induces airway relaxation in mouse models of asthma. *Sci. Transl. Med.* **9**, eaag2288 (2017).
50. C. Laudanna, J. J. Campbell, E. C. Butcher, Role of Rho in chemoattractant-activated leukocyte adhesion through integrins. *Science* **271**, 981–983 (1996).
51. M. Bolomini-Vittori, A. Montresor, C. Giagulli, D. Staunton, B. Rossi, M. Martinello, G. Constantin, C. Laudanna, Regulation of conformer-specific activation of the integrin LFA-1 by a chemokine-triggered Rho signaling module. *Nat. Immunol.* **10**, 185–194 (2009).
52. M. Li, V. Sala, M. C. De Santis, J. Cimino, P. Cappello, N. Pianca, A. Di Bona, J. P. Margaria, M. Martini, E. Lazzarini, F. Pirozzi, L. Rossi, I. Franco, J. Bornbaum, J. Heger, S. Rohrbach,

- A. Perino, C. G. Tocchetti, B. H. F. Lima, M. M. Teixeira, P. E. Porporato, R. Schulz, A. Angelini, M. Sandri, P. Ameri, S. Sciarretta, R. C. P. Lima-Junior, M. Mongillo, T. Zaglia, F. Morello, F. Novelli, E. Hirsch, A. Ghigo, Phosphoinositide 3-kinase gamma inhibition protects from anthracycline cardiotoxicity and reduces tumor growth. *Circulation* **138**, 696–711 (2018).
53. A. Premchandrar, A. Kupniewska, A. Bonna, G. Faure, T. Fraczyk, A. Roldan, B. Hoffmann, M. Faria da Cunha, H. Herrmann, G. L. Lukacs, A. Edelman, M. Dadlez, New insights into interactions between the nucleotide-binding domain of CFTR and keratin 8. *Protein Sci.* **26**, 343–354 (2017).
54. V. Montiel, R. Bella, L. Y. M. Michel, H. Esfahani, D. De Mulder, E. L. Robinson, J. P. Deglasse, M. Tiburcy, P. H. Chow, J. C. Jonas, P. Gilon, B. Steinhorn, T. Michel, C. Beauloye, L. Bertrand, C. Farah, F. D. Zotti, H. Debaix, C. Bouzin, D. Brusa, S. Horman, J. L. Vanoverschelde, O. Bergmann, D. Gillis, M. Rooman, A. Ghigo, S. Geninatti-Crich, A. Yool, W. H. Zimmermann, H. L. Roderick, O. Devuyt, J. L. Balligand, Inhibition of aquaporin-1 prevents myocardial remodeling by blocking the transmembrane transport of hydrogen peroxide. *Sci. Transl. Med.* **12**, eaay2176 (2020).
55. M. R. Ruggiero, S. Baroni, S. Pezzana, G. Ferrante, S. Geninatti Crich, S. Aime, Evidence for the role of intracellular water lifetime as a tumour biomarker obtained by in vivo field-cycling relaxometry. *Angew. Chem. Int. Ed. Engl.* **57**, 7468–7472 (2018).
56. E. Terreno, S. Geninatti Crich, S. Belfiore, L. Biancone, C. Cabella, G. Esposito, A. D. Manazza, S. Aime, Effect of the intracellular localization of a Gd-based imaging probe on the relaxation enhancement of water protons. *Magn. Reson. Med.* **55**, 491–497 (2006).
57. P. Scudieri, I. Musante, E. Caci, A. Venturini, P. Morelli, C. Walter, D. Tosi, A. Palleschi, P. Martin-Vasallo, I. Sermet-Gaudelus, G. Planelles, G. Crambert, L. J. Galletta, Increased expression of ATP12A proton pump in cystic fibrosis airways. *JCI Insight* **3**, e123616 (2018).
58. L. Zhang, M. Gallup, L. Zlock, W. E. Finkbeiner, N. A. McNamara, Rac1 and Cdc42 differentially modulate cigarette smoke-induced airway cell migration through p120-catenin-dependent and -independent pathways. *Am. J. Pathol.* **182**, 1986–1995 (2013).
59. M. Xie, T. C. Rich, C. Scheitrum, M. Conti, W. Richter, Inactivation of multidrug resistance proteins disrupts both cellular extrusion and intracellular degradation of cAMP. *Mol. Pharmacol.* **80**, 281–293 (2011).
60. G. Veit, F. Bossard, J. Goepf, A. S. Verkman, L. J. Galletta, J. W. Hanrahan, G. L. Lukacs, Proinflammatory cytokine secretion is suppressed by TMEM16A or CFTR channel activity in human cystic fibrosis bronchial epithelia. *Mol. Biol. Cell* **23**, 4188–4202 (2012).

Acknowledgments: We would like to thank E. Balmas and L. Conti for discussions. **Funding:** This work was supported by research grants from the Italian Cystic Fibrosis Research Foundation (FFC#25/2014 to E.H., FFC#23/2015 to E.H., FFC#8/2018 to E.H., FFC#4/2016 to A. Ghigo, and FFC#11/2017 to A. Ghigo), Cariplo Foundation (#2015-0880 to A. Ghigo and #2018-0498 to E.H.), Roche Foundation (Bando Roche per la Ricerca 2019 to A. Ghigo), Compagnia di San Paolo (CSTO161109 to E.H.), Telethon Foundation (GGP20079 to A. Ghigo),

the NIH (P30DK065988 to M.G.), Cystic Fibrosis Canada and FRQS Postdoctoral Fellowship (to A.P.), Canadian Institute for Health Research (CIHR) (PJT 153095 to G.L.L.), Cystic Fibrosis Foundation (CFF) (00988G220 to G.L. and BOUCHE15R0 to M.G.), Cystic Fibrosis Canada (to G.L.L.), and the German Federal Ministry of Education and Research (82DZL009B1 to M.A.M.). **Author contributions:** A. Ghigo and E.H. conceived and designed the overall study. A. Ghigo and A. Murabito carried out the core of the experiments and analyzed the data. V.S., A.R.P., and S. Bertolini performed immunoprecipitation and immunoblotting assays. A. Gianotti, E.C., W.R., and N.L.Q. performed short-circuit current measurements in Ussing chambers. A. Montresor performed all experiments with human neutrophils. A.P. performed CFTR phosphoproteomic experiments. F.P. and R.K. carried out all experiments with OVA-sensitized mice. A.D.S. carried out all experiments with macrophages. M. Mergioti, M.R.R., and S. Baroni measured water residence time. E.d.P. and S.C. carried out FIS assays in organoids. M. Matthey and A.C. carried out lung function measurements. R.A.C. performed FRET-based cAMP measurements in epithelial cells. F.C. measured tracheal ring contractility. C.B. measured PI3Kγ MP/PKA-RII dissociation constant. S.V., S.G.C., D.R., M.L., C.G.T., R.L., M.C., X.L., P.M., C.S., V.D.R., F.F., V.F., D.W., B.K.F., M.A.M., J.B., C.L., M.G., G.L.L., and N.P. provided advice on the interpretation of data. A. Ghigo, A. Murabito, and E.H. wrote the manuscript with input from coauthors. All authors reviewed and approved the final manuscript. **Competing interests:** A. Ghigo and E.H. are cofounders and board members of Kither Biotech Srl. A. Ghigo and E.H. are coinventors of patent titled “Novel pi3k gamma inhibitor peptide for treatment of respiratory system diseases” (WO2016103176A1) that is directly associated with the study. M.A.M. reports personal fees for participation in advisory boards or paid consulting from Abbvie, Antabio, Arrowhead Pharmaceuticals, Boehringer Ingelheim, Enterprise Therapeutics, Kither Biotech, Pieris Pharmaceuticals, Santhera, Sterna Biologicals, and Vertex Pharmaceuticals outside the submitted work. P.M. declares consulting activities paid by Kither Biotech and expert testimony fees paid by Vertex Pharmaceuticals. J.B. is inventor on a patent related to organoid swelling and received financial royalties for this contribution from the Royal Dutch Academy of Sciences and Arts. All other authors declare that they have no competing interests. **Data and materials availability:** All data associated with this study are available in the paper or the Supplementary Materials. Individual values and data from main and supplementary figures are presented in data files S1 and S2, respectively. PI3Kγ MP is available to the scientific community upon completion of a material transfer agreement with Kither Biotech Srl. The following cell lines and reagents were obtained through a material transfer agreement between University of Torino and the indicated institution: 16HBE14o- and CFBE41o- cells (University of California San Francisco), wt-CFTR-CFBE41o- and F508del-CFTR-CFBE41o- (University of Alabama at Birmingham), and CFTR antibodies (University of North Carolina–Chapel Hill).

Submitted 2 August 2021
Resubmitted 26 November 2021
Accepted 25 February 2022
Published 30 March 2022
10.1126/scitranslmed.abl6328



Role of Protein Kinase A-Mediated Phosphorylation in CFTR Channel Activity Regulation

Angela Della Sala¹, Giulia Prono², Emilio Hirsch^{1,2*†} and Alessandra Ghigo^{1,2*†}

¹Molecular Biotechnology Center, Department of Molecular Biotechnology and Health Sciences, University of Turin, Turin, Italy, ²Kither Biotech S.r.l., Turin, Italy

OPEN ACCESS

Edited by:

Fabio Mammano,
University of Padua, Italy

Reviewed by:

Steven S. An,
Rutgers Institute for Translational
Medicine and Science, United States
John Cuppoletti,
University of Cincinnati, United States

*Correspondence:

Alessandra Ghigo
alessandra.ghigo@unito.it
Emilio Hirsch
emilio.hirsch@unito.it

[†]These authors have contributed
equally to this work and share senior
authorship

Specialty section:

This article was submitted to
Membrane Physiology and
Membrane Biophysics,
a section of the journal
Frontiers in Physiology

Received: 13 April 2021

Accepted: 10 May 2021

Published: 11 June 2021

Citation:

Della Sala A, Prono G, Hirsch E and
Ghigo A (2021) Role of Protein
Kinase A-Mediated Phosphorylation
in CFTR Channel Activity Regulation.
Front. Physiol. 12:690247.
doi: 10.3389/fphys.2021.690247

Cystic fibrosis transmembrane conductance regulator (CFTR) is an anion channel expressed on the apical membrane of epithelial cells, where it plays a pivotal role in chloride transport and overall tissue homeostasis. CFTR constitutes a unique member of the ATP-binding cassette transporter superfamily, due to its distinctive cytosolic regulatory (R) domain carrying multiple phosphorylation sites that allow the tight regulation of channel activity and gating. Mutations in the *CFTR* gene cause cystic fibrosis, the most common lethal autosomal genetic disease in the Caucasian population. In recent years, major efforts have led to the development of CFTR modulators, small molecules targeting the underlying genetic defect of CF and ultimately rescuing the function of the mutant channel. Recent evidence has highlighted that this class of drugs could also impact on the phosphorylation of the R domain of the channel by protein kinase A (PKA), a key regulatory mechanism that is altered in various CFTR mutants. Therefore, the aim of this review is to summarize the current knowledge on the regulation of the CFTR by PKA-mediated phosphorylation and to provide insights into the different factors that modulate this essential CFTR modification. Finally, the discussion will focus on the impact of CF mutations on PKA-mediated CFTR regulation, as well as on how small molecule CFTR regulators and PKA interact to rescue dysfunctional channels.

Keywords: cystic fibrosis transmembrane conductance regulator, protein kinase A, phosphorylation, cystic fibrosis, VX770, VX809, F508del-CFTR mutation

INTRODUCTION

The cystic fibrosis transmembrane conductance regulator (CFTR) is a cAMP-activated chloride and bicarbonate channel expressed at the apical surface of secretory epithelia, including the airways, sweat glands, gastrointestinal tract, and other tissues (Riordan et al., 1989; Rommens et al., 1989; Riordan, 2008). The CFTR has a critical role in transepithelial ion and fluid secretion and homeostasis, and mutations in this gene have been implied in the pathogenesis of cystic fibrosis (CF; Li and Naren, 2005). CF, the most common life-shortening rare disease among Caucasians, is an autosomal recessive genetic disease affecting around 32,000 individuals in Europe and about 85,000 individuals worldwide (Zolin et al., 2020). The absence of a functional CFTR leads to a decrease in chloride ion secretion that, together with the consequent alteration of water homeostasis, results in the accumulation of dehydrated mucus, recurrent

bacterial infection, and ultimately organ failure. Although CFTR mutations cause a multiorgan disease, respiratory failure is the major cause of morbidity and mortality for CF patients (Ratjen et al., 2015). Although CF nowadays remains an incurable disease, the identification of the defective *CFTR* gene in 1989 (Riordan et al., 1989; Rommens et al., 1989) has prompted significant advances in the development of molecular therapies aimed at addressing the underlying cellular defect (De Boeck and Amaral, 2016; Veit et al., 2016).

The *CFTR* gene, expressed on the long arm of chromosome 7 (Kerem et al., 1989), encodes for a unique member of the large protein superfamily of ATP-binding cassette (ABC) transporters (Klein et al., 1999), which carries a cytosolic regulatory domain that is actively phosphorylated (Collins, 1992; Serohijos et al., 2008). Whereas most of the ABC transporters are active pumps using ATP as the energy source for the transport of small molecules, CFTR is an ATP-gated ion channel where ATP hydrolysis controls channel opening (Dean et al., 2001). Cystic fibrosis transmembrane conductance regulator, like other ABC transporters, is composed of two nucleotide-binding domains (NBDs), involved in channel regulation through ATP binding and hydrolysis, and two transmembrane domains (TMDs), containing six helices that span the plasma membrane to form the ion channel pore (Riordan et al., 1989; Callebaut et al., 2018). In the CFTR, however, the NBD1 domain is linked to the NBD2 one by an additional structural region, a distinctive cytoplasmic regulatory (R) domain with many charged residues and multiple phosphorylation sites that allow the tight regulation of channel activity and gating.

Importantly, the gating of the channel is strictly coupled to the phosphorylation of the R domain by protein kinase A (PKA; Egan et al., 1992; Vergani et al., 2005a,b) and protein kinase C (Chappe et al., 2003; Seavilleklein et al., 2008). PKA-dependent phosphorylation triggers large conformational changes that remove the R region from its position and allow NBDs dimerization to occur. Consequently, ATP binds to the CFTR leading to the opening and activation of the channel, while ATP hydrolysis closes it (Gunderson and Kopito, 1995; Figure 1). In addition to regulating the gating of the channel, PKA-mediated phosphorylation is involved in the regulation of multiple processes, such as CFTR trafficking and stability at the plasma membrane (Chin et al., 2017a).

This review will discuss the role of PKA in CFTR activity regulation, and how this physiological mechanism of channel activation is disrupted by CF mutations. Furthermore, in light of the recent advances in the development of CFTR modulators, we will discuss the impact of these novel molecules on the PKA-mediated regulation of mutant channels.

CFTR GATING REQUIRES PKA-MEDIATED PHOSPHORYLATION

Although the molecular mechanisms underlying CFTR activation have been studied for years, several questions remain unanswered. This section discusses how channel gating strictly depends on

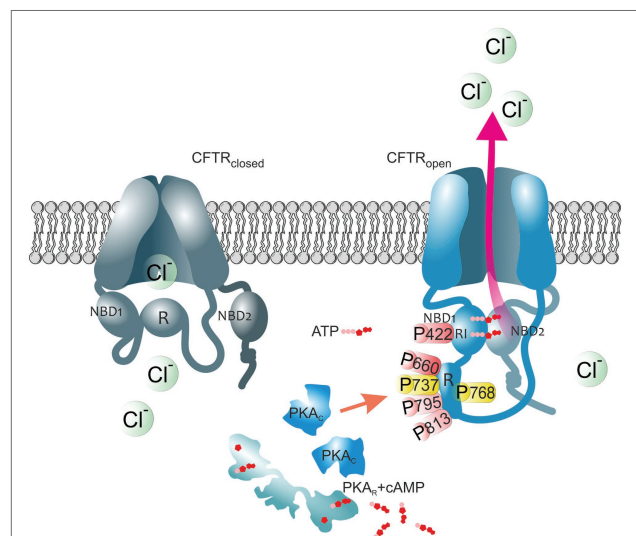


FIGURE 1 | The impact of PKA-mediated phosphorylation on CFTR channel. The cystic fibrosis transmembrane conductance regulator (CFTR) structure consists of two membrane spanning domains, two nucleotide-binding domains (NBD1 and NBD2), and the unique cytoplasmic regulatory (R) domain. Among these, the latter represents a critical site of channel regulation due to its enrichment in protein kinase A (PKA) consensus motifs, with multiple serines and threonines as phosphorylation targets. Moreover, there is an additional phosphorylation site in the regulatory insertion (RI) segment of NBD1. In the closed CFTR state (left channel), the NBD1 interacts with the R domain creating steric hindrances which prevent it from dimerization with NBD2. Upon PKA-dependent phosphorylation (right channel), large conformational changes occur that decrease this interaction leading to the release of the R region from its inhibitory position and allow NBDs dimerization, ultimately ATP binding and CFTR-mediated chloride secretion. Thus, the open probability of the channel is dependent on the access of PKA to the main phospho-sites (S422, S660, S737, S768, S795, and S813). Phospho-sites critical for CFTR channel activation are shown in red. Phosphoserines S737 and S768 are shown in yellow since they have been shown to either activate or inhibit CFTR gating. The role of the major PKA consensus sites in the regulation of CFTR function is detailed in **Table 1**.

the intrinsic structure of the CFTR protein and several posttranslational modifications, primarily phosphorylation.

One of the major challenges to the understanding of the regulation by the R region of the opening and the gating of CFTR has been the resolution of the CFTR structure. A crucial breakthrough has been represented by the construction of medium-high-resolution models of the 3D structures of the full-length CFTR, first from zebrafish (Zhang and Chen, 2016) and then from humans (Liu et al., 2017). These molecular structures of the CFTR, determined using cryo-electron microscopy, provide insights into a dephosphorylated, ATP-free conformation, which represents a closed and inactive state of the channel (Zhang and Chen, 2016; Liu et al., 2017). Of note, Liu and colleagues with the resolution of the human CFTR structure reveal a previously unresolved helix belonging to the R region docked in an inward-facing conformation between the two halves of CFTR, where it acts as a steric block precluding channel opening (Liu et al., 2017). On the other hand, activation of the CFTR channel is strictly coupled to the formation of a

TABLE 1 | PKA phospho-sites in CFTR and their role in channel activity regulation.

PKA consensus site	Domain	Mechanisms involved in PKA-mediated phosphorylation	References
Serine-422	RI-domain of NBD1	Phosphorylation disrupts the interaction with S660 in the R domain promoting NBDs dimerization, formation of the two ATP-binding pockets and CFTR activation	Hudson et al., 2012; Dawson et al., 2013
Serine-737, 768	R-domain	Phosphorylation leads to CFTR channel opening in the 15SA CFTR variant insensitive to PKA. In contrast, phosphorylation by AMPK of these sites maintains CFTR in a closed state	Hegedus et al., 2009; Kongsuphol et al., 2009
Serine-768, 795, 813	R-domain	Phosphorylation leads to CFTR binding to the 14-3-3b isoform in the ER and promotes its forward trafficking to the cell surface	Liang et al., 2012
Serine-660, 700, 795, 813	R-domain	Phosphorylation leads to conformational change and release of the R domain from its inhibitory position, promoting NBDs dimerization and CFTR gating	Rich et al., 1993; Vais et al., 2004; Chen, 2020

closed NBD dimer, and thereby to the initial conformational changes driven by the PKA-dependent phosphorylation of the R domain (Liu et al., 2017; Mihalyi et al., 2020).

Thus, the open probability of the channel is dependent on the access of PKA to the multiple consensus sites in the R domain (Liu et al., 2017), including 18 potential phosphorylation sites (12 serines and 8 threonines) on a 200 residues long domain. Specifically, in the fully phosphorylated protein, eight phosphoserines (residue positions 660, 700, 712, 737, 753, 768, 795, and 813) and partial phosphorylation of serine at position 670 (Baker et al., 2007) have been detected by mass spectrometry (Townsend et al., 1996; Neville et al., 1997) and NMR (Baker et al., 2007). Recently, Lucaks and colleagues implemented a novel CFTR affinity enrichment method, followed by an advanced mass spectrometry technique, to establish the phospho-occupancy of CFTR upon PKA phosphorylation (Schnur et al., 2019). Among the previously described 15 PKA consensus sites, they identified 10 PKA phospho-sites in the R and NBD1 domain of CFTR (serine 422, 660, 670, 686, 700, 712, 737, 753, 768, and 795; Schnur et al., 2019). **Table 1** provides a comprehensive description of the major phospho-sites and their effect on CFTR channel activity regulation. The role of each phosphoserine in the modulation of CFTR activity is quite complex and multiple experiments have been attempted to address this problem by site-direct mutagenesis, where the putative phosphorylation sites in the R region were substituted with alanines (Kanelis et al., 2010; Marasini et al., 2012, 2013). Of note, among such studies, the replacement of serine at position 700, 795, and 813 revealed a decrease in channel open probability (Rich et al., 1993; Vais et al., 2004; Chen, 2020), whereas mutations of serine 737 and 768 increased the activity, thus implying a phospho-dependent inhibitory effect of these residues on the CFTR channel function (Wilkinson et al., 1997; Kongsuphol et al., 2009). Accordingly, phosphorylation of these inhibitory sites by AMPK inhibits CFTR-mediated chloride secretion by maintaining the channel in a closed state (Kongsuphol et al., 2009). These findings appear to be in apparent contrast with the results of the work by Riordan and colleagues aimed at investigating whether individual PKA phospho-sites act cooperatively or distinctly in the regulation of channel activity. This study investigated the impact of the reintroduction of

S737 and S768 in a CFTR variant insensitive to PKA, namely, the 15SA mutant, in which the 15 PKA consensus sites were replaced by alanines (Hegedus et al., 2009). Reintroduction of S737 or S768 or both restored a significant level of channel activation by PKA, thus indicating that phosphorylation of these sites stimulates CFTR channel activity. Furthermore, a mutant CFTR in which all phosphorylation sites have been removed, completely eliminates the PKA-dependent regulation of the channel activity (Xie et al., 2002). In line with this finding, a CFTR mutant containing six or more serine-to-aspartate substitutions mimicking the effect of phosphorylation results in channel opening even in the absence of PKA (Rich et al., 1993).

Overall, these experiments highlight that the effects of PKA-dependent phosphorylation of the R domain are correlated to conformational changes triggered by the negative charges of the phosphate group introduced on phosphoserines (Zhang et al., 2017, 2018; Schnur et al., 2019).

As a confirmation, circular dichroism, X-ray scattering, and NMR experiments showed a reduced density of the phosphorylated structure, suggesting that upon phosphorylation the R domain becomes entirely disordered and less compact (Baker et al., 2007; Bozoky et al., 2013). Further evidence of the structure of phosphorylated CFTR, in its ATP-bound conformation, comes from cryo-electron microscopy (Zhang et al., 2017, 2018). These images, comparing the conformation in a phosphorylated and ATP-bound state (Zhang and Chen, 2016; Liu et al., 2017) with the dephosphorylated and ATP-free conformation (Zhang et al., 2017, 2018), define the structural changes of the two human and zebrafish CFTR orthologs. These structures further reveal the clearly distinct position of the R domain after phosphorylation. Upon PKA binding, phosphorylation promotes the release of the R domain from its inhibitory position, causing NBDs dimerization and flipping of the TMDs into an outward-facing conformation, ultimately leading to channel opening and activation of its ATPase function (Sorum et al., 2015; **Figure 1**).

On the other hand, how phosphorylation triggers the ATPase activity of CFTR has remained unclear. Whereas PKA-mediated phosphorylation of the R domain is absolutely required (Chang et al., 1993; Winter and Welsh, 1997; Seibert et al., 1999), whether ATP binding is essential for CFTR gating is still

controversial. In the following paragraph, we will describe how phosphorylated CFTR channels are gated through ATP-dependent and independent mechanisms.

EFFECTS OF PKA-MEDIATED PHOSPHORYLATION ON ATP BINDING

The widely accepted model of CFTR activation establishes that phosphorylated CFTR channels are gated through an ATP-dependent mechanism that is based on conformational changes (Sorum et al., 2015). In these models, the ATP molecule powers the gating cycle by inducing the opening through NBD1:NBD2 dimerization as well as the closing through its hydrolysis (Higgins and Linton, 2004). While PKA phosphorylation promotes the release of the R domain from its position, the binding of ATP triggers the dimerization of the NBDs that, in turn, leads to channel opening and activation (Vergani et al., 2003, 2005b; Csanady et al., 2010). Therefore, the phosphorylation of the R domain increases the rate of channel opening by stimulating conformational changes that enhance the affinity for ATP (Winter and Welsh, 1997).

Following this obligatory modification, the ATP generally bound only to NBD1 is released, and it binds to the two sites at the NBD1:NBD2 interface (Aleksandrov et al., 2018). Recent studies by Csana and colleagues support a model wherein ATP binding to both NBDs enhances their dimerization and consequently channel opening (Mihalyi et al., 2016). Instead, the ATPase activity at NBD2 subsequently promotes destabilization of the NBD dimer, leading to channel closure (Mihalyi et al., 2016). Additionally, Lewis and colleagues have found that in the CFTR closed state, the NBDs dimer is prevented, due to the inhibitory interaction of the R domain with the regulatory insertion (RI) domain of NBD1 (Lewis et al., 2004). Although the majority of the canonical phosphorylation sites are located within the R domain of CFTR, an additional residue (S422) in the RI region plays a key regulatory function (Lewis et al., 2004). In particular, S422 of the RI domain interacts with S660 in the R domain, creating steric hindrances on NBD1, which prevent it from dimerization with NBD2 (Hudson et al., 2012; Dawson et al., 2013). Upon phosphorylation by PKA of these two serines, the alpha-helical content of both the RI and the R regions decreases (Hudson et al., 2012; Dawson et al., 2013). Therefore, phosphorylation by PKA weakens the interaction between the R domain and NBD1, ultimately allowing the formation of the NBD1:NBD2 dimer (Aleksandrov et al., 2018).

Different from the wild-type CFTR channel, where the gating is dependent on ATP binding, in gating mutants where ATP binding is impaired, the introduction of a second mutation, like the K978C or the NBD2 deletion, restores the open conformation of the channel, but PKA-mediated phosphorylation of the R domain is still required for full channel activation (Eckford et al., 2012). These examples of ATP-independent CFTR channel appear to be regulated by phosphorylation, *via* allosteric interactions between the R domain and the NBD1 region (Eckford et al., 2012). Nonetheless, further studies are required to understand the molecular basis for such ATP-independent gating and CFTR regulation.

Overall, phosphorylation represents an additional level of control of CFTR activity besides ATP binding and hydrolysis. Given that the ATP concentrations within a cell are high enough for constant activation of the channel, phosphorylation is essential for the prevention of futile cycling of the channel between the open and closed conformations (Higgins and Linton, 2004).

EFFECTS OF CF-CAUSING MUTATIONS ON PKA-MEDIATED PHOSPHORYLATION OF CFTR

Considering the essential role of PKA-dependent phosphorylation of the intrinsically disordered R domain in modulating CFTR gating (Hallows et al., 2003; Billet et al., 2015, 2016), it is plausible that CF-causing mutations may disturb this mechanism of channel regulation. The most common CFTR mutation, consisting of the deletion of phenylalanine (F508del) located at the interface between NBD1 and the intracellular loop 4, interferes with the correct R domain folding and assembly (Riordan, 2005; Hwang et al., 2018). As a consequence, the aberrant channel is targeted to early ER-associated degradation (Farinha and Amaral, 2005). Moreover, the resulting thermal instability of this mutant form further contributes to its removal from the plasma membrane (Okuyoneda et al., 2010), which has been shown to contain only 2% of mature F508del-CFTR compared to the normal wild-type (WT) channel amount (Van Goor et al., 2011). Importantly, Wang and colleagues demonstrated that the phosphorylation rate of F508del-CFTR by PKA is significantly lower than that of WT-CFTR, suggesting that the abnormal protein does not constitute a good substrate for the kinase (Wang et al., 2000). The same results were obtained from the analysis of the other two disease-causing CFTR mutations, R170G and A1067T, both occurring in coupling helices that allow the correct channel activation by phosphorylation (Chin et al., 2017b).

Furthermore, a relevant study by Pasyk et al. exploited mass spectrometry to quantitatively assess PKA-mediated phosphorylation of serine 660 of F508del-CFTR at the ER and reported a drastic reduction of phosphorylation upon forskolin stimulation in comparison with the WT form (Pasyk et al., 2009). Interestingly, COPI-mediated retrograde trafficking from the Golgi to the ER, which prevents misfolded F508del-CFTR from successfully reaching the apical cell membrane (Rennolds et al., 2008; Okuyoneda et al., 2010), has been linked to phosphorylation-dependent interactions between the channel and 14-3-3 proteins (Liang et al., 2012). In particular, selective binding of 14-3-3 protein isoforms to specific PKA-phosphorylated sites within the R region decreases this retrograde retrieval, ultimately resulting in augmented CFTR biogenesis. Unfortunately, whether the impaired phosphorylation caused by the deletion of F508 negatively impacts this protein-protein interaction has yet to be elucidated.

Another relevant process that contributes to the maintenance of channel density at the plasma membrane is the endosomal trafficking of the CFTR, which ensures the internalization and recycling of abundant or misfolded proteins (Moore et al., 2007).

Notably, Holleran and collaborators revealed that cell surface F508del-CFTR is targeted to lysosomes and displays defective PKA-regulated exocytosis, consisting of significantly slower rates of translocation to the plasma membrane from the Rab11+/EHD1+ endosomal recycling compartment upon PKA challenge (Holleran et al., 2013). Therefore, these data suggest that the abnormal phosphorylation of the mutant CFTR by PKA could, at least partly, account for the defective peripheral trafficking of the channel. Moreover, it has been shown that the excision of the RI polypeptide from the NBD1 of F508del protein, which contains the additional PKA consensus site S422, may be beneficial for the life cycle of the mutant channel (Aleksandrov et al., 2010). Specifically, removal of this region was found to promote the escape of F508del-CFTR from the ER quality control machinery and thus the increased apical surface stability. In addition, recent evidence confirmed that the amount of phosphorylated S422, which represents a minor PKA target site, is decreased in the aberrant F508del protein (Pankow et al., 2019). However, further analyses are required to clarify whether the presence of the RI hampers the F508del-CFTR stability independently of its phosphorylation state and to evaluate the biological consequence of its reduced phosphorylation in the mutant CFTR.

Another important CFTR genetic defect that could potentially interfere with PKA-mediated phosphorylation of the channel is the G551D mutation, a class III mutation with a worldwide frequency of ~4% (CFF patient registry, 2019). The disease-causing substitution occurs in the NBD1 domain and strongly impairs the ATP-dependent channel gating, without hindering channel trafficking to the plasma membrane (Gregory et al., 1991; Bompadre et al., 2007). Interestingly, Chang and colleagues demonstrated that the R domain of this mutant form undergoes normal phosphorylation despite its lack of ATP binding (Chang et al., 1993). In contrast, a very recent study showed that G551D-CFTR exhibits defective phosphorylation-dependent activation as a result of a decreased sensitivity to PKA-mediated phosphorylation. Stimulation of mutant channels with high doses of PKA induced a remarkable increase in their activity, thus suggesting that the intrinsic phosphorylation defect of G551D-CFTR might be one of the major causes of low basal functionality. Moreover, phosphorylation of the serine residue 737 of G551D occurred at a lesser extent compared to WT-CFTR, highlighting a possible causative factor of the slower activation rate of the aberrant protein (Wang et al., 2020).

Taken together, abnormal PKA-mediated phosphorylation underlies multiple molecular defects observed in mutant CFTR channels and represents a promising therapeutic target for the treatment of CF. Therefore, the following paragraph will focus on how currently available CFTR modulators impact on the phosphorylation of the channel by PKA.

EFFECTS OF CFTR MODULATORS ON PKA-DEPENDENT REGULATION OF CFTR

In recent years, major advances have been made in the field of precision therapy against the underlying cause of CF. A variety of small molecules, designed to target specific channel defects

and collectively known as CFTR modulators, have been developed to improve or even restore the expression, activity, and stability of defective CFTR variants (Lopes-Pacheco, 2016). Of utmost relevance are CFTR correctors, which rescue the misprocessing of mutant CFTRs, and potentiators, that are intended to restore the defective cAMP-dependent chloride channel activity at the cell surface (Lopes-Pacheco, 2016). Nonetheless, how these therapeutic agents act on the PKA-mediated phosphorylation of CFTR mutants is still largely unaddressed.

Importantly, there are some paradigmatic exceptions of CFTR modulating drugs whose relationship with PKA-dependent phosphorylation has been investigated and will be now discussed. The potentiator VX-770 (ivacaftor) is approved both as a single therapy for G551D mutants and as a combination with either the corrector VX-809 (lumacaftor; Connett, 2019) or VX-445 and VX-661 for F508del carriers (Bear, 2020). Importantly, ivacaftor was found to enhance channel activity in an ATP-independent manner (Eckford et al., 2012). However, non-phosphorylated CFTR does not exhibit any significant ion current increase upon VX-770 stimulation, suggesting that its potentiating action is strictly dependent on the phosphorylation state of the channel (Eckford et al., 2012). Conversely, Jih and collaborators demonstrated that this potentiator can increase the activity of a CFTR lacking the R domain, thus arguing with the previous hypotheses of a phosphorylation-dependent mechanism (Jih and Hwang, 2013). Recently, a study by Uliyakina et al. revealed that the absence of the RI domain strongly emphasizes VX-809-mediated rescue of F508del-CFTR but negatively impacts the channel currents stimulated by VX-770 (Uliyakina et al., 2020). Therefore, these two modulators display a contradictory behavior in the absence of the unique region containing the PKA phosphorylation site, S422, but future analyses are needed to dissect the role of RI in mutant CFTR. Additionally, another molecule, VRT-532, which had been formerly identified as a potentiator (Van Goor et al., 2006), showed to significantly amplify the activity of G551D-CFTR mutants. Despite its direct interaction with the aberrant channel (Pasyk et al., 2009), VRT-532 did not induce an increase in CFTR phosphorylation, suggesting that its mechanism of action occurs at stages that are downstream of the PKA kinase activity (Pyle et al., 2011).

Conversely, correctors based on 3-(2-benzyloxy-phenyl)-5-chloromethyl-isoxazoles, like UCCF-152, were found to stimulate potent and rapid phosphorylation of the R domain of WT, temperature-rescued F508del-CFTR and G551D-CFTR, while also increasing iodide currents, leading to their classification as CFTR activators (Pyle et al., 2011). The specific residues phosphorylated upon the interaction with UCCF-152 have not been yet identified, but this isoxazole neither raises cellular cAMP levels nor directly activates PKA, suggesting a possible enhancement of the propensity of the R domain to be phosphorylated by releasing steric hindrances (Sammelson et al., 2003). To date, no additional analyses have been performed to further characterize UCCF-152 as a candidate CF-treating agent. The impact of CF-causing mutations on PKA phosphorylation of CFTR, and the effect of CFTR modulators on the activity of mutant channels is summarized in **Table 2**.

TABLE 2 | Effects of CFTR modulators on PKA-dependent regulation of CFTR mutants.

CFTR mutant	Impact on PKA-mediated phosphorylation	Effects of CFTR modulators	References
F508del	Reduced phosphorylation rate (PKA phospho-sites S442, S660), altered interaction with 14-3-3 proteins, increased COPI-mediated retrograde trafficking, defective PKA-regulated exocytosis	Potentialiation by VX-770 shows contrasting results on phosphorylated and non-phosphorylated mutant CFTR. VX-770-mediated rescue requires S442, while its deletion enhances VX-809 correction. The activator UCCF-152 potentiates the phosphorylation of the R domain	Wang et al., 2000; Pasyk et al., 2009; Pyle et al., 2011; Eckford et al., 2012; Liang et al., 2012; Holleran et al., 2013; Uliyakina et al., 2020
G551D	Reduced phosphorylation (PKA phospho-site S737) and defective phosphorylation-dependent activation	VRT-532 potentiates the activity of the channel. The activator UCCF-152 potentiates the phosphorylation of the R domain	Chang et al., 1993; Pyle et al., 2011; Wang et al., 2020

Overall, our current knowledge of how CFTR modulators interfere or promote PKA-dependent phosphorylation of the channel remains scarce, and future efforts are needed to allow a better understanding of their impact on this essential molecular modification of the channel.

CONCLUSION

In conclusion, PKA-dependent phosphorylation plays a key role in multiple steps during the life cycle of CFTR. While interactions resulting in phosphorylation at the CFTR R domain regulate channel opening and activity, other phosphorylation events at the C and N terminal ends of CFTR modulate channel stability and trafficking at the PM. Importantly, CFTR mutations leading to CF impair different steps of CFTR biogenesis that are regulated by these phosphorylation events. Targeting PKA-mediated phosphorylation thus represents a promising strategy to rescue the activity of different CF-causing CFTR variants. Nonetheless, how correctors and potentiators, including their highly effective combinations, like the recently approved Trikafta, impact on the PKA-mediated phosphorylation of CFTR still needs to be thoroughly investigated. Future studies in this

direction might help to maximize therapeutic efficacy, ultimately normalizing the life expectancy of CF patients.

AUTHOR CONTRIBUTIONS

ADS designed the overall layout and wrote the bulk of the manuscript. GP was involved in the writing of the manuscript and referencing. EH reviewed the manuscript and produced the figure. AG was involved in the editing and critical revision of the manuscript. AG and EH acquired the funding. All authors contributed to the article and approved the submitted version.

FUNDING

This work was supported by the Italian Cystic Fibrosis Research Foundation (FFC#8/2018 to EH), Compagnia di Sanpaolo (CSTO161109 to EH), Cariplo Foundation (#2018-0498 to EH), Roche Foundation (Bando Roche per la Ricerca 2019 to AG), and Telethon Foundation (GGP20079 to AG).

REFERENCES

- Aleksandrov, L. A., Fay, J. F., and Riordan, J. R. (2018). R-domain phosphorylation by protein kinase A stimulates dissociation of unhydrolyzed ATP from the first nucleotide-binding site of the cystic fibrosis transmembrane conductance regulator. *Biochemistry* 57, 5073–5075. doi: 10.1021/acs.biochem.8b00646
- Aleksandrov, A. A., Kota, P., Aleksandrov, L. A., He, L., Jensen, T., Cui, L., et al. (2010). Regulatory insertion removal restores maturation, stability and function of DeltaF508 CFTR. *J. Mol. Biol.* 401, 194–210. doi: 10.1016/j.jmb.2010.06.019
- Baker, J. M., Hudson, R. P., Kanelis, V., Choy, W. Y., Thibodeau, P. H., Thomas, P. J., et al. (2007). CFTR regulatory region interacts with NBD1 predominantly via multiple transient helices. *Nat. Struct. Mol. Biol.* 14, 738–745. doi: 10.1038/nsmb1278
- Bear, C. E. (2020). A therapy for most with cystic fibrosis. *Cell* 180:211. doi: 10.1016/j.cell.2019.12.032
- Billet, A., Jia, Y., Jensen, T. J., Hou, Y. X., Chang, X. B., Riordan, J. R., et al. (2016). Potential sites of CFTR activation by tyrosine kinases. *Channels* 10, 247–251. doi: 10.1080/19336950.2015.1126010
- Billet, A., Jia, Y., Jensen, T., Riordan, J. R., and Hanrahan, J. W. (2015). Regulation of the cystic fibrosis transmembrane conductance regulator anion channel by tyrosine phosphorylation. *FASEB J.* 29, 3945–3953. doi: 10.1096/fj.15-273151
- Bompadre, S. G., Sohma, Y., Li, M., and Hwang, T. C. (2007). G551D and G1349D, two CF-associated mutations in the signature sequences of CFTR, exhibit distinct gating defects. *J. Gen. Physiol.* 129, 285–298. doi: 10.1085/jgp.200609667
- Bozoky, Z., Krzeminski, M., Muhandiram, R., Birtley, J. R., Al-Zahrani, A., Thomas, P. J., et al. (2013). Regulatory R region of the CFTR chloride channel is a dynamic integrator of phospho-dependent intra- and intermolecular interactions. *Proc. Natl. Acad. Sci. U. S. A.* 110, E4427–E4436. doi: 10.1073/pnas.1315104110
- Callebaut, I., Chong, P. A., and Forman-Kay, J. D. (2018). CFTR structure. *J. Cyst. Fibros.* 17, S5–S8. doi: 10.1016/j.jcf.2017.08.008
- CFR patient registry (2019). Cystic Fibrosis Foundation Patient Registry 2019 Annual Data Report.
- Chang, X. B., Tabcharani, J. A., Hou, Y. X., Jensen, T. J., Kartner, N., Alon, N., et al. (1993). Protein kinase A (PKA) still activates CFTR chloride channel after mutagenesis of all 10 PKA consensus phosphorylation sites. *J. Biol. Chem.* 268, 11304–11311. doi: 10.1016/S0021-9258(18)82125-1
- Chappe, V., Hinkson, D. A., Zhu, T., Chang, X. B., Riordan, J. R., and Hanrahan, J. W. (2003). Phosphorylation of protein kinase C sites in NBD1 and the R domain control CFTR channel activation by PKA. *J. Physiol.* 548, 39–52. doi: 10.1113/jphysiol.2002.035790
- Chen, J. H. (2020). Protein kinase A phosphorylation potentiates cystic fibrosis transmembrane conductance regulator gating by relieving autoinhibition on

- the stimulatory C terminus of the regulatory domain. *J. Biol. Chem.* 295, 4577–4590. doi: 10.1074/jbc.RA119.008427
- Chin, S., Hung, M., and Bear, C. E. (2017a). Current insights into the role of PKA phosphorylation in CFTR channel activity and the pharmacological rescue of cystic fibrosis disease-causing mutants. *Cell. Mol. Life Sci.* 74, 57–66. doi: 10.1007/s00018-016-2388-6
- Chin, S., Yang, D., Miles, A. J., Eckford, P. D. W., Molinski, S., Wallace, B. A., et al. (2017b). Attenuation of phosphorylation-dependent activation of cystic fibrosis transmembrane conductance regulator (CFTR) by disease-causing mutations at the transmission interface. *J. Biol. Chem.* 292, 1988–1999. doi: 10.1074/jbc.M116.762633
- Collins, F. S. (1992). Cystic fibrosis: molecular biology and therapeutic implications. *Science* 256, 774–779. doi: 10.1126/science.1375392
- Connett, G. J. (2019). Lumacaftor-ivacaftor in the treatment of cystic fibrosis: design, development and place in therapy. *Drug Des. Devel. Ther.* 13, 2405–2412. doi: 10.2147/DDDT.S153719
- Csanady, L., Vergani, P., and Gadsby, D. C. (2010). Strict coupling between CFTR's catalytic cycle and gating of its Cl⁻ ion pore revealed by distributions of open channel burst durations. *Proc. Natl. Acad. Sci. U. S. A.* 107, 1241–1246. doi: 10.1073/pnas.0911061107
- Dawson, J. E., Farber, P. J., and Forman-Kay, J. D. (2013). Allosteric coupling between the intracellular coupling helix 4 and regulatory sites of the first nucleotide-binding domain of CFTR. *PLoS One* 8:e74347. doi: 10.1371/journal.pone.0074347
- Dean, M., Rzhetsky, A., and Allikmets, R. (2001). The human ATP-binding cassette (ABC) transporter superfamily. *Genome Res.* 11, 1156–1166. doi: 10.1101/gr.GR-1649R
- De Boeck, K., and Amaral, M. D. (2016). Progress in therapies for cystic fibrosis. *Lancet Respir. Med.* 4, 662–674. doi: 10.1016/S2213-2600(16)00023-0
- Eckford, P. D., Li, C., Ramjeesingh, M., and Bear, C. E. (2012). Cystic fibrosis transmembrane conductance regulator (CFTR) potentiator VX-770 (ivacaftor) opens the defective channel gate of mutant CFTR in a phosphorylation-dependent but ATP-independent manner. *J. Biol. Chem.* 287, 36639–36649. doi: 10.1074/jbc.M112.393637
- Egan, M., Flotte, T., Afione, S., Solow, R., Zeitlin, P. L., Carter, B. J., et al. (1992). Defective regulation of outwardly rectifying Cl⁻ channels by protein kinase A corrected by insertion of CFTR. *Nature* 358, 581–584. doi: 10.1038/358581a0
- Farinha, C. M., and Amaral, M. D. (2005). Most F508del-CFTR is targeted to degradation at an early folding checkpoint and independently of calnexin. *Mol. Cell. Biol.* 25, 5242–5252. doi: 10.1128/MCB.25.12.5242-5252.2005
- Gregory, R. J., Rich, D. P., Cheng, S. H., Souza, D. W., Paul, S., Manavalan, P., et al. (1991). Maturation and function of cystic fibrosis transmembrane conductance regulator variants bearing mutations in putative nucleotide-binding domains 1 and 2. *Mol. Cell. Biol.* 11, 3886–3893. doi: 10.1128/MCB.11.8.3886
- Gunderson, K. L., and Kopito, R. R. (1995). Conformational states of CFTR associated with channel gating: the role ATP binding and hydrolysis. *Cell* 82, 231–239. doi: 10.1016/0092-8674(95)90310-0
- Hallows, K. R., Mccane, J. E., Kemp, B. E., Witters, L. A., and Foskett, J. K. (2003). Regulation of channel gating by AMP-activated protein kinase modulates cystic fibrosis transmembrane conductance regulator activity in lung submucosal cells. *J. Biol. Chem.* 278, 998–1004. doi: 10.1074/jbc.M210621200
- Hegedus, T., Aleksandrov, A., Mengos, A., Cui, L., Jensen, T. J., and Riordan, J. R. (2009). Role of individual R domain phosphorylation sites in CFTR regulation by protein kinase A. *Biochim. Biophys. Acta* 1788, 1341–1349. doi: 10.1016/j.bbmem.2009.03.015
- Higgins, C. F., and Linton, K. J. (2004). The ATP switch model for ABC transporters. *Nat. Struct. Mol. Biol.* 11, 918–926. doi: 10.1038/nsmb836
- Holleran, J. P., Zeng, J., Frizzell, R. A., and Watkins, S. C. (2013). Regulated recycling of mutant CFTR is partially restored by pharmacological treatment. *J. Cell Sci.* 126, 2692–2703. doi: 10.1242/jcs.120196
- Hudson, R. P., Chong, P. A., Protasevich, I., Vernon, R., Noy, E., Bihler, H., et al. (2012). Conformational changes relevant to channel activity and folding within the first nucleotide binding domain of the cystic fibrosis transmembrane conductance regulator. *J. Biol. Chem.* 287, 28480–28494. doi: 10.1074/jbc.M112.371138
- Hwang, T. C., Yeh, J. T., Zhang, J., Yu, Y. C., Yeh, H. I., and Destefano, S. (2018). Structural mechanisms of CFTR function and dysfunction. *J. Gen. Physiol.* 150, 539–570. doi: 10.1085/jgp.201711946
- Jih, K. Y., and Hwang, T. C. (2013). Vx-770 potentiates CFTR function by promoting decoupling between the gating cycle and ATP hydrolysis cycle. *Proc. Natl. Acad. Sci. U. S. A.* 110, 4404–4409. doi: 10.1073/pnas.1215982110
- Kanelis, V., Hudson, R. P., Thibodeau, P. H., Thomas, P. J., and Forman-Kay, J. D. (2010). NMR evidence for differential phosphorylation-dependent interactions in WT and DeltaF508 CFTR. *EMBO J.* 29, 263–277. doi: 10.1038/emboj.2009.329
- Kerem, B., Rommens, J. M., Buchanan, J. A., Markiewicz, D., Cox, T. K., Chakravarti, A., et al. (1989). Identification of the cystic fibrosis gene: genetic analysis. *Science* 245, 1073–1080. doi: 10.1126/science.2570460
- Klein, I., Sarkadi, B., and Varadi, A. (1999). An inventory of the human ABC proteins. *Biochim. Biophys. Acta* 1461, 237–262. doi: 10.1016/s0005-2736(99)00161-3
- Kongsuphol, P., Cassidy, D., Hieke, B., Treharne, K. J., Schreiber, R., Mehta, A., et al. (2009). Mechanistic insight into control of CFTR by AMPK. *J. Biol. Chem.* 284, 5645–5653. doi: 10.1074/jbc.M806780200
- Lewis, H. A., Buchanan, S. G., Burley, S. K., Connors, K., Dickey, M., Dorwart, M., et al. (2004). Structure of nucleotide-binding domain 1 of the cystic fibrosis transmembrane conductance regulator. *EMBO J.* 23, 282–293. doi: 10.1038/sj.emboj.7600040
- Li, C., and Naren, A. P. (2005). Macromolecular complexes of cystic fibrosis transmembrane conductance regulator and its interacting partners. *Pharmacol. Ther.* 108, 208–223. doi: 10.1016/j.pharmthera.2005.04.004
- Liang, X., Da Paula, A. C., Bozoky, Z., Zhang, H., Bertrand, C. A., Peters, K. W., et al. (2012). Phosphorylation-dependent 14-3-3 protein interactions regulate CFTR biogenesis. *Mol. Biol. Cell* 23, 996–1009. doi: 10.1091/mbc.E11-08-0662
- Liu, F., Zhang, Z., Csanady, L., Gadsby, D. C., and Chen, J. (2017). Molecular structure of the human CFTR ion channel. *Cell* 169, 85.e8–95.e8. doi: 10.1016/j.cell.2017.02.024
- Lopes-Pacheco, M. (2016). CFTR modulators: shedding light on precision medicine for cystic fibrosis. *Front. Pharmacol.* 7:275. doi: 10.3389/fphar.2016.00275
- Marasini, C., Galeno, L., and Moran, O. (2012). Thermodynamic study of the native and phosphorylated regulatory domain of the CFTR. *Biochem. Biophys. Res. Commun.* 423, 549–552. doi: 10.1016/j.bbrc.2012.05.165
- Marasini, C., Galeno, L., and Moran, O. (2013). A SAXS-based ensemble model of the native and phosphorylated regulatory domain of the CFTR. *Cell. Mol. Life Sci.* 70, 923–933. doi: 10.1007/s00018-012-1172-5
- Mihalyi, C., Iordanov, I., Torocsik, B., and Csanady, L. (2020). Simple binding of protein kinase A prior to phosphorylation allows CFTR anion channels to be opened by nucleotides. *Proc. Natl. Acad. Sci. U. S. A.* 117, 21740–21746. doi: 10.1073/pnas.2007910117
- Mihalyi, C., Torocsik, B., and Csanady, L. (2016). Obligate coupling of CFTR pore opening to tight nucleotide-binding domain dimerization. *elife* 5:e18164. doi: 10.7554/eLife.18164
- Moore, C. A., Milano, S. K., and Benovic, J. L. (2007). Regulation of receptor trafficking by GRKs and arrestins. *Annu. Rev. Physiol.* 69, 451–482. doi: 10.1146/annurev.physiol.69.022405.154712
- Neville, D. C., Rozanas, C. R., Price, E. M., Gruis, D. B., Verkman, A. S., and Townsend, R. R. (1997). Evidence for phosphorylation of serine 753 in CFTR using a novel metal-ion affinity resin and matrix-assisted laser desorption mass spectrometry. *Protein Sci.* 6, 2436–2445. doi: 10.1002/pro.5560061117
- Okiyoneda, T., Barriere, H., Bagdany, M., Rabeh, W. M., Du, K., Hohfeld, J., et al. (2010). Peripheral protein quality control removes unfolded CFTR from the plasma membrane. *Science* 329, 805–810. doi: 10.1126/science.1191542
- Pankow, S., Bamberger, C., and Yates, J. R. 3rd. (2019). A posttranslational modification code for CFTR maturation is altered in cystic fibrosis. *Sci. Signal.* 12:eaa97984. doi: 10.1126/scisignal.aan97984
- Pasyk, S., Li, C., Ramjeesingh, M., and Bear, C. E. (2009). Direct interaction of a small-molecule modulator with G551D-CFTR, a cystic fibrosis-causing mutation associated with severe disease. *Biochem. J.* 418, 185–190. doi: 10.1042/BJ20081424
- Pyle, L. C., Ehrhardt, A., Mitchell, L. H., Fan, L., Ren, A., Naren, A. P., et al. (2011). Regulatory domain phosphorylation to distinguish the mechanistic basis underlying acute CFTR modulators. *Am. J. Phys. Lung Cell. Mol. Phys.* 301, L587–L597. doi: 10.1152/ajplung.00465.2010
- Ratjen, F., Bell, S. C., Rowe, S. M., Goss, C. H., Quittner, A. L., and Bush, A. (2015). Cystic fibrosis. *Nat. Rev. Dis. Primers.* 1:15010. doi: 10.1038/nrdp.2015.10
- Rennolds, J., Tower, C., Musgrove, L., Fan, L., Maloney, K., Clancy, J. P., et al. (2008). Cystic fibrosis transmembrane conductance regulator trafficking is

- mediated by the COPI coat in epithelial cells. *J. Biol. Chem.* 283, 833–839. doi: 10.1074/jbc.M706504200
- Rich, D. P., Berger, H. A., Cheng, S. H., Travis, S. M., Saxena, M., Smith, A. E., et al. (1993). Regulation of the cystic fibrosis transmembrane conductance regulator Cl⁻ channel by negative charge in the R domain. *J. Biol. Chem.* 268, 20259–20267. doi: 10.1016/S0021-9258(20)80723-6
- Riordan, J. R. (2005). Assembly of functional CFTR chloride channels. *Annu. Rev. Physiol.* 67, 701–718. doi: 10.1146/annurev.physiol.67.032003.154107
- Riordan, J. R. (2008). CFTR function and prospects for therapy. *Annu. Rev. Biochem.* 77, 701–726. doi: 10.1146/annurev.biochem.75.103004.142532
- Riordan, J. R., Rommens, J. M., Kerem, B., Alon, N., Rozmahel, R., Grzelczak, Z., et al. (1989). Identification of the cystic fibrosis gene: cloning and characterization of complementary DNA. *Science* 245, 1066–1073. doi: 10.1126/science.2475911
- Rommens, J. M., Iannuzzi, M. C., Kerem, B., Drumm, M. L., Melmer, G., Dean, M., et al. (1989). Identification of the cystic fibrosis gene: chromosome walking and jumping. *Science* 245, 1059–1065. doi: 10.1126/science.2772657
- Sammelson, R. E., Ma, T., Galletta, L. J., Verkman, A. S., and Kurth, M. J. (2003). 3-(2-Benzoyloxyphenyl) isoxazoles and isoxazolines: synthesis and evaluation as CFTR activators. *Bioorg. Med. Chem. Lett.* 13, 2509–2512. doi: 10.1016/S0960-894X(03)00482-7
- Schnur, A., Premchandrar, A., Bagdany, M., and Lukacs, G. L. (2019). Phosphorylation-dependent modulation of CFTR macromolecular signalling complex activity by cigarette smoke condensate in airway epithelia. *Sci. Rep.* 9:12706. doi: 10.1038/s41598-019-48971-y
- Seavilleklein, G., Amer, N., Evagelidis, A., Chappe, F., Irvine, T., Hanrahan, J. W., et al. (2008). PKC phosphorylation modulates PKA-dependent binding of the R domain to other domains of CFTR. *Am. J. Phys. Cell Phys.* 295, C1366–C1375. doi: 10.1152/ajpcell.00034.2008
- Seibert, F. S., Chang, X. B., Aleksandrov, A. A., Clarke, D. M., Hanrahan, J. W., and Riordan, J. R. (1999). Influence of phosphorylation by protein kinase A on CFTR at the cell surface and endoplasmic reticulum. *Biochim. Biophys. Acta* 1461, 275–283. doi: 10.1016/S0005-2736(99)00163-7
- Serohijos, A. W., Hegedus, T., Aleksandrov, A. A., He, L., Cui, L., Dokholyan, N. V., et al. (2008). Phenylalanine-508 mediates a cytoplasmic-membrane domain contact in the CFTR 3D structure crucial to assembly and channel function. *Proc. Natl. Acad. Sci. U. S. A.* 105, 3256–3261. doi: 10.1073/pnas.0800254105
- Sorum, B., Czege, D., and Csanady, L. (2015). Timing of CFTR pore opening and structure of its transition state. *Cell* 163, 724–733. doi: 10.1016/j.cell.2015.09.052
- Townsend, R. R., Lipniunas, P. H., Tulk, B. M., and Verkman, A. S. (1996). Identification of protein kinase A phosphorylation sites on NBD1 and R domains of CFTR using electrospray mass spectrometry with selective phosphate ion monitoring. *Protein Sci.* 5, 1865–1873. doi: 10.1002/pro.5560050912
- Uliyaykina, I., Botelho, H. M., Da Paula, A. C., Afonso, S., Lobo, M. J., Felicio, V., et al. (2020). Full rescue of F508del-CFTR processing and function by CFTR modulators can be achieved by removal of two regulatory regions. *Int. J. Mol. Sci.* 21:4524. doi: 10.3390/ijms21124524
- Vais, H., Zhang, R., and Reenstra, W. W. (2004). Dibasic phosphorylation sites in the R domain of CFTR have stimulatory and inhibitory effects on channel activation. *Am. J. Phys. Cell Phys.* 287, C737–C745. doi: 10.1152/ajpcell.00504.2003
- Van Goor, F., Hadida, S., Grootenhuys, P. D., Burton, B., Stack, J. H., Straley, K. S., et al. (2011). Correction of the F508del-CFTR protein processing defect in vitro by the investigational drug VX-809. *Proc. Natl. Acad. Sci. U. S. A.* 108, 18843–18848. doi: 10.1073/pnas.1105787108
- Van Goor, F., Straley, K. S., Cao, D., Gonzalez, J., Hadida, S., Hazlewood, A., et al. (2006). Rescue of DeltaF508-CFTR trafficking and gating in human cystic fibrosis airway primary cultures by small molecules. *Am. J. Phys. Lung Cell. Mol. Phys.* 290, L1117–L1130. doi: 10.1152/ajplung.00169.2005
- Veit, G., Avramescu, R. G., Chiang, A. N., Houck, S. A., Cai, Z., Peters, K. W., et al. (2016). From CFTR biology toward combinatorial pharmacotherapy: expanded classification of cystic fibrosis mutations. *Mol. Biol. Cell* 27, 424–433. doi: 10.1091/mbc.E14-04-0935
- Vergani, P., Basso, C., Mense, M., Nairn, A. C., and Gadsby, D. C. (2005a). Control of the CFTR channel's gates. *Biochem. Soc. Trans.* 33, 1003–1007. doi: 10.1042/BST20051003
- Vergani, P., Lockless, S. W., Nairn, A. C., and Gadsby, D. C. (2005b). CFTR channel opening by ATP-driven tight dimerization of its nucleotide-binding domains. *Nature* 433, 876–880. doi: 10.1038/nature03313
- Vergani, P., Nairn, A. C., and Gadsby, D. C. (2003). On the mechanism of MgATP-dependent gating of CFTR Cl⁻ channels. *J. Gen. Physiol.* 121, 17–36. doi: 10.1085/jgp.20028673
- Wang, W., Fu, L., Liu, Z., Wen, H., Rab, A., Hong, J. S., et al. (2020). G551D mutation impairs PKA-dependent activation of CFTR channel that can be restored by novel GOF mutations. *Am. J. Phys. Lung Cell. Mol. Phys.* 319, L770–L785. doi: 10.1152/ajplung.00262.2019
- Wang, F., Zeltwanger, S., Hu, S., and Hwang, T. C. (2000). Deletion of phenylalanine 508 causes attenuated phosphorylation-dependent activation of CFTR chloride channels. *J. Physiol.* 524, 637–648. doi: 10.1111/j.1469-7793.2000.00637.x
- Wilkinson, D. J., Strong, T. V., Mansoura, M. K., Wood, D. L., Smith, S. S., Collins, F. S., et al. (1997). CFTR activation: additive effects of stimulatory and inhibitory phosphorylation sites in the R domain. *Am. J. Phys.* 273, L127–L133. doi: 10.1152/ajplung.1997.273.1.L127
- Winter, M. C., and Welsh, M. J. (1997). Stimulation of CFTR activity by its phosphorylated R domain. *Nature* 389, 294–296. doi: 10.1038/38514
- Xie, J., Adams, L. M., Zhao, J., Gerken, T. A., Davis, P. B., and Ma, J. (2002). A short segment of the R domain of cystic fibrosis transmembrane conductance regulator contains channel stimulatory and inhibitory activities that are separable by sequence modification. *J. Biol. Chem.* 277, 23019–23027. doi: 10.1074/jbc.M201661200
- Zhang, Z., and Chen, J. (2016). Atomic structure of the cystic fibrosis transmembrane conductance regulator. *Cell* 167, 1586–1597. doi: 10.1016/j.cell.2016.11.014
- Zhang, Z., Liu, F., and Chen, J. (2017). Conformational changes of CFTR upon phosphorylation and ATP binding. *Cell* 170, 483–491. doi: 10.1016/j.cell.2017.06.041
- Zhang, Z., Liu, F., and Chen, J. (2018). Molecular structure of the ATP-bound, phosphorylated human CFTR. *Proc. Natl. Acad. Sci. U. S. A.* 115, 12757–12762. doi: 10.1073/pnas.1815287115
- Zolin, A., Orenti, A., Naehrich, L., Jung, A., and Van Rens, J. (2020). European Cystic Fibrosis Society Patient Registry Annual Data Report 2018.

Conflict of Interest: AG and EH are founders and board members of Kither Biotech, a company focused on the development of PI3K inhibitors for airway diseases not in conflict with statements in this article. The other co-authors declare no conflict of interest.

Copyright © 2021 Della Sala, Prono, Hirsch and Ghigo. This is an open-access article distributed under the terms of the Creative Commons Attribution License (CC BY). The use, distribution or reproduction in other forums is permitted, provided the original author(s) and the copyright owner(s) are credited and that the original publication in this journal is cited, in accordance with accepted academic practice. No use, distribution or reproduction is permitted which does not comply with these terms.

Roles of phosphatidyl inositol 3 kinase gamma (PI3K γ) in respiratory diseases

Valentina Sala^{1,*}, Angela Della Sala¹, Alessandra Ghigo^{1,2,#} and Emilio Hirsch^{1,2,#,*}

¹ Department of Molecular Biotechnology and Health Sciences, University of Torino, Via Nizza 52, 10126, Torino, Italy.

² Kither Biotech S.r.l. Via Nizza 52, 10126, Torino, Italy.

Equal contribution to senior authorship

* Corresponding Authors:

Emilio Hirsch, via Nizza 52, 10126 Torino, Italy, Tel. +390116706225, Fax: +390116706432; E-mail: emilio.hirsch@unito.it

Valentina Sala, via Nizza 52, 10126 Torino, Italy, Tel. +390116706335, Fax: +390116706432; E-mail: valentina.sala@unito.it

ABSTRACT Phosphatidyl inositol 3 kinase gamma (PI3K γ) is expressed in all the cell types that are involved in airway inflammation and disease, including not only leukocytes, but also structural cells, where it is expressed at very low levels under physiological conditions, while is significantly upregulated after stress. In the airways, PI3K γ behaves as a trigger or a controller, depending on the pathological context. In this review, the contribution of PI3K γ in a plethora of respiratory diseases, spanning from acute lung injury, pulmonary fibrosis, asthma, cystic fibrosis and response to both bacterial and viral pathogens, will be commented.

Received originally: 05.11.2020

in revised form: 15.02.2021,

Accepted 23.02.2021,

Published 08.03.2021.

Keywords: PI3K signaling, chronic respiratory disease, restrictive airway disease, obstructive airway disease, inflammation.

Abbreviations:

AHR – airway hyperresponsiveness; **ASM** – airway smooth muscle; **cAMP** – cyclic adenosine monophosphate; **CF** – cystic fibrosis; **CFTR** – CF transmembrane conductance regulator; **GPCR** – G-protein coupled receptor; **COPD** – chronic obstructive pulmonary disease; **IAV** – influenza A; **IFN** – interferon; **IL** – interleukin; **IPF** – idiopathic pulmonary fibrosis; **KD** – knockdown; **KO** – knockout; **LPS** – lipopolysaccharide; **MIF** – migration inhibitory factor; **NK** – natural killer; **PI3K** – phosphatidyl inositol 3 kinase; **PLY** – pneumolysin; **SNP** – single-nucleotide polymorphisms; **TLR** – Toll-like receptor; **VILI** – ventilation-induced lung injury.

INTRODUCTION

Phosphatidyl inositol 3 kinases (PI3Ks) are a family of lipid kinases that play key roles in a plethora of processes, including cell growth, proliferation and differentiation, tissue morphogenesis, metabolism, and immune function. The PI3K family is divided into three classes with distinct functions, among which the best characterized is class I, which phosphorylates phosphatidylinositol 4,5 bisphosphate in the third position to generate the second messenger phosphatidylinositide 3,4,5 trisphosphate. Class I PI3K subfamily is further divided into two classes: class IA, which is composed of α , β and δ isoforms, and class IB, whose only member is PI3K γ [1]. Class I PI3K isoforms display different expression patterns: while PI3K α and PI3K β are ubiquitously expressed, PI3K δ and PI3K γ have a more restricted expression pattern. Accordingly, deficiency in PI3K α or PI3K β

is embryonic lethal in murine models, whereas PI3K γ or PI3K δ knockout (KO) mice are viable and fertile [2].

In particular, PI3K γ is expressed, at very low levels under physiological conditions, in cell types including cardiomyocytes [3-9], vascular smooth muscle cells [10], and the microglia [11], where it is significantly upregulated after stress.

On the contrary, PI3K γ is constitutively enriched in leukocytes (neutrophils, eosinophils, macrophages, T cells and mast cells) [12]. Consistently, PI3K γ KO mice exposed to natural pathogens/microbiota display altered immune traits that closely mirror the human Inactivated PI3K γ Syndrome (IPGS) [13]. Intriguingly, clinical signs related to loss of PI3K γ include autoimmune cytopenia and infections, as well as pathological infiltration of T cells in barrier organs, including the lungs, that are hyper-responsive to microbial products [13].

Of utmost relevance for respiratory homeostasis and disease, PI3K γ is also expressed in all the other cell types that are involved in airway disease, like endothelial cells [14], fibroblasts [15], and epithelial cells [16, 17].

Besides such diverse expression patterns, class I PI3Ks own non-redundant roles in the response to a variety of stimuli. Class IA PI3Ks, exception done for PI3K β that can be also activated by G-protein Coupled Receptors (GPCRs) [18], are recruited to receptor tyrosine kinases through the SH2 domains of p85-like regulatory subunits. Class IB PI3K γ is composed of the p110 γ catalytic subunit, and of the p101 and p84/p87 subunits. These two adapter companions have important non-redundant roles in coupling PI3K γ to upstream Ras/GPCRs signaling pathways [19]. While p84 is a component of a constitutively-expressed PI3K complex, p101 is part of an inducible PI3K complex [20]. Moreover, the p110 γ /p84 heterodimer is less sensitive to the activation promoted by G $\beta\gamma$ subunits and depends on Ras partnership, while activation of the p110 γ /p101 variant by G $\beta\gamma$ subunits is more favorable and Ras-independent [21]. Importantly, p110 γ acts as an A-kinase anchoring protein (AKAP), being engaged in a functional and physical interaction with PKA that does not involve its kinase activity [7, 8]. Thus, PI3K γ is not only a kinase but also a scaffold protein for PKA in a complex containing type 3 and 4 phosphodiesterases (PDEs). This complex acts in a negative feedback loop, suppressing cyclic adenosine monophosphate (cAMP) levels in the vicinity of the β 2-adrenergic

receptor, through PKA-mediated activation of PDEs [7, 8].

Therefore, acting at the crossroads of multiple pathways [1, 22], PI3K γ is a hub of intracellular signaling. As an example, PI3K γ is activated downstream of GPCRs by both metabolic signals acting on β -adrenergic receptors, and immune signals like chemokines and complement fragments. Moreover, PI3K γ can be activated by pathogen- and damage-associated molecular patterns downstream of Toll-like receptors (TLRs) in myeloid cells [23-25] and cardiomyocytes [5], functioning as a master regulator at the interface between metabolic and immune homeostasis. The relevance of the PI3K γ hub as a regulator and amplifier for diverse and converging signaling pathways is evident in mast cells, where the Fc ϵ RI receptor mediates PI3K γ activation. Yet, the Fc ϵ RI receptor has no direct link to GPCRs, but degranulation relies on PI3K γ [26]. Intriguingly, the combinatorial regulation of PI3K γ heterodimer variants can lead to a remarkable level of signaling specificity, which depends on both the tissue and the physio-pathological context [27].

Moreover, studies demonstrating the effects of knocking out PI3K γ in murine disease models (**Table 1**) led to great interest in the immunological functions and in the potential of PI3K γ as a therapeutic target in inflammatory-driven diseases [15], including those affecting the airways. Within this review, we intend to highlight the relevance of PI3K γ as a trigger or target in a plethora of respiratory diseases, spanning from acute lung injury, pulmonary fibrosis,

TABLE 1. Differential responses of PI3K γ KO mouse models of respiratory diseases.

Pathology	PI3K γ KO phenotype	References
Airway inflammation	Within all studies, PI3K γ -deficient mice are healthy and viable with reduced allergic AHR, inflammation, and remodelling. In the absence of PI3K γ , the chemokine-induced model of airway inflammation displays impaired neutrophils, eosinophils and macrophages chemotaxis, reduced peribronchial fibrosis and TGF- β 1+ cells and lower Smad 2/3 signaling.	[57, 91, 116]
Lung injury, Fibrosis	PI3K γ deficiency confers protection against bleomycin-induced pulmonary injury. PI3K γ KO mice display reduced weight loss, decreased lethality, reduced deposition of lung collagen and lower expression of profibrogenic and proangiogenic genes.	[51]
Lung injury, Inflammation	PI3K γ KO mice display reduced accumulation of neutrophils in an LPS-induced acute lung injury model, and perturbation in E-selectin-mediated adhesion, in response to TNF- α .	[117]
Lung injury, Endotoxemia	Endotoxemia-induced lung edema, neutrophil accumulation, nuclear translocation of NF- κ B and production of proinflammatory cytokines (IL-1 β and TNF- α) in lung neutrophils are reduced in transgenic mice lacking the catalytic subunit of PI3K γ .	[118]
Lung injury, ARDS	In acute lung injury and adult respiratory distress syndrome (ARDS) models, PI3K γ KO mice display reduced histological evidence of lung injury after high volume ventilation and reduced PKB phosphorylation compared to wild-type, independently from inhibitory effects on cytokine release.	[16, 119]
Lung vascular injury, Inflammation	In a model where lung vascular injury was induced by bacteraemia (i.e. by intraperitoneal <i>Escherichia coli</i> injection), PI3K γ KO mice present higher levels of leucocyte accumulation in the lung, and greater microvascular permeability, resulting in lung edema. These results point to PI3K γ as a negative regulator of lung vascular injury in gram-negative sepsis.	[120]

asthma, cystic fibrosis and response to both bacterial and viral pathogens (Figure 1).

PI3K γ ROLE IN RESPIRATORY DISEASES

Ventilator-induced damage

Mechanical ventilation is a life-saving therapy but can contribute to the progression or even initiate lung injury *per se*. Ventilation-induced lung injury (VILI) clinically displays signs of alveolar edema, including increased vascular permeability and accumulation of fluids in the alveoli [28].

In VILI, the mechanical stress induced by ventilation activates the inflammasome in macrophages and endothelial cells, leading to enhanced nitric oxide (NO), oxygen radicals, and peroxynitrite production, which contributes to the

increase of alveolar and vascular permeability [28] and impairs alveolar fluid clearance [29]. In line with these findings, the inhibition of PI3K γ kinase activity specifically in resident lung cells attenuates VILI through the reduction of NO release [30].

Besides NO, the intracellular level of cAMP is critical for the modulation of endothelial permeability [31]. Since PI3K γ can act as a scaffold, independently of its kinase activity, to modulate cAMP levels [7, 8], its role in the formation of edema during VILI has been investigated. Accordingly, PI3K γ knockout lungs are protected from VILI [16]. Moreover, pharmacological combined regimens aimed at blocking PI3K γ kinase activity while increasing cAMP levels attenuate VILI in PI3K γ wild-type lungs de-

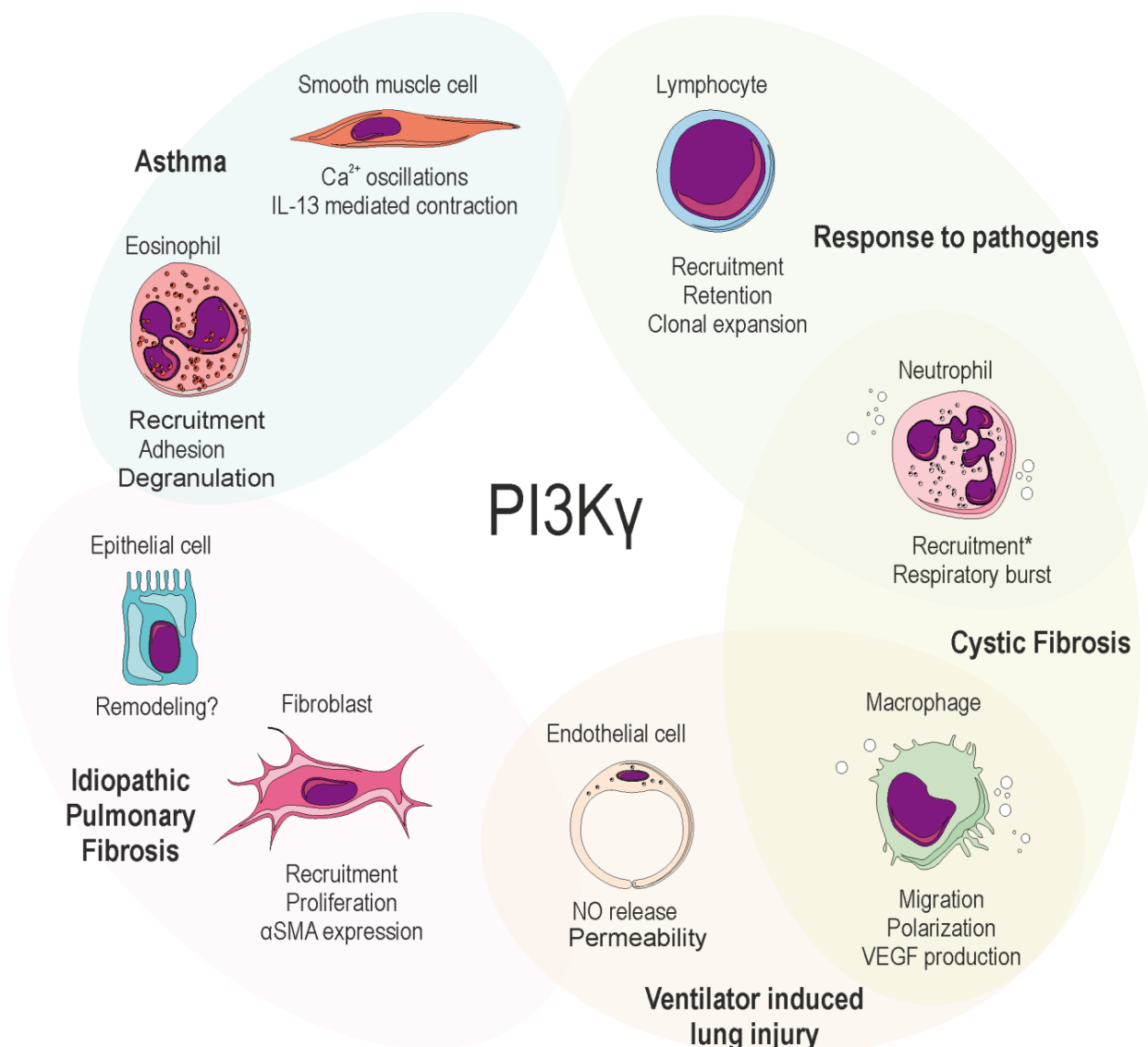


FIGURE 1: Schematic representation of the biological processes induced or mediated by PI3K γ in the cell types that are relevant for respiratory disease. PI3K γ has been involved in almost all target cells shown in the figure using either isoform-selective PI3K inhibitors or genetic engineering. *Neutrophilic recruitment may be enhanced by either activation or inhibition of PI3K γ , depending on the context. NO: Nitric Oxide; α SMA: α -smooth muscle actin; VEGF: Vascular endothelial growth factor; IL-13: Interleukin-13.

prived of circulating leukocytes [30], pointing to the central role of PI3K γ in lung cell types other than the immune cells.

Nevertheless, PI3K γ is largely expressed in leukocytes, whose contribution to Vascular endothelial growth factor (VEGF) production, inflammation and injury in VILI is recognized [32]. A major player in the control of local and systemic immune response is TLR4 [33, 34]. Notably, it has been shown that TLR4 is overexpressed [35], and has a key role in experimental models of VILI [36-39]. In macrophages, upon TLR4 receptor activation, PI3K γ is recruited by Rab8, and is required to activate the Akt/mTOR pathway to bias the cytokine response towards an anti-inflammatory scenario [24]. Therefore, these findings suggest that the contribution of the TLR4/PI3K γ axis to VILI pathogenesis deserves further investigation.

PI3K γ emerged therefore as a possible therapeutic target in the treatment and/or prevention of VILI and edema. However, strategies aimed at blocking PI3K γ kinase dependent and independent activities only in resident inflammatory and parenchymal lung cells, such as airway epithelial cells, should be addressed. This could enable to mitigate potential systemic side effects on the innate immune system on one side, and on different cAMP-responsive cells, like cardiomyocytes, on the other.

Idiopathic pulmonary fibrosis (IPF)

Idiopathic pulmonary fibrosis (IPF) is a chronic, progressive, fibrotic interstitial lung disease of unknown etiology, which occurs primarily in older adults (median age at diagnosis is about 65 years) [40]. Although it is classified as a rare disease (occurring in less than 5/10,000 persons per year), IPF is the most common type of idiopathic interstitial pneumonia, occurring with a frequency comparable to that of stomach, brain and testis cancers [41]. Moreover, the global burden of IPF is extremely high, due to the poor prognosis, with a median survival time of two to four years from diagnosis [42].

Historically, IPF was considered a chronic and progressive inflammatory disorder, which gradually leads to established fibrosis. However, the failure of anti-inflammatory therapies [43] caused a profound revision of this concept [44]. IPF is now thought to result from the concomitance of repetitive local micro-injuries to the ageing alveolar epithelium, genetic factors [45], and environmental risk factors (such as cigarette smoke, drugs, lung microbiome, infections or environmental pollutants) [42, 46]. In turn, intracellular signaling initiated by micro-injuries gives rise to an aberrant communication between epithelial cells and fibroblasts, leading to increased extracellular matrix accumulation, and, ultimately, to lung interstitial remodeling and loss of function.

Within this context, PI3K signaling emerged as a crucial pathway in models of pulmonary fibrosis [47, 48]. In particular, class I PI3Ks play key roles in the homeostasis of all the cell types that are involved in the pathogenesis of IPF. Consistently, an inhaled pan-Class I PI3K inhibitor has been demonstrated to have a protective effect against the rapid, progressive pulmonary fibrosis induced by instillation of bleomycin *in vivo* [48], by reducing the expression of pro-

fibrotic genes, including transforming growth factor- β (TGF- β) and connective tissue growth factor (CTGF) [49]. Among class I isoforms, PI3K γ is overexpressed in myofibroblasts and bronchiolar basal cells in the lungs of IPF patients, and, *ex vivo*, in human IPF primary fibroblasts [50]. Both genetic and pharmacological inhibition of PI3K γ are able to inhibit proliferation as well as α -smooth muscle actin (α SMA) expression in IPF fibroblasts *in vitro* [50]. Accordingly, mice lacking PI3K γ are protected from the accumulation of matrix and leukocytes in the lungs after bleomycin injury [51], pointing to PI3K γ as a promising therapeutic target for IPF.

Recently, the need of pathway-specific biomarkers and genetic phenotyping has emerged in order to identify patient subtypes for new combinatorial trials [52]. In fact, due to its intrinsic complexity, the natural history of IPF is highly variable and the course of the disease in an individual patient is somewhat unpredictable, as some patients experience a rapid lung decline, while others progress much more slowly. Of note, a rapidly progressive disease has been associated with the upregulation of several genes, including TLR9 [53], downstream of which PI3K γ is activated, at least in cardiomyocytes [5]. Moreover, in the past two decades, metabolic dysregulation, impaired mitochondrial autophagy, and mitochondrial dysfunction have been observed in cells of IPF lungs [54].

Overall, these results suggest the intriguing hypothesis that the activation level of PI3K γ might act as a master controller in the different processes that converge on IPF pathogenesis and influence the fate of the lung environment. Whether PI3K γ will be a suitable biomarker or therapeutic target in IPF patients, however, still has to be investigated.

Asthma

The role of PI3K family members in asthma is well documented and pan-class I PI3K topical inhibition is effective against acute and, more importantly, glucocorticoid resistant asthma [49]. Focusing on the specific contribution of PI3K γ to asthma pathogenesis, KO of PI3K γ or treatment with an aerosolized dual inhibitor of PI3K γ and δ (TG100-115), is able to reduce eosinophilic airway hyperresponsiveness (AHR) and inflammation in experimental models [54-57].

Moreover, the PI3K γ -specific inhibitor AS605240 dampens eosinophilic inflammation induced by the CC chemokine eotaxin (CCL11), by suppressing signaling pathways downstream of CC chemokine receptor 3 (CCR3) [58]. In detail, AS605240 inhibits eotaxin-induced chemotaxis, adhesion to Intercellular Adhesion Molecule 1 (ICAM-1), and degranulation of human peripheral blood eosinophils by inhibiting ERK1/2 phosphorylation, without downregulation of surface CCR3 expression [58].

Mechanistically, the pathological role of PI3K γ in asthma implicates the release of inflammatory cell mediators, including macrophage migration inhibitory factor (MIF) and the T-helper type II cytokine Interleukin-13 (IL-13).

MIF participates as a proinflammatory cytokine in both innate and adaptive immune responses, contributing to the

pathogenesis of inflammatory, metabolic, autoimmune, and allergic diseases. Of note, MIF plays a pivotal role in activating the expression of PI3K γ regulatory (p101) and catalytic subunits (p110) [59]. In turn, increased PI3K γ activity is responsible for IL-13-mediated contraction of airway smooth muscle (ASM) cells, the underlying mechanism of AHR induced by allergen sensitization or cytokines in asthma [59–63]. IL-13 receptor and PI3K γ are both expressed in ASM cells, in which they control contractility by regulating Ca²⁺ oscillations [64]. Notably, IL-13, which is increased in the airways of asthmatic patients and correlates with AHR [65], is sufficient [66] and required [67] for the development of allergen-induced AHR. In a translational perspective, targeting PI3K γ , either pharmacologically or by RNA interference, suppresses IL-13-dependent contractility of ASM cells, and, more importantly, intranasal administration of a PI3K γ inhibitor attenuates IL-13-induced AHR in mice [64]. Therefore, dampening IL-13 levels by targeting the upstream PI3K γ signaling might be a feasible and efficient strategy to reduce Ca²⁺ oscillations and contraction in ASMs.

Overall, these data underline the promising therapeutic potential of PI3K γ inhibition in asthma [68].

Cystic Fibrosis

Cystic fibrosis (CF) is the most common genetic disease in the Caucasian population, affecting ~1 in 3,500 persons. The basic defect of CF results from mutations in a single gene encoding for the CF transmembrane conductance regulator (*CFTR*), a 1,480 residues transmembrane glycoprotein that regulates cAMP-mediated chloride (Cl⁻) conductance at the apical surface of secretory epithelia. Impaired secretion of Cl⁻ and bicarbonate triggers dehydration of the airway surface liquid, resulting in increased mucus viscosity and impaired mucociliary clearance. The accumulated mucus ultimately favors colonization by pathogens and resistance to treatments [69]. In turn, airway mucus obstruction and recurrent/persistent bacterial infections trigger a chronic neutrophilic inflammation, which are responsible for the release of neutrophilic elastases and for the ensuing, progressive lung damage and decline of function in CF patients [70].

In this context, the inflammatory response in CF lungs is non-resolving and self-perpetuating. In fact, the vicious cycle of neutrophilic burden and release of noxious mediators, further fuels inflammation and infection, and further contributes to disease progression towards irreversible lung damage. Notably, albeit chronic bacterial infections play a prominent role in the progression of CF lung disease, inflammation was observed in the lungs of asymptomatic CF infants without any apparent established bacterial infection [71], suggesting that sterile inflammation can precede, and possibly promote, infection in early-stage CF lung disease, by favoring the expansion of more pathogenic strains among the lung microbiota. Consistently, recent studies suggest that, upon migration to CF airways, neutrophils undergo a phenotypic reprogramming, leading to dysregulated lifespan, metabolism and effector function, ultimately contributing, together with the epithelium and

resident microbiota, to the evolution of a pathological microenvironment [72].

Therefore, anti-inflammatory therapy, eventually combined with antibiotics, is crucial to prevent lung damage. However, currently used therapeutic strategies show limited clinical benefit. With the aim of filling this gap, the possibility to interfere with leukocyte trafficking into CF airways has been explored. PI3K γ has a key role in this process, triggering signaling pathways evoked by binding of chemotactic factors to GPCRs. Among these, IL-8 represents the principal neutrophil chemoattractant and its elevated concentration characterizes CF lung inflammation. In the CF context, the biological efficacy of both genetic deletion and pharmacological inhibition of PI3K γ in reducing chronic neutrophilic inflammation in the lungs has been demonstrated in β -ENaC overexpressing CF-like mice [73].

While most research on CF inflammation has focused on epithelial cells and neutrophils, macrophages play an important role in the initiation and resolution of pulmonary inflammation. Functional abnormalities have been observed in CF macrophages from experimental models, including newborn CF pigs, and from CF patients, and found to display a constitutive proinflammatory status and hyper-responsiveness to microbial stimuli, supporting the presence of a primary defect in CF macrophages, which seems to be correlated to CFTR channel function [74, 75].

Of note, mucus stasis *per se* might be responsible for the pro-inflammatory polarization of airway macrophages [76], albeit data from CF patients point to a CFTR-dependent defect in the resolution phase of inflammation, due to the inability of CF macrophages to re-polarize to the M2 immunosuppressive phenotype [77]. Notably, blockade of PI3K γ activity promotes M1 macrophage polarization in implanted tumors, and inflammation, albeit M2 polarization has been observed in obese mice lacking PI3K γ [78], suggesting that the cellular context and activation level of PI3K γ might be crucial to determine the fate of macrophages.

Overall, these data would support the relevance of the immune response in CF disease, but whether abnormalities in immune cells, including changes to macrophage polarization, could be corrected using CFTR-directed therapies remains an open question. Whereas blockade of PI3K γ activity by small-molecule inhibitors may represent a valid approach to down-modulate neutrophil recruitment and burst in inflamed tissues, the resulting increased susceptibility to infection might be a potential side effect. Therefore, focused therapeutic windows should be defined for the use of these molecules in CF patients.

PI3K γ IN INFECTIVE DISEASES

Bacterial infections

Streptococcus pneumoniae is the most prevalent gram-positive bacterium causing community-acquired pneumonia, septic meningitis, and otitis media. The pathogenicity of *S. pneumoniae* is largely linked to its ability to produce a variety of virulence factors, among which the most relevant is pneumococcal virulence factor pneumolysin (PLY).

In addition to its ability to form pores in cell membranes, PLY acts as a pathogen-associated molecular pattern by signaling via TLR4 to induce TLR4-dependent cytotoxicity in lung resident macrophages, thus further promoting the bacterial colonization of the lower respiratory tract [35, 79]. Of note, TLR4 activation acts through PI3K γ to shift macrophages towards an anti-inflammatory scenario [24]. Mechanistically, PI3K γ and Rab8a control cytokine production by signaling through mTOR [24], which acts as a hub downstream of TLR4 to bias cytokine responses, inhibiting NF κ B-dependent transcription of pro-inflammatory cytokines, like IL-6 and IL-12, while enhancing STAT3-mediated transcription of the anti-inflammatory cytokine IL-10 [80]. Consistently, either genetic deletion or pharmacologic inhibition of PI3K γ in mice infected with *S. pneumoniae* causes an impaired recruitment of macrophages, associated with a reduced bacterial clearance from the lungs [81]. This, in turn, results in an impaired resolution/repair process and in progressive pneumococcal pneumonia [81]. Similar results have been observed after infection by *Staphylococcus aureus*, as a higher bacterial burden is present in PI3K γ KO mice, due to the reduced recruitment of leukocytes.

On the contrary, PI3K γ deficiency improves the resistance against *Mycobacterium tuberculosis* in the early phase of infection, by increasing T helper IL-17+ (Th17) cells number, production of IL-17, and expression of molecules associated with Th17- cells differentiation and neutrophil recruitment [82]. These findings are in accord with previous data showing increased concentrations of IL-17 in the bronchoalveolar lavage fluid of PI3K γ KO mice challenged with intranasal instillation of lipopolysaccharide (LPS) [4].

Moreover, a deficiency in expression of PI3K γ , along with PI3K δ , enhances the IL-17/G-CSF axis and induces neutrophilia [83].

Of note, the crosstalk between the IL-17 signaling pathway and neutrophils recruitment seems to be time-dependent [84]: while higher neutrophil counts are protective against early tuberculosis infection [85], a pathogenic role of neutrophils during the late stages of tuberculosis has been proposed [86]. Thus, whereas pharmacological inhibition of PI3K γ may be a suitable strategy to inhibit inflammation and limit lung damage in chronic and early-stage lung diseases, it might raise concerns in acute and late-stage infections, where it could result in an impaired host defense against high bacterial burden.

Influenza

The role of PI3K γ in the context of viral infections has been studied in Kaposi's sarcoma-associated herpes virus-induced tumors, where PI3K γ is required for the viral oncogenic signaling [87]. On the other hand, PI3K γ is also important in the regulation of innate immune responses, as well as establishment and resolution of inflammation upon influenza infection. Influenza A (IAV) and B viruses are among the most common causes of acute respiratory diseases of viral origin, accounting for three to five million cases of severe infection and up to 650,000 deaths/year worldwide [88]. In particular, the clinical manifestation of

IAV infection, a highly pathogenic strain, is characterized by an excessive inflammatory response leading to lung damage [89].

Response to IAV infection can be conceptually divided in three stages, which however occur simultaneously through the course of the injury [90]. First, the immune response against the influenza virus is initiated by release of type-I and type-III interferons (IFNs), mainly produced by epithelial cells, which are primarily targeted by IAV, and by dendritic cells. Second, the innate immune system (natural killer (NK) cells, macrophages, and neutrophils), is rapidly recruited to the airways by cytokines and chemokines. Finally, specificity and memory are provided by T cells. PI3K γ plays a crucial role in all these responses, driving production of type-I and type-III IFNs, as well as recruitment of NK and CD8+ T cells, and ultimately controlling viral titers in the infected lungs.

PI3K γ has a pivotal role in the recruitment and survival of macrophages and neutrophils [91, 92], which, however, when excessively activated, might be harmful to the host by leading to lung damage [93, 94]. Recently, PI3K γ has been shown to be essential after IAV infection for the control of recruitment and survival of innate immune cells and for resolution of inflammation [95]. In fact, in PI3K γ KO mice infected by IAV, the increased production of pro-inflammatory cytokines and the accumulation of activated neutrophils in the lungs contribute to lung damage and enhanced lethality. Moreover, PI3K γ controls leukocyte survival and resolution of inflammation, as shown by the reduced number of resolving macrophages and lower IL-10 levels in PI3K γ KO mice infected with IAV. Keeping with that, during IAV infection, this unbalance towards pro-inflammatory signals, to the detriment of pro-resolving signals, finally results in increased lung injury in PI3K γ KO mice.

Recently, the contribution of PI3K γ in regulating priming of CD8+ T cells by resident dendritic cells and NK/lymphocyte migration toward chemokine stimuli in PI3K γ KD/KD (knockdown) [96] and PI3K γ KO mice [45], respectively, has been shown to contribute to the enhanced susceptibility to IAV infection.

Consistent with these findings, PI3K γ orchestrates the antiviral immunity and inflammatory magnitude in response to IAV by distinct mechanisms. Therefore, targeting PI3K γ may not be useful to treat IAV infection, possibly leading to decreased control of the infection, but might be an important diagnostic marker of disease severity. Nevertheless, the contribution of the scaffold and kinase activity of PI3K γ have not been dissected in this context, and attention should be paid to the fact that PI3K γ KO and KD/KD mice do not necessarily have overlapping phenotypes, as previously suggested in the heart [8, 97].

Moreover, the analysis of single-nucleotide polymorphisms (SNPs) on *PIK3CG* gene might be exploited for prognosis. Different genetic polymorphisms on genes encoding for host factors have been investigated to explain the heterogeneity of immune responses to influenza infection and disease outcomes [98]. SNPs on *PIK3CG*, or close to the gene, have been studied in genetic association stud-

ies in a number of diseases, like cardiovascular disease [99], epinephrine-induced aggregation [100] and HDL-cholesterol plasma levels [101]. Importantly, SNPs located in *PIK3CG* gene (rs17847825 and rs2230460) have been associated with disease protection in influenza A(H1N1)pdm09-infected patients [95], thus suggesting the possible use of PI3K γ as a clinical prognostic factor.

CONCLUSIONS

Following the initial characterization of PI3K γ [102, 103] and the patenting of the first PI3K γ -selective inhibitor by Novartis in 2003 for the treatment of respiratory diseases [104], drug discovery efforts in the last decade have validated the value of PI3K γ as a promising therapeutic target, especially for inflammatory disease (for a chronological review of the patented synthetic PI3K γ inhibitor chemotypes see [15] and [105]).

In particular, pharmacological targeting of PI3K γ may be effective in the regulation of the immune system, and therefore in the control of airway diseases driven by an excessive inflammatory response. On the other hand, possible side effects can be expected upon long-term treatment or in the co-occurrence of infections, as highlighted by preclinical work [81]. Similarly, infections have been observed as a significant side effect of the dual PI3K γ δ inhibitor Duvelisib [106]. However, whether and how PI3K γ selective inhibitors predispose to infections is still unknown, as only one compound selectivity targeting PI3K γ , IPI-549 from Infinity Pharmaceuticals, has initiated clinical development so far, though as an anti-cancer agent [105]. Therefore, it cannot be excluded that inhibitors targeting PI3K γ catalytic activity may have opposite effects in the lungs, and only clinical trials will define the nature and the extent of a therapeutic window for these drugs in pulmonary diseases, compared to the more advanced dual PI3K γ δ inhibitors.

Among these, several compounds have reached clinical trial for respiratory diseases (Table 2). For example, Duvelisib was a candidate for mild asthma, but further development in non-oncologic diseases has been stopped,

as the primary end point (changes in maximum allergen-induced Forced Expiratory Volume 1 decrease) was missed in clinical trials. Significant effects were seen, however, on secondary end points, but at a dose potentially leading to serious adverse reactions [107]. Other dual γ δ inhibitors that reached clinical development for respiratory diseases (like asthma and chronic obstructive pulmonary disease (COPD)) include RV1729 and RV6153, from RespiVert, and AZD8154, from AstraZeneca (Table 2). Possibly, an inhalation-based delivery of PI3K γ δ (and PI3K γ) inhibitors could help reducing, if not overcoming, any systemic adverse effect, though impairing the response to respiratory pathogens. In line with this approach, Chiesi Farmaceutici has started a clinical study to investigate the safety, tolerability and pharmacokinetics of the inhaled CHF6523 PI3K inhibitor. As an exploratory assessment, the anti-inflammatory effect of CHF6523 on sputum and blood biomarkers in COPD subjects will be evaluated (Table 2).

Moreover, considering that class IB isoforms can cooperate with class IA and IB PI3Ks in controlling, downstream signaling events, dual inhibition may be desirable to achieve a relevant therapeutic effect [15]. On the other hand, from a safety perspective, a high isoform selectivity is required, especially toward PI3K α and β , which made development of PI3K γ inhibitors difficult, due to the high similarity between isoform sequences. Only recently, new classes of increasingly more specific inhibitors have been generated to block PI3K γ kinase activity [108-110]. However, this approach may not discriminate between the two PI3K γ heteromeric variants, that share the same catalytic p110 γ subunit combined to different regulatory subunits, which hypothetically exert distinct biological functions [27].

Nonetheless, PI3K γ is a multifunctional protein, which is not only involved in the modulation of the Akt/mTOR pathway through its catalytic action, but also in the inhibition of cAMP as a scaffold protein. As cAMP elevation in lungs triggers bronchodilation and anti-inflammatory responses, better definition of the protein-protein interactions driving PI3K γ -mediated cAMP modulation might open the way to novel therapeutic options in airway diseases.

TABLE 2. Clinical development of PI3K γ δ inhibitors for respiratory diseases.

Compound	Developer	Target	Disease	Clinical Trial Identifier	Clinical phase	Status	Subjects enrolled	Duration (weeks)	Refs.
IP-145 (Copiktra®, Duvelisib)	Verastem Oncology, licensed from Infinity Pharmaceuticals	PI3K γ δ inhibitor	Mild Asthma	NCT01653756	2	Completed	50	2	[107, 111, 112]
RV1729	RespiVert	PI3K γ δ inhibitor	Asthma Asthma COPD	NCT01813084 NCT02140320 NCT02140346	1 1 1	Completed Completed Completed	63 49 48	4 2 4	[111, 113, 114]
RV6153	RespiVert	PI3K γ δ inhibitor	Asthma	NCT02517359	1	Terminated	55	4	[105, 111]
AZD8154	AstraZeneca	PI3K γ δ inhibitor	Asthma Asthma Asthma	NCT04480879 NCT04187508 NCT03436316	1 2 1	Terminated Withdrawn Completed	10 - 78	9 - 2	[115]
CHF6523	Chiesi Farmaceutici	PI3K inhibitor	COPD	NCT04032535	1	Recruiting	-	4	

Despite efforts in developing PI3K γ inhibitors in the last decades, only one compound, the dual $\gamma\delta$ inhibitor Duvelisib, has received approval, and its application is limited to oncological malignancies. Therefore, a more profound understanding of the biological role of PI3K γ variants as well as of the impact of its non-catalytic functions in signal transduction is needed in order to foster new tools, and expand fields of intervention for PI3K γ targeting.

ACKNOWLEDGMENTS

This work was supported by the Italian Cystic Fibrosis Research Foundation (FFC#25/2014, FFC#23/2015 and FFC#8/2018 to EH, FFC#4/2016 and FFC#11/2017 to AG), Compagnia di Sanpaolo (CSTO161109 to EH), Cariplo Foundation (#2015-0880 to AG and #2018-0498 to EH), Roche Foundation (Bando Roche per la Ricerca 2019 to AG).

REFERENCES

- Burke JE, Williams RL (2015). Synergy in activating class I PI3Ks. *Trends Biochem Sci* 40(2): 88-100. doi: 10.1016/j.tibs.2014.12.003
- Vanhaesebroeck B (2006). Charging the batteries to heal wounds through PI3K. *Nat Chem Biol* 2(9): 453-455. doi: 10.1038/nchembio0906-453
- Crackower MA, Oudit GY, Koziarzki I, Sarao R, Sun H, Sasaki T, Hirsch E, Suzuki A, Shioi T, Irie-Sasaki J, Sah R, Cheng HY, Rybin VO, Lembo G, Fratta L, Oliveira-dos-Santos AJ, Benovic JL, Kahn CR, Izumo S, Steinberg SF, Wymann MP, Backx PH, Penninger JM (2002). Regulation of myocardial contractility and cell size by distinct PI3K-PTEN signaling pathways. *Cell* 110(6): 737-749. doi: 10.1016/s0092-8674(02)00969-8
- Harris SJ, Ciucian L, Finan PM, Wymann MP, Walker C, Westwick J, Ward SG, Thomas MJ (2012). Genetic ablation of PI3K γ results in defective IL-17RA signalling in T lymphocytes and increased IL-17 levels. *Eur J Immunol* 42(12): 3394-3404. doi: 10.1002/eji.201242463
- Li M, Sala V, De Santis MC, Cimino J, Cappello P, Pianca N, Di Bona A, Margaria JP, Martini M, Lazzarini E, Pirozzi F, Rossi L, Franco I, Bornbaum J, Heger J, Rohrbach S, Perino A, Tocchetti CG, Lima BHF, Teixeira MM, Porporato PE, Schulz R, Angelini A, Sandri M, Ameri P, Sciarretta S, Lima-Júnior RCP, Mongillo M, Zaglia T, Morello F, et al. (2018). Phosphoinositide 3-Kinase Gamma Inhibition Protects From Anthracycline Cardiotoxicity and Reduces Tumor Growth. *Circulation* 138(7): 696-711. doi: 10.1161/circulationaha.117.030352
- Naga Prasad SV, Esposito G, Mao L, Koch WJ, Rockman HA (2000). Gbetagamma-dependent phosphoinositide 3-kinase activation in hearts with in vivo pressure overload hypertrophy. *J Biol Chem* 275(7): 4693-4698. doi: 10.1074/jbc.275.7.4693
- Patrucco E, Notte A, Barberis L, Selvetella G, Maffei A, Brancaccio M, Marengo S, Russo G, Azzolino O, Rybalkin SD, Silengo L, Altruda F, Wetzker R, Wymann MP, Lembo G, Hirsch E (2004). PI3Kgamma modulates the cardiac response to chronic pressure overload by distinct kinase-dependent and -independent effects. *Cell* 118(3): 375-387. doi: 10.1016/j.cell.2004.07.017
- Perino A, Ghigo A, Ferrero E, Morello F, Santulli G, Baillie GS, Damilano F, Dunlop AJ, Pawson C, Walsler R, Levi R, Altruda F, Silengo L, Langeberg LK, Neubauer G, Heymans S, Lembo G, Wymann MP, Wetzker R, Houslay MD, Iaccarino G, Scott JD, Hirsch E (2011). Integrating cardiac PIP3 and cAMP signaling through a PKA anchoring function of p110 γ . *Mol Cell* 42(1): 84-95. doi: 10.1016/j.molcel.2011.01.030
- Perrino C, Schroder JN, Lima B, Villamizar N, Nienaber JJ, Milano CA, Naga Prasad SV (2007). Dynamic regulation of phosphoinositide 3-

CONFLICT OF INTEREST

Alessandra Ghigo and Emilio Hirsch are founders of Kither Biotech S.r.l. Valentina Sala received a contract fee from Kither Biotech S.r.l.

COPYRIGHT

© 2021 Sala *et al.* This is an open-access article released under the terms of the Creative Commons Attribution (CC BY) license, which allows the unrestricted use, distribution, and reproduction in any medium, provided the original author and source are acknowledged.

Please cite this article as: Valentina Sala, Angela Della Sala, Alessandra Ghigo and Emilio Hirsch (2021). Roles of phosphatidylinositol 3 kinase gamma (PI3K γ) in respiratory diseases. *Cell Stress: in press*.

kinase-gamma activity and beta-adrenergic receptor trafficking in end-stage human heart failure. *Circulation* 116(22): 2571-2579. doi: 10.1161/circulationaha.107.706515

10. Yu Q, Li W, Jin R, Yu S, Xie D, Zheng X, Zhong W, Cheng X, Hu S, Li M, Zheng Q, Li G, Song Z (2019). PI3Kgamma (Phosphoinositide 3-Kinase gamma) Regulates Vascular Smooth Muscle Cell Phenotypic Modulation and Neointimal Formation Through CREB (Cyclic AMP-Response Element Binding Protein)/YAP (Yes-Associated Protein) Signaling. *Arterioscler Thromb Vasc Biol* 39(3): e91-e105. doi: 10.1161/ATVBAHA.118.312212

11. Jin R, Yu S, Song Z, Quillin JW, Deas DP, Penninger JM, Nanda A, Granger DN, Li G (2010). Phosphoinositide 3-kinase-gamma expression is upregulated in brain microglia and contributes to ischemia-induced microglial activation in acute experimental stroke. *Biochem Biophys Res Commun* 399(3): 458-464. doi: 10.1016/j.bbrc.2010.07.116

12. Sasaki T, Irie-Sasaki J, Jones RG, Oliveira-dos-Santos AJ, Stanford WL, Bolon B, Wakeham A, Itie A, Bouchard D, Koziarzki I, Joza N, Mak TW, Ohashi PS, Suzuki A, Penninger JM (2000). Function of PI3Kgamma in thymocyte development, T cell activation, and neutrophil migration. *Science* 287(5455): 1040-1046. doi: 10.1126/science.287.5455.1040.

13. Takeda AJ, Maher TJ, Zhang Y, Lanahan SM, Bucklin ML, Compton SR, Tyler PM, Comrie WA, Matsuda M, Olivier KN, Pittaluga S, McElwee JJ, Long Priel DA, Kuhns DB, Williams RL, Mustillo PJ, Wymann MP, Koneti Rao V, Lucas CL (2019). Human PI3Kgamma deficiency and its microbiota-dependent mouse model reveal immunodeficiency and tissue immunopathology. *Nat Commun* 10(1): 4364. doi: 10.1038/s41467-019-12311-5

14. Madeddu P, Kraenkel N, Barcelos LS, Siragusa M, Campagnolo P, Oikawa A, Caporali A, Herman A, Azzolino O, Barberis L, Perino A, Damilano F, Emanuelli C, Hirsch E (2008). Phosphoinositide 3-kinase gamma gene knockout impairs postischemic neovascularization and endothelial progenitor cell functions. *Arterioscler Thromb Vasc Biol* 28(1): 68-76. doi: 10.1161/atvbaha.107.145573

15. Ruckle T, Schwarz MK, Rommel C (2006). PI3Kgamma inhibition: towards an 'aspirin of the 21st century'? *Nat Rev Drug Discov* 5(11): 903-918. doi: 10.1038/nrd2145

16. Lionetti V, Lisi A, Patrucco E, De Giuli P, Milazzo MG, Ceci S, Wymann M, Lena A, Gremigni V, Fanelli V, Hirsch E, Ranieri VM (2006). Lack of phosphoinositide 3-kinase-gamma attenuates ventilator-induced lung injury. *Crit Care Med* 34(1): 134-141. doi: 10.1097/01.ccm.0000190909.70601.2c

17. Montoro DT, Haber AL, Biton M, Vinarsky V, Lin B, Birket SE, Yuan F, Chen S, Leung HM, Villoria J, Rogel N, Burgin G, Tsankov AM, Waghray A, Slyper M, Waldman J, Nguyen L, Dionne D, Rozenblatt-Rosen O, Tata PR, Mou H, Shivaraju M, Bihler H, Mense M, Tearney GJ, Rowe SM, Engelhardt JF, Regev A, Rajagopal J (2018). A revised airway epithelial hierarchy includes CFTR-expressing ionocytes. *Nature* 560(7718): 319-324. doi: 10.1038/s41586-018-0393-7
18. Ciraolo E, Iezzi M, Marone R, Marengo S, Curcio C, Costa C, Azzolino O, Gonella C, Rubinetto C, Wu H, Dastrù W, Martin EL, Silengo L, Altruda F, Turco E, Lanzetti L, Musiani P, Ruckle T, Rommel C, Backer JM, Forni G, Wymann MP, Hirsch E (2008). Phosphoinositide 3-kinase p110beta activity: key role in metabolism and mammary gland cancer but not development. *Sci Signal* 1(36): ra3. doi: 10.1126/scisignal.1161577
19. Kurig B, Shymanets A, Bohnacker T, Prajwal, Brock C, Ahmadian MR, Schaefer M, Gohla A, Harteneck C, Wymann MP, Jeandros E, Nürnberg B (2009). Ras is an indispensable coregulator of the class IB phosphoinositide 3-kinase p87/p110gamma. *Proc Natl Acad Sci U S A* 106(48): 20312-20317. doi: 10.1073/pnas.0905506106
20. Shymanets A, Prajwal, Bucher K, Beer-Hammer S, Harteneck C, Nürnberg B (2013). p87 and p101 subunits are distinct regulators determining class IB phosphoinositide 3-kinase (PI3K) specificity. *J Biol Chem* 288(43): 31059-31068. doi: 10.1074/jbc.M113.508234
21. Schmid MC, Avraamides CJ, Dippold HC, Franco I, Foubert P, Ellies LG, Acevedo LM, Manglicmot JR, Song X, Wrasidlo W, Blair SL, Ginsberg MH, Cheresh DA, Hirsch E, Field SJ, Varner JA (2011). Receptor tyrosine kinases and TLR/IL1Rs unexpectedly activate myeloid cell PI3ky, a single convergent point promoting tumor inflammation and progression. *Cancer Cell* 19(6): 715-727. doi: 10.1016/j.ccr.2011.04.016
22. Fruman DA, Chiu H, Hopkins BD, Bagrodia S, Cantley LC, Abraham RT (2017). The PI3K Pathway in Human Disease. *Cell* 170(4): 605-635. doi: 10.1016/j.cell.2017.07.029
23. Luo L, Wall AA, Tong SJ, Hung Y, Xiao Z, Tarique AA, Sly PD, Fantino E, Marzolo MP, Stow JL (2018). TLR Crosstalk Activates LRP1 to Recruit Rab8a and PI3Ky for Suppression of Inflammatory Responses. *Cell Rep* 24(11): 3033-3044. doi: 10.1016/j.celrep.2018.08.028
24. Luo L, Wall AA, Yeo JC, Condon ND, Norwood SJ, Schoenwaelder S, Chen KW, Jackson S, Jenkins BJ, Hartland EL, Schroder K, Collins BM, Sweet MJ, Stow JL (2014). Rab8a interacts directly with PI3Ky to modulate TLR4-driven PI3K and mTOR signalling. *Nat Commun* 5: 4407. doi: 10.1038/ncomms5407
25. Wall AA, Luo L, Hung Y, Tong SJ, Condon ND, Blumenthal A, Sweet MJ, Stow JL (2017). Small GTPase Rab8a-recruited Phosphatidylinositol 3-Kinase γ Regulates Signaling and Cytokine Outputs from Endosomal Toll-like Receptors. *J Biol Chem* 292(11): 4411-4422. doi: 10.1074/jbc.M116.766337
26. Laffargue M, Calvez R, Finan P, Trifilieff A, Barbier M, Altruda F, Hirsch E, Wymann MP (2002). Phosphoinositide 3-kinase gamma is an essential amplifier of mast cell function. *Immunity* 16(3): 441-451. doi: 10.1016/s1074-7613(02)00282-0
27. Nurnberg B, Beer-Hammer S (2019). Function, Regulation and Biological Roles of PI3Kgamma Variants. *Biomolecules* 9(9): 427. doi: 10.3390/biom9090427.
28. Wang T, Gross C, Desai AA, Zemskov E, Wu X, Garcia AN, Jacobson JR, Yuan JX, Garcia JG, Black SM (2017). Endothelial cell signaling and ventilator-induced lung injury: molecular mechanisms, genomic analyses, and therapeutic targets. *Am J Physiol Lung Cell Mol Physiol* 312(4): L452-L476. doi: 10.1152/ajplung.00231.2016
29. Choi WI, Quinn DA, Park KM, Moufarrej RK, Jafari B, Syrkinina O, Bonventre JV, Hales CA (2003). Systemic microvascular leak in an in vivo rat model of ventilator-induced lung injury. *Am J Respir Crit Care Med* 167(12): 1627-1632. doi: 10.1164/rccm.200210-1216OC
30. Fanelli V, Puntorieri V, Assenzio B, Martin EL, Elia V, Bosco M, Delsedime L, Del Sorbo L, Ferrari A, Italiano S, Ghigo A, Slutsky AS, Hirsch E, Ranieri VM (2010). Pulmonary-derived phosphoinositide 3-kinase gamma (PI3Kgamma) contributes to ventilator-induced lung injury and edema. *Intensive Care Med* 36(11): 1935-1945. doi: 10.1007/s00134-010-2018-y
31. Sayner SL (2011). Emerging themes of cAMP regulation of the pulmonary endothelial barrier. *Am J Physiol Lung Cell Mol Physiol* 300(5): L667-678. doi: 10.1152/ajplung.00433.2010
32. Shi CS, Huang TH, Lin CK, Li JM, Chen MH, Tsai ML, Chang CC (2016). VEGF Production by Ly6C+high Monocytes Contributes to Ventilator-Induced Lung Injury. *PLoS One* 11(10): e0165317. doi: 10.1371/journal.pone.0165317
33. Aderem A, Ulevitch RJ (2000). Toll-like receptors in the induction of the innate immune response. *Nature* 406(6797): 782-787. doi: 10.1038/35021228
34. Perros F, Lambrecht BN, Hammad H (2011). TLR4 signalling in pulmonary stromal cells is critical for inflammation and immunity in the airways. *Respir Res* 12: 125. doi: 10.1186/1465-9921-12-125
35. Villar J, Cabrera NE, Casula M, Flores C, Valladares F, Diaz-Flores L, Muros M, Slutsky AS, Kacmarek RM (2010). Mechanical ventilation modulates TLR4 and IRAK-3 in a non-infectious, ventilator-induced lung injury model. *Respir Res* 11: 27. doi: 10.1186/1465-9921-11-27
36. Ding X, Tong Y, Jin S, Chen Z, Li T, Billiar TR, Pitt BR, Li Q, Zhang LM (2018). Mechanical ventilation enhances extrapulmonary sepsis-induced lung injury: role of WISP1- α v β 5 integrin pathway in TLR4-mediated inflammation and injury. *Crit Care* 22(1): 302. doi: 10.1186/s13054-018-2237-0
37. Hu G, Malik AB, Minshall RD (2010). Toll-like receptor 4 mediates neutrophil sequestration and lung injury induced by endotoxin and hyperinflation. *Crit Care Med* 38(1): 194-201. doi: 10.1097/CCM.0b013e3181bc7c17
38. Li H, Su X, Yan X, Wasserloos K, Chao W, Kaynar AM, Liu ZQ, Leikauf GD, Pitt BR, Zhang LM (2010). Toll-like receptor 4-myeloid differentiation factor 88 signaling contributes to ventilator-induced lung injury in mice. *Anesthesiology* 113(3): 619-629. doi: 10.1097/ALN.0b013e3181e89ab2
39. Vaneker M, Joosten LA, Heunks LM, Snijselaar DG, Halbertsma FJ, van Egmond J, Netea MG, van der Hoeven JG, Scheffer GJ (2008). Low-tidal-volume mechanical ventilation induces a toll-like receptor 4-dependent inflammatory response in healthy mice. *Anesthesiology* 109(3): 465-472. doi: 10.1097/ALN.0b013e318182aef1
40. Raghu G, Collard HR, Egan JJ, Martinez FJ, Behr J, Brown KK, Colby TV, Cordier JF, Flaherty KR, Lasky JA, Lynch DA, Ryu JH, Swigris JJ, Wells AU, Ancochea J, Bouros D, Carvalho C, Costabel U, Ebina M, Hansell DM, Johkoh T, Kim DS, King TE, Kondoh Y, Myers J, Müller NL, Nicholson AG, Richeldi L, Selman M, Dudden RF, et al. (2011). An official ATS/ERS/JRS/ALAT statement: idiopathic pulmonary fibrosis: evidence-based guidelines for diagnosis and management. *Am J Respir Crit Care Med* 183(6): 788-824. doi: 10.1164/rccm.2009-040GL
41. Hutchinson J, Fogarty A, Hubbard R, McKeever T (2015). Global incidence and mortality of idiopathic pulmonary fibrosis: a systematic review. *Eur Respir J* 46(3): 795-806. doi: 10.1183/09031936.00185114
42. Ley B, Collard HR, King TE (2011). Clinical course and prediction of survival in idiopathic pulmonary fibrosis. *Am J Respir Crit Care Med* 183(4): 431-440. doi: 10.1164/rccm.201006-0894CI
43. Idiopathic Pulmonary Fibrosis Clinical Research N, Martinez FJ, de Andrade JA, Anstrom KJ, King TE, Jr., Raghu G (2014). Randomized trial

- of acetylcysteine in idiopathic pulmonary fibrosis. **N Engl J Med** 370(22): 2093-2101. doi: 10.1056/NEJMoa1401739
44. Richeldi L, Collard HR, Jones MG (2017). Idiopathic pulmonary fibrosis. **Lancet** 389(10082): 1941-1952. doi: 10.1016/S0140-6736(17)30866-8
45. Garcia CK (2018). Insights from human genetic studies of lung and organ fibrosis. **J Clin Invest** 128(1): 36-44. doi: 10.1172/jci93556
46. Sauleda J, Núñez B, Sala E, Soriano JB (2018). Idiopathic Pulmonary Fibrosis: Epidemiology, Natural History, Phenotypes. **Med Sci** 6(4): 110. doi: 10.3390/medsci6040110
47. Le Cras TD, Korfhagen TR, Davidson C, Schmidt S, Fenchel M, Ikegami M, Whittsett JA, Hardie WD (2010). Inhibition of PI3K by PX-866 prevents transforming growth factor- α -induced pulmonary fibrosis. **Am J Pathol** 176(2): 679-686. doi: 10.2353/ajpath.2010.090123
48. Mercer PF, Woodcock HV, Eley JD, Platé M, Sulikowski MG, Durrenberger PF, Franklin L, Nanthakumar CB, Man Y, Genovese F, McAnulty RJ, Yang S, Maher TM, Nicholson AG, Blanchard AD, Marshall RP, Lukey PT, Chambers RC (2016). Exploration of a potent PI3 kinase/mTOR inhibitor as a novel anti-fibrotic agent in IPF. **Thorax** 71(8): 701-711. doi: 10.1136/thoraxjnl-2015-207429
49. Campa CC, Silva RL, Margaria JP, Pirali T, Mattos MS, Kraemer LR, Reis DC, Grosa G, Copperi F, Dalmarco EM, Lima-Junior RCP, Aprile S, Sala V, Dal Bello F, Prado DS, Alves-Filho JC, Medana C, Cassali GD, Tron GC, Teixeira MM, Ciraolo E, Russo RC, Hirsch E (2018). Inhalation of the prodrug PI3K inhibitor CL27c improves lung function in asthma and fibrosis. **Nat Commun** 9(1): 5232. doi: 10.1038/s41467-018-07698-6
50. Conte E, Gili E, Fruciano M, Korfei M, Fagone E, Iemmolo M, Lo Furno D, Giuffrida R, Crimi N, Guenther A, Vancheri C (2013). PI3K p110 γ overexpression in idiopathic pulmonary fibrosis lung tissue and fibroblast cells: in vitro effects of its inhibition. **Lab Invest** 93(5): 566-576. doi: 10.1038/labinvest.2013.6
51. Russo RC, Garcia CC, Barcelos LS, Rachid MA, Guabiraba R, Roffê E, Souza AL, Sousa LP, Mirolo M, Doni A, Cassali GD, Pinho V, Locati M, Teixeira MM (2011). Phosphoinositide 3-kinase γ plays a critical role in bleomycin-induced pulmonary inflammation and fibrosis in mice. **J Leukoc Biol** 89(2): 269-282. doi: 10.1189/jlb.0610346
52. Sontake V, Gajjala PR, Kasam RK, Madala SK (2019). New therapeutics based on emerging concepts in pulmonary fibrosis. **Expert Opin Ther Targets** 23(1): 69-81. doi: 10.1080/14728222.2019.1552262
53. Sokai A, Tanizawa K, Handa T, Kanatani K, Kubo T, Ikezoe K, Nakatsuka Y, Tokuda S, Oga T, Hirai T, Nagai S, Chin K, Mishima M (2017). Importance of serial changes in biomarkers in idiopathic pulmonary fibrosis. **ERJ Open Res** 3(3): 00019-2016. doi: 10.1183/23120541.00019-2016
54. Zank DC, Bueno M, Mora AL, Rojas M (2018). Idiopathic Pulmonary Fibrosis: Aging, Mitochondrial Dysfunction, and Cellular Bioenergetics. **Front Med** 5: 10. doi: 10.3389/fmed.2018.00010
55. Doukas J, Eide L, Stebbins K, Racanelli-Layton A, Dellamary L, Martin M, Dneprovskaja E, Noronha G, Soll R, Wrasidlo W, Acevedo LM, Cheresch DA (2009). Aerosolized phosphoinositide 3-kinase gamma/delta inhibitor TG100-115 [3-[2,4-diamino-6-(3-hydroxyphenyl)pteridin-7-yl]phenol] as a therapeutic candidate for asthma and chronic obstructive pulmonary disease. **J Pharmacol Exp Ther** 328(3): 758-765. doi: 10.1124/jpet.108.144311
56. Lim DH, Cho JY, Song DJ, Lee SY, Miller M, Broide DH (2009). PI3K gamma-deficient mice have reduced levels of allergen-induced eosinophilic inflammation and airway remodeling. **Am J Physiol Lung Cell Mol Physiol** 296(2): L210-219. doi: 10.1152/ajplung.90275.2008
57. Takeda M, Ito W, Tanabe M, Ueki S, Kato H, Kihara J, Tanigai T, Chiba T, Yamaguchi K, Kayaba H, Imai Y, Okuyama K, Ohno I, Sasaki T, Chihara J (2009). Allergic airway hyperresponsiveness, inflammation, and remodeling do not develop in phosphoinositide 3-kinase gamma-deficient mice. **J Allergy Clin Immunol** 123(4): 805-812. doi: 10.1016/j.jaci.2008.11.047
58. Saito Y, Takeda M, Nishikawa J, Konno Y, Tamaki M, Itoga M, Kobayashi Y, Moritoki Y, Ito W, Chihara J, Ueki S (2014). The effect of pharmacological PI3K γ inhibitor on eotaxin-induced human eosinophil functions. **Pulm Pharmacol Ther** 27(2): 164-169. doi: 10.1016/j.pupt.2013.11.006
59. Singh AK, Pantouris G, Borosch S, Rojanasthien S, Cho TY (2017). Structural basis for decreased induction of class IB PI3-kinases expression by MIF inhibitors. **J Cell Mol Med** 21(1): 142-153. doi: 10.1111/jcmm.12949
60. Deshpande DA, Penn RB (2006). Targeting G protein-coupled receptor signaling in asthma. **Cell Signal** 18(12): 2105-2120. doi: 10.1016/j.cellsig.2006.04.008
61. Eum SY, Maghni K, Tolloczko B, Eidelman DH, Martin JG (2005). IL-13 may mediate allergen-induced hyperresponsiveness independently of IL-5 or eotaxin by effects on airway smooth muscle. **Am J Physiol Lung Cell Mol Physiol** 288(3): L576-584. doi: 10.1152/ajplung.00380.2003
62. Laporte SA, Oakley RH, Holt JA, Barak LS, Caron MG (2000). The interaction of beta-arrestin with the AP-2 adaptor is required for the clustering of beta 2-adrenergic receptor into clathrin-coated pits. **J Biol Chem** 275(30): 23120-23126. doi: 10.1074/jbc.M002581200
63. Sathish V, Thompson MA, Bailey JP, Pabelick CM, Prakash YS, Sieck GC (2009). Effect of proinflammatory cytokines on regulation of sarcoplasmic reticulum Ca²⁺ reuptake in human airway smooth muscle. **Am J Physiol Lung Cell Mol Physiol** 297(1): L26-34. doi: 10.1152/ajplung.00026.2009
64. Jiang H, Abel PW, Toews ML, Deng C, Casale TB, Xie Y, Tu Y (2010). Phosphoinositide 3-kinase gamma regulates airway smooth muscle contraction by modulating calcium oscillations. **J Pharmacol Exp Ther** 334(3): 703-709. doi: 10.1124/jpet.110.168518
65. Saha SK, Berry MA, Parker D, Siddiqui S, Morgan A, May R, Monk P, Bradding P, Wardlaw AJ, Pavord ID, Brightling CE (2008). Increased sputum and bronchial biopsy IL-13 expression in severe asthma. **J Allergy Clin Immunol** 121(3): 685-691. doi: 10.1016/j.jaci.2008.01.005
66. Wills-Karp M, Luyimbazi J, Xu X, Schofield B, Neben TY, Karp CL, Donaldson DD (1998). Interleukin-13: central mediator of allergic asthma. **Science** 282(5397): 2258-2261. doi: 10.1126/science.282.5397.2258
67. Walter DM, McIntire JJ, Berry G, McKenzie AN, Donaldson DD, DeKruyff RH, Umetsu DT (2001). Critical role for IL-13 in the development of allergen-induced airway hyperreactivity. **J Immunol** 167(8): 4668-4675. doi: 10.4049/jimmunol.167.8.4668
68. Marwick JA, Chung KF, Adcock IM (2010). Phosphatidylinositol 3-kinase isoforms as targets in respiratory disease. **Ther Adv Respir Dis** 4(1): 19-34. doi: 10.1177/1753465809352792
69. Elborn JS (2016). Cystic fibrosis. **Lancet** 388(10059): 2519-2531. doi: 10.1016/s0140-6736(16)00576-6
70. Sly PD, Gangell CL, Chen L, Ware RS, Ranganathan S, Mott LS, Murray CP, Stick SM, Investigators AC (2013). Risk factors for bronchiectasis in children with cystic fibrosis. **N Engl J Med** 368(21): 1963-1970. doi: 10.1056/NEJMoa1301725
71. Stick S, Tiddens H, Aurora P, Gustafsson P, Ranganathan S, Robinson P, Rosenfeld M, Sly P, Ratjen F (2013). Early intervention studies in infants and preschool children with cystic fibrosis: are we ready? **Eur Respir J** 42(2): 527-538. doi: 10.1183/09031936.00108212

72. Margaroli C, Tirouvanziam R (2016). Neutrophil plasticity enables the development of pathological microenvironments: implications for cystic fibrosis airway disease. **Mol Cell Pediatr** 3(1): 38. doi: 10.1186/s40348-016-0066-2
73. Galluzzo M, Ciraolo E, Lucattelli M, Hoxha E, Ulrich M, Campa CC, Lungarella G, Doring G, Zhou-Suckow Z, Mall M, Hirsch E, De Rose V (2015). Genetic Deletion and Pharmacological Inhibition of PI3K γ Reduces Neutrophilic Airway Inflammation and Lung Damage in Mice with Cystic Fibrosis-Like Lung Disease. **Mediators Inflamm** 2015(545417). doi: 10.1155/2015/545417
74. L  v  que M, Le Trionnaire S, Del Porto P, Martin-Chouly C (2017). The impact of impaired macrophage functions in cystic fibrosis disease progression. **J Cyst Fibros** 16(4): 443-453. doi: 10.1016/j.jcf.2016.10.011
75. Paemka L, McCullagh BN, Abou Alaiwa MH, Stoltz DA, Dong Q, Randak CO, Gray RD, McCray PB (2017). Monocyte derived macrophages from CF pigs exhibit increased inflammatory responses at birth. **J Cyst Fibros** 16(4): 471-474. doi: 10.1016/j.jcf.2017.03.007
76. Saini Y, Dang H, Livraghi-Butrico A, Kelly EJ, Jones LC, O'Neal WK, Boucher RC (2014). Gene expression in whole lung and pulmonary macrophages reflects the dynamic pathology associated with airway surface dehydration. **BMC Genomics** 15: 726. doi: 10.1186/1471-2164-15-726
77. Tarique AA, Sly PD, Holt PG, Bosco A, Ware RS, Logan J, Bell SC, Wainwright CE, Fantino E (2017). CFTR-dependent defect in alternatively-activated macrophages in cystic fibrosis. **J Cyst Fibros** 16(4): 475-482. doi: 10.1016/j.jcf.2017.03.011
78. Breasson L, Sardi C, Becattini B, Zani F, Solinas G (2018). PI3K γ ablation does not promote diabetes in. **FASEB J** 32(1): 319-329. doi: 10.1096/fj.201700372RR
79. Ding X, Jin S, Tong Y, Jiang X, Chen Z, Mei S, Zhang L, Billiar TR, Li Q (2017). TLR4 signaling induces TLR3 up-regulation in alveolar macrophages during acute lung injury. **Sci Rep** 7: 34278. doi: 10.1038/srep34278
80. Katholnig K, Linke M, Pham H, Hengstschlager M, Weichhart T (2013). Immune responses of macrophages and dendritic cells regulated by mTOR signalling. **Biochem Soc Trans** 41(4): 927-933. doi: 10.1042/BST20130032
81. Maus UA, Backi M, Winter C, Srivastava M, Schwarz MK, Ruckle T, Paton JC, Briles D, Mack M, Welte T, Maus R, Bohle RM, Seeger W, Rommel C, Hirsch E, Lohmeyer J, Preissner KT (2007). Importance of phosphoinositide 3-kinase gamma in the host defense against pneumococcal infection. **Am J Respir Crit Care Med** 175(9): 958-966. doi: 10.1164/rccm.200610-1533OC
82. Cavalcanti-Neto MP, Prado RQ, Pi  eros AR, S  rgio CA, Bertolini TB, Gembre AF, Ramos SG, Bonato VL (2018). Improvement of the resistance against early Mycobacterium tuberculosis-infection in the absence of PI3K γ enzyme is associated with increase of CD4+IL-17+ cells and neutrophils. **Tuberculosis** 113: 1-9. doi: 10.1016/j.tube.2018.08.009
83. Bucher K, Schmitt F, Mothes B, Blumendeller C, Sch  ll D, Piekorz R, Hirsch E, N  rnberg B, Beer-Hammer S (2017). Deficiency of PI3-Kinase catalytic isoforms p110 γ and p110 δ in mice enhances the IL-17/G-CSF axis and induces neutrophilia. **Cell Commun Signal** 15(1): 28. doi: 10.1186/s12964-017-0185-y
84. Leisching GR (2018). Susceptibility to Tuberculosis Is Associated With PI3K-Dependent Increased Mobilization of Neutrophils. **Front Immunol** 9: 1669. doi: 10.3389/fimmu.2018.01669
85. Martineau AR, Newton SM, Wilkinson KA, Kampmann B, Hall BM, Nawroly N, Packe GE, Davidson RN, Griffiths CJ, Wilkinson RJ (2007). Neutrophil-mediated innate immune resistance to mycobacteria. **J Clin Invest** 117(7): 1988-1994. doi: 10.1172/jci31097
86. Philips JA (2017). Neutrophils: Double agents for TB. **Sci Transl Med** 9(394). doi: 10.1126/scitranslmed.aan6195
87. Martin D, Galisteo R, Molinolo AA, Wetzker R, Hirsch E, Gutkind JS (2011). PI3K γ mediates kaposi's sarcoma-associated herpesvirus vGPCR-induced sarcomagenesis. **Cancer Cell** 19(6): 805-813. doi: 10.1016/j.ccr.2011.05.005
88. Iuliano AD, Roguski KM, Chang HH, Muscatello DJ, Palekar R, Tempia S, Cohen C, Gran JM, Schanzer D, Cowling BJ, Wu P, Kyncl J, Ang LW, Park M, Redlberger-Fritz M, Yu H, Espenhain L, Krishnan A, Emukule G, van Asten L, Pereira da Silva S, Aungkulanon S, Buchholz U, Widdowson MA, Bresee JS, Network GSI-aMC (2018). Estimates of global seasonal influenza-associated respiratory mortality: a modelling study. **Lancet** 391(10127): 1285-1300. doi: 10.1016/s0140-6736(17)33293-2
89. Brandes M, Klauschen F, Kuchen S, Germain RN (2013). A systems analysis identifies a feedforward inflammatory circuit leading to lethal influenza infection. **Cell** 154(1): 197-212. doi: 10.1016/j.cell.2013.06.013
90. Herold S, Becker C, Ridge KM, Budinger GR (2015). Influenza virus-induced lung injury: pathogenesis and implications for treatment. **Eur Respir J** 45(5): 1463-1478. doi: 10.1183/09031936.00186214
91. Hirsch E, Katanaev VL, Garlanda C, Azzolino O, Pirola L, Silengo L, Sozzani S, Mantovani A, Altruda F, Wymann MP (2000). Central role for G protein-coupled phosphoinositide 3-kinase gamma in inflammation. **Science** 287(5455): 1049-1053. doi: 10.1126/science.287.5455.1049
92. Yang KY, Arcaroli J, Kupfner J, Pitts TM, Park JS, Strasshiem D, Perng RP, Abraham E (2003). Involvement of phosphatidylinositol 3-kinase gamma in neutrophil apoptosis. **Cell Signal** 15(2): 225-233. doi: 10.1016/s0898-6568(02)00063-3
93. Akaie T, Noguchi Y, Ijiri S, Setoguchi K, Suga M, Zheng YM, Dietzschold B, Maeda H (1996). Pathogenesis of influenza virus-induced pneumonia: involvement of both nitric oxide and oxygen radicals. **Proc Natl Acad Sci U S A** 93(6): 2448-2453. doi: 10.1073/pnas.93.6.2448
94. Narasaraju T, Yang E, Samy RP, Ng HH, Poh WP, Liew AA, Phoon MC, van Rooijen N, Chow VT (2011). Excessive neutrophils and neutrophil extracellular traps contribute to acute lung injury of influenza pneumonia. **Am J Pathol** 179(1): 199-210. doi: 10.1016/j.ajpath.2011.03.013
95. Garcia CC, Tavares LP, Dias ACF, Kehdy F, Alvarado-Arnez LE, Queiroz-Junior CM, Galv  o I, Lima BH, Matos AR, Goncalves APF, Soriani FM, Moraes MO, Marques JT, Siqueira MM, Machado AMV, Sousa LP, Russo RC, Teixeira MM (2018). Phosphatidylinositol 3 Kinase-Gamma Balances Antiviral and Inflammatory Responses During Influenza A H1N1 Infection: From Murine Model to Genetic Association in Patients. **Front Immunol** 9: 975. doi: 10.3389/fimmu.2018.00975
96. Nobs SP, Schneider C, Heer AK, Huotari J, Helenius A, Kopf M (2016). PI3K γ Is Critical for Dendritic Cell-Mediated CD8+ T Cell Priming and Viral Clearance during Influenza Virus Infection. **PLoS Pathog** 12(3): e1005508. doi: 10.1371/journal.ppat.1005508
97. Ghigo A, Perino A, Mehel H, Zahradnikova A, Jr., Morello F, Leroy J, Nikolaev VO, Damilano F, Cimino J, De Luca E, Richter W, Westenbroek R, Catterall WA, Zhang J, Yan C, Conti M, Gomez AM, Vandecasteele G, Hirsch E, Fischmeister R (2012). Phosphoinositide 3-kinase gamma protects against catecholamine-induced ventricular arrhythmia through protein kinase A-mediated regulation of distinct phosphodiesterases. **Circulation** 126(17): 2073-2083. doi: 10.1161/CIRCULATIONAHA.112.114074

98. To KK, Zhou J, Chan JF, Yuen KY (2015). Host genes and influenza pathogenesis in humans: an emerging paradigm. *Curr Opin Virol* 14: 7-15. doi: 10.1016/j.coviro.2015.04.010
99. Wain LV, Verwoert GC, O'Reilly PF, Shi G, Johnson T, Johnson AD, Bochud M, Rice KM, Henneman P, Smith AV, Ehret GB, Amin N, Larson MG, Mooser V, Hadley D, Dörr M, Bis JC, Aspelund T, Esko T, Janssens AC, Zhao JH, Heath S, Laan M, Fu J, Pistis G, Luan J, Arora P, Lucas G, Pirastu N, Pichler I, et al. (2011). Genome-wide association study identifies six new loci influencing pulse pressure and mean arterial pressure. *Nat Genet* 43(10): 1005-1011. doi: 10.1038/ng.922
100. Johnson AD, Yanek LR, Chen MH, Faraday N, Larson MG, Tofler G, Lin SJ, Kraja AT, Province MA, Yang Q, Becker DM, O'Donnell CJ, Becker LC (2010). Genome-wide meta-analyses identifies seven loci associated with platelet aggregation in response to agonists. *Nat Genet* 42(7): 608-613. doi: 10.1038/ng.604
101. Kächele M, Hennige AM, Machann J, Hieronimus A, Lamprinou A, Machicao F, Schick F, Fritsche A, Stefan N, Nürnberg B, Häring HU, Staiger H (2015). Variation in the Phosphoinositide 3-Kinase Gamma Gene Affects Plasma HDL-Cholesterol without Modification of Metabolic or Inflammatory Markers. *PLoS One* 10(12): e0144494. doi: 10.1371/journal.pone.0144494
102. Stephens L, Smrcka A, Cooke FT, Jackson TR, Sternweis PC, Hawkins PT (1994). A novel phosphoinositide 3 kinase activity in myeloid-derived cells is activated by G protein beta gamma subunits. *Cell* 77(1): 83-93. doi: 10.1016/0092-8674(94)90237-2
103. Stoyanov B, Volinia S, Hanck T, Rubio I, Loubtchenkov M, Malek D, Stoyanova S, Vanhaesebroeck B, Dhand R, Nürnberg B, et al. (1995). Cloning and characterization of a G protein-activated human phosphoinositide-3 kinase. *Science* 269(5224): 690-693. doi: 10.1126/science.7624799
104. Bruce I, F. P., Leblanc C, Mccarthy C, Whitehead L, Blair NE, Bloomfield GC, Hayler J, Kirman L, Oza MS, Shukla L (2003). 5-Phenylthiazole derivatives and their use as phosphatidylinositol 3-kinase (PI3K) inhibitors for the treatment of allergic and inflammatory diseases. WO-03072557.
105. Perry MWD, Abdulai R, Mogemark M, Petersen J, Thomas MJ, Valastro B, Westin Eriksson A (2019). Evolution of PI3K γ and delta Inhibitors for Inflammatory and Autoimmune Diseases. *J Med Chem* 62(10): 4783-4814. doi: 10.1021/acs.jmedchem.8b01298
106. Horwitz SM, Koch R, Porcu P, Oki Y, Moskowitz A, Perez M, Myskowski P, Officer A, Jaffe JD, Morrow SN, Allen K, Douglas M, Stern H, Sweeney J, Kelly P, Kelly V, Aster JC, Weaver D, Foss FM, Weinstock DM (2018). Activity of the PI3K-delta,gamma inhibitor duvelisib in a phase 1 trial and preclinical models of T-cell lymphoma. *Blood* 131(8): 888-898. doi: 10.1182/blood-2017-08-802470
107. Schmalbach T, Fuhr R, Albayaty M, Allen K, Douglas M, Dunbar J, McLaughlin J, Alexander L, McKee C (2015). Duvelisib, a PI3K- δ,γ inhibitor, in subjects with mild asthma. *Eur Respir J* 46(suppl 59): PA2122. doi: 10.1183/13993003.congress-2015.PA2122
108. Bandarage UK, Aronov AM, Cao J, Come JH, Cottrell KM, Davies RJ, Giroux S, Jacobs M, Mahajan S, Messersmith D, Moody CS, Swett R, Xu J (2021). Discovery of a Novel Series of Potent and Selective Alkynylthiazole-Derived PI3K γ Inhibitors. *ACS Med Chem Lett* 12(1): 129-135. doi: 10.1021/acsmedchemlett.0c00573
109. Drew SL, Thomas-Tran R, Beatty JW, Fournier J, Lawson KV, Miles DH, Mata G, Sharif EU, Yan X, Mailyan AK, Ginn E, Chen J, Wong K, Soni D, Dhanota P, Chen PY, Shaqfeh SG, Meleza C, Pham AT, Chen A, Zhao X, Banuelos J, Jin L, Schindler U, Walters MJ, Young SW, Walker NP, Leleti MR, Powers JP, Jeffrey JL (2020). Discovery of Potent and Selective PI3K γ Inhibitors. *J Med Chem* 63(19): 11235-11257. doi: 10.1021/acs.jmedchem.0c01203
110. Miles DH, Yan X, Thomas-Tran R, Fournier J, Sharif EU, Drew SL, Mata G, Lawson KV, Ginn E, Wong K, Soni D, Dhanota P, Shaqfeh SG, Meleza C, Chen A, Pham AT, Park T, Swinarski D, Banuelos J, Schindler U, Walters MJ, Walker NP, Zhao X, Young SW, Chen J, Jin L, Leleti MR, Powers JP, Jeffrey JL (2020). Discovery of Potent and Selective 7-Azaindole Isoindolinone-Based PI3K γ Inhibitors. *ACS Med Chem Lett* 11(11): 2244-2252. doi: 10.1021/acsmedchemlett.0c00387
111. Harding SD, Faccenda E, Southan C, Pawson AJ, Maffia P, Alexander SPH, Davenport AP, Fabbro D, Levi-Schaffer F, Spedding M, Davies JA (2020). The IUPHAR Guide to Immunopharmacology: connecting immunology and pharmacology. *Immunology* 160(1): 10-23. doi: 10.1111/imm.13175
112. Winkler DG, Faia KL, DiNitto JP, Ali JA, White KF, Brophy EE, Pink MM, Proctor JL, Lussier J, Martin CM, Hoyt JG, Tillotson B, Murphy EL, Lim AR, Thomas BD, Macdougall JR, Ren P, Liu Y, Li LS, Jessen KA, Fritz CC, Dunbar JL, Porter JR, Rommel C, Palombella VJ, Changelian PS, Kutok JL (2013). PI3K-delta and PI3K-gamma inhibition by IPI-145 abrogates immune responses and suppresses activity in autoimmune and inflammatory disease models. *Chem Biol* 20(11): 1364-1374. doi: 10.1016/j.chembiol.2013.09.017
113. Mardh CK, Root J, Uddin M, Stenvall K, Malmgren A, Karabelas K, Thomas M (2017). Targets of Neutrophil Influx and Weaponry: Therapeutic Opportunities for Chronic Obstructive Airway Disease. *J Immunol Res* 2017: 5273201. doi: 10.1155/2017/5273201
114. Norman P (2014). Evaluation of WO2013136076: two crystalline forms of the phosphatidylinositol 3-kinase-delta inhibitor RV-1729. *Expert Opin Ther Pat* 24(4): 471-475. doi: 10.1517/13543776.2014.865725
115. Sadiq MW, Asimus S, Kristensson C, Hagberg A, Mäenpää J, Valastro B, Fuhr R, Koernicke T, Keen C, Brailsford W, Betts J (2019). Safety, tolerability and pharmacokinetics (PK) of AZD8154 (a selective PI3K δ inhibitor) after single ascending inhaled doses in healthy volunteers. *Eur Respir J* 54(suppl 63): PA4220. doi: 10.1183/13993003.congress-2019.PA4220
116. Thomas MJ, Smith A, Head DH, Milne L, Nicholls A, Pearce W, Vanhaesebroeck B, Wymann MP, Hirsch E, Trifilieff A, Walker C, Finan P, Westwick J (2005). Airway inflammation: chemokine-induced neutrophilia and the class I phosphoinositide 3-kinases. *Eur J Immunol* 35(4): 1283-1291. doi: 10.1002/eji.200425634
117. Puri KD, Doggett TA, Huang CY, Douangpanya J, Hayflick JS, Turner M, Penninger J, Diacovo TG (2005). The role of endothelial PI3K γ activity in neutrophil trafficking. *Blood* 106(1): 150-157. doi: 10.1182/blood-2005-01-0023
118. Yum HK, Arcaroli J, Kupfner J, Shenkar R, Penninger JM, Sasaki T, Yang KY, Park JS, Abraham E (2001). Involvement of phosphoinositide 3-kinases in neutrophil activation and the development of acute lung injury. *J Immunol* 167(11): 6601-6608. doi: 10.4049/jimmunol.167.11.6601
119. Miyahara T, Hamanaka K, Weber DS, Drake DA, Anghelescu M, Parker JC (2007). Phosphoinositide 3-kinase, Src, and Akt modulate acute ventilation-induced vascular permeability increases in mouse lungs. *Am J Physiol Lung Cell Mol Physiol* 293(1): L11-21. doi: 10.1152/ajplung.00279.2005
120. Ong E, Gao XP, Predescu D, Broman M, Malik AB (2005). Role of phosphatidylinositol 3-kinase-gamma in mediating lung neutrophil sequestration and vascular injury induced by E. coli sepsis. *Am J Physiol Lung Cell Mol Physiol* 289(6): L1094-1103. doi: 10.1152/ajplung.00179.2005



Metabolic Aspects of Anthracycline Cardiotoxicity

Michele Russo, PhD¹

Angela Della Sala, MS¹

Carlo Gabriele Tocchetti, MD, PhD, FISC, FHFA^{2,3,4}

Paolo Ettore Porporato, PhD¹

Alessandra Ghigo, PhD^{1,*} 

Address

^{*1}Department of Molecular Biotechnology and Health Sciences, Molecular Biotechnology Center, University of Torino, Torino, Via Nizza 52, 10126, Torino, Italy
Email: Alessandra.ghigo@unito.it

²Department of Translational Medical Sciences, Federico II University, Naples, Italy

³Interdepartmental Center of Clinical and Translational Sciences (CIRCET), Federico II University, Naples, Italy

⁴Interdepartmental Hypertension Research Center (CIRIAPA), Federico II University, Naples, Italy

© The Author(s) 2021

Michele Russo and Angela Della Sala contributed equally to this work.
This article is part of the Topical Collection on *Cardio-oncology*

Keywords Cardiotoxicity · Cardiac metabolism · Doxorubicin

Opinion statement

Heart failure (HF) is increasingly recognized as the major complication of chemotherapy regimens. Despite the development of modern targeted therapies such as monoclonal antibodies, doxorubicin (DOXO), one of the most cardiotoxic anticancer agents, still remains the treatment of choice for several solid and hematological tumors. The insurgence of cardiotoxicity represents the major limitation to the clinical use of this potent anticancer drug. At the molecular level, cardiac side effects of DOXO have been associated to mitochondrial dysfunction, DNA damage, impairment of iron metabolism, apoptosis, and autophagy dysregulation. On these bases, the antioxidant and iron chelator molecule, dexrazoxane, currently represents the unique FDA-approved cardioprotectant for patients treated with anthracyclines.

A less explored area of research concerns the impact of DOXO on cardiac metabolism. Recent metabolomic studies highlight the possibility that cardiac metabolic alterations may critically contribute to the development of DOXO cardiotoxicity. Among these, the impairment of oxidative phosphorylation and the persistent activation of glycolysis, which are commonly observed in response to DOXO treatment, may undermine the ability of cardiomyocytes to meet the energy demand, eventually leading to energetic failure. Moreover, increasing evidence links DOXO cardiotoxicity to imbalanced insulin signaling and to cardiac insulin resistance.

Published online: 05 February 2021

Although anti-diabetic drugs, such as empagliflozin and metformin, have shown interesting cardioprotective effects *in vitro* and *in vivo* in different models of heart failure, their mechanism of action is unclear, and their use for the treatment of DOXO cardiotoxicity is still unexplored.

This review article aims at summarizing current evidence of the metabolic derangements induced by DOXO and at providing speculations on how key players of cardiac metabolism could be pharmacologically targeted to prevent or cure DOXO cardiomyopathy.

Introduction

Doxorubicin (DOXO) is a highly effective chemotherapeutic drug belonging to non-selective class I anthracycline family [1], widely used for the treatment of several cancers, such as solid tumors, acute leukemia, lymphomas, and breast cancer [2, 3]. However, its clinical use is hampered by its cumulative and irreversible cardiotoxicity, which leads to myocardial dysfunction manifesting as aberrant arrhythmias, ventricular dysfunction, and congestive heart failure, even years after chemotherapy cessation [4–6].

As the number of cancer survivors is steadily increasing, the long-term side effects of DOXO administration are becoming ever more apparent [7]. Despite the exponential growth of the field of cardio-oncology in the last decade, the molecular mechanisms underlying DOXO-induced cardiotoxicity have not been fully elucidated yet [8]. The finding that antioxidants fail to prevent DOXO-induced cardiotoxicity has challenged the classical view according to which oxidative stress is the main determinant of the cardiac side effects of DOXO, suggesting the involvement of additional mechanisms [8, 9]. Among the theories that have been proposed are mitochondrial dysfunction [10], DNA damage [11], defects in iron handling [10], apoptosis [12], and dysregulation of autophagy [13–15].

Although the exact mechanism of DOXO cardiotoxicity remains to be defined, mitochondrial damage and accumulation of dysfunctional mitochondria have been shown as key hallmarks of DOXO-induced cardiotoxic effects [13]. Mitochondria constitute around 50% of the cardiomyocyte volume and are vitally important for energy generation. As DOXO accumulates in the inner mitochondrial membrane by binding cardiolipin, this perturbs mitochondrial protein function and uncouples mitochondrial respiratory chain complexes, eventually impairing ATP

production [16]. Moreover, the ATP deficiency linked to DOXO cardiotoxicity has been directly correlated to alterations of mitochondrial energy metabolism and bioenergetics.

The myocardium can fulfill the elevated metabolic requests thanks to an incredible metabolic flexibility according to which ATP can be generated starting from a variety of energy substrates such as glucose, fatty acids, and ketone bodies. Of note, build-up of each of these carbon sources is associated with increased rates of cardiovascular diseases [17], and, in general, metabolic dysregulations play a critical role in the pathophysiology of heart failure (HF) [18, 19].

The association between metabolic dysregulation and cardiotoxicity has been demonstrated with different cancer therapies, such as copanlisib in relapsed follicular lymphoma [20], nilotinib in chronic myelogenous leukemia [21, 22], and androgen deprivation (AD) in prostate cancer [17], which were found associated to glucose dysregulation and hyperglycemia, or increased cholesterol level. Multiple studies have shown that AD therapy consistently increase insulin resistance, total cholesterol, and the rate of incident diabetes mellitus leading to increased risk of myocardial infarction and sudden cardiac death [23, 24]. However, less is known about the cardiac metabolic dysregulations involved in DOXO cardiotoxicity. Important clues come from a recent clinical study conducted in breast cancer patients treated with anthracyclines [25•], where a metabolite profiling approach has been used to define the early metabolic changes associated with the development of cardiotoxicity. Patients who developed cardiotoxicity display changes in citric acid and aconitic acid, along with an increased level of purine and pyrimidine metabolites in the plasma, that may be related to the systemic DNA

damage induced by chemotherapy [25]. Of note, the identification of early metabolic changes as well as the measurement of circulating metabolites in the plasma could provide insight into the mechanisms associated with the development of DOXO cardiotoxicity.

In further support of the importance of exploring metabolic changes linked to DOXO treatment, there is growing evidence that drugs approved for the treatment of metabolic diseases, such as diabetes, could protect against anthracycline cardiotoxicity. Among them, two anti-diabetic agents, metformin (MET) and empagliflozin (EMPA), have shown promising results since, along with their glucose-lowering effects, they protect against the development of cardiometabolic diseases as well as DOXO-related cardiotoxicity [26, 27]. Moreover,

empagliflozin, a SGLT2 inhibitor, exhibits protective effects in DOXO-induced HF in mice without diabetes [27]. Taken together, these findings suggest that an improved understanding of the mechanisms underlying the regulation of cardiac metabolism in response to DOXO treatment may lead to the identification of novel pharmacological targets as well as the development of new strategies to prevent the cardiotoxic effects of DOXO in cancer patients.

Here, we focus on the description of the molecular processes governing cardiac metabolism whose deregulation has been linked to DOXO cardiotoxicity. Moreover, we discuss how the identification of key players of cardiac metabolism may be instrumental to improve and refine current therapeutic strategies.

DOXO cardiotoxicity and iron metabolism

Impairment of cellular iron metabolism has been suggested as a main source of reactive oxygen species (ROS) in DOXO-induced cardiotoxicity, a theory referred to as “ROS and iron hypothesis” [28, 29]. It has been demonstrated that inside the cell DOXO is reduced to a cytotoxic semiquinone radical (SQ) that is rapidly converted back to the original molecule using O_2 as an electron acceptor [30, 31]. This process leads to superoxide formation that is detoxicated in H_2O_2 , either spontaneously or by superoxide dismutase activity (Fig. 1). The cellular pool of chelatable and redox-active iron, defined as labile iron pool (LIP), strongly reacts with H_2O_2 , generating ROS through Fenton reaction. Furthermore, LIP can directly interact with DOXO, creating DOXO-Fe complexes that drive ROS production [32, 33]. In support of this evidence, it is reported that DOXO interferes with mechanisms involved in cellular iron homeostasis. First, DOXO modulates the mRNA maturation of transferrin receptor and ferritin, through irreversible inactivation of the RNA-binding activity of iron regulatory proteins 1 and 2 (IRP-1 and 2) (Fig. 1) [34, 35]. Moreover, DOXO disrupts the cellular localization of iron, increasing iron/ferritin binding in the cytosol [36] and reducing its release from cellular storages, such as mitochondria (Fig. 1) [35]. In agreement, a mouse model of hereditary hemochromatosis (HH), in which the lack of the *Hfe* gene drives an aberrant iron accumulation in the heart and other organs, is characterized by increased iron accumulation into mitochondria and high susceptibility to DOXO cardiotoxicity. Thus, in response to DOXO treatment, the cytosolic iron concentration is maintained at physiological levels through reduced mobilization of cellular storages and ferritin turnover, but its accumulation within mitochondria compromises mitochondrial iron metabolism [10]. Ichikawa et al. demonstrated, both in vitro and in vivo, that overexpression of the mitochondrial transporter ABCB8 facilitates the efflux of iron from mitochondria, reduces ROS production, and protects against DOXO-induced cardiotoxicity [10]. Iron accumulation into mitochondria has been linked to ferroptosis, a recently described form of iron-dependent cell

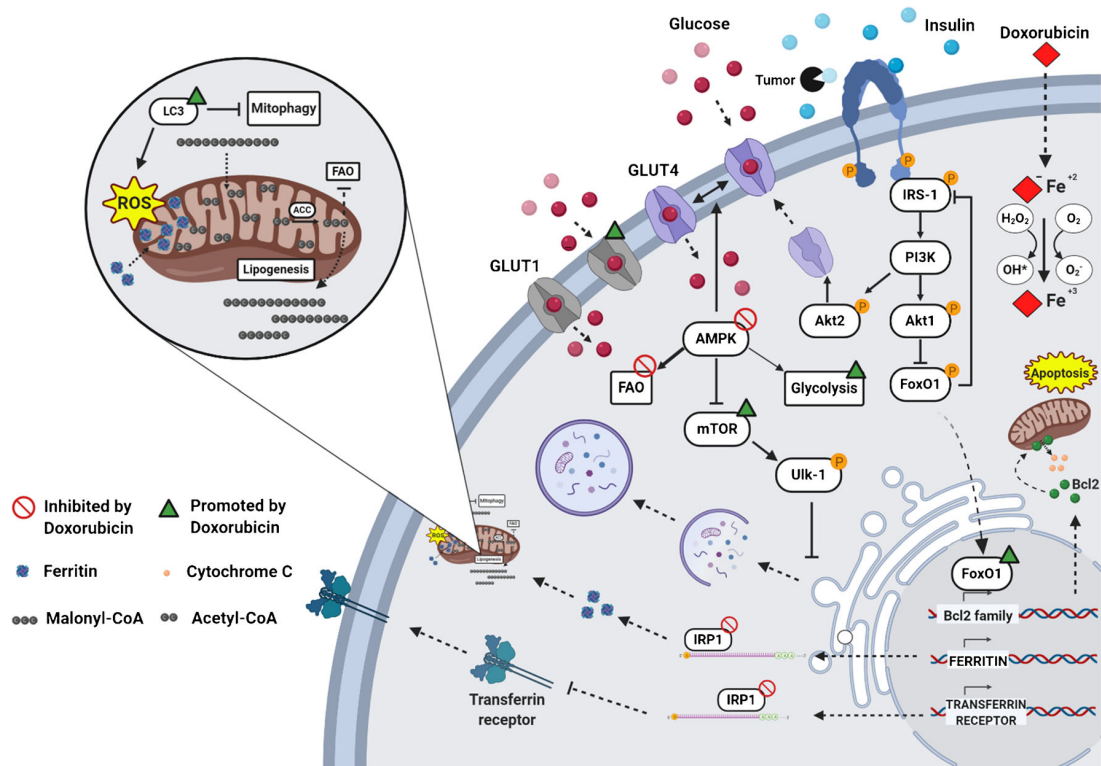


Fig. 1. Metabolic changes induced by DOXO in cardiomyocytes. DOXO interferes with Fe^{2+} metabolism, leading to activation of ferroptosis through ROS production, disruption of IRP-1 activity, and iron accumulation into mitochondria. These events are hallmarks of mitochondrial dysfunction that leads to a block of fatty acid oxidation (FAO) and an increase in glycolysis, as a consequence of AMPK inhibition. Acetyl-CoA carboxylase (ACC), a direct downstream target inhibited by AMPK, is overactivated and catalyzes the formation of Malonyl-CoA, blocking FAO irreversibly. At the plasma membrane, DOXO promotes glucose uptake via GLUT4 through insulin-mediated activation of AMPK and AKT2. In addition, DOXO increases the expression of GLUT1, an insulin-independent glucose transporter, normally absent in the adult heart. Following the insulin desensitization induced by tumor-secreted factors, AKT1 signaling is disrupted and promotes FOXO1 nuclear translocation, inducing the activation of the apoptotic pathway through the expression of pro-apoptotic members of the Bcl-2 family. Finally, DOXO cardiotoxicity has been linked to autophagy dysregulation. DOXO inhibits autophagy by activating mTOR or by blocking AMPK, resulting in accumulation of undegraded autophagosomes and mitochondrial dysfunction with increased production of ROS. This figure was created with [BioRender.com](https://www.biorender.com).

death, which is morphologically, biochemically, and genetically distinct from apoptosis, necrosis, and autophagy. Ferroptosis is featured by mitochondria iron accumulation and lipid peroxidation [37] and has been previously associated with other pathologies, such as cancer [38], stroke [39], and ischemia/reperfusion injuries [40]. Fang and colleagues revealed for the first time the role of ferroptosis in DOXO-induced cardiomyopathy. Mice defective for canonical activators of necroptosis or apoptosis or both, *Ripk3* $^{-/-}$, *Mlkl* $^{-/-}$, or *Fadd* $^{-/-}$ -*Mlkl* $^{-/-}$ respectively, showed typical hallmarks of ferroptosis in cardiomyocytes after DOXO administration. This study demonstrates that ferroptosis is triggered by heme oxygenase-1-mediated heme degradation through an Nrf2-dependent mechanism that drastically induces iron overload into mitochondria and ferroptosis activation [41].

Strategies to reduce iron accumulation into mitochondria in response to DOXO, using, for example, iron chelators, have been explored. Dexrazoxane is the unique molecule approved by FDA for the treatment of DOXO cardiotoxicity, for its dual activity as inhibitor of topoisomerase 2 β (Top-2 β) [42] and iron chelator [41]. By limiting mitochondria iron accumulation in cardiomyocytes [41], dexrazoxane prevents the activation of apoptotic and ferroptotic pathways. Nevertheless, several side effects have been linked to the use of dexrazoxane, including the development of secondary malignancies, myelosuppression [43], and reduction of DOXO antitumoral efficacy as a consequence of the inhibition of the topoisomerase 2 isoform expressed in cancer cells, Top-2 α [44, 45]. Nowadays, some of dexrazoxane-associated side effects have been retracted [46, 47], and further studies elucidate that the cardioprotective effect of dexrazoxane is mainly linked to its inhibition of Top-2 β than its iron-chelating property [48].

On the other hand, specific iron chelators, such as deferiprone [10], deferoxamine [49], and deferasirox [50], failed to counteract DOXO-mediated cardiotoxicity, probably due to their limited lipophilic properties and accessibility to iron mitochondrial storage [51]. Instead, a mild protection against DOXO toxicity has been documented with the small lipophilic iron chelator pyridoxal isonicotinoyl hydrazone and its analogue [52]. Interestingly, the ferroptosis inhibitor ferrostatin-1 has been proved to reduce iron-mediated lipid peroxidation [53, 54]. Mice treated with ferrostatin-1 are protected against DOXO-induced cardiotoxicity, suggesting the use of this molecule as a valid alternative to dexrazoxane [41]. Overall, this evidence suggests that specific iron chelator molecules fail to show a significant cardioprotective effect, likely because of their inability to reach iron storage into mitochondria. In this scenario, the inhibition of ferroptosis may represent a new promising approach to target one of the multiple mechanisms driving DOXO cardiotoxicity.

Cardiac metabolic changes triggered by DOXO: a focus on fatty acid oxidation and glycolysis

Cardiac metabolism is a highly sophisticated mechanism that in physiological conditions uses fatty acids (FAs) as a major source for catabolic reactions while switching to glycolysis in response to several pathological insults [18]. Despite the glycolytic switch that represents an early compensatory event, persistent glucose usage eventually turns maladaptive and leads to energetic failure, where glycolysis and impaired mitochondrial function do not allow cardiomyocytes to meet the cellular energy demand [55]. Studies with animal models have shown that cardiac insulin resistance and metabolic modifications, such as reduced mitochondrial oxidation of glucose, lactate, and fatty acids, are putative early markers of heart stress [56]. In agreement, the inhibition of glucose uptake consequent to insulin signaling desensitization has been identified as one of the prevalent risk factors for HF, and disruption of physiological cardiac metabolism adaptation has been associated with worse prognosis [57]. Despite these observations, the use of insulin-sensitizing agents failed to show improvements in patients and, on the contrary, has been associated with potential risk of cardiac side effects [58]. In line with this evidence, Taegtmeier and co-workers

have proposed insulin resistance as a physiological adaptation to non-ischemic heart damage, protecting cardiomyocytes from substrate overload in dysregulated metabolic states [59]. Impairment of insulin signaling has been reported to reduce glucose uptake and activate fatty acid oxidation in an AMPK-dependent manner [60].

Similarly, cardiotoxic chemotherapeutic drugs have been shown to impair intracellular mechanisms controlling cardiac metabolism [61•]. Specifically, DOXO induces the systemic insulin resistance typical of type II diabetes, with augmented serum triglyceride and blood glucose levels [62, 63], and, at the same time, triggers massive cardiac glucose uptake [64, 65]. Furthermore, DOXO has been demonstrated to affect gene expression involved in aerobic fatty acid oxidation and anaerobic glycolysis (Fig. 1) [66].

A central role in this process is exerted by AMPK, the master sensor of cellular energy status, that acts as a “fuel gauge” [67]. AMPK triggers long-term catabolic pathways that generate ATP, including fatty acid oxidation and glycolysis, while downregulating processes that are dispensable for short-term cell survival, such as the biosynthetic metabolism that rapidly consumes the ATP pool [68]. DOXO-mediated disruption of AMPK drives metabolic disarrangements and cellular substrate overload [69]. Experimental evidence shows that DOXO-induced AMPK inhibition increases glucose uptake after 2 weeks of treatment [70], probably due to concomitant expression of GLUT1 [71], an insulin-independent glucose transporter normally absent in the adult heart. Furthermore, Malonyl-CoA overproduction by acetyl coenzyme A carboxylase (ACC), an enzyme directly inhibited by AMPK [72], irreversibly blocks FAO and increases lipid synthesis and accumulation (Fig. 1) [73]. In agreement, cardiomyocyte-specific overexpression of adipose triglyceride lipase limits FA accumulation and shows a beneficial effect on cardiac function after DOXO treatment [74].

Additionally, in response to cellular stress, AMPK inhibits the activity of enzymes that reduce and consume ATP, such as creatine kinase [75]. DOXO impairs the high-energy phosphate pool through direct inhibition of AMPK [72] and creatine kinase (CK) system [76], reducing the phosphocreatine-to-creatine (PCr/Cr), PCr-to-ATP (PCr/ATP), and ATP-to-ADP (ATP/ADP) ratios [77]. In line with these observations, the recovery of AMPK activity exerts beneficial effect on mitochondria, reducing oxidative stress and preserving mitochondrial energy production [78].

The pivotal role of the AMPK pathway in the cardiac metabolic rearrangements induced by DOXO has been recently confirmed in cardiomyocytes derived from human-induced pluripotent stem cells (hi-PSCs), which have been established as a powerful model for drug toxicity screening on cells isolated from cancer patients under chemotherapy regimen [79••]. In these cells, impairment of gene modulating cardiac metabolism is one of the main effects of chemotherapeutic agents, including DOXO [80]. The use of specific AMPK-inducing agents was proven effective in counteracting the bioenergetic failure linked to the use of trastuzumab [80] and might be a new strategy to counteract the development of cardiotoxicity during chemotherapy regimens. Among these AMPK-restoring agents is metformin, a hypoglycemic drug used to treat patients with type 2 diabetes, which is known to trigger the AMPK pathway in insulin-sensitive organs, such as the heart [81]. Notably, several studies have reported the cardioprotective effects of metformin against DOXO-induced

toxicity [26, 82, 83]. Furthermore, metformin also displays an AMPK-dependent antitumoral activity [84], which makes this molecule a new promising agent to treat patients that suffer both HF and cancer.

Importantly, cancer and cardiovascular diseases are known to share several risk factors, including aging, smoking, overweight, and physical inactivity, but whether these two disease conditions are directly linked is still to be defined [48, 85]. In this context, metabolic diseases have emerged as a common risk factor for both cancer and heart failure [86–89]. Moreover, a clinical study has reported that patients with comorbidities, such as diabetes, dyslipidemia, and obesity, exhibit higher incidence of DOXO-related cardiotoxicity [9]. All these indications suggest that metabolic diseases affect the clinical outcome of patients subjected to DOXO treatment. In this context, insulin signaling plays a fundamental role, in modulating both heart metabolism and cancer growth, with AMPK being one of the main regulators.

In the following paragraph, we will describe how advanced cancer itself dramatically interferes with the cardiac insulin pathway further exacerbating drug-induced toxicity.

Insulin resistance at the crossroad of tumor growth and DOXO cardiotoxicity

Metabolic diseases, such as obesity and diabetes, significantly increase the incidence of HF in patients, where insulin resistance is a common risk factor. Insulin desensitization occurring in this state drastically reduces the important effects of insulin on cardiac tissue. Insulin receptor is widely expressed on the surface of many cell types, including cardiomyocytes, where upon ligand binding and insulin receptor substrates (IRS) 1 and 2 are recruited. IRS1 more than IRS2 is fundamental for regulation of the PI3K/Akt pathway and the MAP kinase cascade, such as ERK, both involved in the control of metabolism and cell survival [90]. Three members of the AKT family are known, AKT1, AKT2, and AKT3, but how these isoforms differentially contribute to cardiac cell function is not completely clear. It has been established that AKT1 is required for cardiomyocyte survival, while AKT2 is essential for the modulation of genes involved in cardiac metabolism. Indeed, AKT2 promotes glucose uptake through the mobilization and fusion of GLUT4-containing vesicles to the plasma membrane (Fig. 1) [90]. Despite the role of AKT during cardiac stress condition is still debated, it is reported that short-term AKT activation may exert cardioprotective effects, enhancing glycolysis and reducing oxidative phosphorylation. Controversially, chronic and long-term activity of AKT1 in the adult heart is associated with high risk of cardiac complications and reduced mitochondrial functions. Following insulin stimulation, AKT1 phosphorylates and blocks FOXO1 nuclear translocation, inhibiting the expression of pro-apoptotic proteins belonging to the Bcl-2 family (Fig. 1) [91]. FOXO1 has emerged as one of the key players in chronic metabolic diseases, promoting hyperglycemia and glucose intolerance [92]. In physiological conditions, pro-survival stimuli was induced by insulin repress FOXO1 activity through PI3K/AKT1 pathway. Following stress stimuli, FOXO1 translocates in the nucleus

and induces a negative feedback on insulin pathway through a JNK-dependent mechanism that drastically reduces IRS-1 activity (Fig.1) [93].

Although the imbalance of insulin signaling has been extensively studied in several models of obesity and type 2 diabetes, only a few studies have addressed its role in DOXO-induced cardiotoxicity, and the underlying molecular mechanisms are still poorly understood. Recent studies demonstrate that aberrant FOXO1 activity is responsible of DOXO-induced cardiotoxicity and its specific pharmacological targeting has been shown to ameliorate the cardiac outcome [94, 95].

In addition to chemotherapy, the tumor itself can negatively affect cardiac insulin signaling. Interestingly, Thackeray et al. have reported that advanced cancer contributes to the impairment of cardiac insulin signaling through secretion of insulin-degrading enzymes, massive glucose adsorption, and reduced production of pancreatic insulin. In this scenario, other cancer-mediated mechanisms, such as promotion of proteolysis by ubiquitin-proteasome and autophagy-related lysosomal pathways, mitochondrial dysfunction, impairment of catabolism and anabolism reactions, and release of the proinflammatory cytokines such as IL-6 and TNF- α [96, 97], further contribute to increasing the risk of heart failure development [91]. In agreement with the well-established pro-survival role of insulin-stimulated AKT1 pathway in cardiomyocytes, administration of low-dose insulin rescues cardiac function in tumor-bearing mice by restoring AKT signaling and autophagy inhibition in cardiomyocytes, without affecting cancer glucose uptake [98••]. Furthermore, expression of a constitutively active form of AKT1 by adenoviral vector prevents heart damage and protects mice from DOXO-induced cardiotoxicity [99], suggesting that the lack of insulin-mediated AKT1 activation during cancer progression could aggravate the cardiotoxicity induced by DOXO. In agreement, previous report shows that insulin depletion is associated with increased accumulation of DOXO into the heart and reduced cardiac function [100].

In addition to defective insulin signaling, the massive glucose uptake by the tumor can deprive cardiac cells of a pivotal energetic source during stress conditions [98]. Particularly, as described by Warburg in 1920, malignant cells based their energy production on the use of glycolysis and generate lactate. This metabolic adaptation, called "Warburg effect", confers the ability to cancer cells to survive in several stress conditions, including anaerobic environment of solid tumor inner mass. In this scenario, the use of 2-deoxyglucose (2-DG), a glucose analogue which blocks glycolysis, represent an interesting therapeutic strategy to treat cancer. 2-DG is phosphorylated to 2-DG-6-P inside the cell by hexokinase and cannot be further metabolized. It is thought that 2-DG-6-P competes with glucose utilization into glycolysis and drastically reduces energy production of cancer cells. Moreover, despite that 2-fluorodeoxy-D-glucose is a more potent glycolysis inhibitor, the main effect of 2-DG is the inhibition of N-linked glycosylation process, causing its high structural similarity to Mannose. The block of oligosaccharide formation required for the assembling of structural lipids and maturation of glycoproteins has been observed to induce tumor cells' death even in aerobic condition [101, 102]). Moreover, further studies were conducted to investigate the combining of 2-DG with others antineoplastic agents. In vivo evidence established that 2-DG co-treatment with adriamycin or paclitaxel increased their antitumoral efficacy against osteosarcoma and non-small cell lung cancers [103]. Previous work showed that caloric restriction

treatment based on the administration of 2-DG prevents DOXO-mediated cardiotoxicity through several mechanisms, including activation of AMPK-dependent mechanism [104].

Of note, the targeted therapy with a 2-DG-based adriamycin complex showed promising results, by specifically targeting tumor growth and, at the same time, limiting the organ toxicity of anthracyclines *in vivo* [105]. Overall, these findings suggest that the tumor itself negatively impacts on cardiac function through secreted factors that act in an endocrine manner and identify dysregulation of the cardiac insulin pathway as a major mechanism whereby the tumor negatively affects cardiac cell survival (Fig. 1).

Autophagy at the crossroad of metabolism and cell survival in DOXO cardiotoxicity

Autophagy is a highly conserved process which is aimed to maintain cell and tissue homeostasis, promoting the elimination of damaged and long-lived organelles and misfolded proteins under both physiological and pathological conditions [106, 13]. Importantly, autophagy plays an essential role in the regulation of cellular metabolism, both in normal conditions and in the setting of energy depletion, since it has been involved in the regulation and mobilization of energy stores, such as lipids and glycogen [107]. Accumulating evidence indicates that the cardiac side effects of DOXO may be closely related to a dysregulation of autophagy signaling and an imbalance in cellular metabolism, leading to intracellular Ca^{2+} accumulation, energy depletion, and mitochondrial dysfunction [108]. However, there is still controversy on whether DOXO inhibits or activates autophagy and whether autophagy activation has a beneficial or maladaptive role in this process [14].

Several studies have revealed that DOXO interferes with the initiation of the autophagic process by modulating the two main regulatory pathways [109], AMPK and mammalian target of rapamycin (mTOR). AMPK and mTOR promote and inhibit autophagy, respectively, by finely regulating the activity of the autophagy activating kinase Ulk-1 (Fig. 1). AMPK is the main metabolic sensor of the cell and is sensitive to changes in AMP:ATP ratio that is indicative of the cellular energy state. In low energy state, activation of AMPK relieves mTOR-inhibition of ULK1, leading to induction of autophagy [110]. Conversely, in the presence of high levels of energy substrates, AMPK activity is antagonized by mTOR which inhibits autophagy [111].

It has been shown that cardiac AMPK is inhibited in response to DOXO [72, 112]. Although the exact mechanism of such regulation remains elusive, re-activation of AMPK has been proposed as a therapeutic strategy to counteract DOXO-induced HF, and the cardioprotective effects of this approach have been linked to reactivation of autophagy [113]. Importantly, promoting a negative energy balance before DOXO treatment, i.e., via starvation or exercise, restores AMPK signaling and autophagy and ultimately reduces DOXO-induced cardiotoxicity [114]. For instance, dietary restriction in rats treated with DOXO modulates the ATP:AMP ratio inducing AMPK activation, increasing fatty acid oxidation rates and ATP levels, and ultimately leads to improved cardiac function [115]. In addition, AMPK activation, and the ensuing reduction in

apoptosis and increase in autophagy, was further achieved in DOX-treated rat neonatal cardiomyocytes with the caloric restriction mimetic 2-deoxyglucose [104].

Mitochondrial dysfunction at the interplay of autophagy and metabolism

The exact link between autophagy and metabolism regulation in the pathogenic sequelae of DOXO cardiomyopathy is still to be defined. However, the prevailing view is that DOXO-induced mitochondrial dysfunction and the ensuing production of reactive oxygen species stand at the crossroad of these two cellular processes. As a consequence of its accumulation within mitochondria, DOXO uncouples mitochondrial respiratory chain complexes, eventually impairing ATP production [16]. In keeping with this model, cardiomyocytes exposed to DOXO exhibit low levels of ATP associated with dysregulation of autophagy [116]. Thus, DOXO cardiotoxicity directly contributes to ATP deficiency, altering mitochondrial energy metabolism and bioenergetics [117], even though it is still debated whether ATP deficiency is the trigger or the result of autophagy deregulation.

Compelling evidence reveals that mitochondrial autophagy or mitophagy is defective in models of DOXO-induced cardiotoxicity [118]. DOXO disrupts cardiac mitochondrial autophagy by inhibiting lysosomal biogenesis and fusion with autophagosomes, thus preventing proper digestion of damaged mitochondria engulfed by autophagosomes [119, 120]. Recently, a comprehensive study by Abdullah et al. showed a direct association between autophagy dysregulation and defects in mitochondrial respiration in the development of DOXO-associated cardiomyopathy [118••]. In this study, both in vivo and in vitro analyses showed that DOXO cardiotoxicity results in a gradual accumulation of autophagosomes (Fig. 1); DOXO-induced autophagosome accumulation, in turn, results in altered expression of proteins involved in the regulation of mitochondrial dynamics and oxidative phosphorylation (OXPHOS and PDH proteins) and in mitochondrial respiratory dysfunction [118••]. Mitochondria isolated from both DOXO-treated hearts and intact neonatal cardiomyocytes exposed to DOXO show decreased oxygen consumption rate, indicating a suppression of mitochondrial bioenergetics [118••]. Such mitochondrial dysfunction could result from defects in mitochondrial substrate uptake or in the activity of the entire TCA cycle, causing cardiomyocyte death by ATP deprivation.

In agreement, another study reports that DOXO-treated cardiomyocytes exhibit decreased levels of ATP which, in turn, activate autophagy [121]. This study demonstrates that DOXO induces the production of 4-hydroxynonenal (4-HNE), a product of lipid peroxidation which is toxic to the heart and that mediates autophagy activation through lipid peroxidation-derived aldehydes [121]. On the other hand, DOXO reduces the expression of the mitochondrial aldehyde dehydrogenase (ALDH2) [122], which has been shown to mediate cardioprotective effects by reducing the production of 4-HNE and ROS [123, 124]. ALDH2 controls 4-HNE-induced autophagy via the regulation of AMPK-Akt-mTOR-signaling pathway. The ALDH2 activator Alda-1 was shown to prevent DOXO effects in neonatal cardiomyocytes, such as downregulation of Akt phosphorylation and upregulation of autophagy

proteins like Beclin-1, Atg5, and LC3-II [121]. In further support of a link between ALDH2 and autophagy regulation in response to DOXO, the autophagy inducer rapamycin could abolish the protective action of Alda-1 against DOXO-induced cardiomyocyte dysfunction, whereas the autophagy inhibitor 3-MA reduced DOXO cardiotoxicity [121]. A similar study by Ge et al. demonstrated that ALDH2 knock-in mice treated with DOXO had better cardiac function compared to DOXO-treated wild-type mice [125]. Taken together, these results suggest that promoting ALDH2 expression and inhibition of 4-HNE-induced autophagy may be a plausible approach to reduce DOXO-induced cardiac dysfunction.

Another possible link between mitochondrial metabolism dysfunction and autophagy dysregulation in DOXO-induced cardiotoxicity could be represented by intracellular calcium signaling [126, 127]. Decuyper et al. reported intracellular Ca^{2+} as one of the regulators of autophagy [128]. In healthy conditions, intracellular Ca^{2+} signaling suppresses autophagy, while under stress conditions and low energy production Ca^{2+} signaling is enhanced and stimulates autophagy. It has been reported that DOXO perturbs the expression of Ca^{2+} -handling proteins and alters Ca^{2+} homeostasis, causing mitochondrial dysfunction and apoptosis in the myocardium [126]. By disrupting Ca^{2+} handling, DOXO dysregulates autophagy in human cardiac progenitor cells (hCPCs), which are important regulators of myocardial homeostasis [127]. In hCPCs, the cytotoxic effects of DOXO induce abnormal cytosolic Ca^{2+} accumulation which, in turn, disrupts mTOR-mediated regulation of autophagy. Additionally, DOXO reduces the expression of the autophagosome marker LC3 and of an anti-senescence marker, SMP30, leading to reduced autophagosome formation and cellular viability, respectively [127]. Accordingly, autophagy activation with the mTOR inhibitor rapamycin rescues DOXO cardiotoxicity in hCPCs, with a significant reduction in DOXO-mediated cytosolic Ca^{2+} accumulation and restored autophagosome formation as well as SMP30 expression [127].

Rapamycin has been also shown to alleviate the autophagic interruption mediated by insulin-like growth factor II receptor α (IGF-IIR α) in DOXO-treated H9c2 cells [129]. IGF-IIR α is a novel stress-inducible contributor to cardiac damage which has been linked to DOXO-induced oxidative stress and autophagy alteration [129]. Interestingly, IGF-IIR α overexpression in combination with DOXO treatment increases LC3 expression and perturbs autophagosomal formation, impairing autophagy both in vitro in H9c2 cells and in vivo in transgenic rat models [129].

Overall, these findings suggest that DOXO-mediated dysregulation of autophagy drives mitochondrial dysfunction via different cytosolic and mitochondrial signaling axes and that restoring autophagy may be a valuable therapeutic approach to target DOXO toxicity.

Metabolic agents as potential strategies to restore autophagy in DOXO cardiotoxicity

Currently, there are no specific treatments for DOXO cardiotoxicity, and cancer patients experiencing cardiac issues are primarily treated with standard heart failure medications, such as renin angiotensin system

blockers and beta blockers. As discussed above, reactivation of AMPK has been proposed as a therapeutic option to treat heart failure associated with different metabolic diseases. Intriguingly, the anti-diabetic drug and AMPK activator, metformin, has been shown to improve cardiac function in a diabetic OVE26 mouse model by increasing autophagy activity [130]. Consistent with these findings, Zilinyi and co-workers reported that co-administration of DOXO and metformin increases autophagic activity and confers cardioprotection in a rat model [26]. This study shows that metformin restores LC3 levels and induces AMPK autophagy initiation, leading to improved cardiac function and reduced DOXO cardiotoxicity [26].

Recently, new hypoglycemic drugs like SGLT2 inhibitors have been shown to restore DOXO-mediated dysregulation of autophagy and to improve cardiac function [131, 132•]. Among these, empagliflozin (EMPA) has showed important cardioprotective effects in both diabetic and non-diabetic *in vivo* models undergoing DOXO treatment [27]. Previous work with diabetic animal models treated with EMPA has led to the hypothesis that EMPA prevents heart failure by improving ATP generation and thereby enhancing cardiac efficiency [132•, 133]. Consistently, Zucker diabetic fatty rats treated with EMPA show enhanced cardiac autophagy via increased AMPK activation [132•]. Moreover, EMPA enhances the cardiac energy pool by increasing cardiac energy production from glucose and fatty acid oxidation, whereas it reduces the cardiac content of sphingolipids and glycerophospholipids, major factors contributing to insulin resistance-induced HF [132•]. Although the effects of EMPA in DOXO-induced cardiotoxicity are still under evaluation, preliminary results have shown improved cardiac function in mice treated with EMPA [27]. Of note, EMPA showed a protective effect against DOXO in H9C2 cells and in DOXO-treated mice [27]. From a mechanistic perspective, EMPA has been shown to increase blood ketone levels, as beta hydroxybutyrate (β OHB) which, in turn, improves cell viability and restores mitochondrial dysfunction, ultimately reducing ROS generation and increasing intracellular ATP levels in cardiomyocytes [27].

In conclusion, these observations unravel the possibility of repurposing metabolic drugs to restore autophagy and mitochondrial metabolism to treat or prevent DOXO cardiotoxicity.

The emerging role of gut microbiota-derived metabolites in DOXO cardiotoxicity

Gut microbiota has been shown to be implicated in several cardiovascular and metabolic diseases, such as atherosclerosis [134], dyslipidemia [135], hypertension [136], chronic kidney disease [137], obesity [138], type I [139] and type II [140] diabetes mellitus, as well as HF [141]. The novel emerging approach of metagenomic has permitted to identify new species of bacteria colonizing human gut that were not able to be cultured *in vitro* [142] and allowed to compare the gut microbiota

composition in patients with HF [141]. It is now well accepted that microbiota-derived metabolites from dietary metabolism influence the pathogenesis of cardiometabolic disorders [143]. These molecules are secreted, degraded, or modified by different metabolic pathways active in intestinal bacteria and can directly or indirectly affect the organism, demonstrating how the gut microbiome can be considered a new and independent endocrine organ in the host [144]. Among the most important metabolites produced by gut microbiota, short chain fatty acids including acetate, propionate, and butyrate have shown an interesting effect on cardiac function in animal models [145]. The cardioprotective effects of butyrate are primarily linked to its epigenetic action since it functions as a potent HDAC inhibitor, and HDAC inhibitors are known to protect the heart from maladaptive hypertrophy and ischemic injuries [146–149]. Furthermore, many studies conducted by Raphaëli and colleagues have elucidated the dual activity of butyrate and its prodrugs which, on the one hand, synergize the antitumoral activity of DOXO in cancer models and, on the other hand, protect the cardiomyocytes against DOXO-induced cardiotoxicity [150–152]. Recently, it has been demonstrated for the first time that *in vivo* oral administration of FBA, a novel synthetic derivative of butyrate, is able to protect the heart from DOXO-induced cardiotoxicity, preventing mitochondrial dysfunction [153]. Thus, the use of GUT-microbiota-derived metabolite as nutraceutical may represent a new promising therapeutic approach for DOXO cardiotoxicity.

Conclusion and future perspectives

The impact of major anticancer treatments on cardiac metabolism has long been ignored and only recently has started to be investigated. The emerging view is that cardiac metabolic alterations may be used not only as early markers of iatrogenic cardiac injury but also as targets for pharmacological interventions aimed at restraining the late-onset and chronic cardiotoxicity associated to the use of anthracyclines. In this scenario, repurposing metabolic drugs for the treatment of cardiotoxicity represents an intriguing approach. The new anti-diabetic drug empagliflozin has proven effective in reducing glucose blood levels and, at the same time, rescuing heart function. However, despite these promising cues, the molecular mechanisms behind the cardioprotective effects of empagliflozin are still mysterious since the putative molecular target of the drug, the sodium-glucose co-transporter-2, is not expressed in cardiomyocytes. Other molecules employed for the treatment of metabolic disorder, such as rosiglitazone, exhibited controversial clinical results [58], thus highlighting the need of further work to clarify these inconsistencies. On the other hand, compelling evidence is available in support of the use of metformin, especially given its dual ability to modulate cardiac metabolism on the one side and to induce cancer cell death in an AMPK-dependent manner on the other side. In perspective, the identification of new and previously undescribed players specifically involved in the metabolic adaptations induced by anthracyclines will pave the way towards the design of new therapeutics that may prevent cardiotoxicity without affecting the antineoplastic properties of the drug.

Acknowledgements

We gratefully acknowledge Enrico Bono for the help with figure preparation and Edoardo Bertero for helpful discussion.

Funding

Open access funding provided by Università degli Studi di Torino within the CRUI-CARE Agreement.

Compliance with Ethical Standards

Conflict of Interest

Michele Russo declares that he has no conflict of interest.

Angela Della Sala declares that she has no conflict of interest.

Carlo Gabriele Tocchetti has received compensation from Alere for service as a consultant and is listed as an inventor on 2 heart failure patents.

Paolo Ettore Porporato declares that he has no conflict of interest.

Alessandra Ghigo is a co-founder and stakeholder of Kither Biotech, a pharmaceutical product company focused on respiratory medicine not in conflict with statements made in this article.

Open Access

This article is licensed under a Creative Commons Attribution 4.0 International License, which permits use, sharing, adaptation, distribution and reproduction in any medium or format, as long as you give appropriate credit to the original author(s) and the source, provide a link to the Creative Commons licence, and indicate if changes were made. The images or other third party material in this article are included in the article's Creative Commons licence, unless indicated otherwise in a credit line to the material. If material is not included in the article's Creative Commons licence and your intended use is not permitted by statutory regulation or exceeds the permitted use, you will need to obtain permission directly from the copyright holder. To view a copy of this licence, visit <http://creativecommons.org/licenses/by/4.0/>.

References and Recommended Reading

Papers of particular interest, published recently, have been highlighted as:

- Of importance
- Of major importance

1. Carvalho C, Santos RX, Cardoso S, Correia S, Oliveira PJ, Santos MS, et al. Doxorubicin: the good, the bad and the ugly effect. *Curr Med Chem*. 2009;16(25):3267–85. <https://doi.org/10.2174/092986709788803312>.
2. Weiss RB. The anthracyclines: will we ever find a better doxorubicin? *Semin Oncol*. 1992;19(6):670–86.
3. Cortes-Funes H, Coronado C. Role of anthracyclines in the era of targeted therapy. *Cardiovasc Toxicol*. 2007;7(2):56–60. <https://doi.org/10.1007/s12012-007-0015-3>.
4. Singal PK, Li T, Kumar D, Danelisen I, Iliskovic N. Adriamycin-induced heart failure: mechanism and modulation. *Mol Cell Biochem*. 2000;207(1–2):77–86. <https://doi.org/10.1023/a:1007094214460>.
5. Cardinale D, Colombo A, Bacchiani G, Tedeschi I, Meroni CA, Veglia F, et al. Early detection of anthracycline cardiotoxicity and improvement with heart failure therapy. *Circulation*. 2015;131(22):1981–8. <https://doi.org/10.1161/CIRCULATIONAHA.114.013777>.
6. Colombo A, Cipolla C, Beggiato M, Cardinale D. Cardiac toxicity of anticancer agents. *Curr Cardiol Rep*.

- 2013;15(5):362. <https://doi.org/10.1007/s11886-013-0362-6>.
7. Ryan TD, Nagarajan R, Godown J. Cardiovascular toxicities in pediatric cancer survivors. *Cardiol Clin*. 2019;37(4):533–44. <https://doi.org/10.1016/j.ccl.2019.07.002>.
 8. Varricchi G, Ameri P, Cadeddu C, Ghigo A, Madonna R, Marone G, et al. Antineoplastic drug-induced cardiotoxicity: a redox perspective. *Front Physiol*. 2018;9:167. <https://doi.org/10.3389/fphys.2018.00167>.
 9. Vejpongsa P, Yeh ET. Prevention of anthracycline-induced cardiotoxicity: challenges and opportunities. *J Am Coll Cardiol*. 2014;64(9):938–45. <https://doi.org/10.1016/j.jacc.2014.06.1167>.
 10. Ichikawa Y, Ghanefar M, Bayeva M, Wu R, Khechaduri A, Naga Prasad SV, et al. Cardiotoxicity of doxorubicin is mediated through mitochondrial iron accumulation. *J Clin Invest*. 2014;124(2):617–30. <https://doi.org/10.1172/JCI72931>.
 11. Lyu YL, Kerrigan JE, Lin CP, Azarova AM, Tsai YC, Ban Y, et al. Topoisomerase IIbeta mediated DNA double-strand breaks: implications in doxorubicin cardiotoxicity and prevention by dexrazoxane. *Cancer Res*. 2007;67(18):8839–46. <https://doi.org/10.1158/0008-5472.CAN-07-1649>.
 12. Kobayashi S, Volden P, Timm D, Mao K, Xu X, Liang Q. Transcription factor GATA4 inhibits doxorubicin-induced autophagy and cardiomyocyte death. *J Biol Chem*. 2010;285(1):793–804. <https://doi.org/10.1074/jbc.M109.070037>.
 13. Koleini N, Kardami E. Autophagy and mitophagy in the context of doxorubicin-induced cardiotoxicity. *Oncotarget*. 2017;8(28):46663–80. <https://doi.org/10.18632/oncotarget.16944>.
 14. Sala V, Della Sala A, Hirsch E, Ghigo A. Signaling pathways underlying anthracycline cardiotoxicity. *Antioxid Redox Signal*. 2020;32(15):1098–114. <https://doi.org/10.1089/ars.2020.8019>.
 15. Mercurio V, Pirozzi F, Lazzarini E, Marone G, Rizzo P, Agnetti G, et al. Models of heart failure based on the cardiotoxicity of anticancer drugs. *J Card Fail*. 2016;22(6):449–58. <https://doi.org/10.1016/j.cardfail.2016.04.008>.
 16. Goormaghtigh E, Chatelain P, Caspers J, Ruysschaert JM. Evidence of a complex between adriamycin derivatives and cardiolipin: possible role in cardiotoxicity. *Biochem Pharmacol*. 1980;29(21):3003–10. [https://doi.org/10.1016/0006-2952\(80\)90050-7](https://doi.org/10.1016/0006-2952(80)90050-7).
 17. Grundy SM, Cleeman JJ, Daniels SR, Donato KA, Eckel RH, Franklin BA, et al. Diagnosis and management of the metabolic syndrome: an American Heart Association/National Heart, Lung, and Blood Institute Scientific Statement. *Circulation*. 2005;112(17):2735–52. <https://doi.org/10.1161/CIRCULATIONAHA.105.169404>.
 18. Bertero E, Maack C. Metabolic remodelling in heart failure. *Nat Rev Cardiol*. 2018;15(8):457–70. <https://doi.org/10.1038/s41569-018-0044-6>
- Broad overview of the physiological processes of cardiac energy metabolism and their pathological alterations in heart failure.
19. McGarrah RW, Crown SB, Zhang GF, Shah SH, Newgard CB. Cardiovascular metabolomics. *Circ Res*. 2018;122(9):1238–58. <https://doi.org/10.1161/CIRCRESAHA.117.311002>
- Discuss the current state of metabolomics, one of the newer omics technologies, emerged as a powerful tool for understanding the metabolic changes that occur in heart failure and ischemic heart disease.
20. Dreyling M, Santoro A, Mollica L, Leppa S, Follows GA, Lenz G, et al. Phosphatidylinositol 3-kinase inhibition by copanlisib in relapsed or refractory indolent lymphoma. *J Clin Oncol : official journal of the American Society of Clinical Oncology*. 2017;35(35):3898–905. <https://doi.org/10.1200/JCO.2017.75.4648>.
 21. Racil Z, Razga F, Drapalova J, Buresova L, Zackova D, Palackova M, et al. Mechanism of impaired glucose metabolism during nilotinib therapy in patients with chronic myelogenous leukemia. *Haematologica*. 2013;98(10):e124–6. <https://doi.org/10.3324/haematol.2013.086355>.
 22. Breccia M, Muscaritoli M, Gentilini F, Latagliata R, Carosino I, Rossi Fanelli F, et al. Impaired fasting glucose level as metabolic side effect of nilotinib in non-diabetic chronic myeloid leukemia patients resistant to imatinib. *Leuk Res*. 2007;31(12):1770–2. <https://doi.org/10.1016/j.leukres.2007.01.024>.
 23. Keating NL, O'Malley A, Freedland SJ, Smith MR. Diabetes and cardiovascular disease during androgen deprivation therapy: observational study of veterans with prostate cancer. *J Natl Cancer Inst*. 2012;104(19):1518–23. <https://doi.org/10.1093/jnci/djs376>.
 24. Oka R, Utsumi T, Endo T, Yano M, Kamijima S, Kamiya N, et al. Effect of androgen deprivation therapy on arterial stiffness and serum lipid profile changes in patients with prostate cancer: a prospective study of initial 6-month follow-up. *Int J Clin Oncol*. 2016;21(2):389–96. <https://doi.org/10.1007/s10147-015-0891-7>.
 25. Asnani A, Shi X, Farrell L, Lall R, Sebag IA, Plana JC, et al. Changes in citric acid cycle and nucleoside metabolism are associated with anthracycline cardiotoxicity in patients with breast cancer. *J Cardiovasc Transl Res*. 2019. <https://doi.org/10.1007/s12265-019-09897-y>
- Clinical study reporting the role in patients of early metabolic changes as insight into the mechanisms associated with the development of chemotherapy-associated cardiotoxicity.
26. Zilinyi R, Czompa A, Czeglédi A, Gajtko A, Pituk D, Lekli I, et al. The cardioprotective effect of metformin in doxorubicin-induced cardiotoxicity: the role of autophagy. *Molecules*. 2018;23(5):1184. <https://doi.org/10.3390/molecules23051184>
- Examine the protective role of metformin and its effect on autophagy in doxorubicin-induced cardiotoxicity.
27. Oh CM, Cho S, Jang JY, Kim H, Chun S, Choi M, et al. Cardioprotective potential of an SGLT2 inhibitor against doxorubicin-induced heart failure. *Korean Circ J*. 2019;49(12):1183–95. <https://doi.org/10.4070/kcj.2019.0180>
- First study reporting the cardioprotective effects of SGLT2 inhibitors in DOXO-induced HF in mice. Treatment with

- empagliflozin prevented the development of DOXO-cardiotoxicity by switching fuel consumption and activating autophagy.
28. Berthiaume JM, Wallace KB. Adriamycin-induced oxidative mitochondrial cardiotoxicity. *Cell Biol Toxicol.* 2007;23(1):15–25. <https://doi.org/10.1007/s10565-006-0140-y>.
 29. Myers C. The role of iron in doxorubicin-induced cardiomyopathy. *Semin Oncol.* 1998;25(4 Suppl 10):10–4.
 30. Keizer HG, Pinedo HM, Schuurhuis GJ, Joenje H. Doxorubicin (adriamycin): a critical review of free radical-dependent mechanisms of cytotoxicity. *Pharmacol Ther.* 1990;47(2):219–31. [https://doi.org/10.1016/0163-7258\(90\)90088-j](https://doi.org/10.1016/0163-7258(90)90088-j).
 31. Riddick DS, Lee C, Ramji S, Chinje EC, Cowen RL, Williams KJ, et al. Cancer chemotherapy and drug metabolism. *Drug Metab Dispos.* 2005;33(8):1083–96. <https://doi.org/10.1124/dmd.105.004374>.
 32. Xu X, Persson HL, Richardson DR. Molecular pharmacology of the interaction of anthracyclines with iron. *Mol Pharmacol.* 2005;68(2):261–71. <https://doi.org/10.1124/mol.105.013383>.
 33. Myers CE, Gianni L, Simone CB, Klecker R, Greene R. Oxidative destruction of erythrocyte ghost membranes catalyzed by the doxorubicin-iron complex. *Biochemistry.* 1982;21(8):1707–12. <https://doi.org/10.1021/bi00537a001>.
 34. Minotti G, Ronchi R, Salvatorelli E, Menna P, Cairo G. Doxorubicin irreversibly inactivates iron regulatory proteins 1 and 2 in cardiomyocytes: evidence for distinct metabolic pathways and implications for iron-mediated cardiotoxicity of antitumor therapy. *Cancer Res.* 2001;61(23):8422–8.
 35. Xu X, Sutak R, Richardson DR. Iron chelation by clinically relevant anthracyclines: alteration in expression of iron-regulated genes and atypical changes in intracellular iron distribution and trafficking. *Mol Pharmacol.* 2008;73(3):833–44. <https://doi.org/10.1124/mol.107.041335>.
 36. Kwok JC, Richardson DR. Anthracyclines induce accumulation of iron in ferritin in myocardial and neoplastic cells: inhibition of the ferritin iron mobilization pathway. *Mol Pharmacol.* 2003;63(4):849–61. <https://doi.org/10.1124/mol.63.4.849>.
 37. Stockwell BR, Friedmann Angeli JP, Bayir H, Bush AI, Conrad M, Dixon SJ, et al. Ferroptosis: a regulated cell death nexus linking metabolism, redox biology, and disease. *Cell.* 2017;171(2):273–85. <https://doi.org/10.1016/j.cell.2017.09.021>.
 38. Mou Y, Wang J, Wu J, He D, Zhang C, Duan C, et al. Ferroptosis, a new form of cell death: opportunities and challenges in cancer. *J Hematol Oncol.* 2019;12(1):34. <https://doi.org/10.1186/s13045-019-0720-y>.
 39. Tuo QZ, Lei P, Jackman KA, Li XL, Xiong H, Li XL, et al. Tau-mediated iron export prevents ferroptotic damage after ischemic stroke. *Mol Psychiatry.* 2017;22(11):1520–30. <https://doi.org/10.1038/mp.2017.171>.
 40. Linkermann A, Skouta R, Himmerkus N, Mulay SR, Dewitz C, De Zen F, et al. Synchronized renal tubular cell death involves ferroptosis. *Proc Natl Acad Sci U S A.* 2014;111(47):16836–41. <https://doi.org/10.1073/pnas.1415518111>.
 - 41.●● Fang X, Wang H, Han D, Xie E, Yang X, Wei J, et al. Ferroptosis as a target for protection against cardiomyopathy. *Proc Natl Acad Sci U S A.* 2019;116(7):2672–80. <https://doi.org/10.1073/pnas.1821022116>
- First evidence that inhibition of Ferroptosis protects from heart dysfunction.
42. Zhang S, Liu X, Bawa-Khalife T, Lu LS, Lyu YL, Liu LF, et al. Identification of the molecular basis of doxorubicin-induced cardiotoxicity. *Nat Med.* 2012;18(11):1639–42. <https://doi.org/10.1038/nm.2919>.
 43. Tebbi CK, London WB, Friedman D, Villaluna D, De Alarcon PA, Constine LS, et al. Dexrazoxane-associated risk for acute myeloid leukemia/myelodysplastic syndrome and other secondary malignancies in pediatric Hodgkin's disease. *J Clin Oncol.* 2007;25(5):493–500. <https://doi.org/10.1200/JCO.2005.02.3879>.
 44. Deng S, Yan T, Nikolova T, Fuhrmann D, Nemecek A, Godtel-Armbrust U, et al. The catalytic topoisomerase II inhibitor dexrazoxane induces DNA breaks, ATF3 and the DNA damage response in cancer cells. *Br J Pharmacol.* 2015;172(9):2246–57. <https://doi.org/10.1111/bph.13046>.
 45. Swain SM, Whaley FS, Gerber MC, Weisberg S, York M, Spicer D, et al. Cardioprotection with dexrazoxane for doxorubicin-containing therapy in advanced breast cancer. *J Clin Oncol.* 1997;15(4):1318–32. <https://doi.org/10.1200/JCO.1997.15.4.1318>.
 46. Reichardt P, Tabone MD, Mora J, Morland B, Jones RL. Risk-benefit of dexrazoxane for preventing anthracycline-related cardiotoxicity: re-evaluating the European labeling. *Future Oncol.* 2018;14(25):2663–76. <https://doi.org/10.2217/fon-2018-0210>.
 47. Seif AE, Walker DM, Li Y, Huang YS, Kavcic M, Torp K, et al. Dexrazoxane exposure and risk of secondary acute myeloid leukemia in pediatric oncology patients. *Pediatr Blood Cancer.* 2015;62(4):704–9. <https://doi.org/10.1002/pbc.25043>.
 48. Bures J, Jirkovska A, Sestak V, Jansova H, Karabanovich G, Roh J, et al. Investigation of novel dexrazoxane analogue JR-311 shows significant cardioprotective effects through topoisomerase IIbeta but not its iron chelating metabolite. *Toxicology.* 2017;392:1–10. <https://doi.org/10.1016/j.tox.2017.09.012>.
 49. Popelova O, Sterba M, Simunek T, Mazurova Y, Guncova I, Hroch M, et al. Deferiprone does not protect against chronic anthracycline cardiotoxicity in vivo. *J Pharmacol Exp Ther.* 2008;326(1):259–69. <https://doi.org/10.1124/jpet.108.137604>.
 50. Hasinoff BB, Patel D, Wu X. The oral iron chelator ICL670A (deferisirox) does not protect myocytes against doxorubicin. *Free Radic Biol Med.*

- 2003;35(11):1469–79. <https://doi.org/10.1016/j.freeradbiomed.2003.08.005>.
51. Zanninelli G, Glickstein H, Breuer W, Milgram P, Brisot P, Hider RC, et al. Chelation and mobilization of cellular iron by different classes of chelators. *Mol Pharmacol*. 1997;51(5):842–52. <https://doi.org/10.1124/mol.51.5.842>.
 52. Schroterova L, Kaiserova H, Baliharova V, Velik J, Gersl V, Kvasnickova E. The effect of new lipophilic chelators on the activities of cytosolic reductases and P450 cytochromes involved in the metabolism of anthracycline antibiotics: studies in vitro. *Physiol Res*. 2004;53(6):683–91.
 53. Miotto G, Rossetto M, Di Paolo ML, Orian L, Venerando R, Roveri A, et al. Insight into the mechanism of ferroptosis inhibition by ferrostatin-1. *Redox Biol*. 2020;28:101328. <https://doi.org/10.1016/j.redox.2019.101328>.
 54. Dixon SJ, Lemberg KM, Lamprecht MR, Skouta R, Zaitsev EM, Gleason CE, et al. Ferroptosis: an iron-dependent form of nonapoptotic cell death. *Cell*. 2012;149(5):1060–72. <https://doi.org/10.1016/j.cell.2012.03.042>.
 55. Stanley WC, Recchia FA, Lopaschuk GD. Myocardial substrate metabolism in the normal and failing heart. *Physiol Rev*. 2005;85(3):1093–129. <https://doi.org/10.1152/physrev.00006.2004>.
 56. Zhang L, Jaswal JS, Ussher JR, Sankaralingam S, Wagg C, Zaugg M, et al. Cardiac insulin-resistance and decreased mitochondrial energy production precede the development of systolic heart failure after pressure-overload hypertrophy. *Circ Heart Fail*. 2013;6(5):1039–48. <https://doi.org/10.1161/CIRCHEARTFAILURE.112.000228>.
 57. Witteles RM, Fowler MB. Insulin-resistant cardiomyopathy clinical evidence, mechanisms, and treatment options. *J Am Coll Cardiol*. 2008;51(2):93–102. <https://doi.org/10.1016/j.jacc.2007.10.021>.
 58. Nissen SE, Wolski K. Effect of rosiglitazone on the risk of myocardial infarction and death from cardiovascular causes. *N Engl J Med*. 2007;356(24):2457–71. <https://doi.org/10.1056/NEJMoa072761>.
 59. Taegtmeier H, Beauloye C, Harmancey R, Hue L. Insulin resistance protects the heart from fuel overload in dysregulated metabolic states. *Am J Physiol Heart Circ Physiol*. 2013;305(12):H1693–7. <https://doi.org/10.1152/ajpheart.00854.2012>.
 60. Long YC, Cheng Z, Copps KD, White MF. Insulin receptor substrates Irs1 and Irs2 coordinate skeletal muscle growth and metabolism via the Akt and AMPK pathways. *Mol Cell Biol*. 2011;31(3):430–41. <https://doi.org/10.1128/MCB.00983-10>.
 61. • Deidda M, Mercurio V, Cuomo A, Noto A, Mercurio G, Cadeddu DC. Metabolomic perspectives in anti-blastic cardiotoxicity and cardioprotection. *Int J Mol Sci*. 2019;20(19):4928. <https://doi.org/10.3390/ijms20194928>
- Recent overview that describes metabolomic approach as a potential and practical tool to investigate the impact of chemotherapy-induced cardiotoxicity.
62. Arunachalam S, Tirupathi Pichiah PB, Achiraman S. Doxorubicin treatment inhibits PPARgamma and may induce lipotoxicity by mimicking a type 2 diabetes-like condition in rodent models. *FEBS Lett*. 2013;587(2):105–10. <https://doi.org/10.1016/j.febslet.2012.11.019>.
 63. de Lima Junior EA, Yamashita AS, Pimentel GD, De Sousa LG, Santos RV, Goncalves CL, et al. Doxorubicin caused severe hyperglycaemia and insulin resistance, mediated by inhibition in AMPk signalling in skeletal muscle. *J Cachexia Sarcopenia Muscle*. 2016;7(5):615–25. <https://doi.org/10.1002/jcsm.12104>.
 64. •• Bauckneht M, Ferrarazzo G, Fiz F, Morbelli S, Sarocchi M, Pastorino F, et al. Doxorubicin effect on myocardial metabolism as a prerequisite for subsequent development of cardiac toxicity: a translational (18)F-FDG PET/CT observation. *J Nucl Med*. 2017;58(10):1638–45. <https://doi.org/10.2967/jnumed.117.191122>
- Translational study that indicates basal cardiac metabolism as predictive factor doxorubicin-induced cardiotoxicity.
65. Sambuceti G, Morbelli S, Cossu V, Marini C, Bauckneht M. Reply: doxorubicin effect on myocardial metabolism as a prerequisite for subsequent development of cardiac toxicity: are there unsuspected confounders? *J Nucl Med*. 2018;59(4):713–4. <https://doi.org/10.2967/jnumed.117.206797>.
 66. Carvalho RA, Sousa RP, Cadete VJ, Lopaschuk GD, Palmeira CM, Bjork JA, et al. Metabolic remodeling associated with subchronic doxorubicin cardiomyopathy. *Toxicology*. 2010;270(2–3):92–8. <https://doi.org/10.1016/j.tox.2010.01.019>.
 67. Hardie DG, Carling D. The AMP-activated protein kinase—fuel gauge of the mammalian cell? *Eur J Biochem*. 1997;246(2):259–73. <https://doi.org/10.1111/j.1432-1033.1997.00259.x>.
 68. Hardie DG. AMP-activated protein kinase: a master switch in glucose and lipid metabolism. *Rev Endocr Metab Disord*. 2004;5(2):119–25. <https://doi.org/10.1023/B:REMD.0000021433.63915.bb>.
 69. Gratia S, Kay L, Potenza L, Seffouh A, Novel-Chate V, Schnebelen C, et al. Inhibition of AMPK signalling by doxorubicin: at the crossroads of the cardiac responses to energetic, oxidative, and genotoxic stress. *Cardiovasc Res*. 2012;95(3):290–9. <https://doi.org/10.1093/cvr/cvs134>.
 70. Bulten BF, Sollini M, Boni R, Massri K, de Geus-Oei LF, van Laarhoven HWM, et al. Cardiac molecular pathways influenced by doxorubicin treatment in mice. *Sci Rep*. 2019;9(1):2514. <https://doi.org/10.1038/s41598-019-38986-w>.
 71. Hrelia S, Fiorentini D, Maraldi T, Angeloni C, Bordoni A, Biagi PL, et al. Doxorubicin induces early lipid peroxidation associated with changes in glucose transport in cultured cardiomyocytes. *Biochim Biophys Acta*. 2002;1567(1–2):150–6. [https://doi.org/10.1016/S0005-2736\(02\)00612-0](https://doi.org/10.1016/S0005-2736(02)00612-0).

72. Tokarska-Schlattner M, Zaugg M, da Silva R, Lucchinetti E, Schaub MC, Wallimann T, et al. Acute toxicity of doxorubicin on isolated perfused heart: response of kinases regulating energy supply. *Am J Physiol Heart Circ Physiol*. 2005;289(1):H37–47. <https://doi.org/10.1152/ajpheart.01057.2004>.
73. Long YC, Zierath JR. AMP-activated protein kinase signaling in metabolic regulation. *J Clin Invest*. 2006;116(7):1776–83. <https://doi.org/10.1172/JCI29044>.
74. Nagendran J, Kienesberger PC, Pulinilkunnil T, Zordoky BN, Sung MM, Kim T, et al. Cardiomyocyte specific adipose triglyceride lipase overexpression prevents doxorubicin induced cardiac dysfunction in female mice. *Heart*. 2013;99(14):1041–7. <https://doi.org/10.1136/heartjnl-2013-303843>.
75. Ponticos M, Lu QL, Morgan JE, Hardie DG, Partridge TA, Carling D. Dual regulation of the AMP-activated protein kinase provides a novel mechanism for the control of creatine kinase in skeletal muscle. *EMBO J*. 1998;17(6):1688–99. <https://doi.org/10.1093/emboj/17.6.1688>.
76. Gupta A, Rohlfen C, Leppo MK, Chacko VP, Wang Y, Steenbergen C, et al. Creatine kinase-overexpression improves myocardial energetics, contractile dysfunction and survival in murine doxorubicin cardiotoxicity. *PLoS One*. 2013;8(10):e74675. <https://doi.org/10.1371/journal.pone.0074675>.
77. Octavia Y, Tocchetti CG, Gabrielson KL, Janssens S, Crijns HJ, Moens AL. Doxorubicin-induced cardiomyopathy: from molecular mechanisms to therapeutic strategies. *J Mol Cell Cardiol*. 2012;52(6):1213–25. <https://doi.org/10.1016/j.yjmcc.2012.03.006>.
78. Liu D, Ma Z, Di S, Yang Y, Yang J, Xu L, et al. AMPK/PGC1 α activation by melatonin attenuates acute doxorubicin cardiotoxicity via alleviating mitochondrial oxidative damage and apoptosis. *Free Radic Biol Med*. 2018;129:59–72. <https://doi.org/10.1016/j.freeradbiomed.2018.08.032>.
- 79.●● Sharma A, McKeithan WL, Serrano R, Kitani T, Burridge PW, Del Alamo JC, et al. Use of human induced pluripotent stem cell-derived cardiomyocytes to assess drug cardiotoxicity. *Nat Protoc*. 2018;13(12):3018–41. <https://doi.org/10.1038/s41596-018-0076-8>
- Assessment of a new biological platform to investigate the drug-induced cardiotoxicity in human induced pluripotent stem cell-derived cardiomyocytes.
80. Cunha-Oliveira T, Ferreira LL, Coelho AR, Deus CM, Oliveira PJ. Doxorubicin triggers bioenergetic failure and p53 activation in mouse stem cell-derived cardiomyocytes. *Toxicol Appl Pharmacol*. 2018;348:1–13. <https://doi.org/10.1016/j.taap.2018.04.009>.
81. Musi N, Hirshman MF, Nygren J, Svanfeldt M, Bavenholm P, Rooyackers O, et al. Metformin increases AMP-activated protein kinase activity in skeletal muscle of subjects with type 2 diabetes. *Diabetes*. 2002;51(7):2074–81. <https://doi.org/10.2337/diabetes.51.7.2074>.
82. Asensio-Lopez MC, Sanchez-Mas J, Pascual-Figal DA, Abenza S, Perez-Martinez MT, Valdes M, et al. Involvement of ferritin heavy chain in the preventive effect of metformin against doxorubicin-induced cardiotoxicity. *Free Radic Biol Med*. 2013;57:188–200. <https://doi.org/10.1016/j.freeradbiomed.2012.09.009>.
- 83.●● Kitani T, Ong SG, Lam CK, Rhee JW, Zhang JZ, Oikonomopoulos A, et al. Human-induced pluripotent stem cell model of trastuzumab-induced cardiac dysfunction in patients with breast cancer. *Circulation*. 2019;139(21):2451–65. <https://doi.org/10.1161/CIRCULATIONAHA.118.037357>
- Evaluation of Trastuzumab-induced cardiotoxicity on human induced pluripotent stem cell-model derived from patients.
84. Choi YK, Park KG. Metabolic roles of AMPK and metformin in cancer cells. *Mol Cell*. 2013;36(4):279–87. <https://doi.org/10.1007/s10059-013-0169-8>.
85. Lopez-Otin C, Blasco MA, Partridge L, Serrano M, Kroemer G. The hallmarks of aging. *Cell*. 2013;153(6):1194–217. <https://doi.org/10.1016/j.cell.2013.05.039>.
- 86.●● Aboumsallem JP, Moslehi J, de Boer RA. Reverse cardio-oncology: cancer development in patients with cardiovascular disease. *J Am Heart Assoc*. 2020;9(2):e013754. <https://doi.org/10.1161/JAHA.119.013754>
- Recent overview on Heart Failure-associated factors inducing Cancer.
- 87.●● de Boer RA, Meijers WC, van der Meer P, van Veldhuisen DJ. Cancer and heart disease: associations and relations. *Eur J Heart Fail*. 2019;21(12):1515–25. <https://doi.org/10.1002/ejhf.1539>
- Emerging evidence of cancer and heart diseases interplay.
- 88.●● Meijers WC, de Boer RA. Common risk factors for heart failure and cancer. *Cardiovasc Res*. 2019;115(5):844–53. <https://doi.org/10.1093/cvr/cvz035>
- Highlighting of common risk factors shared between heart failure and cancer.
- 89.● Ameri P, Canepa M, Anker MS, Belenkov Y, Bergler-Klein J, Cohen-Solal A, et al. Cancer diagnosis in patients with heart failure: epidemiology, clinical implications and gaps in knowledge. *Eur J Heart Fail*. 2018;20(5):879–87. <https://doi.org/10.1002/ejhf.1165>
- Guideline of cancer diagnosis in patients with heart failure.
90. DeBosch B, Sambandam N, Weinheimer C, Courtois M, Muslin AJ. Akt2 regulates cardiac metabolism and cardiomyocyte survival. *J Biol Chem*. 2006;281(43):32841–51. <https://doi.org/10.1074/jbc.M513087200>.
91. Riehle C, Abel ED. Insulin signaling and heart failure. *Circ Res*. 2016;118(7):1151–69. <https://doi.org/10.1161/CIRCRESAHA.116.306206>.
92. Gross DN, van den Heuvel AP, Birnbaum MJ. The role of FoxO in the regulation of metabolism. *Oncogene*. 2008;27(16):2320–36. <https://doi.org/10.1038/onc.2008.25>.

93. Eijkelenboom A, Burgering BM. FOXOs: signalling integrators for homeostasis maintenance. *Nat Rev Mol Cell Biol.* 2013;14(2):83–97. <https://doi.org/10.1038/nrm3507>.
- 94.● Xia P, Chen J, Liu Y, Fletcher M, Jensen BC, Cheng Z. Doxorubicin induces cardiomyocyte apoptosis and atrophy through cyclin-dependent kinase 2-mediated activation of forkhead box O1. *J Biol Chem.* 2020;295(13):4265–76. <https://doi.org/10.1074/jbc.RA119.011571>
- New study that indicates FOXO1 as a potential target in DOXO-induced cardiotoxicity.
95. Oh J, Lee BS, Lim G, Lim H, Lee CJ, Park S, et al. Atorvastatin protects cardiomyocyte from doxorubicin toxicity by modulating survivin expression through FOXO1 inhibition. *J Mol Cell Cardiol.* 2020;138:244–55. <https://doi.org/10.1016/j.yjmcc.2019.12.007>.
96. Hill JA, Olson EN. Cardiac plasticity. *N Engl J Med.* 2008;358(13):1370–80. <https://doi.org/10.1056/NEJMra072139>.
97. Honors MA, Kinzig KP. The role of insulin resistance in the development of muscle wasting during cancer cachexia. *J Cachexia Sarcopenia Muscle.* 2012;3(1):5–11. <https://doi.org/10.1007/s13539-011-0051-5>.
- 98.●● Thackeray JT, Pietzsch S, Stapel B, Ricke-Hoch M, Lee CW, Bankstahl JP, et al. Insulin supplementation attenuates cancer-induced cardiomyopathy and slows tumor disease progression. *JCI Insight.* 2017;2(10):e93098. <https://doi.org/10.1172/jci.insight.93098>
- Important evidence that describes the effect of cancer on cardiac insulin signalling.
99. Taniyama Y, Walsh K. Elevated myocardial Akt signalling ameliorates doxorubicin-induced congestive heart failure and promotes heart growth. *J Mol Cell Cardiol.* 2002;34(10):1241–7. <https://doi.org/10.1006/jmcc.2002.2068>.
100. Al-Shabanah OA, El-Kashef HA, Badary OA, Al-Bekairi AM, Elmazar MM. Effect of streptozotocin-induced hyperglycaemia on intravenous pharmacokinetics and acute cardiotoxicity of doxorubicin in rats. *Pharmacol Res.* 2000;41(1):31–7. <https://doi.org/10.1006/phrs.1999.0568>.
101. Kurtoglu M, Maher JC, Lampidis TJ. Differential toxic mechanisms of 2-deoxy-D-glucose versus 2-fluorodeoxy-D-glucose in hypoxic and normoxic tumor cells. *Antioxid Redox Signal.* 2007;9(9):1383–90. <https://doi.org/10.1089/ars.2007.1714>.
102. Pajak B, Siwiak E, Soltyka M, Priebe A, Zielinski R, Fokt I, et al. 2-Deoxy-d-glucose and its analogs: from diagnostic to therapeutic agents. *Int J Mol Sci.* 2019;21(1):234. <https://doi.org/10.3390/ijms21010234>.
103. Maschek G, Savaraj N, Priebe W, Braunschweiger P, Hamilton K, Tidmarsh GF, et al. 2-deoxy-D-glucose increases the efficacy of adriamycin and paclitaxel in human osteosarcoma and non-small cell lung cancers in vivo. *Cancer Res.* 2004;64(1):31–4. <https://doi.org/10.1158/0008-5472.can-03-3294>.
104. Chen K, Xu X, Kobayashi S, Timm D, Jepperson T, Liang Q. Caloric restriction mimetic 2-deoxyglucose antagonizes doxorubicin-induced cardiomyocyte death by multiple mechanisms. *J Biol Chem.* 2011;286(25):21993–2006. <https://doi.org/10.1074/jbc.M111.225805>.
105. Cao J, Cui S, Li S, Du C, Tian J, Wan S, et al. Targeted cancer therapy with a 2-deoxyglucose-based adriamycin complex. *Cancer Res.* 2013;73(4):1362–73. <https://doi.org/10.1158/0008-5472.CAN-12-2072>.
106. Lekli I, Haines DD, Balla G, Tosaki A. Autophagy: an adaptive physiological countermeasure to cellular senescence and ischaemia/reperfusion-associated cardiac arrhythmias. *J Cell Mol Med.* 2017;21(6):1058–72. <https://doi.org/10.1111/jcmm.13053>.
107. Cuervo AM, Macian F. Autophagy, nutrition and immunology. *Mol Asp Med.* 2012;33(1):2–13. <https://doi.org/10.1016/j.mam.2011.09.001>.
108. Kawaguchi T, Takemura G, Kanamori H, Takeyama T, Watanabe T, Morishita K, et al. Prior starvation mitigates acute doxorubicin cardiotoxicity through restoration of autophagy in affected cardiomyocytes. *Cardiovasc Res.* 2012;96(3):456–65. <https://doi.org/10.1093/cvr/cvs282>.
109. Heras-Sandoval D, Perez-Rojas JM, Hernandez-Damian J, Pedraza-Chaverri J. The role of PI3K/AKT/mTOR pathway in the modulation of autophagy and the clearance of protein aggregates in neurodegeneration. *Cell Signal.* 2014;26(12):2694–701. <https://doi.org/10.1016/j.cellsig.2014.08.019>.
110. Kim J, Kundu M, Viollet B, Guan KL. AMPK and mTOR regulate autophagy through direct phosphorylation of Ulk1. *Nat Cell Biol.* 2011;13(2):132–41. <https://doi.org/10.1038/ncb2152>.
111. Laplante M, Sabatini DM. mTOR signaling in growth control and disease. *Cell.* 2012;149(2):274–93. <https://doi.org/10.1016/j.cell.2012.03.017>.
112. Barpe DR, Rosa DD, Froehlich PE. Pharmacokinetic evaluation of doxorubicin plasma levels in normal and overweight patients with breast cancer and simulation of dose adjustment by different indexes of body mass. *Eur J Pharm Sci : official journal of the European Federation for Pharmaceutical Sciences.* 2010;41(3–4):458–63. <https://doi.org/10.1016/j.ejps.2010.07.015>.
113. Li Y, Wang Y, Zou M, Chen C, Chen Y, Xue R, et al. AMPK blunts chronic heart failure by inhibiting autophagy. *Biosci Rep.* 2018;38(4):BSR20170982. <https://doi.org/10.1042/BSR20170982>.
114. Canto C, Auwerx J. Calorie restriction: is AMPK a key sensor and effector? *Physiology (Bethesda).* 2011;26(4):214–24. <https://doi.org/10.1152/physiol.00010.2011>.
115. Mitra MS, Donthamsetty S, White B, Latendresse JR, Mehendale HM. Mechanism of protection of moderately diet restricted rats against doxorubicin-induced acute cardiotoxicity. *Toxicol Appl Pharmacol.* 2007;225(1):90–101. <https://doi.org/10.1016/j.taap.2007.07.018>.

116. Lv X, Yu X, Wang Y, Wang F, Li H, Wang Y, et al. Berberine inhibits doxorubicin-triggered cardiomyocyte apoptosis via attenuating mitochondrial dysfunction and increasing Bcl-2 expression. *PLoS One*. 2012;7(10):e47351. <https://doi.org/10.1371/journal.pone.0047351>.
117. Trites MJ, Clugston RD. The role of adipose triglyceride lipase in lipid and glucose homeostasis: lessons from transgenic mice. *Lipids Health Dis*. 2019;18(1):204. <https://doi.org/10.1186/s12944-019-1151-z>.
- 118.●● Abdullah CS, Alam S, Aishwarya R, Miriyala S, Bhuiyan MAN, Panchatcharam M, et al. Doxorubicin-induced cardiomyopathy associated with inhibition of autophagic degradation process and defects in mitochondrial respiration. *Sci Rep*. 2019;9(1):2002. <https://doi.org/10.1038/s41598-018-37862-3>
- Time course study of DOXO treatment showing impairment of autophagy, mitochondrial dynamics, and bioenergetics in both acute and chronic mouse models of DOXO-associated cardiomyopathy.
119. Wang P, Wang L, Lu J, Hu Y, Wang Q, Li Z, et al. SESN2 protects against doxorubicin-induced cardiomyopathy via rescuing mitophagy and improving mitochondrial function. *J Mol Cell Cardiol*. 2019;133:125–37. <https://doi.org/10.1016/j.yjmcc.2019.06.005>.
120. Dhingra R, Margulets V, Chowdhury SR, Thliveris J, Jassal D, Fernyhough P, et al. Bnip3 mediates doxorubicin-induced cardiac myocyte necrosis and mortality through changes in mitochondrial signaling. *Proc Natl Acad Sci U S A*. 2014;111(51):E5537–44. <https://doi.org/10.1073/pnas.1414665111>.
121. Sun A, Cheng Y, Zhang Y, Zhang Q, Wang S, Tian S, et al. Aldehyde dehydrogenase 2 ameliorates doxorubicin-induced myocardial dysfunction through detoxification of 4-HNE and suppression of autophagy. *J Mol Cell Cardiol*. 2014;71:92–104. <https://doi.org/10.1016/j.yjmcc.2014.01.002>.
122. Zhang Y, Ren J. ALDH2 in alcoholic heart diseases: molecular mechanism and clinical implications. *Pharmacol Ther*. 2011;132(1):86–95. <https://doi.org/10.1016/j.pharmthera.2011.05.008>.
123. Chen CH, Budas GR, Churchill EN, Disatnik MH, Hurlley TD, Mochly-Rosen D. Activation of aldehyde dehydrogenase-2 reduces ischemic damage to the heart. *Science*. 2008;321(5895):1493–5. <https://doi.org/10.1126/science.1158554>.
124. Doser TA, Turdi S, Thomas DP, Epstein PN, Li SY, Ren J. Transgenic overexpression of aldehyde dehydrogenase-2 rescues chronic alcohol intake-induced myocardial hypertrophy and contractile dysfunction. *Circulation*. 2009;119(14):1941–9. <https://doi.org/10.1161/CIRCULATIONAHA.108.823799>.
125. Ge W, Yuan M, Ceylan AF, Wang X, Ren J. Mitochondrial aldehyde dehydrogenase protects against doxorubicin cardiotoxicity through a transient receptor potential channel vanilloid 1-mediated mechanism. *Biochim Biophys Acta*. 2016;1862(4):622–34. <https://doi.org/10.1016/j.bbadis.2015.12.014>.
126. Cardoso S, Santos RX, Carvalho C, Correia S, Pereira GC, Pereira SS, et al. Doxorubicin increases the susceptibility of brain mitochondria to Ca(2+)-induced permeability transition and oxidative damage. *Free Radic Biol Med*. 2008;45(10):1395–402. <https://doi.org/10.1016/j.freeradbiomed.2008.08.008>.
127. Park JH, Choi SH, Kim H, Ji ST, Jang WB, Kim JH, et al. Doxorubicin regulates autophagy signals via accumulation of cytosolic Ca(2+) in human cardiac progenitor cells. *Int J Mol Sci*. 2016;17(10):1680. <https://doi.org/10.3390/ijms17101680>.
128. Decuyper JP, Bultynck G, Parys JB. A dual role for Ca(2+) in autophagy regulation. *Cell Calcium*. 2011;50(3):242–50. <https://doi.org/10.1016/j.ceca.2011.04.001>.
129. Pandey S, Kuo WW, Shen CY, Yeh YL, Ho TJ, Chen RJ, et al. Insulin-like growth factor II receptor-alpha is a novel stress-inducible contributor to cardiac damage underpinning doxorubicin-induced oxidative stress and perturbed mitochondrial autophagy. *Am J Phys Cell Phys*. 2019;317(2):C235–C43. <https://doi.org/10.1152/ajpcell.00079.2019>.
130. Xie Z, Lau K, Eby B, Lozano P, He C, Pennington B, et al. Improvement of cardiac functions by chronic metformin treatment is associated with enhanced cardiac autophagy in diabetic OVE26 mice. *Diabetes*. 2011;60(6):1770–8. <https://doi.org/10.2337/db10-0351>.
131. Xu C, Wang W, Zhong J, Lei F, Xu N, Zhang Y, et al. Canagliflozin exerts anti-inflammatory effects by inhibiting intracellular glucose metabolism and promoting autophagy in immune cells. *Biochem Pharmacol*. 2018;152:45–59. <https://doi.org/10.1016/j.bcp.2018.03.013>.
- 132.● Verma S, Rawat S, Ho KL, Wagg CS, Zhang L, Teoh H, et al. Empagliflozin increases cardiac energy production in diabetes: novel translational insights into the heart failure benefits of SGLT2 inhibitors. *JACC Basic Transl Sci*. 2018;3(5):575–87. <https://doi.org/10.1016/j.jacbts.2018.07.006>
- Recent study suggesting the beneficial impact on cardiac function of Empagliflozin, a new antidiabetic class. The authors evaluated cardiac energy production and substrate use in diabetic mice treated with Empagliflozin.
133. Hammoudi N, Jeong D, Singh R, Farhat A, Komajda M, Mayoux E, et al. Empagliflozin improves left ventricular diastolic dysfunction in a genetic model of type 2 diabetes. *Cardiovasc Drugs Ther*. 2017;31(3):233–46. <https://doi.org/10.1007/s10557-017-6734-1>.
134. Karlsson FH, Fak F, Nookaew I, Tremaroli V, Fagerberg B, Petranovic D, et al. Symptomatic atherosclerosis is associated with an altered gut metagenome. *Nat Commun*. 2012;3:1245. <https://doi.org/10.1038/ncomms2266>.

135. Fu J, Bonder MJ, Cenit MC, Tigchelaar EF, Maatman A, Dekens JA, et al. The gut microbiome contributes to a substantial proportion of the variation in blood lipids. *Circ Res*. 2015;117(9):817–24. <https://doi.org/10.1161/CIRCRESAHA.115.306807>.
136. Marques FZ, Mackay CR, Kaye DM. Beyond gut feelings: how the gut microbiota regulates blood pressure. *Nat Rev Cardiol*. 2018;15(1):20–32. <https://doi.org/10.1038/nrcardio.2017.120>.
137. Tang WH, Wang Z, Kennedy DJ, Wu Y, Buffa JA, Agatista-Boyle B, et al. Gut microbiota-dependent trimethylamine N-oxide (TMAO) pathway contributes to both development of renal insufficiency and mortality risk in chronic kidney disease. *Circ Res*. 2015;116(3):448–55. <https://doi.org/10.1161/CIRCRESAHA.116.305360>.
138. Tumbaugh PJ, Ley RE, Mahowald MA, Magrini V, Mardis ER, Gordon JL. An obesity-associated gut microbiome with increased capacity for energy harvest. *Nature*. 2006;444(7122):1027–31. <https://doi.org/10.1038/nature05414>.
139. Wen L, Ley RE, Volchkov PY, Stranges PB, Avanesyan L, Stonebraker AC, et al. Innate immunity and intestinal microbiota in the development of type 1 diabetes. *Nature*. 2008;455(7216):1109–13. <https://doi.org/10.1038/nature07336>.
140. Qin J, Li Y, Cai Z, Li S, Zhu J, Zhang F, et al. A metagenome-wide association study of gut microbiota in type 2 diabetes. *Nature*. 2012;490(7418):55–60. <https://doi.org/10.1038/nature11450>.
141. Tang WHW, Li DY, Hazen SL. Dietary metabolism, the gut microbiome, and heart failure. *Nat Rev Cardiol*. 2019;16(3):137–54. <https://doi.org/10.1038/s41569-018-0108-7>.
142. Zhu A, Sunagawa S, Mende DR, Bork P. Inter-individual differences in the gene content of human gut bacterial species. *Genome Biol*. 2015;16:82. <https://doi.org/10.1186/s13059-015-0646-9>.
143. Tremaroli V, Backhed F. Functional interactions between the gut microbiota and host metabolism. *Nature*. 2012;489(7415):242–9. <https://doi.org/10.1038/nature11552>.
144. Brown JM, Hazen SL. The gut microbial endocrine organ: bacterially derived signals driving cardiometabolic diseases. *Annu Rev Med*. 2015;66:343–59. <https://doi.org/10.1146/annurev-med-060513-093205>.
145. Li L, Hua Y, Ren J. Short-chain fatty acid propionate alleviates Akt2 knockout-induced myocardial contractile dysfunction. *Exp Diabetes Res*. 2012;2012:851717. <https://doi.org/10.1155/2012/851717>.
146. Antos CL, McKinsey TA, Dreitz M, Hollingsworth LM, Zhang CL, Schreiber K, et al. Dose-dependent blockade to cardiomyocyte hypertrophy by histone deacetylase inhibitors. *J Biol Chem*. 2003;278(31):28930–7. <https://doi.org/10.1074/jbc.M303113200>.
147. Gallo P, Latronico MV, Gallo P, Grimaldi S, Borgia F, Todaro M, et al. Inhibition of class I histone deacetylase with an apicidin derivative prevents cardiac hypertrophy and failure. *Cardiovasc Res*. 2008;80(3):416–24. <https://doi.org/10.1093/cvr/cvn215>.
148. Granger A, Abdullah I, Huebner F, Stout A, Wang T, Huebner T, et al. Histone deacetylase inhibition reduces myocardial ischemia-reperfusion injury in mice. *FASEB J*. 2008;22(10):3549–60. <https://doi.org/10.1096/fj.08-108548>.
149. Kong Y, Tannous P, Lu G, Berenji K, Rothermel BA, Olson EN, et al. Suppression of class I and II histone deacetylases blunts pressure-overload cardiac hypertrophy. *Circulation*. 2006;113(22):2579–88. <https://doi.org/10.1161/CIRCULATIONAHA.106.625467>.
150. Moyal L, Goldfeiz N, Gorovitz B, Rephaeli A, Tal E, Tarasenko N, et al. AN-7, a butyric acid prodrug, sensitizes cutaneous T-cell lymphoma cell lines to doxorubicin via inhibition of DNA double strand breaks repair. *Investig New Drugs*. 2018;36(1):1–9. <https://doi.org/10.1007/s10637-017-0500-x>.
151. Rephaeli A, Waks-Yona S, Nudelman A, Tarasenko I, Tarasenko N, Phillips DR, et al. Anticancer prodrugs of butyric acid and formaldehyde protect against doxorubicin-induced cardiotoxicity. *Br J Cancer*. 2007;96(11):1667–74. <https://doi.org/10.1038/sj.bjc.6603781>.
152. Tarasenko N, Kessler-Icekson G, Boer P, Inbal A, Schlesinger H, Phillips DR, et al. The histone deacetylase inhibitor butyroyloxymethyl diethylphosphate (AN-7) protects normal cells against toxicity of anticancer agents while augmenting their anticancer activity. *Investig New Drugs*. 2012;30(1):130–43. <https://doi.org/10.1007/s10637-010-9542-z>.
153. Russo M, Guida F, Paparo L, Trinchese G, Aitoro R, Avagliano C, et al. The novel butyrate derivative phenylalanine-butylamide protects from doxorubicin-induced cardiotoxicity. *Eur J Heart Fail*. 2019;21(4):519–28. <https://doi.org/10.1002/ejhf.1439>
- Butyrate-derived molecule prevents cardiac mitochondria dysfunction in the heart.

Publisher's note

Springer Nature remains neutral with regard to jurisdictional claims in published maps and institutional affiliations.

Forum Review Article

Signaling pathways underlying anthracycline cardiotoxicity

Valentina Sala^{1*}, Angela Della Sala^{1*}, Emilio Hirsch¹ and Alessandra Ghigo¹

¹Department of Molecular Biotechnology and Health Sciences, University of Torino, Via Nizza 52, 10126, Torino, Italy

* equal contributors

Abbreviated title: Signaling pathways in anthracycline cardiotoxicity

Address correspondence to: Alessandra Ghigo, Department of Molecular Biotechnology and Health Sciences, University of Torino, Via Nizza 52, 10126, Torino, Italy Tel

+390116706335, Fax. +390116706452, alessandra.ghigo@unito.it

Word count: 7510

Reference numbers: 148

Number of greyscale illustrations: 0

Number of color illustrations: 7 (online 7)

Number of tables: 1

Keywords: Anthracyclines, cardiotoxicity, reactive oxygen species, DNA damage, calcium homeostasis, autophagy

Abstract

Significance: The cardiac side effects of hematological treatments are a major issue of the growing population of cancer survivors, often affecting patient survival even more than the tumor for which the treatment was initially prescribed. Among the most cardiotoxic drugs are anthracyclines, highly potent anti-tumor agents, which still represent a mainstay in the treatment of hematological and solid tumors. Unfortunately, diagnosis, prevention and treatment of cardiotoxicity are still unmet clinical needs which call for a better understanding of the molecular mechanism behind the pathology.

Recent Advances: This review article will discuss recent findings on the pathomechanisms underlying the cardiotoxicity of anthracyclines, spanning from DNA and mitochondrial damage to calcium homeostasis, autophagy and apoptosis. Special emphasis will be given to the role of reactive oxygen species and their interplay with major signaling pathways.

Critical Issues: Although new promising therapeutic targets and new drugs have started to be identified, their efficacy has been mainly proven in preclinical studies and requires clinical validation.

Future Directions: Future studies are awaited to confirm the relevance of recently uncovered targets, as well as identifying new druggable pathways, in more clinically relevant models, including for example human induced pluripotent stem cell-derived cardiomyocytes.

Introduction

In the last 20 years, major advances in oncological treatments have significantly reduced cancer death rates, but concomitantly highlighted cardiac disease as the leading cause of morbidity and premature mortality among cancer survivors. This is a critical issue, especially for patients who are often diagnosed at young age, like lymphoma and leukemia patients, and are commonly treated with highly cardiotoxic drugs like anthracyclines (ANTs). ANTs are potent anticancer agents that not only kill transformed cells, but significantly damage cardiomyocytes that, unable to regenerate, carry life-long alterations culminating in heart failure. ANT cardiotoxicity commonly occurs well after cancer remission, and is generally irreversible and refractory to standard heart failure pharmacotherapy, leading to a poor prognosis (40, 140).

Early diagnosis of cardiotoxicity before overt cardiac deterioration occurs, i.e. when the disease is still in a reversible and treatable phase, currently represents an unmet clinical need. Similarly, treatment options for patients diagnosed with cardiotoxicity are limited, since small trials have shown only modest efficacy of standard heart failure treatments in patients with ANT cardiotoxicity. Antioxidants revealed to be equally ineffective, thus challenging the classical view in which reactive oxygen species (ROS) are the major culprits of the cardiac side effects of ANTs (127). In the last ten years, the field of Cardio-Oncology has grown exponentially and has led to the awareness that the scenario of the molecular mechanisms behind ANT cardiotoxicity is more complex than previously anticipated, and not just centered around the role of ROS (122).

The scope of this review article is to provide a comprehensive description of the major signaling pathways that are affected by ANTs within cardiomyocytes and whose deregulation has been causally linked to ANT cardiotoxicity. The role of ROS as signaling intermediates of ANT cardiotoxicity will be emphasized.

1. DNA damage at the interplay of ROS, apoptosis and mitochondrial dysfunction

The antineoplastic action of ANTs is linked to their ability to induce DNA damage, through both direct and indirect mechanisms, predominantly in proliferating cells in S- and G2-phase. On one side, ANTs intercalate into DNA, and form bulky adducts as well as crosslinks that interfere with DNA replication and transcription. On the other side, ANTs can damage DNA by increasing the production of ROS, that in turn lead to oxidized

nucleotides, base mismatches, point mutations and DNA single strand breaks. Last, ANTs interfere directly with DNA helicase activity and the ensuing DNA strand separation, as well as with type 2 topoisomerases (Top2) and DNA unwinding. The relevance of Top2 poisoning by ANTs recently emerged as a leading cause of cardiotoxicity, so that Top2 and the intertwined signaling pathways have been identified as promising therapeutic targets. On the other hand, the role of ROS has been reconsidered. Albeit initially considered as the triggering event of cardiotoxicity (the so-called ROS-driven hypothesis), oxidative stress is now recognized as a secondary event, associated to nuclear and mitochondrial DNA damage (126).

1.1. The ROS-driven hypothesis

The susceptibility of cardiomyocytes to ROS-induced damage is related to their limited antioxidant resources. As a consequence of their prevalent oxidative metabolism, the antioxidant systems of cardiomyocytes are almost completely saturated at steady state (36) and any further source of ROS, like ANTs, can exhaust their antioxidant capacity more rapidly than in any other cell type. ANTs are responsible for ROS generation, since they are reductively activated to a semiquinone radical. This, in turn, undergoes redox cycling, thereby producing superoxide ($O_2^{\cdot-}$) and hydrogen peroxide (H_2O_2). A further mechanism of ANT-mediated ROS production involves iron. In the presence of iron, ANTs can form Fe^{3+} -anthracycline complexes, which catalyze the Fenton's reaction, where H_2O_2 is converted to various ROS species, including the cytotoxic hydroxyl radicals (OH^{\cdot}) (121, 22) (Figure 1). The ensuing massive ROS generation ultimately leads to cardiac cell death (17, 115).

Albeit ROS have long been recognized as pivotal mediators of ANT cardiotoxicity, the initial ROS-driven hypothesis has been challenged by a series of studies showing modest effects of ROS scavengers and iron chelators in preventing ANT cardiac side effects in chronic settings. Importantly, N-acetyl cysteine or combinations of antioxidants have been tested, with variable outcomes, but did not protect patients from ANTs cardiotoxicity (114). Intriguingly, none has matched the effectiveness of Dexrazoxane (ICRF-187 or DXR), a bisdioxopiperazine agent structurally related to EDTA but with more potent chelating/antioxidant activities (118). This finding led to the hypothesis that the mechanism of action of DXR might be other than iron-binding.

Yet, the contribution of redox cycling and primary ROS production to ANTs cardiotoxicity is debated, and the most recent view is that the enhanced ROS generation is a secondary phenomenon resulting from mitochondrial dysfunction (48) or endoplasmic reticulum stress caused by accumulation of misfolded proteins (83).

1.2. Topoisomerase 2 poisoning and inhibition

In 2012, Zhang et al. showed that the production of ROS could also be secondary to the interaction of ANTs with the beta isoform of topoisomerase 2 (Top2) (12). DNA Topoisomerases 2 are responsible for the catalysis of the transient breaking and adjoining of DNA double helix during DNA replication and transcription (18). As an intermediate of this process, a DNA-Top2 covalent complex, the so-called cleavage complex, is formed. ANTs act like Top2 poisons in stabilizing the complex, thereby preventing the re-ligation of DNA and leading to the formation of DNA double-strand breaks, which are potent inducers of the DNA damage response (Figure 2).

The DNA damage response to genotoxic stress is mainly regulated by three members of the phosphatidylinositol 3-kinase related kinase (Pikk) family: DNA-dependent protein kinase (DNA-Pk), ataxia-telangiectasia-mutated (ATM); and ATM and Rad3-related (ATR) (62,66). The initial processing of double-strand DNA breaks, prior to repair, is mediated by the heterotrimeric MRN complex, composed of Mre11, Rad50 and Nbs1 proteins. Upon recognition of double strand breaks by the MRN complex, ATM kinase is activated, leading to the phosphorylation of key regulators of cell cycle progression and DNA repair (78). However, if double-strand breaks are not properly repaired, DNA damage activates a set of apoptotic signaling routes, including the ATM/ATR-p53, as well as necroptosis (78, 102).

DNA damage-induced cell death is the key mechanism behind the anticancer action of ANTs and, at the same time, is responsible for their cardiotoxicity. Notably, the effects of ANTs in proliferating (tumor) and non-proliferating (cardiomyocytes) cells are mediated by two distinct isoforms of Top2 (Figure 3). While the alpha isoform of Top2 (Top2- α) is overexpressed in proliferating cells in S and G2 phase, and it is almost undetectable in quiescent tissues, Top2- β is the unique isoform expressed by adult mammalian cardiomyocytes (12) and mature iPSC-derived cardiomyocytes (4, 15). The interaction of doxorubicin (Doxo) with Top2- α generates a ternary Top2-Doxo-DNA cleavage complex that triggers tumor cell death. Similarly, the Top2- β -Doxo-DNA complex induces DNA

6

double strand breaks and activates a DNA damage response that is responsible for cardiomyocytes death. In cardiomyocytes, the activation of p53 stimulates DNA repair processes, but concomitantly represses genes involved in mitochondrial biogenesis (like PGC-1) and oxidative phosphorylation, impairs the ratio between beta-cell lymphoma 2 (Bcl2) and Bcl2 associated X (140), culminating in cardiac cell death (143,86). Consistently, p53-knockout mice and adult mouse hearts expressing cardiac myocyte-restricted dominant-interfering p53 are partially protected against Doxo-induced cell death and myocardial dysfunction (147). The observed protection in these models likely stems from both inhibition of apoptosis and preserved mammalian target of rapamycin (mTOR) signaling, which may contribute to prevent cardiac mass reduction (147).

In further agreement with the role of Top2- β in ANT cardiotoxicity, murine embryonic fibroblasts (72) and cardiomyocytes (12) lacking Top2- β are protected from Doxo-induced damage. Of note, Top2- β appears to be a key player in the cardiotoxicity elicited by ANTs not only when they are used in monotherapy, but also in the setting of combinatorial regimens, like with monoclonal antibodies. For instance, both Doxo and Trastuzumab alone induce Top2- β protein downregulation in cardiomyocytes, which is exacerbated in combined treatments. This further reduction in Top2- β activity leads to enhanced ROS production and apoptosis, and might be one of the reasons of the aggravated cardiotoxicity of combination therapies compared to single agents (53). Of note, Atwal *et al.* showed that, *in vitro*, 10 μ M Doxo (or higher) can interfere with the action of other drugs that act as Top2 poisons, like etoposide, thus hindering the overall anti-cancer efficacy of combined treatments (4).

Given the selective expression of the beta isoform in cardiomyocytes, the development of Top2- α specific drugs may provide a valuable means to reduce cardiotoxicity, whilst maintaining the anti-cancer efficacy of the drug. This is a key aspect to be considered in the development of cardioprotective agents against ANT toxicity. On these grounds, the increased risk of secondary malignancies in patients treated with Dexrazoxane (DXR) has limited its application as cardioprotective agent in the past, though its use in children and adolescents has been recently reconsidered (98). Mechanistically, the cardioprotective action of DXR has been suggested to be independent of its antioxidant properties, rather it has been ascribed to its ability to compete with ATP binding on Top2- β , thereby producing

a configuration change that prevents the formation of a complex with ANTs (72). In accord with this view, the DXR analogue JR-311 shows significant cardioprotective effects which depend on Top2- β modulation, while being independent from its iron chelating properties (10). Despite its cardioprotective function, caution is still used while prescribing DXR, and this drug is nowadays not recommended for children aged 0-18 years who are expected to receive a cumulative dose of Doxo (or other anthracycline) lower than 300 mg/m². Considering the isoform selectivity and opposing effects of Top2 poisoning *versus* inhibition, it is reasonable to assume that all patients receiving ANTs would benefit from the development of new therapeutic regimens including Top2- α specific poisons and Top2- β specific inhibitors.

1.3. *Rac1 as a master regulator of DNA damage and ROS production*

As Top2 emerged as a good pharmacological target to prevent ANT cardiotoxicity, new Top2 regulators have started to be investigated. Among these, Rac1 has been shown to contribute to Doxo-mediated cardiomyocyte death (for a complete review see (38)), in both ROS-dependent and ROS-independent manners (73) (Figure 4). Rac1 is a small guanosine triphosphate (GTP)-bound protein, belonging to the Rho family, a group of molecular switches and signal transducers that transmit extracellular stimuli from the inner plasma membrane to intracellular signaling pathways. Rac1 is involved in a variety of cellular processes, such as cell-cell and cell-substrate adhesion, polarization, migration, invasion, proliferation, transcription, vesicle formation and apoptosis, which depend on its spatio-temporal distribution (94). Several studies have identified the presence of a nuclear pool of Rac1, and have unraveled the mechanisms underlying its nuclear localization (94), which include DNA damage itself (41). This is in agreement with the finding that oxidized DNA bases can act as Rac1 GEFs (35). In the nucleus, Rac1 was recently found associated with Top2 (108), where it is responsible for the activation of a DNA damage-ATM-p53-apoptosis pathway (139).

Pharmacological inhibition of Rac1 signaling with NSC23766 interferes with Doxo genotoxicity by preventing the formation of the cleavage complex, thereby reducing the generation of double strand breaks and the activation of the DNA damage response (46). Of note, the effect of NSC23766 can be further improved by the lipid-lowering drug Lovastatin (46). Inhibition of the HMG-CoA reductase by statins causes the depletion of the

cellular pool of isoprene precursors, which are essential for the C-terminal prenylation, and the subsequent membrane localization, of Rho proteins (26). Thus, prevention of Rac1 prenylation by statins promotes Rac1 translocation to the nucleus, suggesting that the therapeutic effect of statins might be linked to the upregulation of the nuclear pool of Rac1 versus the cytosolic counterpart. Nevertheless, the mechanism by which nuclear Rac1 regulates Top2 activity is still unclear and deserves further experimental efforts. It was shown that, in acute (73) and sub-acute (39) models of ANT cardiotoxicity, cardiac Rac1 knockout confers cardioprotection by means of ROS-independent as well as ROS-dependent mechanisms. In fact, Rac1 contributes to the assembly and activation of the phagocyte nicotinamide adenine dinucleotide phosphate (NADPH) oxidase complex (42), and cardiomyocyte-specific deletion of Rac1 was shown to impair Doxo-induced NADPH oxidase activation, ROS production, DNA fragmentation, cardiomyocyte apoptosis, and finally improve cardiac function. Consistently, mice with impaired Nox2 NADPH oxidase complex are less sensitive to ANTs (145).

Overall, statins interfere with two of the main mechanisms underlying ANTs cardiotoxicity, i.e. ROS production and Top2-mediated DNA damage. Their beneficial effect in models of ANT cardiotoxicity and their favorable tolerability make them promising candidates for the prevention and/or treatment of ANTs cardiotoxicity, as confirmed in small-scale clinical studies (1). More importantly, statins may sensitize certain tumors to chemotherapy, thereby enhancing the anti-cancer efficiency of ANT regimens and at the same time protecting the heart (25).

1.4. *mtDNA and mitochondrial homeostasis*

Another interesting aspect related to Top2 poisoning by ANTs is that both Top2- α and - β isoforms were found in mitochondria (70, 141). Top2- β is likely the most relevant isoform in cardiac mitochondria (141). In cardiomyocytes, ANT-mediated Top2- β poisoning might affect not only nuclear DNA, but also mitochondrial DNA (mtDNA), further contributing to increased ROS production and cytotoxicity. Accordingly, ANT-related chronic heart failure is characterized by imbalanced mitochondrial mass and reduced nuclear expression of genes pivotal to mitochondrial biogenesis and homeostasis (54). These include the peroxisome proliferator activated receptor- γ (PPAR γ) coactivator-1 α and β (PGC-1 α and β), nuclear respiratory factor 1 (NRF1) and mitochondrial transcription factor A (TFAM).

Accordingly, the protective effect exerted by the histone deacetylase and PGC-1 α activator, Sirtuin 1 (SIRT1) against ANTs cardiotoxicity (11) is likely due, at least in part, to the regulation of mitochondrial biogenesis.

In addition, ANTs can induce mitochondrial damage through the uncoupling of the electron transport chain, disruption of mitochondrial membrane potential and generation of ROS, especially in conjunction with mitochondrial iron metabolism (32). However, the relative contribution of direct Top2 poisoning and of secondary oxidation of nucleotides by ROS on mtDNA depletion has yet to be clarified.

Recently, Jean *et al.* (51) showed that mice treated with a modified form of Doxo, which exclusively targets mitochondria but not nuclei, are resistant to ANT cardiotoxicity, downsizing the contribution of mtDNA damage to the disease. On the other hand, Khiati *et al.* (56) showed that mice lacking mitochondrial Top1 (mtTOP1) are hypersensitive to ANTs, and display severe mitochondrial damage. Doxo-induced mitochondrial defects, including mitochondrial cristae disorganization and impaired production of respiratory chain proteins, ultimately result in decreased O₂ consumption, increased ROS production, and cardiac damage leading to lethality.

2. ANT-induced impairment of Calcium Handling

The failure of antioxidants to protect against ANT cardiotoxicity led to the view that ROS likely represent signaling intermediates of Doxo-induced damage, but not the triggering event of ANT cardiotoxicity. Increasing evidence highlights the impairment of cellular and mitochondrial Ca²⁺ signaling, rather than the induction of oxidative stress, as one of the primary pathological events.

2.1. Cytosolic Ca²⁺ impairment

Isolated cardiac myocytes perfused with Doxo show increased Ca²⁺ sparks occurrence and decreased Ca²⁺ transients (104). Of note, the doxorubicin metabolite, doxorubicinol, has been shown to target calsequestrin type 2 (CSQ2), thus increasing cytoplasmic Ca²⁺ concentration and favoring arrhythmic conditions (1) (Figure 5). Doxo also inhibits the transcription of the sarcoplasmic reticulum Ca²⁺-ATPase 2a (SERCA2a) and therefore reduces Ca²⁺ uptake in the SR (2). Moreover, Doxo and its metabolite doxorubicinol modify ryanodine receptor (RyR) and SERCA2a activity by binding to the proteins and *via* thiol oxidation (37), and induce Calcium/Calmodulin-dependent protein kinase-II (CaMKII)-

10

dependent Ca^{2+} leakage from the SR (104, 124). Overall, the effects on RyR, SERCA2a and phospholamban (PLN), mediated by activation of PKA and CaMKII, result in transient intracellular Ca^{2+} alterations. These, in turn, lead to a temporary depression of Ca^{2+} transients that precedes structural defects and overt cardiac dysfunction in models of cardiotoxicity induced by chronic low-dose Doxo (69). Albeit it is known that ROS activate both PKA and CaMKII (8, 141), the two main regulators of the excitation-contraction coupling, the contribution of β -adrenergic signaling in the setting of ANT cardiotoxicity has been postulated, but still requires experimental confirmation (69).

The ensuing disruption of sarcoplasmic Ca^{2+} handling machinery leads to intracellular Ca^{2+} overload and, finally, to sarcomeric disarray and myofibril deterioration, that is further aggravated by Doxo-activated Ca^{2+} -dependent calpain proteases (68).

2.2. Mitochondrial Ca^{2+} impairment

Besides excessive accumulation of Ca^{2+} in the cytoplasm, impaired Ca^{2+} fluxes have been reported in mitochondria in response to Doxo treatment (19). Ca^{2+} enters mitochondria through the mitochondrial calcium uniporter (MCU) and, above a physiological threshold, mitochondrial Ca^{2+} triggers the opening of the permeability transition pore (MTP), resulting in dissipation of transmembrane potential, mitochondrial swelling, and increased permeability of the outer membrane to apoptotic factors, such as cytochrome c (142). In turn, in the cytosol, cytochrome c forms a complex with the adaptor protein apoptosis protease activator protein-1 (Apaf-1) and caspase-9, the so-called apoptosome, which finally activates the apoptotic cascade (142).

2.3. Emerging therapeutic strategies to rescue Ca^{2+} homeostasis

As the relevance of SR Ca^{2+} leakage in ANT cardiotoxicity emerged, new therapeutic approaches have been explored, including cardiac gene therapy with the GRP78 chaperone, which is responsible for amelioration of SR stress (124). Intriguingly, adeno-associated virus (AAV)-mediated GRP78 overexpression partly protects cardiomyocytes from Doxo-induced cell death by modulating Ca^{2+} /CAMKII-dependent pathways and preventing p53 accumulation (124). This study suggests that SR stress is a valuable therapeutic target in the context of Doxo-induced, and possibly other, cardiac disease.

Further highlighting the central role of CaMKII in this process, it has been recently demonstrated that pharmacological or genetic blockade of L-type Ca^{2+} channel (LTCC)

attenuates Doxo-induced cardiomyocyte apoptosis by suppressing intracellular Ca^{2+} accumulation and the ensuing activation of CaMKII-NF- κ B pathway (49). Hence, LTCC blockers might be potential therapeutic agents against ANT-induced cardiomyopathy.

Recently, Efentakis *et al.* showed that targeting both impaired cytosolic Ca^{2+} homeostasis and mitochondrial alterations is a promising strategy. A single dose of Levosimendan, an inotropic vasodilator (92) that is clinically used for the treatment of decompensated heart failure (24), prevented sub-chronic Doxo-induced cardiotoxicity, as indicated by preserved LV systolic function and structure, by acting on cAMP/PKA and PLN pathway (23). Intriguingly, Levosimendan and its active metabolite OR-1896 act as PDE3 inhibitors, with whom they share structural similarity (90). Of note, besides counteracting cytoplasmic Ca^{2+} accumulation, Levosimendan displays anti-inflammatory and antioxidant activities, sensitizes Troponin C to Ca^{2+} (inotropic effect) and activates the ATP-sensitive K^+ channel (24), events that all converge into a cardioprotective effect.

As increased intracellular Ca^{2+} levels emerged as key triggers of ROS production, which, in turn, further disrupts intracellular and mitochondrial Ca^{2+} homeostasis, new therapeutic tools aimed at preventing or restoring Ca^{2+} balance may prove effective against ANT-induced toxicity.

3. The controversial role of autophagy in ANT-induced cardiotoxicity

The finding that antioxidants and iron chelators fail to prevent ANT cardiotoxicity suggested that additional mechanisms may be involved and, among these, autophagy recently emerged to play a key role (55). However, there is still controversy regarding its beneficial *versus* maladaptive role in ANT-induced cardiotoxicity (111).

3.1. AMPK/mTOR signaling pathway

Autophagy is the major cellular recycling process, essential for maintaining cellular homeostasis (113). The initiation of autophagy is under the control of ATG1, also known as activated unc-51-like autophagy activating kinase 1 (Ulk-1), which phosphorylates Beclin-1 (5, 85), thus triggering the formation of autophagosomes. The activity of Ulk-1 is under the control of adenosine monophosphate-activated protein kinase (AMPK) and mammalian target of rapamycin (mTOR) signaling pathways. AMPK and mTOR promote and inhibit autophagy, respectively, by finely regulating the kinase activity of Ulk-1. Consistently ANTs

have been found to interfere with mTOR and AMPK regulatory pathways leading to autophagy dysregulation.

3.2. ANTs inhibit autophagy

ANTs activate mTOR that, in turn, induces the inhibitory phosphorylation of Ulk-1 at Ser757, thereby preventing Ulk-1-mediated autophagosome initiation (132). On the other hand, ANTs inhibit the phosphorylation of AMPK, an upstream positive regulator of autophagy initiation, further contributing to the block of the autophagic process. Interestingly, Li *et al.* (65) recently identified another kinase which is involved in autophagy regulation, and whose activity is critically affected by ANTs. The authors show that, in cardiomyocytes, Doxo engages PI3K γ signaling, converging on autophagy inhibition and maladaptive metabolic reprogramming. In particular, Doxo activates PI3K γ /Akt signaling downstream of Toll-like receptor 9 (TLR9), leading to increased phosphorylation of mTOR and of its downstream target Ulk-1 and, in turn, to autophagy inhibition. Accordingly, genetic or pharmacological blockade of PI3K γ reactivates autophagy by releasing the inhibitory brake of mTOR, and protects the heart against ANT-induced cardiotoxicity (65). Notably, the enhanced autophagy triggered by PI3K γ inhibition protects cardiomyocytes against multiple Doxo-induced toxic effects, such as DNA damage, Ca²⁺ dysregulation and ROS production. Indeed, in cardiomyocytes, Doxo treatment results in ROS accumulation, which is further enhanced by the addition of the autophagy blocker BafA1, while being reduced by PI3K γ inhibition. Of note, BafA1 completely abrogated the protective effect of PI3K γ blockade, thus corroborating the view that PI3K γ inhibition protects against Doxo-induced oxidative stress and cardiotoxicity via activation of autophagy (65).

Another recent study (131) confirms that Doxo impairs the autophagic flux and the transcription of autophagy-related genes by increasing the expression and phosphorylation of mTOR. Activated mTOR, indeed, retains in the cytoplasm the transcriptional regulator TFEB, that normally drives the expression of autophagy and lysosomal genes, such as LAMP1 (57, 109, 110, 132, 148). The transcriptional activity of TFEB is inhibited by Doxo-induced phosphorylation of mTOR, whereas the impaired nuclear localization of TFEB causes the decline of lysosomal biogenesis and function (77, 82), resulting in increased levels of Beclin-1, LC3-II and P62. In line with these findings, inhibition of mTOR activity with Torin-1 in H9c2 cardiomyoblasts restores the nuclear

localization of TFEB and autophagy, preventing Doxo-induced apoptosis and improving cell viability (6).

In contrast, Zhu *et al.* report that mice with cardiomyocyte-specific and constitutively active mTOR are protected against ANT-induced acute cardiac dysfunction (147). In this work, authors observed that Doxo treatment *in vivo* decreases mTOR activity, as evidenced by decreased mTOR phosphorylation, inducing cardiomyocyte death and mass reduction, while the activation of the mTOR pathway effectively retains normal cardiac mass and function.

3.3. ANTs induce autophagy

In line with Zhu *et al.*, other studies have reported that ANTs increase autophagy, leading to maladaptive cardiac remodeling. A first study of 2009 by Luo *et al.* (71) demonstrated that ANTs induce an upregulation of the autophagy-related marker Beclin-1, and autophagic vacuole formation. In agreement with this study, Kobayashi *et al.* (58) showed that Doxo markedly increases LC3-II protein expression, leading to cardiomyocyte death via inhibition of anti-apoptotic protein B-cell lymphoma 2 (Bcl2), a negative regulator of Beclin-1. Conversely, Bcl2 is directly upregulated by the transcription factor GATA4 (61), that appears to participate to autophagy regulation (58) also by binding to and blocking Beclin-1 (93). Of note, the preservation of GATA4 activity attenuates Doxo cardiotoxicity by inhibiting autophagy through modulation of the expression of Bcl2 and autophagy-related genes.

Li *et al.* (64) further investigated the role of Beclin-1 in ANT cardiotoxicity *in vivo* using Beclin-1 heterozygous deficient mice (Beclin-1 +/-), since Beclin-1 knock out is embryonic lethal. Beclin-1 +/- hearts emerged to be protected against ANT-induced damage. Moreover, Beclin-1 inhibition limits the initiation of autophagy, thus preventing the accumulation of damaged cellular components within autophagosomes and reducing cardiomyocyte apoptosis (58, 64). Consistently, later studies confirmed the activation of autophagy as a primary cause of cardiomyocyte programmed cell death in response to ANTs and suggested inhibition of autophagy as a valuable tool to significantly improve cardiac function and prevent ANT-induced cardiotoxicity (71, 134, 142).

Although autophagy has been revealed as an important mechanism underlying ANT-induced cardiotoxicity, whether ANTs induce or inhibit autophagy (Figure 6), and if

autophagy is beneficial or harmful in this context is still a matter of debate. Future studies are awaited to clarify the scenario.

4. Mitophagy as a key mechanism of ANT-induced cardiotoxicity

Mitochondria, as principal integrators of energy metabolism, are particularly important for maintaining cellular ATP levels to sustain myocardial contractile activity and cardiomyocyte survival. Growing evidence demonstrates that structural damage and dysfunction of these organelles are implicated in the development of cardiovascular diseases, including Doxo-induced cardiomyopathy (28). Of note, Doxo preferentially accumulates inside mitochondria: as a cationic drug, it binds to cardiolipin, an anionic-charged phospholipid located in the inner mitochondrial membrane leading to mitochondrial engulfment and toxicity (31). A selective form of mitochondrial autophagy, namely mitophagy, plays a pivotal role in the regulation of mitochondrial homeostasis, by regulating and eliminating dysfunctional organelles (59). In cardiomyocytes, mitophagy occurs via two pathways: (i) the PTEN-induced kinase 1 (PINK1)/Parkin (E3 ubiquitin ligase) pathway and (112) BH3-only protein Bcl2-like 19 kDa-interacting protein 3 (BNIP3)/BNIP3-like protein Nix, an effector of apoptosis pathway (105). In the following paragraphs, we will describe how these two pathways are affected by ANTs.

4.1. BNIP3 and BNIP3L/Nix

Both BNIP3 and BNIP3L/Nix act on the outer mitochondrial membrane as direct mitophagy receptors, as they have a LC3-II recognition motive (94), thereby allowing autophagosomal engulfment of mitochondria. ANTs lead to severe necrosis in cardiomyocytes, promoting up-regulation and translocation of BNIP3 to the mitochondrial membrane which, in turn, triggers the opening of the permeability transition pore and the increase in ROS production (Figure 7) (20). Conversely, inhibition of BNIP3, with either shRNA against BNIP3 or through the expression of a mutant BNIP3 that fails to target mitochondria, rescues ANT-induced defects of the mitochondrial respiratory chain *in vitro* in cultured cardiomyocytes. Furthermore, mitochondria morphology and cardiac function are preserved in BNIP3 knock-out mice (BNIP3 $-/-$) treated with ANTs, confirming a maladaptive role of BNIP3 in ANT cardiotoxicity (20). Additionally, BNIP3 activation in cardiomyocytes treated with ANTs is associated to loss of nuclear Hmgb1 and release of

classical markers of necrosis (i.e., LDH and cTnT), supporting a primary role of BNIP3 in necrosis (20).

New compelling evidence establishes that nuclear factor- κ B (NF- κ B) signaling, which transcriptionally silences BNIP3 activation under basal conditions, is dramatically reduced in cardiac myocytes treated with Doxo (19). This, in turn, promotes BNIP3 gene activation, mitochondrial injury including calcium influx, permeability transition pore opening, and necrotic cell death. Interestingly, restoring NF- κ B signaling suppresses BNIP3 expression, mitochondrial perturbations, and necrotic cell death, thus suggesting a new potential therapeutic approach for cancer patients treated with Doxo.

4.2. PINK1/Parkin pathway

On the other hand, PINK1 accumulates and recruits Parkin to the outer membrane of depolarized mitochondria, mediating the ubiquitination of mitochondrial proteins and their recognition by p62 and LC3, consequently leading to the initiation of mitochondrial autophagy (105).

In Doxo-induced cardiomyopathy, mitophagy is critically involved in the elimination of vacuolated and dysfunctional mitochondria (47). Hull *et al.* demonstrated that PINK1/Parkin-dependent mitophagy is suppressed early after ANT treatment (2–8 days post-treatment), but is restored at a later stage, when PINK1 and Parkin are significantly upregulated. Interestingly, the mitophagy inhibitor peptide, Mdivi-1, prevents Doxo-induced cardiotoxicity, indicating that excessive mitophagy contributes to Doxo-cardiotoxicity (29).

Nevertheless, the molecular mechanisms by which ANTs inhibit mitophagy have still to be uncovered. A recent study provides novel and compelling evidence that overexpression of SESN2, a member of the sestrins family, protects cardiomyocytes against Doxo-induced cardiomyopathy *via* the improvement of mitochondrial function and rescue of mitophagy (131). Of note, the expression of SESN2 is significantly reduced following Doxo stimulation, *in vitro* and *in vivo*. Mechanistically, SESN2 interacts with Parkin and p62, and promotes Parkin recruitment to mitochondria, subsequently activating mitophagy. These results establish SESN2 as a new player in the regulation of mitochondrial function and provide a potential therapeutic approach to prevent Doxo-induced cardiomyopathy.

16

Interestingly, mitophagy appears to be co-regulated with mitochondrial biogenesis, through a shared signaling pathway involving nuclear translocation of NRFs and a functional interaction between PGC-1 α and Parkin (137). Doxo inhibits the expression of PGC-1 α and its downstream targets, nuclear respiratory factor 1 (NRF1) and mitochondrial transcription factor A (TFAM), thus reducing the expression of mitochondrial proteins. Inhibition of mitophagy by mdivi-1 attenuates Doxo-mediated activation of the PINK1/Parkin pathway and rescues mitochondrial biogenesis by preserving the expression of PGC-1 α (137).

5. Association between apoptosis and autophagic dysregulation

The present section focuses on the interplay between a naturally programmed cell death process, apoptosis, and the cellular recycling process of autophagy. Autophagy and apoptosis have a key role in maintaining cellular homeostasis and respond to similar types of signals and stress, including increased intracellular Ca²⁺ concentration and ROS accumulation.

5.1 Autophagy promotes apoptosis

Apoptosis is regulated by Bcl2 and p53 genes, which are closely associated with autophagy. In general, autophagy restrains apoptosis, while apoptosis-associated caspase activation shuts off the autophagic process (76). However, in particular cases, such as following Doxo stimulation, autophagy is associated with high levels of apoptotic cell death. Autophagy is dramatically increased in Doxo-treated cardiomyocytes, and associates with increased cleavage of caspase 3 and PARP, which indicate apoptosis initiation (58). Similarly, in HUVECs, Doxo induces autophagy early after treatment (since 3 hours), while the level of apoptosis as well as lysosomal membrane permeabilization (LMP) and mitochondrial outer membrane permeabilization (MOMP) increase at later stages (12 hours) (52). This finding implies that Doxo-induced autophagy and the ensuing autophagy-dependent LMP are upstream events, followed by distal events including MOMP and cytochrome c release, which finally triggers caspase-dependent apoptosis. Consistently, inhibition of Doxo-induced autophagy, through the autophagy inhibitor 3-MA or Beclin-1 knockdown, results in significant attenuation of cell death (52, 58). Conversely, activation of autophagy by rapamycin or Beclin-1 expression exacerbate apoptosis in H9C2 cells and in mice hearts treated with Doxo (134).

In addition, Doxo-induced cell death correlates with depletion of GATA4, a transcription factor essential for cardiomyocyte growth and survival (89). GATA4 is both sufficient and necessary to inhibit autophagy by controlling the gene expression of Bcl2, a survival factor with anti-autophagy activity (93). Concurrently, GATA4 reduction induces an up-regulation of ATG genes through p53, leading to the excessive activation of autophagic flux, that ultimately contributes to Doxo-induced cardiomyocyte death.

5.2. Autophagy inhibits apoptosis

The above presented findings are challenged by the observation that activation of autophagy, by stimuli such as AMPK activation by glucose-depletion or mTOR inhibition by rapamycin, results in enhanced cell viability and reduced apoptosis following Doxo treatment in H9C2 cardiomyoblasts and mice overexpressing GFP-LC3 (117). In this study, the induction of autophagy by rapamycin reduces the activity of cleaved caspase-3, thus supporting an inhibitory role of autophagy on apoptosis, and indicating a therapeutic potential of rapamycin against Doxo-induced myocardial damage (117).

Further confirming the beneficial role of autophagy against apoptosis, it has been shown that autophagy inhibition, by decreasing the expression of AMPK or knocking-out AMPK α 1 in mice (AMPK α 1 $^{-/-}$), increases the sensitivity to Doxo-induced apoptosis, while restoration of autophagy by adenovirus-mediated AMPK constitutive activation (AMPK-CA) or 5-aminoimidazole-4-carboxamide ribonucleoside (AICAR) significantly limits the iatrogenic effects of Doxo (130). Consistently, genetic deletion of AMPK α 1 (AMPK α 1 $^{-/-}$) enhances Doxo-related reduction of p53 phosphorylation, establishing a critical role of AMPK in Doxo-induced p53-dependent DNA damage and apoptosis (130).

Similarly, Doxo inhibits autophagy by activating E2F1/mTORC1 pathway and further induces apoptosis by activating E2F1/AMP-activated protein kinase α 2 (AMPK α 2) pathway in starved H9C2 cardiomyoblasts (33). The same result was observed in a mouse model of Doxo-induced cardiotoxicity, in both myocardial ischemic and non-ischemic conditions, in which resveratrol was able to repress E2F1, thereby activating autophagy and reducing apoptosis (33).

Finally, p53, that is mostly studied for its role as a transcription factor, displays a key role in cell death and autophagy regulation (13, 119). Accumulation of cytosolic p53 can directly activate BAX to permeabilize mitochondria, thereby inducing caspase activation and

18

apoptosis (13). p53 also functions as an endogenous repressor of autophagy (80). An additional function of cytosolic p53 has been discovered in Doxo-treated cardiomyocytes (44), in that it inhibits mitophagy by blocking Parkin translocation to damaged mitochondria (Figure 7). The inhibition of Parkin-mediated mitophagy compromises mitochondrial function, resulting in aging-related and Doxo-mediated decrease in cardiac contractility. In keeping with this mechanism, p53-deficient mice and Parkin-overexpressing cardiomyocytes show a less severe decline of mitochondrial integrity and cell death after treatment with Doxo (44).

6. Inflammation-mediated cell death in ANT cardiotoxicity

Inflammation appears to be significantly involved in Doxo-induced cardiotoxicity (81), as acute and chronic myocarditis occur in a dose-dependent manner in patients treated with Doxo (63). Doxo triggers the inflammatory signaling cascades by promoting the release of different cytokines, including interleukin-1 and TNF- α , in combination with the activation of various signaling pathways, such as the nuclear factor- κ B (NF- κ B), p38-MAPK, and the autophagy pathways (97, 107).

NF- κ B is a master regulator of the inflammatory cascade and is maintained in the cytoplasm in an inactive form by the inhibitor of κ B protein (IKK). Upon Doxo treatment, inhibition of autophagy and the ensuing p62 overexpression induce IKK signaling downstream of Toll-like receptors (TLRs), thereby engaging NF- κ B and triggering the inflammatory response. Conversely, when autophagy is upregulated, p62 is reduced and blocks the NF- κ B signaling pathway (146). Therefore, upregulation of autophagy by AMPK/mTOR signaling pathway results in an anti-inflammatory effect, with a reduction of inflammatory cytokine production (97).

In addition, Doxo induces the expression of TLRs which contribute to cardiac damage in virtue of their role in the activation of pro-inflammatory NF- κ B (96). TLRs are a class of thirteen members normally expressed in leukocytes in response to microbial pathogens or dead/damaged cell structures, but recent studies uncover their implication in Doxo-mediated cellular injury and related inflammation (101). Among them, TLR2 and TLR4 are found also in cardiomyocytes and are implicated in ANT-induced cardiotoxicity. TLR2 regulates cytokine release, such as TNF α , IL6 and IL1 β , through NF- κ B activation, as NF- κ B DNA binding activity is increased in wild-type but reduced in TLR2-/- mice after Doxo

administration (87). Of note, genetic ablation and pharmacological inhibition of TLR2 in mice and in cardiomyocytes, respectively, treated with Doxo results cardioprotective, with reduced release of cytokines, and enhanced mice survival (87), as well as prevention of cardiomyocyte death, cardiac dysfunction and inflammation (74, 106, 136).

On the contrary, the role of TLR4 in ANT cardiotoxicity is still controversial. On one side, it controls cardiac inflammation and appears to be involved in Doxo-induced cardiomyopathy through the inhibition of the transcription factor GATA4, since cardiac inflammation is decreased in TLR4 knock-out mice (TLR4^{-/-}) (99). On the other side, blockage of TLR4 with neutralizing antibodies results in an enhanced inflammation and inhibition of autophagy (74). New compelling evidence about TLR4 implication in Doxo-induced cardiac inflammation has been showed by Dargani *et al.* (120). They demonstrate the implication of TLR4 in a new form of programmed cell death characterized by proinflammation, termed pyroptosis. In this study, Doxo activates TLR4-pyrin domain containing-3 (NLRP3) and caspase-1, leading to inflammasome formation and pyroptotic cell death in H9c2 cells (120). Moreover, Doxo stimulates the release of cytokines and inflammatory markers, such as interleukins (IL) (IL-1 β , IL-6), tumor necrosis factor (TNF- α) and nuclear factor- κ B (NF- κ B) (34), which are associated to cardiac dysfunction and apoptosis. Interestingly, the use of embryonic stem cell-derived exosomes (ES-Exos) inhibits TLR4 and NLRP3 inflammasome markers and inflammasome-induced pyroptosis in mice under Doxo treatment, by inducing the release of anti-inflammatory cytokines, such as IL-10 (116, 120). Moreover, ES-Exos transplanted mice results in improved cardiac function, suggesting protective effects of ES-Exos that could be used as a future therapeutic option to treat Doxo-induced cardiac dysfunction (116, 120).

7. Emerging role of microRNAs in anthracycline cardiotoxicity

Recently, microRNAs (miRNAs or miRs), a class of endogenous 22-nucleotide noncoding RNAs, emerged as pivotal modulators of target genes in a variety of heart disease conditions, such as myocardial infarction and hypertensive heart disease (14), as well as Doxo-induced myocardial injury. Of note, several studies have shown increased levels of circulating miRNAs, including miR-21, miR-34a, miR-146a and miR-532-3p in response to Doxo treatment (125).

20

Doxo treatment significantly increases miR-21 expression in both mouse heart tissue and H9C2 cells, whereas Doxo-induced apoptosis results attenuated by miR-21 overexpression in cardiomyocytes through the modulation of the anti-proliferative factor, B cell translocation gene 2 (Btg2) (123).

Regarding the role of miR-146a, Tong *et al.* showed that in a model of acute Doxo cardiotoxicity, miR-146a overexpression further aggravates Doxo-mediated myocardial apoptosis, by targeting a key component of neuregulin-1-ErbB signaling, ErbB4. The increased expression of miR-146a drives ErbB4 downregulation and leads to cardiomyocyte death, while inhibition of miR-146a or overexpression of ErbB4 could prevent and improve cardiomyocyte survival (123). On the other hand, Pan *et al.* recently proved a protective role of miR-146a in a different model of Doxo cardiotoxicity characterized by a low-dose Doxo treatment leading to late-onset cardiomyopathy (91). In this study, the expression of miR-146 is significantly reduced upon Doxo treatment, leading to cardiomyocytes death and, on the other hand, to autophagy inhibition. Of note, these pathological events are reversed by overexpression of miR-146a, which plays an anti-apoptotic role through the p53 pathway. In particular, by targeting TATA-binding protein (TBP) associated factor 9b (TAF9b), a coactivator and stabilizer of p53, miR-146 downregulates the expression of p53, thereby attenuating apoptosis and restoring autophagy in cardiomyocytes (91). New compelling evidence about the implication of miR-146a-5p in Doxo-induced cardiotoxicity has been recently provided by the work of Milano *et al.* (79). The authors demonstrate that intravenous administration of human cardiac progenitor cells (CPCs) exosomes, highly enriched in miR-146-a5p, attenuates Doxo/Trastuzumab-mediated oxidative stress in cardiomyocytes. Hence, specific silencing of miR-146-a5p results in enhanced Doxo-induced cell death (79).

In addition, recent findings demonstrate that miR-34a levels are increased and trigger senescence and apoptotic mechanisms involving p16^{INK4a} and p53 in rat CPCs exposed to Doxo (87). Mesenchymal stem cell (MSC)-based therapies have been reported to modulate Doxo-induced cellular senescence in H9C2 cells via inhibition of miR-34a (133). The mechanism underlying the anti-senescence function of MSCs involves the miR34a-SIRT1-p53 axis, where the inhibition of miR-34a leads to a reduction of p53 and activation of SIRT1, which elongates telomere length and increases telomerase activity (133).

Another miR, miR-532-3p, has been recently shown to have a pro-apoptotic role, inducing mitochondrial fission and apoptosis in Doxo-treated cardiomyocytes. Mechanistically, these effects are explained by a negative regulation of the expression of apoptosis repressor with caspase recruitment domain (ARC) (128).

In addition, Doxo induces miRNA-320a overexpression, that leads to cardiac dysfunction and endothelial injury by dysregulating the vascular endothelial growth factor (VEGF) signaling pathway (137). Accordingly, miR-320a-knockdown mice have attenuated damage of endothelial cells as well as reduced cardiac dysfunction in response to Doxo.

On the other hand, a number of miRNAs, such as the miR-30 family, are downregulated by ANTs. Of note, the miR-30 family has a protective role against Doxo-induced cardiotoxicity by targeting multiple members of the β -adrenergic pathway, such as β 1AR, β 2AR and Gai-2, as well as members of the mitochondrial apoptotic pathway, like the pro-apoptotic gene BNIP3L (100).

Overall, the differential and altered expression of miRNAs in response to ANT treatment highlights the possibility of exploiting microRNAs not only as therapeutic targets, but also as diagnostic biomarkers, as in the case of miR-216b, that it is up-regulated in the first stage of Doxo-induced cardiotoxicity and may act as an early marker of cardiac damage (60).

8. Future perspectives for the treatment of ANT-induced cardiotoxicity

A basic requirement for clinically relevant cardioprotective strategies is the ability to preserve the efficacy of the anti-cancer treatment. Even more interesting are pharmacological approaches which potentially provide a dual beneficial effect, the so-called ability to “kill two birds with one stone” (106), where the cardioprotective agent not only prevents the cardiac side effect of chemotherapy, but also enhances its anti-tumor action.

Among this class of dual drugs are CYP1 inhibitors, derived from Visnagin, which have been recently shown to be promising therapeutic agents against Doxo-induced cardiotoxicity (3). CYP1 belongs to a family of highly conserved monooxygenases that are usually responsible for the metabolism of toxic compounds, including polycyclic aromatic hydrocarbons that share structural similarity with Doxo (112).

On one side, CYP1 plays an important role in the metabolism of polyunsaturated fatty acids (21), such as arachidonic acid metabolites, which have been previously implicated in the pathogenesis of Doxo cardiotoxicity (75). Moreover, CYP1, in particular the CYP1B1 isoform that is overexpressed in a wide range of tumor types, including breast cancer (84), plays a role in estrogen-mediated tumor formation (9, 67). These observations suggest that CYP1 inhibition may simultaneously confer cardioprotection, while enhancing the antitumor effect of Doxo, and make CYP1 inhibitors appealing candidates for future clinical trials.

Besides CYP1, neuregulin, an agonist of the receptor tyrosine kinases belonging to the epidermal growth factor receptor (EGFR) family, has elicited interest as a potential therapeutic against ANT cardiotoxicity. EGFR family includes EGFR/HER1/ErbB1, ErbB2/HER2 (that has no ligand), ErbB3/HER3, and ErbB4/HER4 and among these, ErbB2 and ErbB4 are expressed in differentiated cardiomyocytes. Evidence for the involvement of the ErbB family in ANT cardiotoxicity emerged from the increased risk of cardiotoxicity in patients receiving concurrent Doxo and Trastuzumab (103), a monoclonal antibody targeting ErbB2 receptor used to treat HER2-positive breast and advanced stomach cancer. Moreover, in mouse models of cardiotoxicity, ANTs downregulate cardiac expression of ErbB4, potentially by increasing the levels of miR-146a (43). On the other hand, cardiac-specific overexpression of ErbB2 in mice is protective against cardiac damage (16), including that elicited by ANTs, likely through the upregulation of antioxidant mechanisms (7).

Neuregulin-1 acts as a primary ligand to initiate ErbB signaling, and plays a critical role in cardiomyocyte development, homeostasis and disease (88). Albeit administration of neuregulin-1 reduces ANT-induced cardiomyocyte apoptosis *via* PI3K/Akt (27), its use as a cardioprotectant is limited by potential pro-neoplastic effects (45). Ongoing work is focusing on the development of an engineered neuregulin, displaying reduced neoplastic potential, but preserved cardioprotective function, in mice (50). Neuregulin-mediated cardioprotection thus appears to be a promising approach for patients undergoing treatment with ANTs and deserves further studies and clinical validation.

Conclusions

The exponential growth of the field of Cardio-Oncology of the last decade has greatly expanded our knowledge of the molecular basis of chemotherapy-related cardiotoxicity. The emerging view is that cardiotoxic anti-cancer drugs, like anthracyclines, affect intertwined signaling pathways, which are key to survival of cancer cells, but also of cardiomyocytes. Despite reactive oxygen species are no longer considered the main determinant of cardiotoxicity, they are crucial signaling intermediates that intervene in the response of cardiomyocytes to cardiotoxic insults. The current hope is that the signaling pathways that have just emerged to be targeted by ANTs could be therapeutically manipulated to prevent and/or treat cardiotoxicity. While some pharmacological approaches have already been tested in preclinical models, the way toward the clinical application is still arduous and requires conclusive validation of the most promising targets in models that faithfully reflect the fundamental biology or cardiotoxic responses of the human myocardium. These include for instance human induced pluripotent stem cell-derived cardiomyocytes, which are just emerging as a powerful tool for drug discovery and the realization of precision medicine in Cardio-Oncology (30, 95).

Acknowledgements

This work was supported by grants from Progetto d'Ateneo-Compagnia di San Paolo (PICANCAR to AG), Fondazione Cariplo (GR 2017-0800 to VS), Ricerca Sanitaria Finalizzata (GR-2013-02355449 fellowship to VS) and Leducq Foundation (09CVD01 to EH). We gratefully acknowledge Giulia Prono for figure layout.

Author Disclosure Statement

Prof. Ghigo and Hirsch are co-founders and board members of Kither Biotech, a startup biotech focused on the development of PI3K inhibitors.

Abbreviations Used

AMPK = Adenosine Monophosphate-Activated Protein Kinase	LTCC = L-type Ca ²⁺ Channel
AMPK-CA = AMPK Constitutive Activation	miRNA/ miR = microRNA
ANT = Anthracycline	mtDNA = Mitochondrial DNA
ATG = Autophagy-related Genes	mTOR = Mammalian Target of Rapamycin
ATM = Ataxia-Telangiectasia-mutated kinase	NADPH = Nicotinamide Adenine Dinucleotide Phosphate
ATR = ATM and Rad3-mutated Related kinase	NF-κB = Nuclear Factor-κB
BAX = Bcl2-associated X	Nox = NADPH Oxidase Complex
Bcl2 = Beta-cell lymphoma 2	NRF1 = Nuclear Respiratory Factor 1
BNIP3 = BH3-only protein Bcl-2-like 19 kDa-interacting protein 3	PGC-1 = PPARγ Coactivator 1
CaMKII = Calcium/Calmodulin-dependent protein kinase-II	PI3K = Phosphatidylinositol 3-Kinase
CPC = Cardiac Progenitor Cell	PINK1 = PTEN-induced kinase 1
CYP = Cytochrome P450	PKA = Protein Kinase A
Doxo = Doxorubicin	PPARγ = Peroxisome Proliferator Activated Receptor-γ
DXR = Dexrazoxane	ROS = Reactive Oxygen Species
EGFR = Epidermal Growth Factor Receptor	RyR = Ryanodine Receptor
ES-Exos = Embryonic Stem Cell-derived Exosomes	SERCA = Sarco-Endoplasmic Reticulum Calcium ATPase
IKK = Inhibitor of κB protein	SESN2 = Sestrin-2
IL = Interleukin	SR = Sarcoplasmic Reticulum
LC3 = Microtubule-associated protein 1A/1B-light chain 3	TFEB = Transcription Factor EB
	TLR = Toll-like Receptor
	TNF-α = Tumor Necrosis Factor α
	Top2 = Type 2 Topoisomerase
	Ulk-1 = Unc-51-like autophagy activating kinase 1

References

1. Acar Z, Kale A, Turgut M, Demircan S, Durna K, Demir S, Meric M and Agac MT. Efficiency of atorvastatin in the protection of anthracycline-induced cardiomyopathy. *J Am Coll Cardiol* 58: 988-989, 2011.
2. Arai M, Yoguchi A, Takizawa T, Yokoyama T, Kanda T, Kurabayashi M and Nagai R. Mechanism of doxorubicin-induced inhibition of sarcoplasmic reticulum Ca(2+)-ATPase gene transcription. *Circ Res* 86: 8-14, 2000.
3. Asnani A, Zheng B, Liu Y, Wang Y, Chen HH, Vohra A, Chi A, Cornella-Taracido I, Wang H, Johns DG, Sosnovik DE and Peterson RT. Highly potent visnagin derivatives inhibit Cyp1 and prevent doxorubicin cardiotoxicity. *JCI Insight* 3, 2018.
4. Atwal M, Swan RL, Rowe C, Lee KC, Lee DC, Armstrong L, Cowell IG and Austin CA. Intercalating TOP2 Poisons Attenuate Topoisomerase Action at Higher Concentrations. *Mol Pharmacol* 96: 475-484, 2019.
5. Backer JM. The intricate regulation and complex functions of the Class III phosphoinositide 3-kinase Vps34. *Biochem J* 473: 2251-2271, 2016.
6. Bartlett JJ, Trivedi PC, Yeung P, Kienesberger PC and Puliniikunnil T. Doxorubicin impairs cardiomyocyte viability by suppressing transcription factor EB expression and disrupting autophagy. *Biochem J* 473: 3769-3789, 2016.
7. Belmonte F, Das S, Sysa-Shah P, Sivakumaran V, Stanley B, Guo X, Paolucci N, Aon MA, Nagane M, Kuppusamy P, Steenbergen C and Gabrielson K. ErbB2 overexpression upregulates antioxidant enzymes, reduces basal levels of reactive oxygen species, and protects against doxorubicin cardiotoxicity. *Am J Physiol Heart Circ Physiol* 309: H1271-1280, 2015.
8. Brennan JP, Bardswell SC, Burgoyne JR, Fuller W, Schroder E, Wait R, Begum S, Kentish JC and Eaton P. Oxidant-induced activation of type I protein kinase A is mediated by RI subunit interprotein disulfide bond formation. *J Biol Chem* 281: 21827-21836, 2006.

9. Bruno RD and Njar VC. Targeting cytochrome P450 enzymes: a new approach in anti-cancer drug development. *Bioorg Med Chem* 15: 5047-5060, 2007.
10. Bures J, Jirkovska A, Sestak V, Jansova H, Karabanovich G, Roh J, Sterba M, Simunek T and Kovarikova P. Investigation of novel dexrazoxane analogue JR-311 shows significant cardioprotective effects through topoisomerase IIbeta but not its iron chelating metabolite. *Toxicology* 392: 1-10, 2017.
11. Cappetta D, Esposito G, Piegari E, Russo R, Ciuffreda LP, Rivellino A, Berrino L, Rossi F, De Angelis A and Urbanek K. SIRT1 activation attenuates diastolic dysfunction by reducing cardiac fibrosis in a model of anthracycline cardiomyopathy. *Int J Cardiol* 205: 99-110, 2016.
12. Capranico G, Tinelli S, Austin CA, Fisher ML and Zunino F. Different patterns of gene expression of topoisomerase II isoforms in differentiated tissues during murine development. *Biochim Biophys Acta* 1132: 43-48, 1992.
13. Chipuk JE, Kuwana T, Bouchier-Hayes L, Droin NM, Newmeyer DD, Schuler M and Green DR. Direct activation of Bax by p53 mediates mitochondrial membrane permeabilization and apoptosis. *Science* 303: 1010-1014, 2004.
14. Creemers EE, Tijssen AJ and Pinto YM. Circulating microRNAs: novel biomarkers and extracellular communicators in cardiovascular disease? *Circ Res* 110: 483-495, 2012.
15. Cui N, Wu F, Lu WJ, Bai R, Ke B, Liu T, Li L, Lan F and Cui M. Doxorubicin-induced cardiotoxicity is maturation dependent due to the shift from topoisomerase IIalpha to IIbeta in human stem cell derived cardiomyocytes. *J Cell Mol Med* 23: 4627-4639, 2019.
16. D'Uva G, Aharonov A, Lauriola M, Kain D, Yahalom-Ronen Y, Carvalho S, Weisinger K, Bassat E, Rajchman D, Yifa O, Lysenko M, Konfino T, Hegesh J, Brenner O, Neeman M, Yarden Y, Leor J, Sarig R, Harvey RP and Tzahor E. ERBB2 triggers mammalian heart regeneration by promoting cardiomyocyte dedifferentiation and proliferation. *Nat Cell Biol* 17: 627-638, 2015.

17. Deng S, Kruger A, Kleschyov AL, Kalinowski L, Daiber A and Wojnowski L. Gp91phox-containing NAD(P)H oxidase increases superoxide formation by doxorubicin and NADPH. *Free Radic Biol Med* 42: 466-473, 2007.
18. Dewese JE and Osheroff N. The DNA cleavage reaction of topoisomerase II: wolf in sheep's clothing. *Nucleic Acids Res* 37: 738-748, 2009.
19. Dhingra R, Guberman M, Rabinovich-Nikitin I, Gerstein J, Margulets V, Gang H, Madden N, Thliveris J and Kirshenbaum LA. Impaired NF-kappaB signalling underlies cyclophilin D-mediated mitochondrial permeability transition pore opening in doxorubicin cardiomyopathy. *Cardiovasc Res*, 2019.
20. Dhingra R, Margulets V, Chowdhury SR, Thliveris J, Jassal D, Fernyhough P, Dorn GW, 2nd and Kirshenbaum LA. Bnip3 mediates doxorubicin-induced cardiac myocyte necrosis and mortality through changes in mitochondrial signaling. *Proc Natl Acad Sci U S A* 111: E5537-5544, 2014.
21. Divanovic S, Dalli J, Jorge-Nebert LF, Flick LM, Galvez-Peralta M, Boespflug ND, Stankiewicz TE, Fitzgerald JM, Somarathna M, Karp CL, Serhan CN and Nebert DW. Contributions of the three CYP1 monooxygenases to pro-inflammatory and inflammation-resolution lipid mediator pathways. *J Immunol* 191: 3347-3357, 2013.
22. Doroshov JH and Davies KJ. Redox cycling of anthracyclines by cardiac mitochondria. II. Formation of superoxide anion, hydrogen peroxide, and hydroxyl radical. *J Biol Chem* 261: 3068-3074, 1986.
23. Efentakis P, Varela A, Chavdoula E, Sigala F, Sanoudou D, Tenta R, Gioti K, Kostomitsopoulos N, Papapetropoulos A, Tasouli A, Farmakis D, Davos CH, Klinakis A, Suter T, Cokkinos DV, Iliodromitis EK, Wenzel P and Andreadou I. Levosimendan prevents doxorubicin-induced cardiotoxicity in time- and dose dependent manner: Implications for inotropy. *Cardiovasc Res*, 2019.

24. Farmakis D, Alvarez J, Gal TB, Brito D, Fedele F, Fonseca C, Gordon AC, Gotsman I, Grossini E, Guarracino F, Harjola VP, Hellman Y, Heunks L, Ivancan V, Karavidas A, Kivikko M, Lomivorotov V, Longrois D, Masip J, Metra M, Morelli A, Nikolaou M, Papp Z, Parkhomenko A, Poelzl G, Pollesello P, Ravn HB, Rex S, Riha H, Ricksten SE, Schwinger RHG, Vrtovec B, Yilmaz MB, Zielinska M and Parissis J. Levosimendan beyond inotropy and acute heart failure: Evidence of pleiotropic effects on the heart and other organs: An expert panel position paper. *Int J Cardiol* 222: 303-312, 2016.
25. Feleszko W, Mlynarczuk I, Balkowiec-Iskra EZ, Czajka A, Switaj T, Stoklosa T, Giermasz A and Jakobisiak M. Lovastatin potentiates antitumor activity and attenuates cardiotoxicity of doxorubicin in three tumor models in mice. *Clin Cancer Res* 6: 2044-2052, 2000.
26. Fritz G and Henninger C. Rho GTPases: Novel Players in the Regulation of the DNA Damage Response? *Biomolecules* 5: 2417-2434, 2015.
27. Fukazawa R, Miller TA, Kuramochi Y, Frantz S, Kim YD, Marchionni MA, Kelly RA and Sawyer DB. Neuregulin-1 protects ventricular myocytes from anthracycline-induced apoptosis via erbB4-dependent activation of PI3-kinase/Akt. *J Mol Cell Cardiol* 35: 1473-1479, 2003.
28. Gao S, Li H, Feng XJ, Li M, Liu ZP, Cai Y, Lu J, Huang XY, Wang JJ, Li Q, Chen SR, Ye JT and Liu PQ. alpha-Enolase plays a catalytically independent role in doxorubicin-induced cardiomyocyte apoptosis and mitochondrial dysfunction. *J Mol Cell Cardiol* 79: 92-103, 2015.
29. Gharanei M, Hussain A, Janneh O and Maddock H. Attenuation of doxorubicin-induced cardiotoxicity by mdivi-1: a mitochondrial division/mitophagy inhibitor. *PLoS One* 8: e77713, 2013.
30. Gintant G, Burridge P, Gepstein L, Harding S, Herron T, Hong C, Jalife J and Wu JC. Use of Human Induced Pluripotent Stem Cell-Derived Cardiomyocytes in Preclinical Cancer Drug Cardiotoxicity Testing: A Scientific Statement From the American Heart Association. *Circ Res* 125: e75-e92, 2019.

31. Goormaghtigh E, Huart P, Praet M, Brasseur R and Ruyschaert JM. Structure of the adriamycin-cardiolipin complex. Role in mitochondrial toxicity. *Biophys Chem* 35: 247-257, 1990.
32. Gorini S, De Angelis A, Berrino L, Malara N, Rosano G and Ferraro E. Chemotherapeutic Drugs and Mitochondrial Dysfunction: Focus on Doxorubicin, Trastuzumab, and Sunitinib. *Oxid Med Cell Longev* 2018: 7582730, 2018.
33. Gu J, Fan YQ, Zhang HL, Pan JA, Yu JY, Zhang JF and Wang CQ. Resveratrol suppresses doxorubicin-induced cardiotoxicity by disrupting E2F1 mediated autophagy inhibition and apoptosis promotion. *Biochem Pharmacol* 150: 202-213, 2018.
34. Guo R, Lin J, Xu W, Shen N, Mo L, Zhang C and Feng J. Hydrogen sulfide attenuates doxorubicin-induced cardiotoxicity by inhibition of the p38 MAPK pathway in H9c2 cells. *Int J Mol Med* 31: 644-650, 2013.
35. Hajas G, Bacsı A, Aguilera-Aguirre L, Hegde ML, Tapas KH, Sur S, Radak Z, Ba X and Boldogh I. 8-Oxoguanine DNA glycosylase-1 links DNA repair to cellular signaling via the activation of the small GTPase Rac1. *Free Radic Biol Med* 61: 384-394, 2013.
36. Halestrap AP. Calcium, mitochondria and reperfusion injury: a pore way to die. *Biochem Soc Trans* 34: 232-237, 2006.
37. Hanna AD, Lam A, Tham S, Dulhunty AF and Beard NA. Adverse effects of doxorubicin and its metabolic product on cardiac RyR2 and SERCA2A. *Mol Pharmacol* 86: 438-449, 2014.
38. Henninger C and Fritz G. Statins in anthracycline-induced cardiotoxicity: Rac and Rho, and the heartbreakers. *Cell Death Dis* 8: e2564, 2017.
39. Henninger C, Pohlmann S, Ziegler V, Ohlig J, Schmitt J and Fritz G. Distinct contribution of Rac1 expression in cardiomyocytes to anthracycline-induced cardiac injury. *Biochem Pharmacol* 164: 82-93, 2019.

40. Hilfiker-Kleiner D, Ardehali H, Fischmeister R, Burridge P, Hirsch E and Lyon AR. Late onset heart failure after childhood chemotherapy. *Eur Heart J* 40: 798-800, 2019.
41. Hinde E, Yokomori K, Gaus K, Hahn KM and Gratton E. Fluctuation-based imaging of nuclear Rac1 activation by protein oligomerisation. *Sci Rep* 4: 4219, 2014.
42. Hordijk PL. Regulation of NADPH oxidases: the role of Rac proteins. *Circ Res* 98: 453-462, 2006.
43. Horie T, Ono K, Nishi H, Nagao K, Kinoshita M, Watanabe S, Kuwabara Y, Nakashima Y, Takanabe-Mori R, Nishi E, Hasegawa K, Kita T and Kimura T. Acute doxorubicin cardiotoxicity is associated with miR-146a-induced inhibition of the neuregulin-ErbB pathway. *Cardiovasc Res* 87: 656-664, 2010.
44. Hoshino A, Mita Y, Okawa Y, Ariyoshi M, Iwai-Kanai E, Ueyama T, Ikeda K, Ogata T and Matoba S. Cytosolic p53 inhibits Parkin-mediated mitophagy and promotes mitochondrial dysfunction in the mouse heart. *Nat Commun* 4: 2308, 2013.
45. Hsieh SY, He JR, Hsu CY, Chen WJ, Bera R, Lin KY, Shih TC, Yu MC, Lin YJ, Chang CJ, Weng WH and Huang SF. Neuregulin/erythroblastic leukemia viral oncogene homolog 3 autocrine loop contributes to invasion and early recurrence of human hepatoma. *Hepatology* 53: 504-516, 2011.
46. Huelsenbeck SC, Schorr A, Roos WP, Huelsenbeck J, Henninger C, Kaina B and Fritz G. Rac1 protein signaling is required for DNA damage response stimulated by topoisomerase II poisons. *J Biol Chem* 287: 38590-38599, 2012.
47. Hull TD, Boddu R, Guo L, Tisher CC, Traylor AM, Patel B, Joseph R, Prabhu SD, Suliman HB, Piantadosi CA, Agarwal A and George JF. Heme oxygenase-1 regulates mitochondrial quality control in the heart. *JCI Insight* 1: e85817, 2016.
48. Ichikawa Y, Ghanefar M, Bayeva M, Wu R, Khechaduri A, Naga Prasad SV, Mutharasan RK, Naik TJ and Ardehali H. Cardiotoxicity of doxorubicin is mediated through mitochondrial iron accumulation. *J Clin Invest* 124: 617-630, 2014.

49. Ikeda S, Matsushima S, Okabe K, Ikeda M, Ishikita A, Tadokoro T, Enzan N, Yamamoto T, Sada M, Deguchi H, Morimoto S, Ide T and Tsutsui H. Blockade of L-type Ca(2+) channel attenuates doxorubicin-induced cardiomyopathy via suppression of CaMKII-NF-kappaB pathway. *Sci Rep* 9: 9850, 2019.
50. Jay SM, Murthy AC, Hawkins JF, Wortzel JR, Steinhauser ML, Alvarez LM, Gannon J, Macrae CA, Griffith LG and Lee RT. An engineered bivalent neuregulin protects against doxorubicin-induced cardiotoxicity with reduced proneoplastic potential. *Circulation* 128: 152-161, 2013.
51. Jean SR, Tulumello DV, Riganti C, Liyanage SU, Schimmer AD and Kelley SO. Mitochondrial Targeting of Doxorubicin Eliminates Nuclear Effects Associated with Cardiotoxicity. *ACS Chem Biol* 10: 2007-2015, 2015.
52. Jiang C, Jiang L, Li Q, Liu X, Zhang T, Yang G, Zhang C, Wang N, Sun X and Jiang L. Pyrroloquinoline quinine ameliorates doxorubicin-induced autophagy-dependent apoptosis via lysosomal-mitochondrial axis in vascular endothelial cells. *Toxicology* 425: 152238, 2019.
53. Jiang J, Mohan N, Endo Y, Shen Y and Wu WJ. Type IIB DNA topoisomerase is downregulated by trastuzumab and doxorubicin to synergize cardiotoxicity. *Oncotarget* 9: 6095-6108, 2018.
54. Jirkovsky E, Popelova O, Krivakova-Stankova P, Vavrova A, Hroch M, Haskova P, Brackova-Dolezelova E, Micuda S, Adamcova M, Simunek T, Cervinkova Z, Gersl V and Sterba M. Chronic anthracycline cardiotoxicity: molecular and functional analysis with focus on nuclear factor erythroid 2-related factor 2 and mitochondrial biogenesis pathways. *J Pharmacol Exp Ther* 343: 468-478, 2012.
55. Johnson R, Shabalala S, Louw J, Kappo AP and Muller CJF. Aspalathin Reverts Doxorubicin-Induced Cardiotoxicity through Increased Autophagy and Decreased Expression of p53/mTOR/p62 Signaling. *Molecules* 22, 2017.

56. Khiati S, Dalla Rosa I, Sourbier C, Ma X, Rao VA, Neckers LM, Zhang H and Pommier Y. Mitochondrial topoisomerase I (top1mt) is a novel limiting factor of doxorubicin cardiotoxicity. *Clin Cancer Res* 20: 4873-4881, 2014.
57. Kim SH, Kim G, Han DH, Lee M, Kim I, Kim B, Kim KH, Song YM, Yoo JE, Wang HJ, Bae SH, Lee YH, Lee BW, Kang ES, Cha BS and Lee MS. Ezetimibe ameliorates steatohepatitis via AMP activated protein kinase-TFEB-mediated activation of autophagy and NLRP3 inflammasome inhibition. *Autophagy* 13: 1767-1781, 2017.
58. Kobayashi S, Volden P, Timm D, Mao K, Xu X and Liang Q. Transcription factor GATA4 inhibits doxorubicin-induced autophagy and cardiomyocyte death. *J Biol Chem* 285: 793-804, 2010.
59. Koleini N and Kardami E. Autophagy and mitophagy in the context of doxorubicin-induced cardiotoxicity. *Oncotarget* 8: 46663-46680, 2017.
60. Lazzarini E, Balbi C, Altieri P, Pfeffer U, Gambini E, Canepa M, Varesio L, Bosco MC, Coviello D, Pompilio G, Brunelli C, Cancedda R, Ameri P and Bollini S. The human amniotic fluid stem cell secretome effectively counteracts doxorubicin-induced cardiotoxicity. *Sci Rep* 6: 29994, 2016.
61. Lee KF, Simon H, Chen H, Bates B, Hung MC and Hauser C. Requirement for neuregulin receptor erbB2 in neural and cardiac development. *Nature* 378: 394-398, 1995.
62. Lempiainen H and Halazonetis TD. Emerging common themes in regulation of PIKKs and PI3Ks. *EMBO J* 28: 3067-3073, 2009.
63. Li DL and Hill JA. Cardiomyocyte autophagy and cancer chemotherapy. *J Mol Cell Cardiol* 71: 54-61, 2014.
64. Li DL, Wang ZV, Ding G, Tan W, Luo X, Criollo A, Xie M, Jiang N, May H, Kyrychenko V, Schneider JW, Gillette TG and Hill JA. Doxorubicin Blocks Cardiomyocyte Autophagic Flux by Inhibiting Lysosome Acidification. *Circulation* 133: 1668-1687, 2016.

65. Li M, Sala V, De Santis MC, Cimino J, Cappello P, Pianca N, Di Bona A, Margaria JP, Martini M, Lazzarini E, Pirozzi F, Rossi L, Franco I, Bornbaum J, Heger J, Rohrbach S, Perino A, Tocchetti CG, Lima BHF, Teixeira MM, Porporato PE, Schulz R, Angelini A, Sandri M, Ameri P, Sciarretta S, Lima-Junior RCP, Mongillo M, Zaglia T, Morello F, Novelli F, Hirsch E and Ghigo A. Phosphoinositide 3-Kinase Gamma Inhibition Protects From Anthracycline Cardiotoxicity and Reduces Tumor Growth. *Circulation* 138: 696-711, 2018.
66. Li Z, Pearlman AH and Hsieh P. DNA mismatch repair and the DNA damage response. *DNA Repair (Amst)* 38: 94-101, 2016.
67. Liehr JG and Ricci MJ. 4-Hydroxylation of estrogens as marker of human mammary tumors. *Proc Natl Acad Sci U S A* 93: 3294-3296, 1996.
68. Lim CC, Zuppinger C, Guo X, Kuster GM, Helmes M, Eppenberger HM, Suter TM, Liao R and Sawyer DB. Anthracyclines induce calpain-dependent titin proteolysis and necrosis in cardiomyocytes. *J Biol Chem* 279: 8290-8299, 2004.
69. Llach A, Mazevet M, Mateo P, Villejouvert O, Ridoux A, Rucker-Martin C, Ribeiro M, Fischmeister R, Crozatier B, Benitah JP, Morel E and Gomez AM. Progression of excitation-contraction coupling defects in doxorubicin cardiotoxicity. *J Mol Cell Cardiol* 126: 129-139, 2019.
70. Low RL, Orton S and Friedman DB. A truncated form of DNA topoisomerase IIbeta associates with the mtDNA genome in mammalian mitochondria. *Eur J Biochem* 270: 4173-4186, 2003.
71. Luo P, Zhu Y, Chen M, Yan H, Yang B, Yang X and He Q. HMGB1 contributes to adriamycin-induced cardiotoxicity via up-regulating autophagy. *Toxicol Lett* 292: 115-122, 2018.
72. Lyu YL, Kerrigan JE, Lin CP, Azarova AM, Tsai YC, Ban Y and Liu LF. Topoisomerase IIbeta mediated DNA double-strand breaks: implications in doxorubicin cardiotoxicity and prevention by dexrazoxane. *Cancer Res* 67: 8839-8846, 2007.

73. Ma J, Wang Y, Zheng D, Wei M, Xu H and Peng T. Rac1 signalling mediates doxorubicin-induced cardiotoxicity through both reactive oxygen species-dependent and -independent pathways. *Cardiovasc Res* 97: 77-87, 2013.
74. Ma Y, Zhang X, Bao H, Mi S, Cai W, Yan H, Wang Q, Wang Z, Yan J, Fan GC, Lindsey ML and Hu Z. Toll-like receptor (TLR) 2 and TLR4 differentially regulate doxorubicin induced cardiomyopathy in mice. *PLoS One* 7: e40763, 2012.
75. Maayah ZH, Althurwi HN, Abdelhamid G, Lesyk G, Jurasz P and El-Kadi AO. CYP1B1 inhibition attenuates doxorubicin-induced cardiotoxicity through a mid-chain HETEs-dependent mechanism. *Pharmacol Res* 105: 28-43, 2016.
76. Marino G, Niso-Santano M, Baehrecke EH and Kroemer G. Self-consumption: the interplay of autophagy and apoptosis. *Nat Rev Mol Cell Biol* 15: 81-94, 2014.
77. Martina JA, Chen Y, Gucek M and Puertollano R. MTORC1 functions as a transcriptional regulator of autophagy by preventing nuclear transport of TFEB. *Autophagy* 8: 903-914, 2012.
78. Matt S and Hofmann TG. The DNA damage-induced cell death response: a roadmap to kill cancer cells. *Cell Mol Life Sci* 73: 2829-2850, 2016.
79. Milano G, Biemmi V, Lazzarini E, Balbi C, Ciullo A, Bolis S, Ameri P, Di Silvestre D, Mauri P, Barile L and Vassalli G. Intravenous administration of cardiac progenitor cell-derived exosomes protects against doxorubicin/trastuzumab-induced cardiac toxicity. *Cardiovasc Res*, 2019.
80. Moll UM, Wolff S, Speidel D and Deppert W. Transcription-independent proapoptotic functions of p53. *Curr Opin Cell Biol* 17: 631-636, 2005.
81. Monkkonen T and Debnath J. Inflammatory signaling cascades and autophagy in cancer. *Autophagy* 14: 190-198, 2018.

82. Moruno-Manchon JF, Uzor NE, Kesler SR, Wefel JS, Townley DM, Nagaraja AS, Pradeep S, Mangala LS, Sood AK and Tsvetkov AS. TFEB ameliorates the impairment of the autophagy-lysosome pathway in neurons induced by doxorubicin. *Aging (Albany NY)* 8: 3507-3519, 2016.
83. Murphy MP. Mitochondrial dysfunction indirectly elevates ROS production by the endoplasmic reticulum. *Cell Metab* 18: 145-146, 2013.
84. Murray GI, Taylor MC, McFadyen MC, McKay JA, Greenlee WF, Burke MD and Melvin WT. Tumor-specific expression of cytochrome P450 CYP1B1. *Cancer Res* 57: 3026-3031, 1997.
85. Nazarko VY and Zhong Q. ULK1 targets Beclin-1 in autophagy. *Nat Cell Biol* 15: 727-728, 2013.
86. Nebigil CG and Desaubry L. Updates in Anthracycline-Mediated Cardiotoxicity. *Front Pharmacol* 9: 1262, 2018.
87. Nozaki N, Shishido T, Takeishi Y and Kubota I. Modulation of doxorubicin-induced cardiac dysfunction in toll-like receptor-2-knockout mice. *Circulation* 110: 2869-2874, 2004.
88. Odiete O, Hill MF and Sawyer DB. Neuregulin in cardiovascular development and disease. *Circ Res* 111: 1376-1385, 2012.
89. Oka T, Maillet M, Watt AJ, Schwartz RJ, Aronow BJ, Duncan SA and Molkentin JD. Cardiac-specific deletion of Gata4 reveals its requirement for hypertrophy, compensation, and myocyte viability. *Circ Res* 98: 837-845, 2006.
90. Orstavik O, Manfra O, Andressen KW, Andersen GO, Skomedal T, Osnes JB, Levy FO and Krobert KA. The inotropic effect of the active metabolite of levosimendan, OR-1896, is mediated through inhibition of PDE3 in rat ventricular myocardium. *PLoS One* 10: e0115547, 2015.

91. Pan JA, Tang Y, Yu JY, Zhang H, Zhang JF, Wang CQ and Gu J. miR-146a attenuates apoptosis and modulates autophagy by targeting TAF9b/P53 pathway in doxorubicin-induced cardiotoxicity. *Cell Death Dis* 10: 668, 2019.
92. Papp Z, Edes I, Fruhwald S, De Hert SG, Salmenpera M, Leppikangas H, Mebazaa A, Landoni G, Grossini E, Caimmi P, Morelli A, Guarracino F, Schwinger RH, Meyer S, Algotsson L, Wikstrom BG, Jorgensen K, Filippatos G, Parissis JT, Gonzalez MJ, Parkhomenko A, Yilmaz MB, Kivikko M, Pollesello P and Follath F. Levosimendan: molecular mechanisms and clinical implications: consensus of experts on the mechanisms of action of levosimendan. *Int J Cardiol* 159: 82-87, 2012.
93. Pattingre S, Tassa A, Qu X, Garuti R, Liang XH, Mizushima N, Packer M, Schneider MD and Levine B. Bcl-2 antiapoptotic proteins inhibit Beclin 1-dependent autophagy. *Cell* 122: 927-939, 2005.
94. Payapilly A and Malliri A. Compartmentalisation of RAC1 signalling. *Curr Opin Cell Biol* 54: 50-56, 2018.
95. Pinheiro EA, Fetterman KA and Burrige PW. hiPSCs in cardio-oncology: deciphering the genomics. *Cardiovasc Res* 115: 935-948, 2019.
96. Pop-Moldovan AL, Trofenciu NM, Darabantiu DA, Precup C, Branea H, Christodorescu R and Puschita M. Customized laboratory TLR4 and TLR2 detection method from peripheral human blood for early detection of doxorubicin-induced cardiotoxicity. *Cancer Gene Ther* 24: 203-207, 2017.
97. Qing G, Yan P and Xiao G. Hsp90 inhibition results in autophagy-mediated proteasome-independent degradation of I κ B kinase (IKK). *Cell Res* 16: 895-901, 2006.
98. Reichardt P, Tabone MD, Mora J, Morland B and Jones RL. Risk-benefit of dexrazoxane for preventing anthracycline-related cardiotoxicity: re-evaluating the European labeling. *Future Oncol* 14: 2663-2676, 2018.

99. Riad A, Bien S, Gratz M, Escher F, Westermann D, Heimesaat MM, Bereswill S, Krieg T, Felix SB, Schultheiss HP, Kroemer HK and Tschöpe C. Toll-like receptor-4 deficiency attenuates doxorubicin-induced cardiomyopathy in mice. *Eur J Heart Fail* 10: 233-243, 2008.
100. Roca-Alonso L, Castellano L, Mills A, Dabrowska AF, Sikkell MB, Pellegrino L, Jacob J, Frampton AE, Krell J, Coombes RC, Harding SE, Lyon AR and Stebbing J. Myocardial MiR-30 downregulation triggered by doxorubicin drives alterations in beta-adrenergic signaling and enhances apoptosis. *Cell Death Dis* 6: e1754, 2015.
101. Rock FL, Hardiman G, Timans JC, Kastelein RA and Bazan JF. A family of human receptors structurally related to *Drosophila* Toll. *Proc Natl Acad Sci U S A* 95: 588-593, 1998.
102. Roos WP and Kaina B. DNA damage-induced cell death: from specific DNA lesions to the DNA damage response and apoptosis. *Cancer Lett* 332: 237-248, 2013.
103. Russell SD, Blackwell KL, Lawrence J, Phippen JE, Jr., Roe MT, Wood F, Paton V, Holmgren E and Mahaffey KW. Independent adjudication of symptomatic heart failure with the use of doxorubicin and cyclophosphamide followed by trastuzumab adjuvant therapy: a combined review of cardiac data from the National Surgical Adjuvant breast and Bowel Project B-31 and the North Central Cancer Treatment Group N9831 clinical trials. *J Clin Oncol* 28: 3416-3421, 2010.
104. Sag CM, Kohler AC, Anderson ME, Backs J and Maier LS. CaMKII-dependent SR Ca leak contributes to doxorubicin-induced impaired Ca handling in isolated cardiac myocytes. *J Mol Cell Cardiol* 51: 749-759, 2011.
105. Saito T and Sadoshima J. Molecular mechanisms of mitochondrial autophagy/mitophagy in the heart. *Circ Res* 116: 1477-1490, 2015.
106. Sala V, Li M and Ghigo A. New avenues in cardio-oncology. *Aging (Albany NY)* 11: 1075-1076, 2019.

107. Salminen A, Hyttinen JM, Kauppinen A and Kaarniranta K. Context-Dependent Regulation of Autophagy by IKK-NF-kappaB Signaling: Impact on the Aging Process. *Int J Cell Biol* 2012: 849541, 2012.
108. Sandrock K, Bielek H, Schradi K, Schmidt G and Klugbauer N. The nuclear import of the small GTPase Rac1 is mediated by the direct interaction with karyopherin alpha2. *Traffic* 11: 198-209, 2010.
109. Settembre C, Fraldi A, Medina DL and Ballabio A. Signals from the lysosome: a control centre for cellular clearance and energy metabolism. *Nat Rev Mol Cell Biol* 14: 283-296, 2013.
110. Sha Y, Rao L, Settembre C, Ballabio A and Eissa NT. STUB1 regulates TFEB-induced autophagy-lysosome pathway. *EMBO J* 36: 2544-2552, 2017.
111. Shabalala S, Muller CJF, Louw J and Johnson R. Polyphenols, autophagy and doxorubicin-induced cardiotoxicity. *Life Sci* 180: 160-170, 2017.
112. Shimada T and Fujii-Kuriyama Y. Metabolic activation of polycyclic aromatic hydrocarbons to carcinogens by cytochromes P450 1A1 and 1B1. *Cancer Sci* 95: 1-6, 2004.
113. Shirakabe A, Ikeda Y, Sciarretta S, Zablocki DK and Sadoshima J. Aging and Autophagy in the Heart. *Circ Res* 118: 1563-1576, 2016.
114. Simunek T, Sterba M, Popelova O, Adamcova M, Hrdina R and Gersl V. Anthracycline-induced cardiotoxicity: overview of studies examining the roles of oxidative stress and free cellular iron. *Pharmacol Rep* 61: 154-171, 2009.
115. Singal PK and Iliskovic N. Doxorubicin-induced cardiomyopathy. *N Engl J Med* 339: 900-905, 1998.
116. Singla DK, Johnson TA and Tavakoli Dargani Z. Exosome Treatment Enhances Anti-Inflammatory M2 Macrophages and Reduces Inflammation-Induced Pyroptosis in Doxorubicin-Induced Cardiomyopathy. *Cells* 8, 2019.

117. Sishi BJ, Loos B, van Rooyen J and Engelbrecht AM. Autophagy upregulation promotes survival and attenuates doxorubicin-induced cardiotoxicity. *Biochem Pharmacol* 85: 124-134, 2013.
118. Sterba M, Popelova O, Vavrova A, Jirkovsky E, Kovarikova P, Gersl V and Simunek T. Oxidative stress, redox signaling, and metal chelation in anthracycline cardiotoxicity and pharmacological cardioprotection. *Antioxid Redox Signal* 18: 899-929, 2013.
119. Tasdemir E, Maiuri MC, Galluzzi L, Vitale I, Djavaheri-Mergny M, D'Amelio M, Criollo A, Morselli E, Zhu C, Harper F, Nannmark U, Samara C, Pinton P, Vicencio JM, Carnuccio R, Moll UM, Madeo F, Paterlini-Brechot P, Rizzuto R, Szabadkai G, Pierron G, Blomgren K, Tavernarakis N, Codogno P, Cecconi F and Kroemer G. Regulation of autophagy by cytoplasmic p53. *Nat Cell Biol* 10: 676-687, 2008.
120. Tavakoli Dargani Z and Singla DK. Embryonic stem cell-derived exosomes inhibit doxorubicin-induced TLR4-NLRP3-mediated cell death-pyroptosis. *Am J Physiol Heart Circ Physiol* 317: H460-H471, 2019.
121. Thayer WS. Adriamycin stimulated superoxide formation in submitochondrial particles. *Chem Biol Interact* 19: 265-278, 1977.
122. Tocchetti CG, Cadeddu C, Di Lisi D, Femmino S, Madonna R, Mele D, Monte I, Novo G, Penna C, Pepe A, Spallarossa P, Varricchi G, Zito C, Pagliaro P and Mercurio G. From Molecular Mechanisms to Clinical Management of Antineoplastic Drug-Induced Cardiovascular Toxicity: A Translational Overview. *Antioxid Redox Signal* 30: 2110-2153, 2019.
123. Tong Z, Jiang B, Wu Y, Liu Y, Li Y, Gao M, Jiang Y, Lv Q and Xiao X. MiR-21 Protected Cardiomyocytes against Doxorubicin-Induced Apoptosis by Targeting BTG2. *Int J Mol Sci* 16: 14511-14525, 2015.
124. Tscheschner H, Meinhardt E, Schlegel P, Jungmann A, Lehmann LH, Muller OJ, Most P, Katus HA and Raake PW. CaMKII activation participates in doxorubicin cardiotoxicity and is attenuated by moderate GRP78 overexpression. *PLoS One* 14: e0215992, 2019.

125. Vacchi-Suzzi C, Bauer Y, Berridge BR, Bongiovanni S, Gerrish K, Hamadeh HK, Letzkus M, Lyon J, Moggs J, Paules RS, Pognan F, Staedtler F, Vidgeon-Hart MP, Grenet O and Couttet P. Perturbation of microRNAs in rat heart during chronic doxorubicin treatment. *PLoS One* 7: e40395, 2012.
126. Varricchi G, Ameri P, Cadeddu C, Ghigo A, Madonna R, Marone G, Mercurio V, Monte I, Novo G, Parrella P, Pirozzi F, Pecoraro A, Spallarossa P, Zito C, Mercurio G, Pagliaro P and Tocchetti CG. Antineoplastic Drug-Induced Cardiotoxicity: A Redox Perspective. *Front Physiol* 9: 167, 2018.
127. Vejpongsa P and Yeh ET. Prevention of anthracycline-induced cardiotoxicity: challenges and opportunities. *J Am Coll Cardiol* 64: 938-945, 2014.
128. Wang JX, Zhang XJ, Feng C, Sun T, Wang K, Wang Y, Zhou LY and Li PF. MicroRNA-532-3p regulates mitochondrial fission through targeting apoptosis repressor with caspase recruitment domain in doxorubicin cardiotoxicity. *Cell Death Dis* 6: e1677, 2015.
129. Wang P, Wang L, Lu J, Hu Y, Wang Q, Li Z, Cai S, Liang L, Guo K, Xie J, Wang J, Lan R, Shen J and Liu P. SESN2 protects against doxorubicin-induced cardiomyopathy via rescuing mitophagy and improving mitochondrial function. *J Mol Cell Cardiol* 133: 125-137, 2019.
130. Wang S, Song P and Zou MH. Inhibition of AMP-activated protein kinase alpha (AMPKalpha) by doxorubicin accentuates genotoxic stress and cell death in mouse embryonic fibroblasts and cardiomyocytes: role of p53 and SIRT1. *J Biol Chem* 287: 8001-8012, 2012.
131. Wang X, Li C, Wang Q, Li W, Guo D, Zhang X, Shao M, Chen X, Ma L, Zhang Q, Wang W and Wang Y. Tanshinone IIA Restores Dynamic Balance of Autophagosome/Autolysosome in Doxorubicin-Induced Cardiotoxicity via Targeting Beclin1/LAMP1. *Cancers (Basel)* 11, 2019.
132. Wong PM, Feng Y, Wang J, Shi R and Jiang X. Regulation of autophagy by coordinated action of mTORC1 and protein phosphatase 2A. *Nat Commun* 6: 8048, 2015.

133. Xia W and Hou M. Mesenchymal stem cells confer resistance to doxorubicin-induced cardiac senescence by inhibiting microRNA-34a. *Oncol Lett* 15: 10037-10046, 2018.
134. Xu X, Chen K, Kobayashi S, Timm D and Liang Q. Resveratrol attenuates doxorubicin-induced cardiomyocyte death via inhibition of p70 S6 kinase 1-mediated autophagy. *J Pharmacol Exp Ther* 341: 183-195, 2012.
135. Xu ZM, Li CB, Liu QL, Li P and Yang H. Ginsenoside Rg1 Prevents Doxorubicin-Induced Cardiotoxicity through the Inhibition of Autophagy and Endoplasmic Reticulum Stress in Mice. *Int J Mol Sci* 19, 2018.
136. Yao Y, Xu X, Zhang G, Zhang Y, Qian W and Rui T. Role of HMGB1 in doxorubicin-induced myocardial apoptosis and its regulation pathway. *Basic Res Cardiol* 107: 267, 2012.
137. Yin J, Guo J, Zhang Q, Cui L, Zhang L, Zhang T, Zhao J, Li J, Middleton A, Carmichael PL and Peng S. Doxorubicin-induced mitophagy and mitochondrial damage is associated with dysregulation of the PINK1/parkin pathway. *Toxicol In Vitro* 51: 1-10, 2018.
138. Yin Z, Zhao Y, Li H, Yan M, Zhou L, Chen C and Wang DW. miR-320a mediates doxorubicin-induced cardiotoxicity by targeting VEGF signal pathway. *Aging (Albany NY)* 8: 192-207, 2016.
139. Yoshida M, Shiojima I, Ikeda H and Komuro I. Chronic doxorubicin cardiotoxicity is mediated by oxidative DNA damage-ATM-p53-apoptosis pathway and attenuated by pitavastatin through the inhibition of Rac1 activity. *J Mol Cell Cardiol* 47: 698-705, 2009.
140. Zamorano JL, Lancellotti P, Rodriguez Munoz D, Aboyans V, Asteggiano R, Galderisi M, Habib G, Lenihan DJ, Lip GY, Lyon AR, Lopez Fernandez T, Mohty D, Piepoli MF, Tamargo J, Torbicki A, Suter TM, Zamorano JL, Aboyans V, Achenbach S, Agewall S, Badimon L, Baron-Esquivias G, Baumgartner H, Bax JJ, Bueno H, Carerj S, Dean V, Erol C, Fitzsimons D, Gaemperli O, Kirchhof P, Kolh P, Lancellotti P, Lip GY, Nihoyannopoulos P, Piepoli MF, Ponikowski P, Roffi M, Torbicki A, Vaz Carneiro A, Windecker S, Authors/Task Force M, Guidelines ESCCfP and Document R. 2016 ESC Position Paper on cancer treatments and cardiovascular toxicity developed under the auspices of the ESC

Committee for Practice Guidelines: The Task Force for cancer treatments and cardiovascular toxicity of the European Society of Cardiology (ESC). *Eur J Heart Fail* 19: 9-42, 2017.

141. Zhang H, Zhang YW, Yasukawa T, Dalla Rosa I, Khiati S and Pommier Y. Increased negative supercoiling of mtDNA in TOP1mt knockout mice and presence of topoisomerases IIalpha and IIbeta in vertebrate mitochondria. *Nucleic Acids Res* 42: 7259-7267, 2014.

142. Zhang QL, Yang JJ and Zhang HS. Carvedilol (CAR) combined with carnosic acid (CAA) attenuates doxorubicin-induced cardiotoxicity by suppressing excessive oxidative stress, inflammation, apoptosis and autophagy. *Biomed Pharmacother* 109: 71-83, 2019.

143. Zhang S, Liu X, Bawa-Khalfe T, Lu LS, Lyu YL, Liu LF and Yeh ET. Identification of the molecular basis of doxorubicin-induced cardiotoxicity. *Nat Med* 18: 1639-1642, 2012.

144. Zhang YW, Shi J, Li YJ and Wei L. Cardiomyocyte death in doxorubicin-induced cardiotoxicity. *Arch Immunol Ther Exp (Warsz)* 57: 435-445, 2009.

145. Zhao Y, McLaughlin D, Robinson E, Harvey AP, Hookham MB, Shah AM, McDermott BJ and Grieve DJ. Nox2 NADPH oxidase promotes pathologic cardiac remodeling associated with Doxorubicin chemotherapy. *Cancer Res* 70: 9287-9297, 2010.

146. Zhou HF, Yan H, Hu Y, Springer LE, Yang X, Wickline SA, Pan D, Lanza GM and Pham CT. Fumagillin prodrug nanotherapy suppresses macrophage inflammatory response via endothelial nitric oxide. *ACS Nano* 8: 7305-7317, 2014.

147. Zhu W, Soonpaa MH, Chen H, Shen W, Payne RM, Liechty EA, Caldwell RL, Shou W and Field LJ. Acute doxorubicin cardiotoxicity is associated with p53-induced inhibition of the mammalian target of rapamycin pathway. *Circulation* 119: 99-106, 2009.

148. Zhu Z, Yang C, Iyaswamy A, Krishnamoorthi S, Sreenivasmurthy SG, Liu J, Wang Z, Tong BC, Song J, Lu J, Cheung KH and Li M. Balancing mTOR Signaling and Autophagy in the Treatment of Parkinson's Disease. *Int J Mol Sci* 20, 2019.

Figure Legends

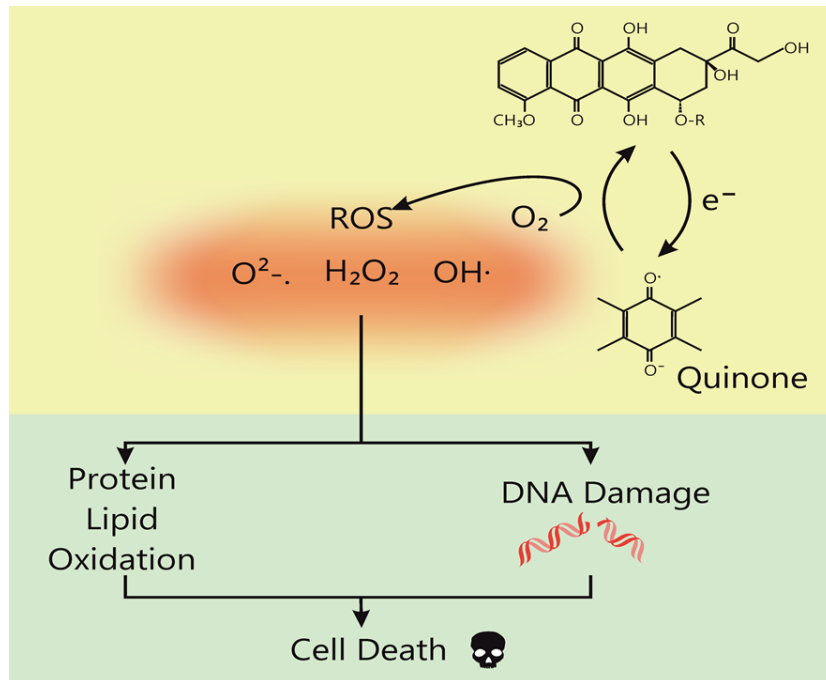


FIG. 1. The ROS-driven hypothesis of anthracycline (ANT)-induced injury.

The classic “ROS-driven hypothesis” points to the generation of reactive oxygen species (ROS) by the quinone moiety of anthracyclines as the leading cause of ANT cardiotoxicity. To see this illustration in color, the reader is referred to the online version of this article at www.liebertpub.com/ars.

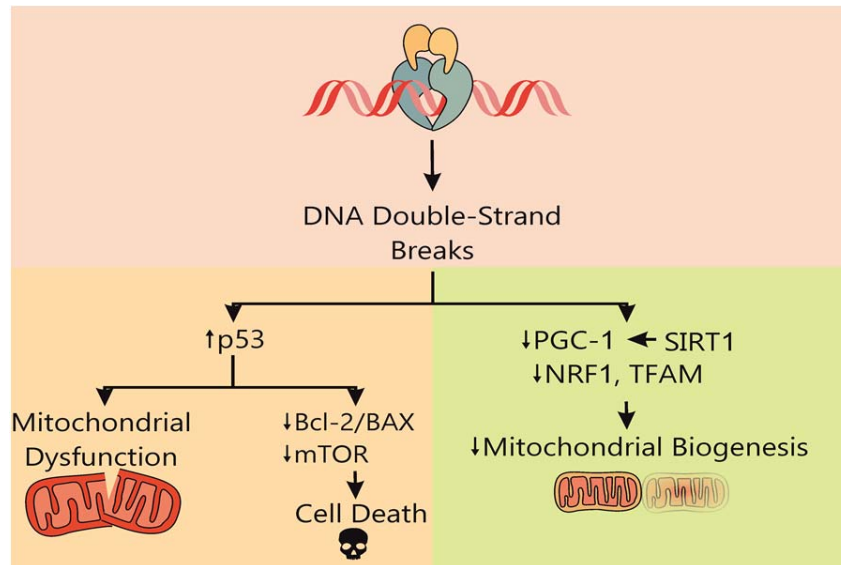


FIG. 2. New mechanisms of anthracycline (ANT)-induced injury to cardiac cells.

According to the most widely accepted view, ANT toxicity is caused by poisoning of topoisomerase 2 beta (Top2- β), which leads to accumulation of double-stranded DNA breaks. This results in the activation of the p53 tumor-suppressor pathway and the ensuing mitochondrial dysfunction, ROS generation, imbalanced pro-survival/pro-apoptotic signals (Bcl2/BAX and mTOR) and, finally, to cardiac cell death (left panel). DNA damage simultaneously impairs mitochondrial biogenesis by affecting peroxisome-proliferator-activated receptor α coactivator 1 (PGC-1), nuclear respiratory factor 1 (NRF1) and mitochondrial transcription factor A (TFAM) (right panel). To see this illustration in color, the reader is referred to the online version of this article at www.liebertpub.com/ars.

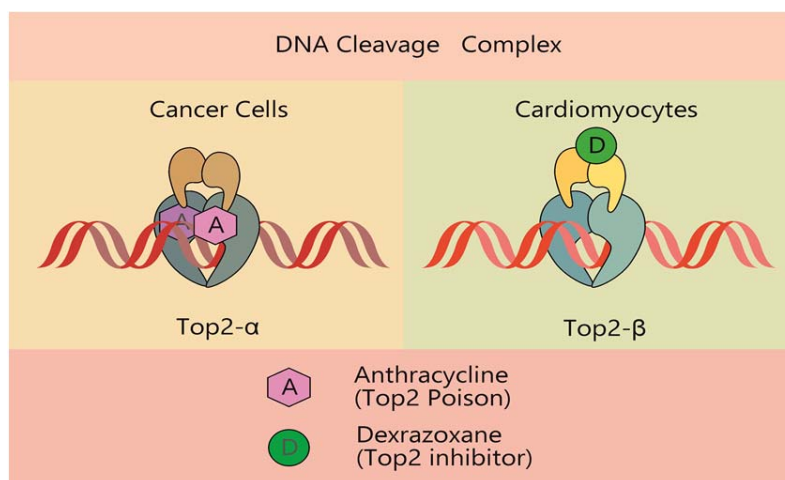


FIG. 3. Mechanism of anthracycline (ANT)-mediated cell injury and death in cancer cells and cardiomyocytes.

The anti-cancer action of ANTs is linked to the poisoning of Top2- α . In cardiomyocytes, the Top2- β isoform is prevalent and represents the major target of ANTs. Dexrazoxane (DXR) protects against ANT cardiotoxicity by interfering with the binding of ANTs to Top2- β , thus preventing the poisoning and the loss of function of Top2. To see this illustration in color, the reader is referred to the online version of this article at www.liebertpub.com/ars.

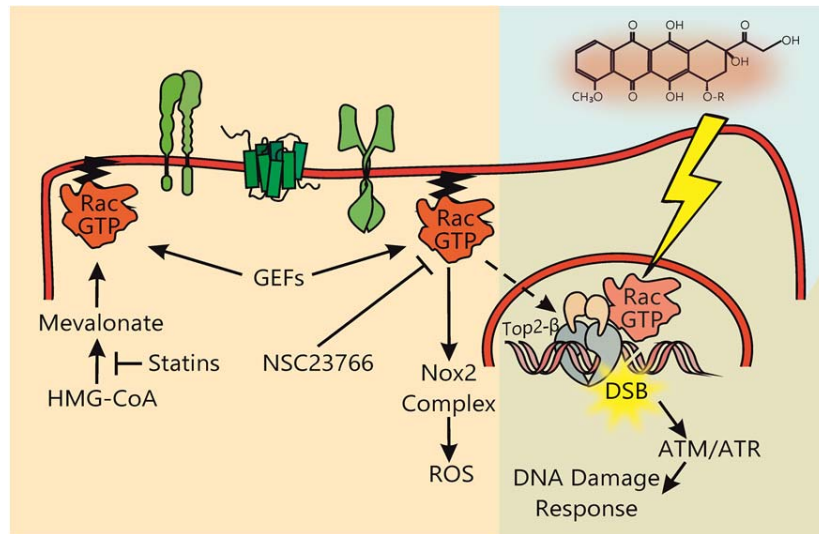


FIG. 4. Geno-protective effect of pharmacological inhibition of Rac1 signaling.

Rac1 signaling contributes to ANT-induced cardiotoxicity by regulating Nox2 NADPH oxidase complex and via a ROS-independent nuclear mechanism, leading to the formation of DNA double-stranded breaks and subsequent activation of the ATM/ATR-p53 pathway. In the nucleus, Rac1 binds to and regulates the activity of topoisomerase 2 (Top2). Inhibition of the HMG-CoA reductase (mevalonate pathway) by statins causes depletion of the cellular pool of isoprene precursors, which are essential for membrane localization of Rac1. Pharmacological targeting of Rac1 by statins or by the Rac1 inhibitor (NSC23766) attenuates ROS production and DNA damage response. To see this illustration in color, the reader is referred to the online version of this article at www.liebertpub.com/ars.

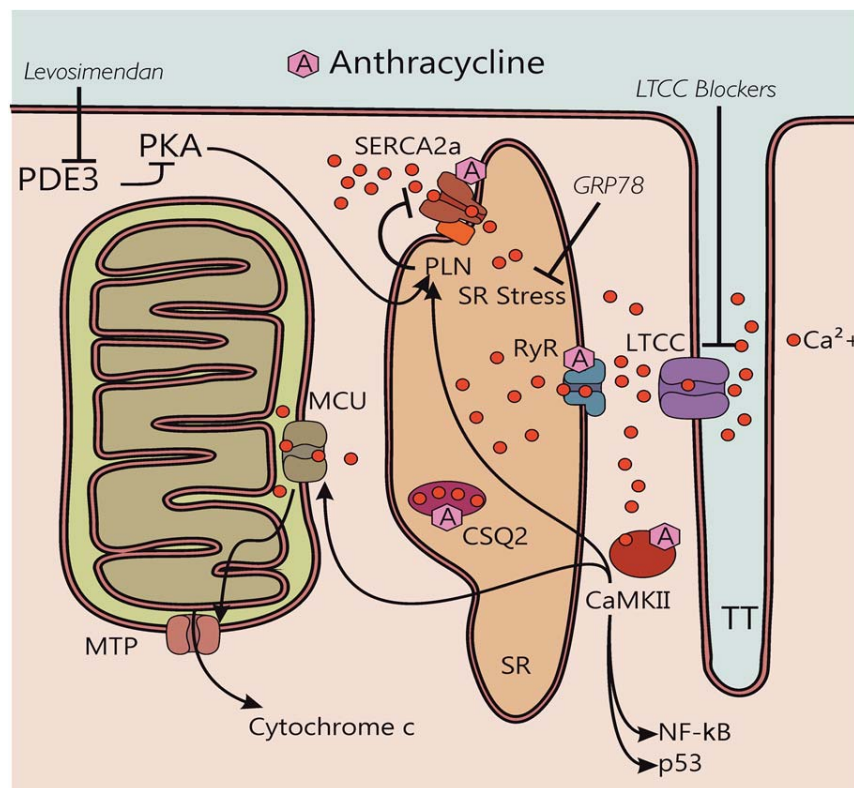


FIG. 5. Calcium overload as a central event in anthracycline (ANT)-induced cardiotoxicity. Doxorubicin (Doxo) and its metabolite, doxorubicinol, affect the activity of different Ca²⁺-handling proteins of cardiomyocytes. Doxorubicinol target calsequestrin type 2 (CSQ2) in the sarcoplasmic reticulum (SR), thus increasing cytoplasmic Ca²⁺ concentration, while Doxo inhibits the transcription of the sarcoplasmic reticulum Ca²⁺-ATPase 2a (SERCA2a), thereby reducing Ca²⁺ reuptake in the SR. Doxo and its metabolite doxorubicinol both modify the activity of ryanodine receptor (RyR) and SERCA2a and induce Calcium/Calmodulin-dependent protein kinase-II (CaMKII)-dependent Ca²⁺ leakage from the SR. ANT-mediated deregulation of CaMKII also impact on mitochondrial Ca²⁺ regulation. CaMKII is responsible for the activation of nuclear factor-kappa B (NF-κB) and p53 signaling and leads to increased Ca²⁺ influx in mitochondria through mitochondrial calcium Ca²⁺ uniporter (MCU). Mitochondrial Ca²⁺ overload, in turn, triggers mitochondrial permeability transition pore (MTP) opening and release of proapoptotic cytochrome c. Pharmacological targeting of key regulators of Ca²⁺ signaling, such as phosphodiesterase 3 (PDE3) by Levosimendan or L-type Ca²⁺ channels (LTCC) by LTCC blockers, as well as

chaperone-mediated alleviation of SR stress (GRP78 overexpression) are emerging therapies against ANT cardiotoxicity. To see this illustration in color, the reader is referred to the online version of this article at www.liebertpub.com/ars.

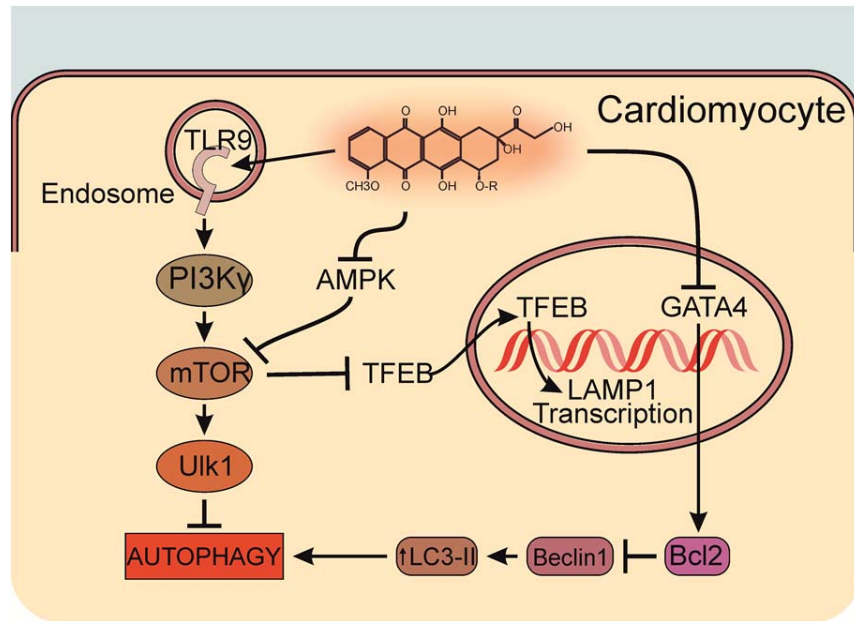


FIG.6. Overview of anthracycline (ANT)-induced dysregulation of autophagy

Autophagy deregulation is a key mechanism underlying ANT-induced cardiotoxicity, although its beneficial versus maladaptive role is still controversial. Cardiomyocyte exposure to ANTs perturbs AMPK, Akt and mTOR signaling pathways, which are all upstream regulators of autophagy. ANTs inhibit the autophagic process by activating mTOR or by blocking AMPK. Furthermore, doxorubicin (Doxo) engages PI3K γ signaling downstream of Toll-like receptor 9 (TLR9), converging on inhibitory phosphorylation of Ulk-1 at Ser757 and preventing autophagosome initiation. Additionally, activated mTOR restricts TFEB in the cytoplasm and inhibits the transcription of autophagy-related genes, such as LAMP1. Conversely, Doxo blocks the activity of GATA4, thereby inhibiting the transcription of anti-apoptotic protein B-cell lymphoma 2 (Bcl2), a negative regulator of Beclin-1. As a result, the autophagy-related marker Beclin-1 and LC3-II are upregulated and lead to cardiomyocyte death. Restoration of GATA4 attenuates Doxo cardiotoxicity by upregulating Bcl2 and in turn inhibiting autophagy. To see this illustration in color, the reader is referred to the online version of this article at www.liebertpub.com/ars.

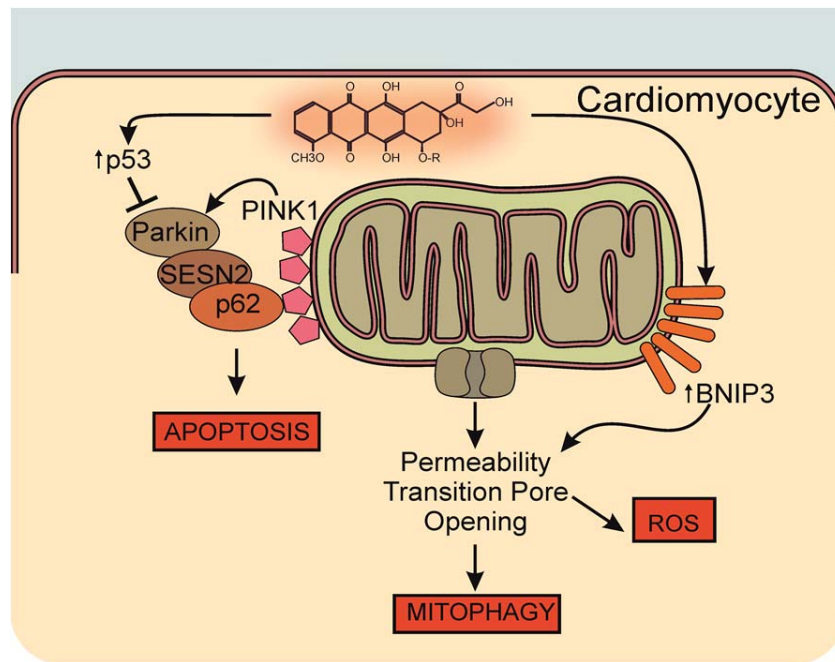


FIG. 7. Mechanism of anthracycline (ANT)-mediated mitochondrial damage and cells death

Normally, mitochondrial homeostasis is regulated through a selective form of autophagy, namely mitophagy. Under stress conditions, PTEN-induced kinase 1 (PINK1) aggregates and recruits Parkin to the mitochondrial outer membrane mediating the ubiquitination of mitochondrial proteins and their recognition by p62, consequently leading to the initiation of mitophagy. However, Doxo-induced p53 accumulation inhibits mitophagy by suppressing Parkin translocation and interaction with SESN2 and p62, therefore inducing cardiomyocytes apoptosis. Conversely, in models of acute cardiotoxicity induced by high dose ANTs, BNIP3-induced mitophagy has a maladaptive role. Up-regulation and translocation of BNIP3 leads to the permeability transition pore opening and increased ROS production. To see this illustration in color, the reader is referred to the online version of this article at www.liebertpub.com/ars.

Table 1: Relevant and emerging therapeutic approaches to counteract ANT-induced cardiotoxicity

Compound/Therapeutic approach	Mechanism of action	References
ICRF-187 or Dexrazoxane (EDTA derivative)	Iron chelation, catalytic inhibition of Topoisomerase 2	(115, 86, 72)
JR-311 (Dexrazoxane analogue)	Catalytic inhibition of Topoisomerase 2	(53)
NSC23766	Rac1 inhibition	(108)
Statins (e.g. Lovastatin)	HMGC-CoA reductase inhibition, prevention of Rac1 prenylation, tumor sensitization to chemotherapy	(108, 42, 145)
Adeno-associated virus overexpressing GRP78 chaperone	Amelioration of Sarcoplasmic Reticulum stress	(2)
Nifedipine, Amlodipine	LTCC blockade	(19)
Levosimendan	Restoration of Ca ²⁺ homeostasis, inotropic vasodilation, anti-inflammatory and anti-oxidant action	(144, 49, 92)
5-Aminoimidazole-4-carboxamide ribonucleotide (AICAR) or adenoviral expression of AMPK-CA	Activation of AMPK	(89)
TLR4 isotype-matched IgG Ab; TLR2- TLR4 embryonic stem cell-derived exosomes (ES-Exos)	TLR2-4 inhibition	(87, 99, 120)
Mesenchymal stem cells	Inhibition of miR-34a-SIRT1-p53 axis	(123)
CPC exosomes	Inhibition of miR-146a-5p target genes	(79)